1993-12

The evolution of jet features during the 1993 East Coast White Hurricane: a case study using the Global Spectral Model

Kraft, Anton J.

Monterey, California. Naval Postgraduate School

NAVAL POSTGRADUATE SCHOOL
Monterey, California

THESIS

THE EVOLUTION OF JET FEATURES DURING THE 1993 EAST COAST "WHITE HURRICANE": A CASE STUDY USING THE GLOBAL SPECTRAL MODEL

by

Anton J. Kraft

December, 1993

Thesis Advisor: Patricia M. Pauley
Co-Advisor: Paul A. Hirschberg

REPORT DOCUMENTATION PAGE

Form Approved OMB No. 0704

1. AGENCY USE ONLY *(Leave blank)*	2. REPORT DATE	3. REPORT TYPE AND DATES COVERED
	December 1993.	Master's Thesis

4. TITLE AND SUBTITLE THE EVOLUTION OF JET STREAK FEATURES DURING THE 1993 EAST COAST "WHITE HURRICANE": A CASE STUDY USING THE GLOBAL SPECTRAL MODEL.

5. FUNDING NUMBERS

6. AUTHOR(S) Anton J. Kraft, LT, USN

7. PERFORMING ORGANIZATION NAME(S) AND ADDRESS(ES)
Naval Postgraduate School
Monterey CA 93943-5000

8. PERFORMING ORGANIZATION REPORT NUMBER

9. SPONSORING/MONITORING AGENCY NAME(S) AND ADDRESS(ES)

10. SPONSORING/MONITORING AGENCY REPORT NUMBER

11. SUPPLEMENTARY NOTES The views expressed in this thesis are those of the author and do not reflect the official policy or position of the Department of Defense or the U.S. Government.

12a. DISTRIBUTION/AVAILABILITY STATEMENT
Approved for public release; distribution is unlimited.

12b. DISTRIBUTION CODE
*A

13.

ABSTRACT *(maximum 200 words)*

During the period of 12 through 14 March 1993 a major snow storm, later described as a "White Hurricane," formed over the Gulf of Mexico, moved east-northeast across the Florida panhandle, and then headed northeast along the eastern seaboard. The extreme weather produced by this storm was responsible for 243 deaths and $1 billion in property damage. Because the storm was accompanied by unusually strong jet streaks, a diagnostic of the storm kinetic energy contents and generation of kinetic energy was undertaken. The vertically integrated kinetic energy (IKE) and vertically integrated generation of kinetic energy (IGK) are shown to be effective tools in determining how jet streaks influenced the development of this storm. Specifically, IKE can indicate geographically where jet streak maxima are located, whereas IGK can provide a measure of the effect of transverse circulations aloft. In addition, IGK combined with IKE can indicate if the jet streak is weakening or strengthening. The data used in this case study were primarily the National Weather Service's Global Spectral Model aviation forecast and analysis. These data were further interpolated for use in VISUAL, which is a meteorological diagnostic and display program developed primarily at the Naval Postgraduate School.

14. SUBJECT TERMS

15. NUMBER OF PAGES 179

16. PRICE CODE

17. SECURITY CLASSIFICATION OF REPORT	18. SECURITY CLASSIFICATION OF THIS PAGE	19. SECURITY CLASSIFICATION OF ABSTRACT	20. LIMITATION OF ABSTRACT
Unclassified	Unclassified	Unclassified	UL

NSN 7540-01-280-5500 Standard Form 298 (Rev. 2-89)
Prescribed by ANSI Std. 239-18

Approved for public release; distribution is unlimited.

The evolution of jet features during the 1993
East Coast "WHITE HURRICANE": A case study
using the Global Spectral Model

by

Anton J. Kraft
Lieutenant, United States Navy
B.S., The Citadel, 1984

Submitted in partial fulfillment
of the requirements for the degree of

MASTER OF SCIENCE IN METEOROLOGY AND PHYSICAL OCEANOGRAPHY

from the

NAVAL POSTGRADUATE SCHOOL
December 1993

Author: [redacted]
Anton J. Kraft

Approved by: [redacted]
Patricia M. Pauley, Thesis Advisor

[redacted]
Paul A. Hirschberg, Co-Advisor

[redacted]
Robert L. Haney, Chairman
Department of Meteorology

ABSTRACT

During the period of 12 through 14 March 1993 a major snow storm, later described as a "White Hurricane," formed over the Gulf of Mexico, moved east-northeast across the Florida panhandle, and then headed northeast along the eastern seaboard. The extreme weather produced by this storm was responsible for 243 deaths and $1 billion in property damage. Because the storm was accompanied by unusually strong jet streaks, a diagnostic of the storm kinetic energy contents and generation of kinetic energy was undertaken. The vertically integrated kinetic energy (IKE) and vertically integrated generation of kinetic energy (IGK) are shown to be effective tools in determining how jet streaks influenced the development of this storm. Specifically, IKE can indicate geographically where jet streak maxima are located, whereas IGK can provide a measure of the effect of transverse circulations aloft. In addition, IGK combined with IKE can indicate if the jet streak is weakening or strengthening. The data used in this case study were primarily the National Weather Service's Global Spectral Model aviation forecast and analysis. These data were further interpolated for use in VISUAL, which is a meteorological diagnostic and display program developed primarily at the Naval Postgraduate School.

TABLE OF CONTENTS

ACKNOWLEDGEMENTS

First, I want to thank my family for all the support especially my wife Teresa. Second, I want to thank my thesis advisor, Dr. Patricia M. Pauley for the proper guidance throughout the thick and thin of putting this thesis together. Third, I thank my Co-Advisor, Dr. Paul A. Hirschberg, who was diligent and thorough. A special thanks goes out to Mr. Steve Drake, who never wavered from requests nor questions I had concerning VISUAL. He is and always will be the "GOD" of VISUAL. Lastly, I want to thank (Sir) Isaac Pauley, for he always provided a smile, a change of pace or a reality check.

I. INTRODUCTION

Over the three day period, 12 through 14 March, a snow storm along the Eastern Seaboard produced some of the most severe weather ever recorded (DeAngelis 1992). Some identified this storm as a "White Hurricane", and many meteorologists labeled it "the storm of the century". Indeed, this very powerful and destructive extratropical cyclone had the force and energy levels of a hurricane.

This storm did not have the strongest winds or the lowest sea-level pressure ever recorded, nor did it the greatest 24 h sea-level pressure decrease. It was labeled "the storm of the century" because the adverse weather it produced had such a large impact on human activity. Heavy wet snow, high winds, and tornadoes were among the most damaging characteristics of this "White Hurricane" according to the National Climate Data Center's (NCDC) Research Customer Service Group, the Naval Oceanography Command News (May 1993), and the Mariners Weather Log (Spring 1993). The following are some highlights of the storm reported by the NCDC group (March 1993):

- At least 243 deaths have been attributed to the storm, plus 48 missing at sea. This is over three times the combined death toll of 79 attributed to hurricanes Hugo and Andrew.

- Thousands of people were isolated by record snowfalls, especially in the Georgia, North Carolina, and Virginia mountains. Over 100 hikers were rescued from the North Carolina and Tennessee mountains. Curfews were enforced in many counties and cities as 'states of emergency' were declared. The National Guard was deployed in many areas, especially in the North Carolina mountains

- For the first time, every major airport on the East Coast was closed at one time or another by the storm.

- Hundreds of roof collapses were reported due to the weight of the heavy snow. Over three million customers were without electrical power at one time due to fallen trees and high winds.

- At least 18 homes fell into the sea on Long Island due to the pounding surf. About 200 homes along North Carolina's Outer Banks were damaged and potentially uninhabitable.

- Florida was struck by at least 27 tornadoes in at least 15 counties. Twenty-six deaths in Florida were attributed either to the tornadoes or their severe weather. A nine foot storm surge was reported in the Appalachicola area. Also, up to six inches of snow fell in the Florida panhandle.

- Three storm-related deaths were reported in Quebec, one in Ontario, and three Cuba (Havana was blacked out). A tornado left 5000 people homeless in Reynosa, Mexico (near the Texas border).

- Highest recorded wind gusts included:
  110 MPH in Franklin County, Fl
  110 MPH in Mount Washington, NH
  101 MPH on Flattop Mountain, NC
  98 MPH in South Timbalier, LA
  92 MPH in South Marsh Island, LA
  90 MPH in Myrtle Beach, SC
  89 MPH in Fire Island, NY
  83 MPH in Vero Beach, FL
  81 MPH in Boston, MA
  71 MPH in La Guardia Arpt, NY

- Snowfall totals included:
  50 inches on Mount Mitchell, NC (14-foot drifts)
  44 inches in Snowshoe, WV
  43 inches in Syracuse, NY
  35 inches in Portland, ME
  35 inches in Lincoln, NH
  30 inches in Beckley, WV
  29 inches in Page County, VA
  27 inches in Albany, NY
  25 inches in Pittsburgh, PA
  24 inches in Mountain City, GA

20 inches in Chattanooga, TN
19 inches in Asheville, NC
17 inches near Birmingham, AL (6-foot drifts)
16 inches in Roanoke, VA
13 inches in Washington, DC
9 inches in Boston, MA
4 inches in Atlanta, GA

- Record low temperatures included (some records for March):
  -5 degrees in Elkins, WV
  -4 degrees in Waynesville, NC
  1 degree in Pittsburgh, PA
  2 degrees in Asheville, NC and Birmingham, AL
  6 degrees in Knoxville, TN
  8 degrees in Greensboro, NC
  9 degrees in Beckley, WV
  11 degrees in Chattanooga, TN and Philadelphia, PA
  15 degrees in New York-JFK and Washington, DC
  17 degrees in Montgomery, AL
  18 degrees in Columbia, SC and Atlanta, GA
  19 degrees in Augusta, GA
  21 degrees in Mobile, AL
  25 degrees in Savannah, GA and Pensacola, FL
  31 degrees in Daytona Beach, FL

- Record low sea-level pressures included:
  28.38 inches in White Plains, NY
  28.43 inches in Philadelphia, PA
  28.43 inches in JFK Arpt, NY
  28.45 inches in Dover, DE
  28.51 inches in Boston, MA
  28.53 inches in Augusta, ME
  28.54 inches in Norfolk, VA
  28.54 inches in Washington, DC
  28.61 inches in Raleigh-Durham, NC
  28.64 inches in Columbia, SC
  28.73 inches in Augusta, GA
  28.74 inches in Greenville-Spartanburg, SC
  28.89 inches in Asheville, NC

- A spokesman for the National Weather Service's (NWS) special studies branch said that the volume of water that fell as snow may be unprecedented. For example, the NWS office at the Asheville, NC, airport reported a snow/water ratio of 4.2

to 1 from core samples of new snow. Numerous other core samples taken in a nearby area by an NCDC employee verified this 'very wet snow' with similar results. This equated to four to five inches of liquid equivalent precipitation (or even higher in some areas) from the storm. Areas north of Asheville which reported up to four feet of snow probably received 'dryer' snow with similar liquid amounts. Due to the weight of the heavy snow, damage to trees and buildings was extensive. Polk County, NC reported 99% of its electrical customers without power at one point during the storm.

- Preliminary damage estimates were as high as $1 billion.

- Comparisons to the Blizzard of 1888 are now being made. A few facts from the '88 storm:
  400 people killed
  50 inches of snow in Saratoga Springs, NY
  48 inches of snow in Albany, NY
  22 inches of snow in New York City
  Snow drifts over the tops of houses from New York to New England
  80 mph wind gusts common

  Although the '88 storm was probably more severe in the Northeast and New England, it did not affect the entire eastern seaboard to the extent that the 1993 storm did.

Clearly, this "White Hurricane" affected the lives of almost everybody living on the East Coast, including U.S. sailors stationed there. The track of the storm (Fig. 1) shows that the cyclone formed over the western Gulf of Mexico; at 1200 UTC 12 March 1993, it was analyzed with a sea-level pressure of 1000 mb. Initially, the storm moved to the east-northeast through the Florida panhandle, and then headed northeast along the coast. The cyclone's lowest sea-level pressure was recorded on 0000 UTC 14 March 1993 over Delaware. Just prior to this time, the storm passed over Norfolk, VA, which is the Navy's largest home port. In addition, it tracked over or near every other U.S. Naval base along the East Coast from Florida to Massachusetts. Finally, the strongest

winds associated with the system were offshore, and these winds moved through every U.S. Navy Operations Area (OPAREA) in the Western Atlantic Ocean.

In order to better understand this infamous storm, its synoptic scale and mesoscale features must be studied. As will be shown in Chapter IV, the cyclone was accompanied by unusually strong jet streaks. An analysis of kinetic energy was therefore undertaken to investigate this aspect of the storm. In addition, the generation of kinetic energy was also examined to illuminate how the jet streaks were maintained against frictional dissipation. As will be shown, this type of study can help naval meteorologists better understand and more importantly, provide better forecasts of such damaging storms to Fleet Commanders, who can then better provide for the safety of all U.S. naval personnel under their command.

With this in mind, the primary objective of this thesis is to determine, using kinetic energy concepts, how jet streaks influenced the development of this storm. In order to meet this objective, this thesis will be organized in the following manner: Chapter II will provide background information on how jet streaks interact in the development of surface cyclones. Chapter III presents a description of the forecast model used, the National Meteorological Center's Global Spectral Model, as well as how and why further postprocessing of the data was done. Chapter III also introduces VISUAL, which is a meteorological diagnostic display program developed primarily at the Naval Postgraduate School. In chapter IV, a synoptic diagnosis will be preformed, which focuses on the large-scale surface features as well as upper-level features associated with the storm including jet streaks. Chapter IV will also provide detailed comparisons of the

differences between the forecasts and the analyses. Chapter V focuses on the energetics diagnoses. Specifically, vertically integrated kinetic energy (IKE) and vertically integrated generation of kinetic energy (IGK) will be presented. The final chapter contains conclusions and recommendations for future research.

II. BACKGROUND

T.N. Carlson (1991, page 244) states explosively developing cyclones can have pressure falls of 10 to 20 mb over 12 hours, have pressure decreases from 960 to 980 mb and occasionally have hurricane force winds over a large area. The most widely quoted definition of an explosively developing cyclone is given by Sanders and Gyakum (1980). They define an explosively developing extratropical cyclone or "bomb" as an extratropical surface cyclone whose central pressure falls an average of at least one mb h^{-1} for 24 h, geostrophically adjusted to 60°N using the formula ($\sin\phi/\sin 60°$) where ϕ is the average latitude of the storm. Wash et al. (1992) used a threshold deepening rate of one mb h^{-1} for a period of 12-h using the same geostrophic adjustment to select explosive cyclones for their study using data from the First GARP Global Experiment (January-February 1979). Sanders and Gyakum (1980) found that these "bombs" were a predominantly maritime, cold-season event usually found within or ahead of the planetary-scale troughs. The storm studied in this thesis more than meets the criterion for an explosively developing cyclone, with its central pressure decrease of 32 mb from 18Z/12 Mar 93 to 18Z/13 Mar 93 and 17 mb from 06Z/13 Mar 93 to 18Z/13 Mar 93.

Note that the emphasis in the definitions above is on the tendency of the central pressure of these storms as a measure of intensification. Following Haltiner and Martin (1957, page 321), an equation for the tendency of sea-level pressure can be written as

$$\frac{\partial p_s}{\partial t} + \boldsymbol{V}_s \cdot \nabla_h p_s + w_s \frac{\partial p_s}{\partial z} = -\int_o^{p_s} \nabla_p \cdot \boldsymbol{V} dp. \qquad (2.1)$$

Recognizing that $w_s = 0$ and rearranging terms yields

$$\frac{\partial p_s}{\partial t} = -\boldsymbol{V}_s \cdot \nabla_h p_s - \int_o^{p_s} \nabla_p \cdot \boldsymbol{V} dp. \qquad (2.2)$$

For cyclonic development, the right-hand side of (2.2) must be negative. Since the first term yields positive values for the frictional inflow that characterizes cyclones, the second term in (2.2) must be negative for development to occur. Furthermore, since cyclones are associated with upward motion, there should be low-level convergence and upper-level divergence by continuity. Thus, as noted by Uccellini (1990), in order to get a negative pressure tendency at the surface and a deepening storm, upper-level divergence must dominate the integral in (2.2). Physically, upper-level divergence leads to a net reduction of mass in the column, which is needed for cyclonic development since sea-level pressure in a hydrostatic atmosphere is equal to the weight of the overlying atmosphere. So, the importance of knowing (or inferring) upper-level divergence cannot be overemphasized.

Due to the difficulty of measuring divergence aloft, these fields are often approximated by the vorticity advection field (Fig. 2B), with divergence (convergence) associated with positive (negative) vorticity advection. Thus, divergence is expected downstream of troughs and convergence upstream of troughs (Fig. 2A). Sanders and Gyakum (1980) and Sanders (1986,1987) have confirmed through climatological studies that rapid development commences as a trough and its associated region of PVA

propagate within 500 km upstream of a cyclogenetic region. The importance of vorticity is reflected in one of Sanders and Auciello's (1987) checklist questions for the prediction of explosive cyclogenesis. Specifically, they ask "Does a 500 mb absolute vorticity maximum of $17x10^{-5}$ (on NGM) or more exist in the initial analysis in an area from 30° N to 50° N and 85° W to 110° W?"

In addition to the importance of divergence/convergence (PVA/NVA) associated with trough/ridge patterns, Uccellini (1990) describes other features common to rapid cyclogenesis. One of these features is the presence of secondary circulations in the entrance/exit regions of jet streaks. The Sanders and Auciello (1987) checklist agrees with the question "Does a jet streak of 110 kts or greater exist at 250 or 300 mb within a 300 nm (550 km) radius in the semicircle south of the initial vorticity maximum?".

In order to see how secondary circulations can arise in the vicinity of jet streaks, consider the simple example of a geostrophic straight jet streak where the horizontal wind is represented primarily by the geostrophic wind. In the entrance region of the jet streak (Fig. 3), the windspeed/kinetic energy is increasing in the alongstream direction. The ageostrophic wind is therefore southerly (for a westerly jet) with the largest ageostrophic windspeed found right at the jet axis. Ageostrophic windspeed decreases both to the north and south of this ageostrophic maximum leads to convergence to the north and divergence to the south (Fig. 3A). The reverse argument is true for the exit region of a geostrophic straight jet. Windspeed/kinetic energy is decreasing in the alongstream direction which produces a northerly ageostrophic wind for a westerly jet. The maximum ageostrophic windspeed in the exit region, like the entrance region, is at the

jet axis with divergence to the north and convergence to the south (Fig. 3A). These circulation patterns, shown in Figs. 3A and 3B are consistent with the vorticity advection concepts described by Riehl et al. (1952) and depicted in Fig. 3C.

The transverse (cross-stream) ageostrophic pattern represents the upper-branch of the transverse secondary circulation. By continuity, upper-level divergence/convergence is associated with low-level convergence/divergence and upward/downward motion. The lower branch of the secondary circulation is given by ageostrophic winds which are oriented from the area of low-level divergence toward the area of low-level convergence (Fig. 3B). The circulation in the entrance region of the idealized jet streak has warm air rising and cold air sinking, and as mentioned above, is marked at jet level by a transverse ageostrophic component toward the cyclonic-shear side of the jet and toward lower isobaric heights (Fig. 3A). Thus, this thermally direct transverse circulation converts available potential energy into kinetic energy for parcels accelerating into the jet streak. Conversely, in the thermally indirect circulation of the exit region, warm (cold) air is sinking (rising), and the transverse ageostrophic component at jet level is directed toward the anticyclonic-shear side of the jet streak toward higher isobaric heights (Fig. 3A), and therefore converts kinetic energy to available potential energy for parcels decelerating out of the jet streak (Uccellini and Kocin 1987).

Unfortunately, idealized geostrophic straight jet streaks are not often found in nature. For instance, complications in the conceptualization are introduced when a jet streak is curved. Carlson (1991, page 369) notes that in situations where the jet is curved, curvature effects may be more important than shear in indicating the sign of the

vorticity advection and hence the divergence. Carlson also notes that it is surprising how little curvature is required in order for the curvature effect to be significant when the wind speed is large. When curvature becomes important, a single positive vorticity maximum is found rather than the maximum/minimum couplet as depicted in Fig. 3C, implying a two-quadrant jet streak model vice the four-quadrant model discussed above. Therefore you either have PVA or NVA in the exit region and the opposite (NVA or PVA) in the entrance region. Carlson shows that ascent may be strongest in the front-left quadrant, even in curved jet situations.

Kinetic energy per unit mass, defined as

$$k = \frac{1}{2}\,(u^2 + v^2)\,, \qquad (2.3)$$

is a logical variable to evaluate in studying a cyclone system characterized by strong jet streaks, such as the March 1993 case. In addition, the direct and indirect transverse circulations associated with the jet streaks can be sites of large energy conversion between available potential energy and kinetic energy. Consequently, the diagnostic tool used in this study is the Eulerian kinetic energy budget, which relates kinetic energy content, local kinetic energy changes, and forcing mechanisms responsible for those changes (Smith 1980), and is given by

$$\frac{\partial K}{\partial t} = \frac{\partial}{\partial t}\left(\frac{1}{g}\int_{p_u}^{p_s} k\,dp\right) = \frac{1}{g}\int_{p_u}^{p_s} [\,\boldsymbol{V}\cdot\nabla_p\phi]\,dp + \frac{1}{g}\int_{p_u}^{p_s} [\nabla_p\cdot k\boldsymbol{V}]\,dp$$
$$- \frac{1}{g}\int_{p_u}^{p_s} \left[\frac{\partial \omega k}{\partial p}\right] dp + \frac{1}{g}\int_{p_u}^{p_s} \boldsymbol{V}\cdot\boldsymbol{F}\,dp. \qquad (2.4)$$

The terms in this equation from left to right represent the following physical processes: (1) the Eulerian time rate of change of kinetic energy, (2) the mechanical generation of kinetic energy by cross-contour flow, (3) the horizontal flux divergence of kinetic energy, (4) the vertical flux divergence of kinetic energy, and (5) frictional dissipation of kinetic energy. In this study we are primarily interested in the kinetic energy content and the generation of kinetic energy, which is the primary source term in the budget equation (2.4). The horizontal and vertical flux divergence terms represent the redistribution of kinetic energy and so result in the propagation of jet streaks, which is only of secondary interest. The frictional dissipation term is typically computed as a residual, and also will not be studied here.

In order to examine spatial distributions of these quantities from (2.4), vertically integrated point values of these quantities were examined in lieu of area-averaging. The first is vertically integrated kinetic energy (IKE), which can show an integrated view of the windspeed field (kinetic energy content) through some predetermined layer, usually the surface to the top of the atmosphere. Specifically, IKE is defined as

$$\boldsymbol{IKE} = \frac{1}{g}\int_{p_u}^{p_s} k\,dp. \qquad (2.5)$$

Substituting from (2.3) yields

$$IKE = \frac{1}{2g}\int_{p_u}^{p_s} [u^2 + v^2]\, dp. \qquad (2.6)$$

which shows the relationship between IKE and windspeed.

Similarly, the vertically integrated generation of kinetic energy (IGK) is given by

$$IGK = \frac{1}{g}\int_{p_u}^{p_s} [-\mathbf{V}\cdot\nabla\phi]\, dp. \qquad (2.7)$$

Kung (1966) notes that the kinetic energy generation term reflects the production or destruction of kinetic energy by cross-contour flow. Clearly, the transverse circulations about jet streaks can have a large impact on this term. This can be seen by noting that the relationship of IGK to the ageostrophic cross-contour flow in (2.7) becomes

$$IGK = \int_{p_u}^{p_s} [-\mathbf{V}_{ag}\cdot\nabla z]\, dp, \qquad (2.8)$$

since $\phi = gz$ and $\mathbf{V}_g \bullet \nabla z = 0$. This expression gives us a means of examining the energy generation caused by secondary circulations as described above.

III. METHODOLOGY

The diagnostics presented in this thesis were computed from forecast model output as well as analyses. The model output provides greater internal consistency between variables, greater temporal consistency, and more smaller-scale detail. The analyses and diagnostics computed from them provide verification for the model output and diagnostics. This chapter describes the model used to generate the forecast series examined as well as the processing and diagnostic technique.

A. MODEL DESCRIPTION

The forecast model used in this thesis is the National Meteorological Center's (NMC) global numerical forecast model. According to Kanamitsu et al. (1991) this model, often referred to as the Global Spectral Model (GSM), is used for global data assimilation, aviation forecasts, and medium-range forecasts. The Global Data Assimilation System (GDAS) is the process by which analyses and forecasts are combined in order to provide initial conditions for worldwide aviation (72 h) and medium-range (3 - 10 days) guidance (Kanamitsu 1989). GDAS is run at 0000, 0600, 1200 and 1800 UTC with a late data cutoff to produce a 6-h forecast that is used as the first-guess field for the analysis of various numerical forecasts. The aviation forecast (AVN) is run at 0000 and 1200 UTC with a short data cutoff to produce a 72-h forecast primarily for short-range weather prediction. An AVN run was used for the data set in

this study. Finally, the medium-range forecast (MRF) is run only at 0000 UTC with a late data cutoff to produce a 10-day forecast primarily for medium-range guidance.

The initial conditions for the AVN run of the GSM are based on a GDAS first-guess followed by a spectral statistical interpolation (SSI) analysis. The goal of SSI which was implemented in June 1991 is to make the analysis as close as possible to the observations and the first-guess field (Derber et al. 1991). The first-guess field from the 6-h GDAS forecast is first interpolated to the observation points in order to calculate the differences (increments) between the observations and the first-guess field. According to Derber et al. (1991), the SSI analysis variables are closely related to the spectral coefficients used in the model. In addition, a more realistic dynamical constraint between the wind and mass fields is applied. Thus, the need for model initialization is eliminated which means the SSI is therefore used directly as the forecast model initial condition.

According to Kanamitsu (1989), the GSM is a hydrostatic primitive equation model that produces predictions of winds, temperature, surface pressure, humidity, and precipitation amount. The model uses the spectral method for its horizontal representation of variables and the Phillips (1957) sigma coordinates in the vertical. The model has 18 layers, six of which are below 850 mb to represent the boundary layer and two of which are in the stratosphere. A semi-implicit scheme is used in time differencing, resulting in relatively long time steps. Model physics includes convective precipitation following Kuo (1965,1974) and stable precipitation in regions of grid-scale saturation. The model uses the Geophysical Fluid Dynamics Laboratory (GFDL)'s

boundary layer package as well as the GFDL radiation package. Furthermore, in March 1991 a number of changes to GDAS were incorporated to improve the AVN and MRF. Kanamitsu et al. (1991) list the improvements:

- The horizontal resolution of the forecast model was increased from triangular truncation wavenumber T80 to T126, which corresponds to an equivalent increase in grid resolution from 160 km to 105 km.
- The use of enhanced orography has been discontinued and replaced by mean orography.
- A new marine-stratus parameterization was introduced.
- A new mass-conservation constraint was implemented.
- The horizontal diffusion in the medium scales was reduced by adopting the Leith formulation.

B. POST PROCESSING

NMC distributes the aviation model analyses and forecasts on a 2.5° latitude x 5.0° longitude grid at mandatory levels. The data on the NMC grid was interpolated onto a finer mesh to decrease the error in calculating derivative quantities. Specifically, a multiquadric interpolation scheme (Nuss and Titley 1994) was used to interpolate the field to a 60 x 44 point Lambert conformal grid centered at 40° N, 85° W with a horizontal grid spacing of approximately 90 km. The domain and terrain field are seen in Fig. 4. These fields were then interpolated vertically, from 1000 mb to 100 mb, in 50 mb increments.

C. VISUAL DIAGNOSTICS

Products used in this study, including synoptic charts as well as energetics quantities, were produced with VISUAL. VISUAL is a meteorological diagnostic and display program that uses GKS primitives and National Center for Atmospheric Research (NCAR) Graphics utility routines to examine meteorological grids and observations. The program was originally developed by Prof. Wendell Nuss from similar code available at NCAR during the early 1980's. The code has been extensively modified over a number of years through the efforts of Wendell Nuss, Steve Drake, Paul Hirschberg, Randy Pauley, Teddy Holt and others (VISUAL Manual 1993).

VISUAL was modified to permit the computation of IKE and IGK from equations (2.6) and (2.8). The vertical integral was approximated using the trapezoid rule, such that

$$\frac{1}{g}\int_{p_1}^{p_2} \chi \, dp = \frac{1}{g}\sum_{k=2}^{n} \frac{(\chi_k + \chi_{k-1})\,\Delta p}{2}, \qquad (3.1)$$

where χ represents the integrand in either (2.6) or (2.8). The limits of integration, p_1 and p_2, can be specified by the user. For the diagnostics presented here, the lower limit was set to 950 mb to minimize the influence of below-ground grid points at 1000 mb, and the upper limit was set to the highest level available -- 100 mb. Integrals from 950 mb to 700 mb and from 700 mb to 100 mb were also examined to investigate low-level and upper-level processes separately.

A routine to compute area average quantities was also written to yield values which can be compared with area-averages from previous studies. The area averages on a conformal grid is defined as

$$\overline{\chi} = \frac{\sum \frac{1}{m}\chi}{\sum \frac{1}{m}}, \qquad (3.2)$$

where m is the map scale factor and the summations are over all grid points.

IV. SYNOPTIC CONDITIONS

As discussed in the Introduction, the so called "storm of the century" formed over the western Gulf of Mexico off the southeastern Texas coast at 1200 UTC 12 March 1993. Figure 1 shows that the storm initially tracked east-northeast to the Florida panhandle and then moved northeast up the Eastern Seaboard. The analyzed sea-level pressure decreased slowly from 1000 mb at 1200 UTC March 1993 to 998 mb at 1800 UTC 12 March 1993. After 1800 UTC 12 March 1993 the analyzed central sea-level pressure dropped rapidly for 30-h to 960 mb by 0000 UTC 14 March 1993 (Fig. 5). After this time it began to weaken slowly. Figure 5 shows a comparison of the analyzed sea-level pressures to that of the 12 - 48 h GSM forecast initialized at 1200 UTC 12 March 1993 (abbreviated 12Z/12). The 12-h forecast shows a weaker than analyzed storm as does the 18-h forecast. Thereafter, however, the model begins to deepen the central pressure at a rate similar to that actually observed. The following chapter will provide a synoptic overview, including the upper-levels, of the storm while comparing the GSM forecasts to the analyses as well as NMC analyses when available.

A. 0000 UTC 13 MARCH 1993

The incipient frontal cyclone over the Gulf of Mexico, which has a central pressure of 989 mb on the NMC surface analysis for 00Z/13 (Fig. 6A), is the subject of this thesis. There has been no change in the central pressure over the previous three hours, but the system is becoming more organized. From Texas to North Carolina the surface

flow has become cyclonic, and the isobaric gradient has tightened due to a strong high pressure system centered over North Dakota. North-northwest winds ranging from 25 to 40 kts are observed to the west of the low center. The system has a cold front extending southward from the low center and a warm front extending to the northeast through southern Georgia. A squall line is analyzed parallel to and east of the cold front. A trough, which may be a coastal front, extends from Cape Hatteras to southern Georgia. Moderate snowfall is analyzed over Alabama and Mississippi with some heavier snow reported over southeastern Tennessee. A second low center, which is computer-generated, is analyzed at 998 mb south of the 989 mb low.

The AVN analysis valid at 00Z/13 (Fig. 7A) has the low center located over the Gulf of Mexico with a central pressure of 1001 mb. The position of the center is in excellent agreement with NMC's 998 mb computer-generated low center on the NMC analysis. The lowest computer-generated isobar around the low in the NMC analysis is at 1000 mb, but ship observations west of the low center and satellite imagery (Fig. 9) support the central pressure of 989 mb and the more northern position indicated by the analyst. In any event, this discrepancy, implies some uncertainty in the observed central pressure. In addition, the interpolation of the model output to a 2.5 degree grid may also have slightly altered the predicted central pressure, but certainly not by 12 mb. The location and the intensity of both the cold front and the warm front, inferred from the thickness packing, are in close agreement with the NMC analysis.

The GOES infrared imagery (Fig. 9) for 0001 UTC 13 March 1993 validates the storm's intensity at this time. This image exhibits the cloud pattern expected more for

a 989 mb storm and associated frontal systems than for the computer-generated 998 mb central pressure. For example, the classic comma-shape cloud pattern is beginning to form with the cold front clearly defined as well as the prefrontal squall line.

The 12-h spectral forecast (Fig. 8A), initialized at 1200 UTC 12 March (12Z/12) and valid at 0000 UTC 13 March (00Z/13), places the low center over the Gulf of Mexico with a central pressure of 1001 mb. The position of the center is in excellent agreement with the AVN analysis and with NMC's 998 mb computer-generated low center on the NMC analysis. The location and the intensity of both the cold front and the warm front on the 12-h forecast, like the AVN analysis, are in close agreement with the NMC analysis. Overall this forecast is in excellent agreement with the AVN analysis at this time, but in disagreement with the NMC analysis and the satellite image.

The NMC 500 mb analysis (Fig. 6B) shows a trough extending from Lake Superior southwest to northern Texas. A weaker trough is shown extending from Louisiana southward through the Gulf of Mexico. The axis of the latter trough is upstream of the surface low, placing the associated positive vorticity advection (PVA) over the surface low and thus favoring further development.

The 500 mb AVN analysis valid at 00Z/13 (Fig. 7B) like the NMC analysis has a trough extending from Lake Superior southwest to northern Texas, and a weaker trough extending from Louisiana southward through the Gulf of Mexico. As with the NMC analysis (Fig. 6B), PVA is over the surface low favoring development. Overall, this AVN analysis is in excellent agreement with the NMC analysis.

The 12-h 500 mb forecast valid at 00Z/13 (Fig. 8B) is also in excellent agreement with both the NMC and AVN analyses. The analyzed trough over the central United States is well predicted in this 12-h forecast although the position of the forecasted trough over the Gulf of Mexico is further east of the analyzed position and the heights up to 6 dm greater. Along the trough axis the absolute vorticity maximum associated with the Gulf of Mexico trough is forecast at $15x10^{-5}$ s^{-1} yielding PVA over the surface low. Again, this shows excellent upper-level support for further development of the surface low.

At 300 mb at this time, the NMC analysis (Fig. 6C) has a trough extending from Minnesota through Oklahoma then down along the Texas coast. A 150 kt (75 m/s) jet streak, with a 175 kt observation over Dayton, is centered over Ohio/Pennsylvania, and is oriented southwest to northeast. Based on the idealized jet streak model, it is not positioned to support further development of the surface low since its right-rear quadrant is over the southern states vice the Gulf of Mexico. Upstream of the trough axis a 130 kt (65 m/s) jet streak is centered over northwestern Texas.

The 300 mb AVN analysis valid at 00Z/13 (Fig. 7C) is in excellent agreement with the NMC analysis. The trough axis extends from Minnesota to the Texas coast like the NMC analysis (Fig. 6C). The 65 m/s (130 kt) upstream jet streak is 10 m/s (20 kt) less than the analyzed upstream jet streak on the NMC analysis, but the location over northwestern Texas is in excellent agreement. The 80 m/s (160 kt) downstream jet streak is centered over Indiana just a little west of the NMC analysis.

The 300 mb forecast valid at 00Z/13 (Fig 8C) like the NMC analysis also places 70 m/s (140 kt) jet over Ohio/Pennsylvania oriented southwest to northeast. As in the NMC and AVN analyses, its right-rear quadrant is over the southern states, therefore providing little support for the surface low. Upstream of the trough axis, both the analysis and the 12-h forecast have a northwest-to-southeast oriented 65-70 m/s (130-140 kt) jet streak centered over the Texas panhandle. It also is currently not in an ideal position to provide support to the surface low with its left-front quadrant over southeastern Texas.

B. 0600 UTC 13 MARCH 1993

Over the subsequent 6-h, the NMC surface analysis (Fig. 10A) portrays the low center as moving northeast to a position over the Florida panhandle. The system has deepened 6 mb to a central pressure of 983 mb, but the lowest computer-generated isobar is at 992 mb. The associated cold front extends from the low center to the west of southern Florida and then to the east of the Yucatan Peninsula. The strongest winds continue to be west of the low center along the coastal regions of the Gulf Coast states. Winds up to 40 kts and temperatures in the mid-30's are reported over this region. Along the eastern coast of Florida in the warm sector of the cyclone, a moderate southeasterly flow (20-30 kts) is reported ahead of the cold front with temperatures in the mid-70's, implying a strong front. The warm front has moved over the southern portion of the hypothesized coastal front along the coast from Georgia to North Carolina. As for the northern portion of the coastal trough, it extends from the warm front to the

northeast along the North Carolina coast. The extensive prefrontal squall line runs from west of Tampa to northeastern Florida. Along the eastern seaboard, a cold northerly flow dominates with the winds becoming more northeasterly and temperatures becoming warmer along the coast.

The 18-h surface forecast valid at 06Z/13 (Fig. 11A) has the low center again at 1001 mb. There is no change in central pressure from the 12-h forecast, although the pressure gradient around the low center is becoming tighter. Overall the placement of the major synoptic features and the flow pattern are in good agreement with the surface analysis, even though the intensity is off by 18 mb. The thickness pattern implies that the system cold front extends to the southwest of the low center rather than south.

The 18-h 500 mb forecast (Fig. 11B) continues to have a weak trough extending north to south through the Gulf of Mexico with PVA over the surface low center. In the 18-h 300 mb forecast (Fig. 11C), the trough axis extends north to south through the Gulf of Mexico west of the 500 mb trough axis as before. The jet streak downstream of the trough axis remains oriented southwest to northeast with a maximum wind speed of 80 m/s (160 kts). The surface low has moved under the outer edge of the right-rear quadrant of the jet streak, and as a result the jet is now in position to support further development of the surface low. On the other hand, upstream of the trough axis the jet centered over Texas has weakened, and is now at 60 m/s (120 kts). It is not in position to aid in the development of the surface low with its left-front quadrant over the western Gulf of Mexico. Overall the surface low should continue to develop with this forecasted 500 mb and 300 mb support.

C. 1200 UTC 13 MARCH 1993

The storm continues to develop and is now moving north with its center over eastern Georgia. The NMC surface analysis valid at 12Z/13 (Fig. 12A) has the central pressure down 10 mb in 6-h to 973 mb. During the past 6-h, the cold front has passed over Florida, and is positioned just off the eastern Florida coast. Winds behind the cold front are westerly at 20 to 25 kts. The warm front has replaced the coastal trough and extends northeast from the low center paralleling the coast. The pre-frontal squall line has persisted, and continues to move ahead of and parallel to the cold front. The ridge extending from Minnesota to Texas is bringing cold polar air from the north behind the system, and as a result snow is being observed as far south as central Georgia. Heavy snow associated with the warm front and local topography is observed over northwestern Virginia, West Virginia, Maryland and Pennsylvania.

The AVN analysis valid at 12Z/13 (Fig. 13A) has the low center over Charleston, SC north of the position in the NMC analysis. The central pressure of the low is 982 mb, 11 mb weaker than the NMC analysis. However, frontal positions are in excellent agreement with the NMC analysis. The thermal fields show cold air advection (CAA) extending over the Gulf of Mexico behind the cold front and warm air advection (WAA) north of the warm front. With the exception of the error in central sea-level pressure, the computer analysis is general agreement with the NMC analysis.

The GOES infra-red imagery valid at 1201 UTC 13 March 1993 (Fig. 15) shows a well organized comma-cloud pattern around the low center. The dry slot is beginning

to wrap around the low center. The pre-frontal squall line again shows up quite well as does the cold front moving through Florida.

The 24-h forecast valid at 12Z/13 (Fig. 14A) has the low center too far north over Charleston, SC deepening 9 mb to a central pressure of 992 mb -- a 19 mb error compared to the NMC manual analysis. The thermal field is beginning to show the characteristic "S" shape pattern that typifies the period of most rapid development, but not to the extent depicted in the AVN analysis (Fig. 13A). CAA is shown to the west and southwest of the low center with WAA to the northeast. Frontal positions and the overall flow pattern are in fairly good agreement with the surface analysis. The sea-level pressure of the ridge (>1036 mb) over Texas is stronger than the analysis (1034 mb), and is centered a little to the northwest over the panhandle instead of over central Texas.

The 500 mb NMC analysis valid at 12Z/13 (Fig. 12B) has the stronger longwave trough beginning to phase with the weaker trough over the Gulf of Mexico. The overall trough has a south-southeast to north-northwest orientation over the eastern Gulf of Mexico. The trough is in an excellent position for continued upper-level support of the surface low by providing PVA over the surface low. Ridging downstream of the trough has developed over the previously mentioned region of heavy snow -- likely a result of latent heating. As a result the confluent trough seen 12 h earlier has become a diffluent trough which should have stronger PVA.

The 500 mb AVN analysis valid at 12Z/13 (Fig. 13B) is in fairly good agreement with the NMC analysis except for the details of the trough over the southeastern states. The longwave trough is not as sharp as on the NMC analysis likely due to computer

postprocessing or smoothing of the data. For example, the 5280 m contour on the AVN analysis runs through central Mississippi and Alabama, whereas the same contour is further north and sharper in the NMC analysis. The ridge over the Western Atlantic which extends over the east-central states has less amplitude than the NMC analysis.

The 24-h 500 mb forecast valid at 12Z/13 (Fig. 14B) has the longwave trough in phase with the weaker trough over the Gulf of Mexico. The absolute vorticity maximum in the base of the longwave trough over central Mississippi is valued at $22x10^{-5}$ s^{-1} compared to $24x10^{-5}$ s^{-1} over southern Alabama in the AVN analysis. This yields PVA over the forecast surface low, which provides necessary support for further development, but weaker than indicated in the analysis. This forecast versus analysis PVA difference can be attributed primarily to the difference in the ridge over the Virginias. The 24-h forecast ridge has less amplitude, which leads to a weaker vorticity gradient and therefore less PVA. For example, over this region significant differences exist in both the 5280 and 5340 m contours.

The 300 mb NMC analysis valid at this time (Fig. 12C) has moved the trough axis from central Texas to the eastern Gulf of Mexico in the past 12-h. During this period, the trough has also deepened significantly, gaining more of a southeast to northwest orientation in the southern part of the trough. Downstream of the trough axis, a 160 kt (80 m/s) jet streak centered over Newfoundland dominates the eastern seaboard. A second maximum of 150 kt (75 m/s) is analyzed over Quebec. The surface low has remained downstream of the trough axis in position for further development. The upstream jet streak is centered over the Gulf of Mexico with a maximum wind speed of

over 150 kts (75 m/s). It is moving into position to provide additional support with its left-front quadrant over eastern Florida/Georgia.

Like the 500 mb AVN analysis, the 300 mb AVN analysis valid at 12Z/13 (Fig. 13C) is in good agreement with the NMC analysis except in the amplitude of the ridge over the east central states. In addition, the two primary jet streaks have some differences. For instance, the upstream jet streak is centered over the northern Gulf of Mexico with a maximum value of 65 m/s (130 kts), while the NMC analysis has the upstream jet streak in the same location but with a maximum of 150 kts (75 m/s). The downstream jet streak location is in good agreement, but has a maximum of 90 m/s (180 kts). This is 20 kts (10 m/s) greater than the NMC downstream jet streak.

The trough axis on the 24-h 300 mb forecast (Fig. 14C) is positioned further west than in the analysis, but the strength of the forecast trough is similar to that of the analyzed trough. The 80 m/s (160 kt) downstream jet streak is forecast to be centered over northern New York. As in the analysis, this jet is in excellent position to support further development of the surface low. The 60 m/s (120 kt) upstream jet has not changed in intensity over the past 6-h, and is now centered over southern Louisiana. This is in contrast to the analyzed jet streak over the Gulf of Mexico with a 150 kt (75 m/s) jet maximum. This forecast jet streak is moving into good position to provide additional support to the surface low. Therefore, this 24-h forecast supports further development of the surface low.

D. 1800 UTC 13 MARCH 1993

In the 6-h ending at 18Z/13, the NMC central pressure has dropped another 9 mb to 966 mb which represents a decrease of 23 mb in the previous 18-h. The NMC surface analysis valid at 18Z/13 (Fig. 16) places the low center just inland of the eastern North Carolina coast. The cyclonic flow about the storm dominates the entire eastern seaboard from the New England states to Key West, Florida. For the first time, NMC has analyzed an occluded front from the low center to the triple point over Cape Hatteras, North Carolina. The cold front extends from the triple point to the southeast to 30.0°N/072.5°W then to the southwest east of the Bahamas Islands. The warm front extends eastward from the triple point over the Western Atlantic. Winds over Florida are out of the west and range from 25 to 35 kts. Along the Gulf Coast, winds are out of the northwest at 20 to 25 kts, and temperatures are in the upper 30's to lower 40's. Over the New England states winds are out of the northeast with temperatures ranging from the low teens to low 20's. Snow is analyzed over the entire region north of Georgia, with heavy snow observed from West Virginia to the New England states. The ridge extending from Minnesota to Texas continues bringing in cold air to the system, and southerly flow over the Western Atlantic including the warm waters of the Gulf Stream provides warm moist air. This juxtaposition of cold polar air and warm moist tropical air plays a major role in the continued development of the surface features, including the generation of more snow along the eastern seaboard.

The 30-h forecast valid at 18Z/13 (Fig. 17A) is in excellent agreement with the analysis in positioning the low center over eastern North Carolina and in depicting

cyclonic flow from New England to Key West. This forecast has the low deepening 12 mb to 980 mb in the past 6-h and 21 mb in the past 18-h. This is an error of 14 mb at this time, though the forecast has the low deepening 12 mb when it actually deepened only 9 mb. Over the past 6-h the thermal pattern has gained a more defined "S" shape with CAA to the south and west of the low center and WAA to the north and east, and it agrees well with an occluded cyclone. The contorted thermal pattern suggests the amount of deepening that has occurred.

The 30-h 500 mb forecast (Fig. 17B) has the base of the longwave trough over Northern Alabama and Georgia with the trough axis running along western Florida. The absolute vorticity maximum in the base of the longwave trough is valued at $25x10^{-5}$ s^{-1}. This provides strong PVA over Georgia and South Carolina, but over North Carolina PVA is weak. Therefore, even with this increase in absolute vorticity, the weak PVA over North Carolina implies the storm is beginning to lose some upper-level support.

At 300 mb (Fig. 17C) the forecast has the trough axis extending through the eastern Gulf of Mexico just upstream of the 500 mb trough axis. The right-rear quadrant of the downstream jet extends only as far south as Virginia, and therefore is not forecast over the surface low. This jet streak is no longer supporting development of the surface cyclone as it continues to move northeast of the surface low center. On the other hand, the jet streak which was upstream of the trough axis at prior analysis and forecast times is at the base of the trough. This 55 m/s (110 kt) jet streak is forecast at this time to only lose 5 m/s over the next 6-h even though it is moving through the base of the trough. Ageostrophic flow at the base of the trough opposes geostrophic flow. Thus,

to lose only 5 m/s implies a strong jet streak. In its current forecast position this jet is centered over the Florida panhandle with its left-front quadrant over the Georgia and South Carolina border. The left-front quadrant continues to move closer to being in excellent position to provide added support for continued deepening of the surface low.

E. 0000 UTC 14 MARCH 1993

At 21Z/13 the low center was analyzed over eastern Virginia with a central pressure of 960 mb. The low had deepened 6 mb over the previous 3-h, but over the following 3-h remained at 960 mb according to the NMC surface analysis valid at 00Z/14 (Fig. 18A). To attain this 960 mb central pressure, the low has deepened 29 mb over 24 h, and therefore easily qualifies as a rapid deepener. At this time, the low center is over eastern Maryland as the system continues to dominate the entire eastern seaboard. In addition, the system has a well developed occlusion. The occluded front extends from the low center northeast along the coast to the triple point just offshore south of Long Island, New York. The warm front extends east-southeast from the triple point, while the cold front extends to the south. Temperatures in the low to mid 30's are observed over Georgia with snow reported as far south as northern Florida. Heavy snow still continues to be observed from West Virginia to New England.

The AVN analysis valid at 00Z/14 (Fig. 19A) is in excellent agreement with the NMC low center location over Maryland, but has the sea-level pressure analyzed at 968 mb -- an 8 mb error. Frontal positions are in excellent agreement with the NMC analysis. The thermal field shows that CAA continues over the Gulf of Mexico and now

also over the Western Atlantic behind the cold front. The overall flow pattern is in good agreement with the NMC analysis.

The GOES infrared imagery for 0001 UTC 14 March (Fig. 21) shows the system cold front over the Western Atlantic. It also shows multilayered clouds associated with the occlusion remaining over the eastern seaboard north of South Carolina. The extent of the cold air behind this system can be seen by the cellular convection implied by the medium gray shading over the Western Atlantic and the Gulf of Mexico.

The 36-h forecast valid at 00Z/14 (Fig. 20A) is in excellent agreement with the NMC analysis low center position over Maryland. The forecast has the low deepening 11 mb over 6-h from 980 mb down to 969 mb compared to the 6 mb/6-h deepening rate that was observed in the NMC analysis. This is a 9 mb error in central pressure compared to the 19 mb error on the 24-h forecast. The forecast deepening rate is 23 mb in 24-h also qualifying it as a rapid deepener. The forecast continues to show excellent agreement with the overall surface wind pattern and with the low dominating the eastern seaboard. As for the thermal pattern, it continues to agree with the analyzed occlusion and frontal position. CAA is south of the low center and has extended over the Western Atlantic southeast of the low center. WAA is north and northwest of the low center.

On the 500 mb NMC analysis valid at 00Z/14 (Fig. 18B) a closed low has formed over the Virginia/West Virginia border with a central height of 5100 m. Both wind and height observations support a closed circulation in this region. The trough axis extends from this low center south through Florida. This 500 mb low center position is upstream of the surface low, and hence indicating weak PVA over the surface cyclone center.

Unlike the NMC analysis, the 500 mb AVN analysis valid at 00Z/14 (Fig. 19B) does not have a closed low over the Virginia/West Virginia border. The AVN analysis does, however, have an area of low heights over this region. The 5160 m contour, which is closed on the NMC analysis, appears to be very close to being closed on the AVN analysis. With this exception, the two analyses are in good agreement, including the ridging over the Western Atlantic, which extends over the New England states and Canadian Maritimes. Two vorticity maxima are indicated in the trough, one just west of the surface low and the other on the Georgia/South Carolina border. The northern maxima is the stronger of the two at $24x10^{-5}$ s^{-1}, the southern has a maximum value of $22x10^{-5}$ s^{-1}.

The 36-h 500 mb forecast (Fig. 20B) also does not have a closed low, but the configuration of the 5160 m contour is very similar to that in the AVN analysis. The forecast heights over this region are in close agreement with the analysis. In contrast to the AVN analysis, the 36-h forecast has a single vorticity maximum located on the Georgia/South Carolina border at $24x10^{-5}$ s^{-1}. Weak PVA is forecast over the surface low again implies that the system is losing upper-level support.

The 300 mb trough continues to move east. According to the 300 mb NMC analysis valid at 00Z/14 (Fig. 18C), the trough axis remains oriented northwest to southeast and runs from Kentucky through Florida. The downstream jet has propagated nearly out of the display domain. The jet streak, which was upstream of the trough axis at 12Z/13, is now downstream of the trough axis with maximum winds greater than 170 kts (85 m/s). The left-front quadrant of the jet is over the surface low center. In this

position, the analyzed jet streak is in position to provide for further development of the system, but as stated earlier the analysis is showing the low starting to fill.

The 300 mb AVN analysis valid at 00Z/14 (Fig. 19C), like the NMC analysis, portrays the downstream jet streak as no longer affecting the low pressure system. This jet streak has propagated farther to the east and has a maximum windspeed of 100 m/s (200 kts). Like the NMC analysis, the jet streak, which was upstream of the trough is now downstream, with a maximum of 80 m/s (160 kts) -- 5 m/s (10 kts) slower than the NMC analysis. The location of the AVN analysis jet streak is in excellent agreement. As in the 12Z/13 300 mb AVN analysis, the trough axis is not as sharp as in the NMC analysis. Overall, though, the AVN analysis is in good agreement with the NMC analysis.

The 36-h 300 mb forecast (Fig. 20C) has the orientation and position of the trough axis in close agreement with the analysis. Again the eastern ridge is not as strong as in the analysis. The 8760 m contours are similar, but the 8640 m contours differ significantly. The east coast jet, which is greater than 60 m/s (120 kt) but significantly weaker than analyzed, does not extend as far north as in the analysis. The maximum windspeeds are located off the South Carolina coast, compared to just off Cape Hatteras in the analysis. As with the analysis, this jet was upstream of the trough axis on the 24-h forecast, but now is in position downstream of the trough axis to provide for further development of the surface low. Interestingly, although jet streak locations over the surface low on the 300 mb analysis and forecast correspond well, the observed low is filling, while the forecast low is still deepening.

F. 0600 UTC 14 MARCH 1993

By 03Z/14 the NMC analysis had the low centered over Delaware and weakening 2 mb to a central pressure of 962 mb. The NMC surface analysis valid at 06Z/14 (Fig. 22) has the low center over New Jersey remaining at 962 mb. The occluded front extends from the low center northeast to the offshore triple point just southeast of Maine. The system warm front extends to the southeast of the triple point and cold front to the south. The effects of the storm are still being felt as far south as Florida as the system continues to move northeast, with temperatures in the low 30's observed over northern Florida. The northeastern states continue to have heavy snow, as well as the southern states of Tennessee and North Carolina.

The 42-h forecast valid at 06Z/14 (Fig. 23A) has the low center over New Jersey in excellent agreement with the analysis. The overall flow pattern in the forecast is also in good agreement with the analysis, with the system dominating the entire eastern seaboard. Unlike the analysis which shows the system weakening, the forecast has the system deepening 7 mb over the previous 6-h to 962 mb. Thus, the 24- h forecast had a 19 mb error, the 36 h forecast had a 9 mb error, but the 42-h forecast has 0 mb error as a result of the excessive deepening predicted at this stage of the cyclone development. The thermal pattern remains the same as in the 36-h forecast, with CAA to the south and southeast of the low center and WAA to the north and northeast.

The 500 mb NMC analysis valid at 00Z/14 depicts a closed low, which was not present in the corresponding 36-h 500 mb forecast. However, the 42-h 500 mb forecast

valid at 06Z/14 (Fig. 23B) forms a closed low over Pennsylvania. In this position the predicted 500 mb low can still provide weak PVA over the surface low.

At 300 mb the 42-h forecast valid at 06Z/14 (Fig. 23C) has the base of the trough axis over Ohio and West Virginia with a strong indication that a closed low may form over this region. The trough axis extends through Virginia and North Carolina. The jet streak downstream of the base of this trough is greater than 70 m/s (140 kt), and is still in good position for further development of the surface low with its left-front quadrant over the surface low. As with the 36-h forecast, the observed storm is filling, but the predicted storm is still deepening.

G. 1200 UTC 14 MARCH 1993

At 09Z/14, NMC analyzes the low center over New York again at 962 mb. The NMC surface analysis valid at 12Z/14 (Fig. 24A) has the low moving to the northeast, centered over New England and at a central pressure of 966 mb. The occlusion extends from the low center northeast along the coast to the triple point over Nova Scotia. Northwest winds dominate the eastern seaboard as the system moves further north. The ridge extending from Minnesota to Louisiana continues to funnel cold polar air southeastward. Temperatures over central Florida are observed in the high twenties to low thirties. The northeastern states continue to have heavy snowfall as the system brings in moisture from the warm waters of the Western Atlantic.

The AVN generated analysis valid at 12Z/14 (Fig. 25A) has the low center at 967 mb and, like the NMC analysis, located over New England. The sea-level pressure error

which was 11 mb at 12Z/13 and 8 mb at 00Z/14 is now one mb likely reflecting the influence of the first-guess field on this analysis. The frontal positions are in excellent agreement with the NMC analysis as CAA continues over the Western Atlantic behind the cold front. Note the troughing in the sea-level pressure analysis over Nova Scotia, indicating the location of the occluded front.

GOES infrared imagery valid for 1201 UTC 14 March (Fig. 27) shows the cold front well off the coast. Cellular convection in the cold polar air being advected over the warmer waters of the Gulf of Mexico and Gulf Stream is seen as medium gray areas. Multilayered clouds are still seen over northern Virginia and also to the north and northeast.

The 48-h surface forecast valid at 12Z/14 (Fig 26A) indicates that the system deepened another 2 mb over the past 6-h to a central pressure of 960 mb, now 6 mb stronger than observed. The overall wind pattern and position of the low center again are in excellent agreement with both the NMC and AVN analyses. The thermal pattern remains the same as in the 42-h forecast. CAA is beginning to extend to the east of the low center, and WAA extends to the west. This thermal advection pattern suggests the system should begin to weaken.

The 500 mb NMC analysis valid at 12Z/14 (Fig. 24B) has the closed low deepening 170 m over 12-h and moving northeast of the surface low center. The trough axis extends to the south-southeast over the surface low. Although the closed low deepens, the system is becoming vertically stacked and therefore is losing upper-level 500 mb support.

As at 00Z/14, the 500 mb AVN analysis valid at 12Z/14 (Fig. 25B) does not have a closed low, but does have a broad area of low heights. The 5040 m contour in the vicinity of the closed low on the NMC analysis is located similarly on the AVN analysis. In general, aside from the closed low, the AVN is in good agreement with the NMC analysis.

In contrast, the 48-h 500 mb forecast valid at 12Z/14 (Fig. 26B) shows a deeper closed low than in the NMC analysis. Over the previous 12-h this forecast low has deepened 240 m. The forecast also has the trough axis extending to the south over the surface low. The vorticity pattern shows neutral vorticity advection beginning to move over the surface low. Therefore, as with the analysis, the forecast does not support further development of the surface low.

At 300 mb, the NMC analyzed pattern (Fig. 24C) has moved slowly to the east. The trough axis remains oriented northwest to southeast and extends just off the Florida coast. The 190 kt (95 m/s) jet streak off the east coast is rapidly moving north, with its left-front quadrant no longer over the surface low. This again argues against further development of the system.

The 300 mb AVN analysis valid at 12Z/14 (Fig. 25C) has a jet maximum of 80 m/s (160 kts) compared to the 190 kts (95 m/s) jet maximum in the analysis. This 190 kt (95 m/s) maximum is east of Virginia and further south than AVN analyzed 80 m/s (160 kt) jet maximum which is east of Long Island, NY. However, the 75 m/s (150 kt) isotach in the AVN analysis is in good agreement with the 150 kt (75 m/s) isotach in the NMC analysis, especially at its northern end.

The 48-h 300 mb forecast valid at 12Z/14 (Fig. 26.C) is generally in good agreement with the AVN analysis, but places the 75 m/s (150 kt) jet maximum off Cape Hatteras, NC -- much farther south than in the AVN analyses. The forecast jet is strengthening, though not as much as the observed, and is no longer in position to provide the necessary support for continued development of the surface low.

In summary, the 12-14 March storm was a significant weather event that severely hampered naval operations along the east coast. A notable feature of the storm was the presence of two strong jet streaks. How the evolution of these jet streaks may have influenced the cyclone system is addressed in the next section by evaluating terms in the kinetic energy budget equation. As demonstrated in this section, the success of the AVN analysis and forecasts in capturing details of the development of the storm make them a viable data set from which to base these calculations.

V. RESULTS

A. INTEGRATED KINETIC ENERGY (IKE)

Three different views of IKE will be presented in this section. The first view will be an integration over the whole atmospheric column (WA) from 950 to 100 mb levels. Similarly, UA will be a integration over the upper atmosphere from 700 to 100 mb. Finally, LA will be an integration over the lower atmosphere from 950 to 700 mb. The 950 mb level was chosen as the lower limit of integration because it was close to ground level but not below it. The 100 mb level was chosen as the upper limit of integration both by convention and because it was the highest data level available. Finally, the 700 mb level was chosen as the level dividing the LA and UA subintegrals; it is the mandatory level which best separates the closed circulations at low-levels from the open-wave features aloft.

These three views of IKE will enable us to examine the upper-level IKE and lower-level IKE separately, as well as to determine how much the LA IKE contributes to the WA IKE. Overall, we should expect to see the locations of upper-level jet streaks, which are the dominant features in the wind field, reflected in UA IKE maps as maxima. Similarly, the WA IKE maxima should be representative of upper-level jet streaks and so should be similar in location and strength to the UA IKE maxima for the same times. It will be of interest to examine how much the LA IKE, which will be representative of the strong low-level winds in the vicinity of the surface cyclone, contributes to WA IKE.

Unless otherwise noted, the IKE values described in this section are from the AVN model forecast.

1. 0000 UTC 13 MARCH 1993

The WA IKE for the 12-h forecast verifying at 00Z/13, depicted in Fig. 28A, closely resembles the 300 mb isotachs for the same time (Fig. 8C). Two main IKE maxima are indicated, one upstream (maximum 70×10^5 J m^{-2}) and one downstream (maximum 85×10^5 J m^{-2}) of the trough axis. These maxima are associated with the two main 300 mb jet streaks previously discussed. The upstream WA IKE maximum is centered exactly on the center of the 300 mb upstream jet streak (Fig. 8C). However, the downstream IKE maximum is not centered on the 300 mb downstream jet streak, but rather on the exit region of the jet. There is a 200 mb jet streak maximum (55 m/s, not shown) over this region shifting the IKE maximum. The axis of minimum WA IKE extends from Minnesota to eastern Texas and closely corresponds to the 300 mb trough axis at this time.

The UA IKE (Fig. 28C) is very similar to the WA in both magnitude and pattern. The UA maxima upstream and downstream of the main trough are in the same locations and have nearly the same magnitudes (70×10^5 J m^{-2} and 85×10^5 J m^{-2}, respectively). Conversely, the LA IKE, depicted in Fig. 28B, is weak throughout the entire domain with values less than 10×10^5 J m^{-2}. The largest values are in the northeastern corner of the domain where a strong surface cyclone is located (Fig. 8A). In addition, a weak double maximum (4×10^5 J m^{-2}) is located over the Gulf of Mexico essentially straddling the position of the surface low center that is the subject of this thesis.

Like the forecast IKE, the WA IKE computed from the AVN analysis (Fig. 29A) resembles the 300 mb isotachs for the same time (Fig. 7C) in the vicinity of the upstream maximum. The maximum analyzed WA IKE is $65x10^5$ J m^{-2} compared to a forecast maximum of $70x10^5$ J m^{-2}, but both centers are located in northeastern New Mexico. Downstream, there are two maxima in the analyzed WA IKE. One is located over the 300 mb jet streak with a maximum value of $85x10^5$ J m^{-2}, and the other is just located downstream over a 200 mb streak (not shown) as in the corresponding forecast, but with a maximum value of $95x10^5$ J m^{-2} compared to $85x10^5$ J m^{-2} in the forecast. Large differences between the analyzed and forecast WA IKE exist over southern Ohio as a result. Lower values of analyzed WA IKE compared to the forecast are also present along the 300 trough line.

The analyzed UA IKE (Fig. 29C) field is quite similar to the analyzed WA IKE field, reflecting the small values present in the LA IKE field. The analyzed LA IKE (Fig. 29B) is in good agreement with the forecast LA IKE for the same time. A similar double maximum is present over the Gulf of Mexico, with larger values in the analysis.

2. 0600 UTC 13 MARCH 1993

The forecast upstream IKE maximum for both the WA and UA is $65x10^5$ J m^{-2} at 06Z/13 (Figs. 30A and 30C), both having moved southeast, and weakened over the past 6-h. This corresponds well to the 300 mb jet streak (Fig. 11C), movement, and weakening trend through the same time period. The downstream IKE maximum for both the WA and UA moves east ahead of the 300 mb jet streak and strengthens to $85x10^5$ J m^{-20}. This IKE strengthening is a direct result of the intensification of both the 300 mb

downstream jet streak (Fig. 11C) as well as the 200 mb downstream jet streak (not shown). In addition, mid-level flow, 600 to 400 mb (not shown), increases over this region.

As at the previous map time, the axis of minimum WA and UA IKE over the Mississippi Valley reflects the 300 mb trough axis. Even with both the upstream 300 mb jet streak and WA and UA IKE maxima weakening, the forecast LA IKE maximum (Fig. 30B) over this region increases slightly to $6x10^5$ J m^{-2} associated with an increase in lower tropospheric winds (1000 to 850 mb) west of the developing surface cyclone. A second increasing weak maximum ($7x10^5$ J m^{-2}) over southern Florida remains southeast of the surface low. The winds at 850 mb (not shown) are the strongest component in the LA IKE in this region. This area contributes to a weak WA IKE maximum ($52x10^5$ J m^{-2}), as depicted in Figs. 30A and 30C. In addition, a weak 300 mb jet streak (Fig. 11C) over this region also contributes to the maximum IKE aloft as seen in the $45x10^5$ J m^{-2} UA IKE maximum (Fig. 30C).

3. 1200 UTC 13 MARCH 1993

At 12Z/13, the forecast WA IKE upstream maximum (Fig. 31A) is $70x10^5$ J m^{-2}. It continues to move southeast and has increased $5x10^5$ J m^{-2} over the past 6-h although the upstream UA maximum (Fig. 31C) remains at $65x10^5$ J m^{-2}. The location of the WA and UA upstream IKE maxima continues to be over the largest winds associated with the 300 mb upstream jet streak (Fig. 14C). However, a new WA maximum of $95x10^5$ J m^{-2} appears downstream of the 300 mb trough. This maximum also appears in the UA IKE field at $90x10^5$ J m^{-2}. The location of this maximum lines up well with the downstream

jet streak maximum at 300 mb. From Minnesota through Illinois and into western Tennessee, the axis of minimum WA and UA IKE matches the 300 mb (Fig. 14C) trough axis, but south of western Tennessee the IKE minimums extend southeastward to the Florida panhandle. On the 300 mb chart (Fig. 14C) valid at this time, the southeast curvature of the 300 mb trough axis is hard to ascertain, but the 300 mb NMC analysis (Fig. 12C) for this time clearly shows the trough axis with a southeastward bend toward the Florida panhandle. The eastward movement of the trough axis is also reflected in the axis of minimum WA and UA IKE moving eastward. Clearly the axis of minimum WA and UA IKE provides an accurate estimate of the location and movement of the 300 mb trough axis.

Two weak maxima continue to be present in the forecast LA IKE field (Fig. 31B). The western maximum of $8x10^5$ J m^{-2} is now under the upstream UA maximum and appears to be separating from the surface cyclone to the east. This maximum is representative of strong northerly winds in the lower troposphere (1000 - 850 mb; not shown) ahead of the surface ridge. Conversely, the eastern LA maximum of $12x10^5$ J m^{-2} is under a UA relative minimum. This LA maximum represents the stronger low level (1000 - 700 mb) winds associated with surface cyclone. In addition, it should be noted that at this time a broad region of minimum LA IKE over the southeastern states and west of the eastern LA maximum has formed.

In the AVN analysis, the location of the WA IKE maxima (Fig. 32A) reflects the location of the analyzed jet streaks for this time (Fig 13C). The upstream maximum is over the northern Gulf of Mexico at $95x10^5$ J m-2, further southeast than the forecast

WA IKE upstream maximum and $25x10^5$ J m^{-2} stronger. This reflects the difference in the forecast upstream jet streak, which had a maximum of 60 m/s (120 kt), and the analyzed upstream jet streak, which had a maximum of 65 m/s (130 kt). The UA IKE maximum of $85x10^5$ J m^{-2} (Fig. 32C) is located over the same region and as expected, is much stronger than in the forecast.

A second IKE maximum offshore of the Georgia/Florida border is seen in the WA and UA fields at $95x10^5$ J m^{-2} and $75x10^5$ J m^{-2}, respectively. This area is located where a 55 m/s (110 kt) jet maximum is analyzed (Fig. 13C). It should be noted though, that a 300 mb jet streak was not in the model forecasts over this region for this time. This forecast error yields large differences between the analyzed and forecast IKE over this area. A $20x10^5$ J m^{-2} maximum associated with the surface cyclone is evident in the analyzed LA IKE (Fig. 32B). This maximum is greater than the forecast LA IKE by $6x10^5$ J m^{-2} for the same time, and shows a much greater increase over the previous 6-h than the forecast. Similar to the forecast but more defined, a region of LA IKE minimum has formed over Georgia.

The analyzed downstream IKE maximum in both the WA and UA fields is centered over Maine and the Canadian Maritimes. The maximum values for both are $115x10^5$ J m^{-2}. The location of the corresponding forecast WA and UA IKE maxima is approximately 5 degrees farther west, and weaker in strength at $95x10^5$ J m^{-2} for the WA and $90x10^5$ J m^{-2} for the UA. Again, the locations and strengths of analyzed IKE maxima are reflections of the analyzed jet streaks. The axis of minimum IKE in the analysis also closely corresponds to the analyzed 300 mb trough pattern.

4. 1800 UTC 13 MARCH 1993

The forecast upstream WA IKE maximum (Fig. 33A) valid at 18Z/13 strengthened by more than $10x10^5$ J m^{-2} over the past 6-h as did the upstream UA maximum (Fig. 33C), in spite of a weakening of the 300 mb upstream jet streak (Fig. 17C). However, winds at low-levels (1000 - 700 mb; not shown) have increased over this region, as can be seen in the LA IKE (Fig. 33B). The downstream IKE maximum is located over the Canadian Maritimes at this time, having moved northeast and strengthened to $110x10^5$ J m^{-2} in the WA and $105x10^5$ J m^{-2} in the UA fields. This is in good agreement with the 300 mb jet streak also centered over the Canadian Maritimes.

The LA IKE maximum located to the southeast of the surface low over the past 18-h has moved to the east of the surface low, east of Cape Hatteras, and strengthened to $20x10^5$ J m^{-2} (Fig. 33B). This strengthening of LA IKE is attributed to the strengthening low-level circulation (1000 - 700 mb) and is in the vicinity of the cold front off the coast of Virginia and Cape Hatteras. This low-level maximum is reflected in a WA maximum of $85x10^5$ J m^{-2} at this time east-northeast of the low center. On the UA map, Fig. 33C, this maximum is not shown, confirming its low-level source. Also, west of the LA IKE maximum, the IKE minimum is more defined and is centered over western Virginia/North Carolina border. A secondary LA maximum remains under the UA maximum now south of the Florida panhandle.

5. 0000 UTC 14 MARCH 1993

The primary IKE maximum in both the WA and UA forecast fields that were upstream of the 300 trough at 18Z/13, propagated around the trough axis and

strengthened considerably over the next 6-h. By 00Z/14, the location of these maxima on both the WA and UA maps (Figs. 34A and 34C) is south of the surface low, with values of $105x10^5$ J m^{-2} and $90x10^5$ J m^{-2}, respectively. This IKE maximum is in the same location as the 300 mb 65 m/s (130 kt) jet streak (Fig. 20C), which also strengthened and propagated around the trough axis during the last 6-h. The downstream IKE maximum is moved east and strengthened, and is located offshore and east of the Canadian Maritimes at $120x10^5$ J m^{-2}. Although the axis of minimum IKE for both WA and UA correspond well to the 300 mb trough axis from Lake Superior through eastern Kentucky, the IKE maximum itself is nearly on the trough line. East of the surface low and located offshore (Fig. 34B) is a $24x10^5$ J m^{-2} LA maximum. This LA maximum strengthened over the past 6-h, as did the surface cyclone and the low-level winds. In addition, the LA IKE minimum persists west of this LA maximum centered over northern Virginia. The secondary LA maximum southwest of the low 6-h ago is less apparent.

The analyzed WA, UA and LA IKE maxima for this time (Fig. 35) have nearly the same locations as the forecasted IKE described above, although the analyzed strengths are much greater than the forecasted IKEs. The WA and UA maxima just of Cape Hatteras are $160x10^5$ J m^{-2} and $135x10^5$ J m^{-2}, respectively, compared to $105x10^5$ J m^{-2} and $90x10^5$ J m^{-2} in the forecast. There is a position difference in the UA maximum, with the analyzed maximum roughly 500 km northeast of the forecast maximum. The downstream WA and UA maxima is offshore and east of the Canadian Maritimes like the forecast, but has a value of $160x10^5$ J m^{-2}. Also, as in the forecast, the UA IKE

maximum is representative of the 300 mb jet streak over this region both in location and in strength. The analyzed LA maximum is $30x10^5$ J m^{-2} and has strengthened, reflecting the continued increase in winds at low levels east of the storm center. The analyzed LA minimum is positioned over northern Virginia like the forecast LA minimum.

6. 0600 UTC 14 MARCH 1993

Over the next 6-h, the 300 mb jet streak located southeast of the surface low as discussed in Chapter IV strengthened with maximum winds of 75 m/s (150 kts) in the 06Z/14 forecast (Fig. 23C), and has continued to move north-northeast. This jet streak is reflected in a stronger IKE maximum for both the WA and UA at $140x10^5$ J m^{-2} and $115x10^5$ J m^{-2} respectively (Figs. 36A and 36C), which has also moved north-northeast. The downstream maximum east of the Canadian Maritimes is out of the domain at this time. The LA maximum (Fig. 36B) remained east of the surface low and has increased $4x10^5$ J m^{-2} over the past 6 h to $28x10^5$ J m^{-2}, reflecting the strengthening of the forecast surface low surface and low-level winds east of the low center. The LA minimum is still west of the LA maximum centered over eastern Pennsylvania.

7. 1200 UTC 14 MARCH 1993

As at 06Z/14, the forecast WA and UA IKE maxima (Figs. 37A and 37C) are east of the surface low. However, the IKE maximum is at the north end of the 300 mb jet streak, reflecting the contribution of other levels. Both maxima have increased by $10x10^5$ J m^{-2} to $150x10^5$ J m^{-2} for the WA, and $125x10^5$ J m^{-2} for the UA. Again, this is expected since the 300 mb jet streak has also increased. The LA IKE maximum (Fig.

37B) has increased slightly to $26x10^5$ J m^{-2}. At this time, the forecast has the surface low at its lowest central pressure. The LA minimum moves north and is centered over eastern New York.

As at earlier times, the analyzed IKE maxima are stronger than the forecast. The WA IKE (Fig. 38A) maximum is $180x10^5$ J m^{-2}, having increased $20x10^5$ J m^{-2} over the past 12 h. At the same time, the UA IKE (Fig. 38C) maximum is $150x10^5$ J m^{-2}, having increased $15x10^5$ J m^{-2} over the past 12 h. Unlike the WA IKE forecast maximum, the analyzed IKE maximum location agrees with the analyzed 300 mb jet streak (Fig. 25C). Similar to the forecast, the analyzed LA IKE maximum is east of the surface low at $28x10^5$ J m^{-2}, but unlike the forecast, it has weakened $2x10^5$ J m^{-2} over the past 12-h. Since the analyzed surface low has filled over the past 12-h and the associated low-level winds offshore have also weakened, a weakening in the analyzed LA IKE is to be expected. The LA minimum moves north-northeast and is centered over the New England states further to the northeast than the forecast.

B. INTEGRATED GENERATION OF KINETIC ENERGY (IGK)

As detailed in the previous section, IKE values associated with the upstream 300 mb jet streak and with the surface cyclone more than doubled between 00Z/13 and 12Z/14. In this section, we examine the processes responsible for this impressive increase in IKE, by evaluating IGK, the primary source term in the kinetic energy budget.

As with IKE, three different views of IGK will be presented: 1) WA - whole atmosphere - representing the 950 to 100 mb layer, 2) UA - upper atmosphere - representing the 700 to 100 mb layer, and 3) LA - lower atmosphere - representing the 950 to 700 mb layer. These three formulations of IGK will enable us to evaluate upper- and lower-level IGK as well as how much each contributes to the WA IGK. Recall, that IGK measures the strength of changes in windspeed associated with cross-contour flow on an isobaric surface. Positive (negative) values are present in geographic locations where generation (destruction) of kinetic energy exist. Since IGK is related to cross-contour flow, large values are expected in the lower troposphere where friction is important and in the entrance and exit regions of upper-level jet streaks where transverse ageostrophic circulations are present. Typically, in the entrance region, ageostrophic winds are oriented toward lower heights which creates positive IGK values and acceleration of the flow. This results in the generation of kinetic energy. In the exit region, ageostrophic winds are oriented toward higher heights which produces negative IGK values and deceleration of the flow. This results in destruction of kinetic energy. In the vicinity of a low pressure center near the ground where friction is important, we should expect to find positive values of IGK since ageostrophic frictional winds around a low are oriented toward the low center -- positive IGK.

In order to assist in the discussion of the IGK diagnoses, 300 mb and 850 mb ageostrophic winds will be plotted on the UA and LA IGK analysis, respectively. Finally, unless otherwise noted, the IGK values described in this section are from the AVN model forecast.

1. 0000 UTC 13 March 1993

In the WA and UA there are two main areas of IGK at this time. Centered over Texas, there is a large negative maximum of IGK, which for the WA (Fig. 39A) is -200 W m^{-2} and for the UA (Fig. 39C) is -250 W m^{-2}. Figure 41C shows that the exit region of the upstream 300 mb jet streak is over Texas as well. Figure 41B shows that this region exhibits a large amount of 300 mb cross-contour flow towards higher heights and thus negative IGK. A difference between the WA and the UA IGK associated with the exit region of this upstream jet streak can be seen over central Texas where there is a broad area of positive IGK (30 W m^{-2}, Fig. 39B). The reason behind this difference can be found in Fig. 41A which shows that the ageostrophic wind at 850 mb moves across the contours from higher heights over Texas towards lower heights over the Gulf of Mexico. This would be expected for the lower branch of a transverse circulation. There is a large positive region of IKE over this same region of negative IGK indicating a weakening trend of the upstream jet streak.

The other main region of WA and UA IGK is a large positive area centered over Mississippi. The IGK maxima are 300 W m^{-2} and 250 W m^{-2} for the WA and UA, respectively. This large positive IGK area is associated with the entrance region of the downstream jet streak (Fig. 41C), a region of expected positive IGK. Figure 41B shows 300 mb cross-contour flow towards lower heights over this area of positive IGK. Also, there are large positive values of IKE over this region indicating a strengthening trend of the downstream jet streak. Significantly, this diagnostic shows that the exit region of

the upstream jet streak and the entrance region of the downstream jet streak are the two energetically active regions at this time.

Using the AVN analysis, the IGK fields (Fig. 40) are similar to the forecast IGK fields (Fig. 39). The area of negative IGK upstream is in excellent agreement with the forecast. Both the WA and UA IGK (Figs. 40A and 40C) have negative maxima of -200 W m^{-2}. The analyzed LA IGK has a weak positive maximum of 40 W m^{-2} over the southeastern Texas coast, stronger and farther southeast compared to the forecast. As in the forecast, there is a large region of positive IGK for both the WA and UA (Figs. 40A and 40C), but this region is centered over western Tennessee vice Mississippi. The analyzed IGK maximum is 400 W m^{-2} for both the WA and UA, greater than the forecast IGK maximum. As in the forecast, comparison of the analysis IGK values with IKE maxima shows a weakening trend for the upstream jet streak whereas the downstream jet streak shows a strengthening trend.

2. 0600 UTC 13 MARCH 1993

By 06Z/13, the area of large negative WA and UA IGK which was centered over central Texas at 00Z/13 had moved east, and is now centered over eastern Texas (Figs. 42A and 42C). The exit region of the upstream jet streak has also moved eastward (Fig. 43C) at this time. The strength of this IGK negative maximum has weakened region by 50 W m^{-2} for both the WA and UA to -150 W m^{-2} and -200 W m^{-2}, respectively. The upstream 300 mb jet streak is also weakening, as discussed earlier. As before, Fig. 43B portrays ageostrophic cross-contour flow towards higher heights in this region. Positive LA IGK values (Fig. 42B) to the west and southeast of the surface low are verified in

Fig. 43A, which show, 850 mb cross-contour flow towards the low center. Like 00Z/13, comparison with WA and UA IKE maxima indicates a weakening trend of the upstream jet streak since large positive IKE values exist over the upstream negative IGK region discussed above and a strengthening trend of the downstream jet streak due to large positive IKE over the downstream positive IGK region.

The large region of positive WA and UA IGK, which was over Mississippi at 00Z/13 has moved northeast as has the entrance region of the 300 mb downstream jet streak. This positive IGK region for both WA and UA is now centered over eastern Tennessee (Figs. 42A and 42C) at 300 W m^{-2}. Again, Fig. 43B shows ageostrophic cross-contour flow towards lower heights over this region at 300 mb. This large area of positive IGK shows that the entrance region of the downstream jet streak is important. Specifically, it is the right-rear quadrant of the entrance region of this jet streak that maybe affecting the surface low at this time.

3. 1200 UTC 13 MARCH 1993

The area of negative forecast IGK associated with the upstream jet streak is weakening in both the WA and UA at this time (Figs. 44A and 44C). The 300 mb upstream jet streak (Fig. 46C) is also weakening as it propagates toward the 300 mb trough axis. The IGK negative maximum for both the WA and UA is -100 W m^{-2}. The large positive region of IGK continues to move northeast and is now centered over western Pennsylvania (Fig. 44A and 44C). The downstream jet streak is also propagating northeast at this time and its entrance region is over the region of large positive IGK. The maximum values of IGK for WA and UA are 300 W m^{-2} and 250 W

m^{-2}, respectively. Figure 46B shows the cross-contour flow at 300 mb that verifies the location of both the negative and positive IGK regions. Again, the region of the jet streak most energetically active, maybe the most influential in the development of the surface low. Like previous times (00Z/13, 06Z/13), IKE maximums compared with IGK regions discussed above show a weakening trend associated with the upstream jet streak and a strengthening trend associated with the downstream jet streak.

In the LA (Fig. 44B), there are positive values of IGK around the surface low with the largest values offshore over the Western Atlantic. This is verified by the significant amount of ageostrophic flow towards the low center and perpendicular to the 850 mb contours (Fig. 46A).

The IGK values produced from the AVN analysis (Fig. 45) has IGK maxima that are similar to the forecast locations, but stronger in intensity. For instance, the region of large positive IGK centered over western Pennsylvania on the forecast is centered over northeastern Ohio at 350 W m^{-2} for WA (Fig. 45A) and 300 W m^{-2} for the UA (Fig. 45C). The negative values over the exit region of the downstream jet streak are smaller than -50 W m^{-2} for the WA and approximately -50 W m^{-2} for the UA, in a very small region over the southern tip of Mississippi. The analyzed exit region of the downstream jet streak was therefore not as active as the forecast. The analyzed LA (Fig. 45B) has positive IGK around the surface low with larger positive values over the Western Atlantic at 90 W m^{-2}. Again the analyzed fields produced larger IGK values over the Western Atlantic in the LA than the forecast. A comparison of the analyzed IKE to analyzed IGK

fields at this time result in the same conclusions as the forecast comparison discussed above.

4. 1800 UTC 13 MARCH 1993

By 18Z/13, the surface low began to lose support from the downstream jet streak as it rapidly moved eastward, but gained support from the upstream jet streak as it propagated around the trough axis. The downstream jet streak continued to have a very energetically active entrance region. The WA and UA IGK (Figs. 47A and 47C) show this area continued to move northeastward, and was now centered over Lake Erie at 300 W m^{-2} for each field. Large positive values of IKE over this region suggest a continued strengthening trend of this downstream jet streak. Figure 48C shows the upstream jet streak to be centered over the Florida panhandle, but not reflected very well in the WA and UA IGK (Figs. 47A and 47C) at this time. The LA IGK (Fig. 47B) continues to show positive values around the surface low with the maximum positive values over the Western Atlantic. The 850 mb ageostrophic winds (Fig. 48A) show strong cross-contour flow in this region.

5. 0000 UTC 14 MARCH 1993

The positive IGK maximum that was over Lake Erie at 18Z/13 has moved northeast over Canada, and remains at 300 W m^{-2} for both WA and UA (Figs. 49A and 49C). Large positive IKE values over this region indicates a continued strengthening trend of the jet streak associated in this region. The main jet streak feature (Fig. 51C) at this time is the 65 m/s (130 kt) isotach maximum, which is near the base of the 300

mb trough centered off the South Carolina coast. There is a small region of negative WA IGK at -50 W m^{-2} and a somewhat larger negative UA IGK region at -100 W m^{-2} over Virginia and North Carolina. This region of negative IGK marks the exit region of the 300 mb jet streak shown in Fig. 51C with ageostrophic winds shown in Fig. 51B. A large region of positive IGK associated with the entrance region of this jet streak southeast of Charleston, SC is shown for the WA and UA at 200 W m^{-2}. This suggests that the entrance regions are most active at this time, although the exit region of the upstream jet streak is becoming more active. The IKE results (Fig. 34), for this time, compared with IGK values suggest weakening of the exit region and a strengthening of the entrance region of the upstream jet streak. The LA IGK (Fig. 49B) continues to show large positive values around the surface low with the largest offshore values up to 110 W m^{-2}. Again, the 850 mb ageostrophic winds (Fig. 51A) show the cross-contour flow in this region.

The analyzed IGK for this time has a positive maximum over Canada like the forecast, but weaker at 200 W m^{-2} for both WA and UA (Figs. 50A and 50C). The most noteworthy discrepancy between the analyzed and forecast IGK is the large analyzed IGK negative maximum east of Virginia Beach at -400 W m^{-2} for the WA and -450 W m^{-2} for the UA. This is further east and much more stronger than the forecast IGK, indicating that the exit region of this jet streak is more active than in the forecast. The maximum positive IGK is southeast of Cape Hatteras, at 350 W m^{-2} for the WA and 200 W m^{-2} for the UA. The LA IGK is substantial in this region, with values approaching 150 W m^{-2}.

Analyzed IKE results (Fig. 35) compared with the IGK analyzed values result in the same conclusions as the forecast comparison discussed above.

6. 0600 UTC 14 MARCH 1993

The Western Atlantic jet streak (Fig. 53C) is strengthening at this time as are its transverse circulations. The negative IGK region associated with the exit region of this jet has increased in value to -250 W m^{-2} for both WA and UA (Figs. 52A and 52C). Positive IKE values over this region (Fig. 36) would suggest that this exit region is showing a weakening trend. The positive IGK region associated with the jet entrance region has also increased to 400 W m^{-2} for both WA and UA. Large positive IKE values over this region of positive IGK indicate strengthening of the entrance region. The LA (Fig. 52B) continues to show positive IGK around the surface low with the largest positive IGK offshore at 110 W m^{-2}. The 850 mb and 300 mb ageostrophic flow verifies the cross-contour flow over the regions discussed above (Fig. 53A and 53B).

7. 1200 UTC 14 MARCH 1993

Between 06Z/14 and 12Z/14, the Western Atlantic 300 mb jet streak (Fig. 56C) moved northeast and strengthened over the period as did the WA and UA IGK maxima (Figs. 54A and 54C). By 12Z/14, the large negative region associated with the exit region of this jet streak is centered over Maine and has maintained its strength over the past 6-h at -250 W m^{-2} for both WA and UA. The large positive region associated with the entrance region also has moved northeast and has weakened over the past 6-h to 250 W m^{-2}. The LA IGK (Fig. 54B) continues to have positive values around the surface low

with the largest IGK offshore. Again, the 850 mb and 300 mb ageostrophic winds (Fig. 56A and 56B) verify the locations of the maxima IGK. As in previous times (00Z/14, 06Z/14), the comparison of the IGK to IKE values for this time, shows a weakening trend of the exit region and a strengthening trend of the entrance region of the primary jet streak over the Western Atlantic.

The AVN analysis (Fig. 55) places the negative IGK associated with the Western Atlantic jet streak (Fig. 56C) further east over the Canadian Maritimes at -300 W m^{-2} for both WA and UA (Figs. 55A and 55C). The positive IGK associated with the entrance region has weakened and has become more disorganized. The analyzed LA IGK (Fig. 55B) continues to be similar to the forecast, but stronger offshore. Once more, similar conclusions as are ascertained by comparing the analyzed IKE to analyzed IGK fields.

VI. CONCLUSIONS

A. DISCUSSION AND CONCLUSIONS

This study examined the structure, evolution and effects of jet features during the 12-14 March 1993 extratropical "white hurricane" cyclone. A two-fold approach was taken to investigate the jet streaks associated with the development of the storm, using the aviation run (AVN) of the Global Spectral Model (GSM) and NMC and AVN analyses. First, a detailed synoptic overview showed the qualitative linkage between synoptic features and the jet streaks through the life cycle of the storm and also provided a comparison between a forecast and the AVN and NMC analyses. Secondly, kinetic energy concepts were utilized to quantify the development of the jet streaks and the possible effect they had on the system development.

Specifically, the synoptic overview provided evidence that the storm was heavily influenced by two strong jet streaks. Initially, the cyclone began to deepen rapidly as it was influenced by the right-rear quadrant of a downstream jet streak. While this downstream jet streak propagated eastward away from the surface cyclone, the system continued to deepen rapidly as it became influenced by the left-front quadrant of a rapidly propagating upstream jet streak. The evolution of these two jet streaks provided the storm with continuous jet streak influence throughout its life cycle.

A comparison of the GSM forecast and the NMC manual and Aviation (AVN) analyses showed that the GSM forecast initialized at 1200 UTC 13 March 1993 was slow

to deepen the system initially, but that it did an excellent job of predicting the deepening rate after the 18-h forecast time. However, the forecast continued to deepen the storm after 0000 UTC 14 March 1993, when the observed storm began to weaken. In particular, the errors in the forecast central pressure relative to the NMC manual analysis were 19 mb, 9 mb, and 6 mb at 1200 UTC 13 March, 0000 UTC 14 March, and 1200 UTC 14 March, respectively. It is interesting to note that the error in the AVN analysis relative to the NMC manual analysis also decrease with time, with values of 11 mb, 8 mb, and 1 mb at the respective map times. The likely reason for this is the influence of the forecast first guess field on the AVN analysis. Even so, the locations of forecast synoptic-scale features including the jet streaks were in good agreement with both the analyses, although forecast maximum windspeeds in the jet streaks were typically weaker *than observed*. Despite these shortcomings, the GSM did an outstanding job in the general simulation of this storm.

Spatial analyses of vertically integrated kinetic energy (IKE), defined as the vertical integral of the square of the windspeed, were produced to examine the structure of the strong jet streaks and low-level circulation associated with the storm throughout its life cycle. Since the highest winds are concentrated in upper-tropospheric jet streaks, fields of IKE integrated over either the whole atmosphere (WA -- 950 to 100 mb) or the upper atmosphere (UA -- 700 to 100 mb) depict geographically where the upper-level jet maxima are located. For this case, IKE maxima coincided with 300 mb windspeed maxima at most times, reflecting that the strongest winds were usually at 300 mb. The only exceptions were early in the life cycle (00Z/13) of the storm when the strongest

winds associated with the downstream jet streak were at 200 mb. It was found that IKE provides a useful perspective from which to examine the three-dimensional nature of jet streaks on a single chart. In addition, the IKE for the lower atmosphere (LA -- 950 to 700 mb) can also indicate where low-level winds are greatest in the vicinity of the surface low.

The spatial kinetic energy results reported in this thesis can be area-average to facilitate comparisons with previous studies. For example, the area-average IKE values for the WA (Table 1) are similar to the area-average kinetic energy content values of Smith and Dare (1985). Their results were for a storm that deepened 20 mb in 24-h and which displayed an area-average kinetic energy content increase from 34.4×10^5 J m^{-2} to 51.2×10^5 J m^{-2} over this time period. Both the forecasted and analyzed WA area-average IKE show an increasing trend while the storm is deepening, but a weakening of these values is found in the analysis when the storm begins to fill at 12Z/14. Conversely, the area average IKE for the LA (Table 1) shows an increasing rate for both forecasted and analyzed LA throughout the time period. The LA IKE values are smaller in magnitude reflecting the small influence of the lower-atmosphere on the vertically integrated kinetic energy. For both WA and LA, the analysis has stronger values of area-average IKE than the forecast. Although this is to be expected due to an under forecast of the storm, forecasted IKE still gives an excellent indication of the analyzed IKE.

The generation or source term in the kinetic energy budget equation was also studied for this case. Specifically, this term, the vertically integrated generation of kinetic energy (IGK), is defined as the vertical integral of the dot product of the wind

and the height gradient. Because of the orientation between the transverse ageostrophic flow and the height gradient, IGK illuminates where jet streak entrance and exit regions are more energetically active, that is, where more energy transformation is taking place. Therefore, IGK can provide a measure of the effect of transverse circulations aloft. As discussed above, the storm under study here was influenced by the entrance region of one jet streak initially, and then by the exit region of another. During the period of time when the surface cyclone was influenced by the entrance region of the downstream jet streak, the IGK analyses indicated that this portion of the jet streak was quite active in the vicinity of the surface cyclone. As the influence shifted to the exit region of the upstream jet streak, IGK portrayed a similar increase in magnitude in that region.

In addition, comparison of IGK and IKE can indicate if a jet streak is weakening or strengthening. When a region of positive IGK is located geographically over a region of maximum IKE, strengthening of this maximum is expected because the frictional influence over the jet is minimal. On the other hand, a region of negative IGK over a region of maximum IKE indicates a weakening maximum.

Area-average IGK values for this storm are presented in Table 2. These IGK values do not compare as well to the area-average generation of kinetic energy values presented by Smith and Dare (1985) as the area-average IKE values. In their study, the area-average of generation of kinetic energy oscillates back and forth between large positive and small negative values whereas WA IGK is positive throughout the life cycle of the storm in this case. As with IKE, WA IGK values show an increasing/decreasing trend reflecting the intensification/weakening of the storm system. In addition, area-

average LA IGK values, like LA IKE values are small in comparison to WA IGK early in the storm evolution (00Z/13 - 12Z/13), but less so latter on (00Z/14 - 12Z/14). This results in consistent with the changes in low-level circulation. Finally, due to under forecasting, analyzed area-average values of WA and LA IGK are larger than forecast area-average IGK. This difference is small, however, because of the ability of the forecast to capture the WA and LA IGK fields well.

B. RECOMMENDATIONS

The the results of this thesis suggests fruitful avenues of future research. First, the complete kinetic energy budget associated with this storm should be calculated using (2.4) to determine among other things the frictional dissipation term. Secondly, a comparison of NMC's Global Spectral Model used in this study with NMC's Nested Grid Model should be undertaken to examine any model differences. Thirdly, a study of the influence of the effects of diabatic processes to the development of this storm system and in particular, to the evolution of the jet streaks would be of great interest. Finally, IKE and IGK charts generated from model runs should be regularly output to determine the value of these products to the operational forecaster .

THIS PAGE INTENTIONALLY LEFT BLANK

APPENDIX

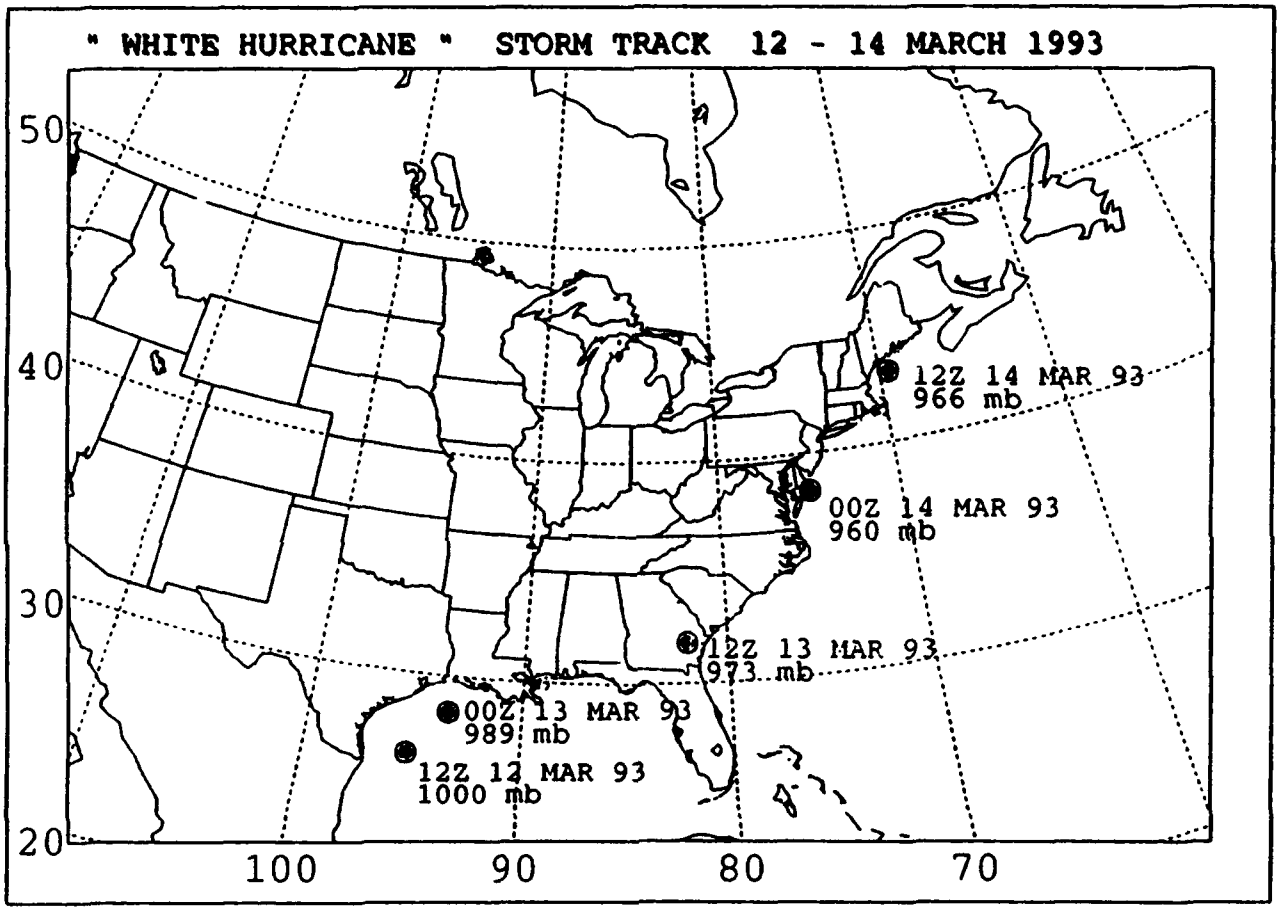

Figure 1. The 12-hourly surface cyclone center positions from the NMC analysis and central sea-level pressures between 1200 UTC 12 March and 1200 UTC 14 March 1993.

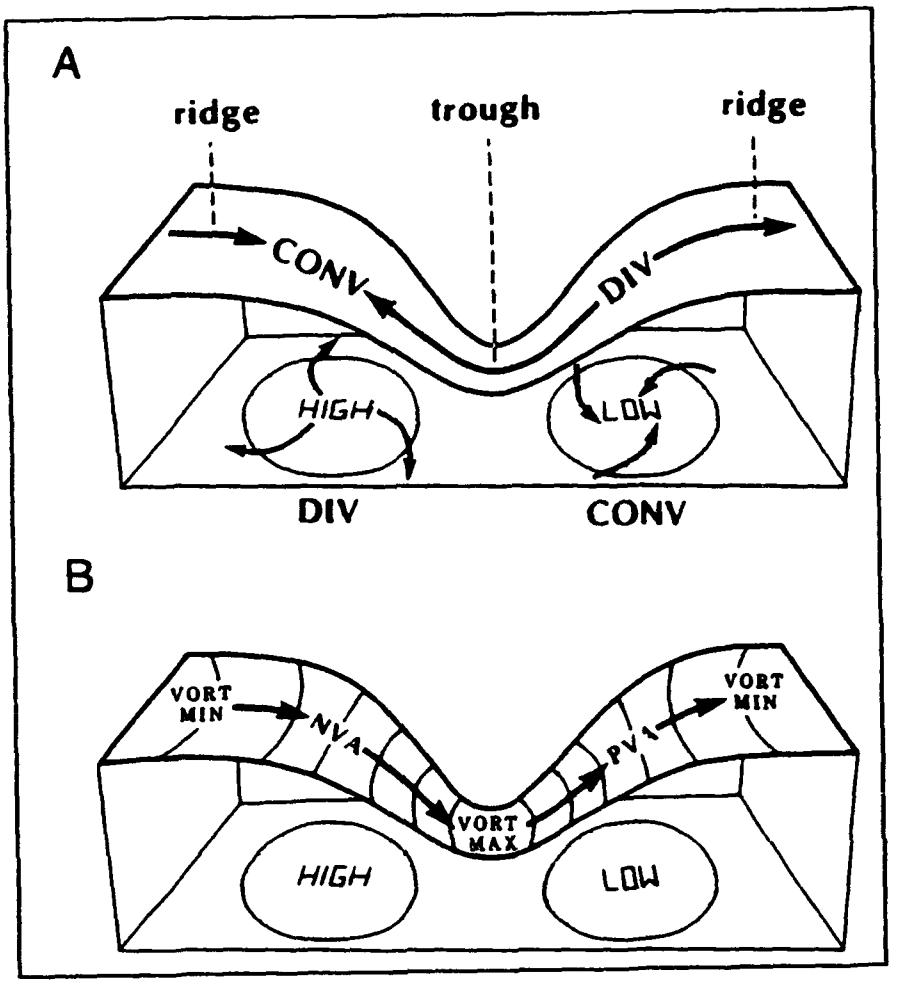

Figure 2. (**A**) Schematic relating the alongstream ageostrophic wind (arrows) to patterns of divergence associated with an upper-level trough/ridge system; (**B**) Schematic of maximum (cyclonic) and minimum (anticyclonic) relative vorticity centers and advections associated with an idealized upper-level trough/ridge system (Kocin and Uccellini 1990).

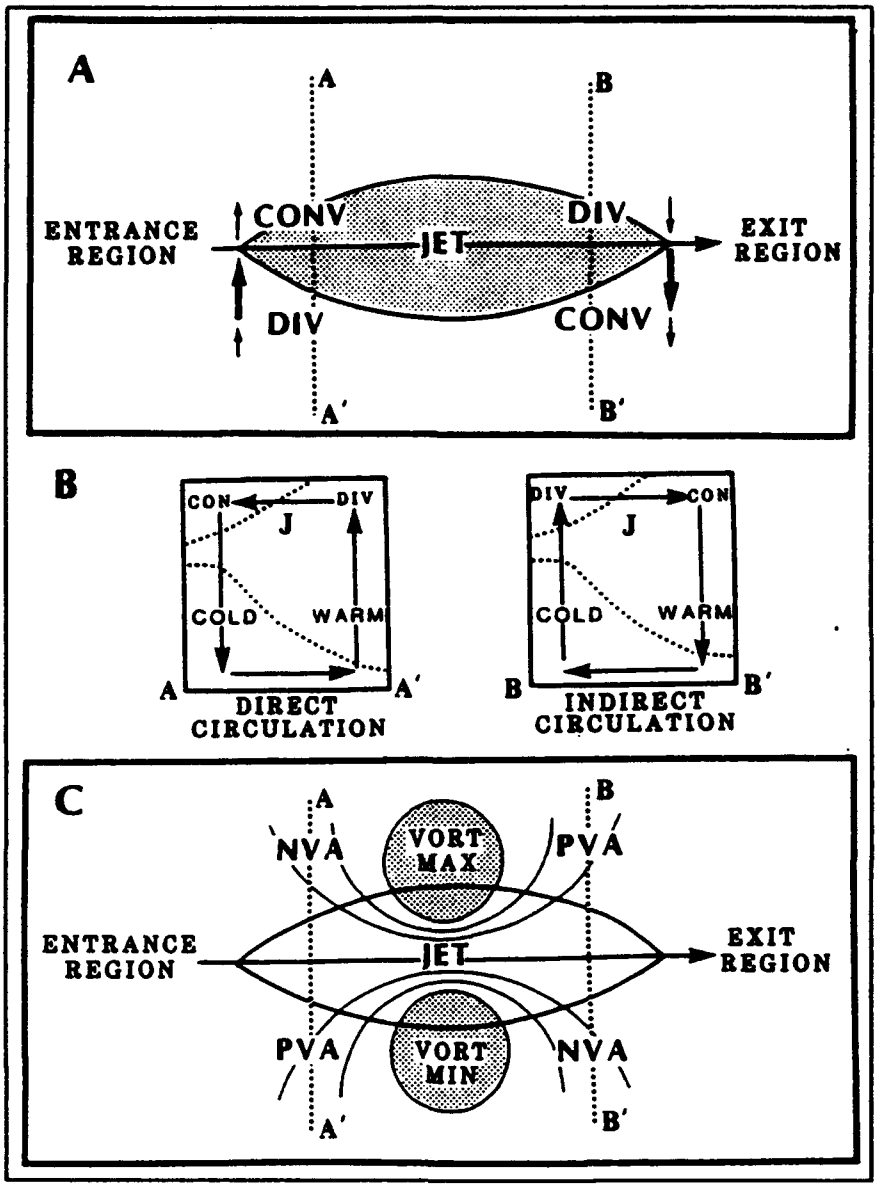

Figure 3. (**A**) Schematic of the transverse ageostrophic wind within jet entrance and exit regions; (**B**) Vertical cross-sections of direct (AA') and indirect (BB') circulations within the jet entrance and exit regions; (**C**) Schematic of maximum and minimum relative vorticity centers, and associated PVA and NVA patterns, associated with a straight jet streak (Kocin and Uccellini 1990).

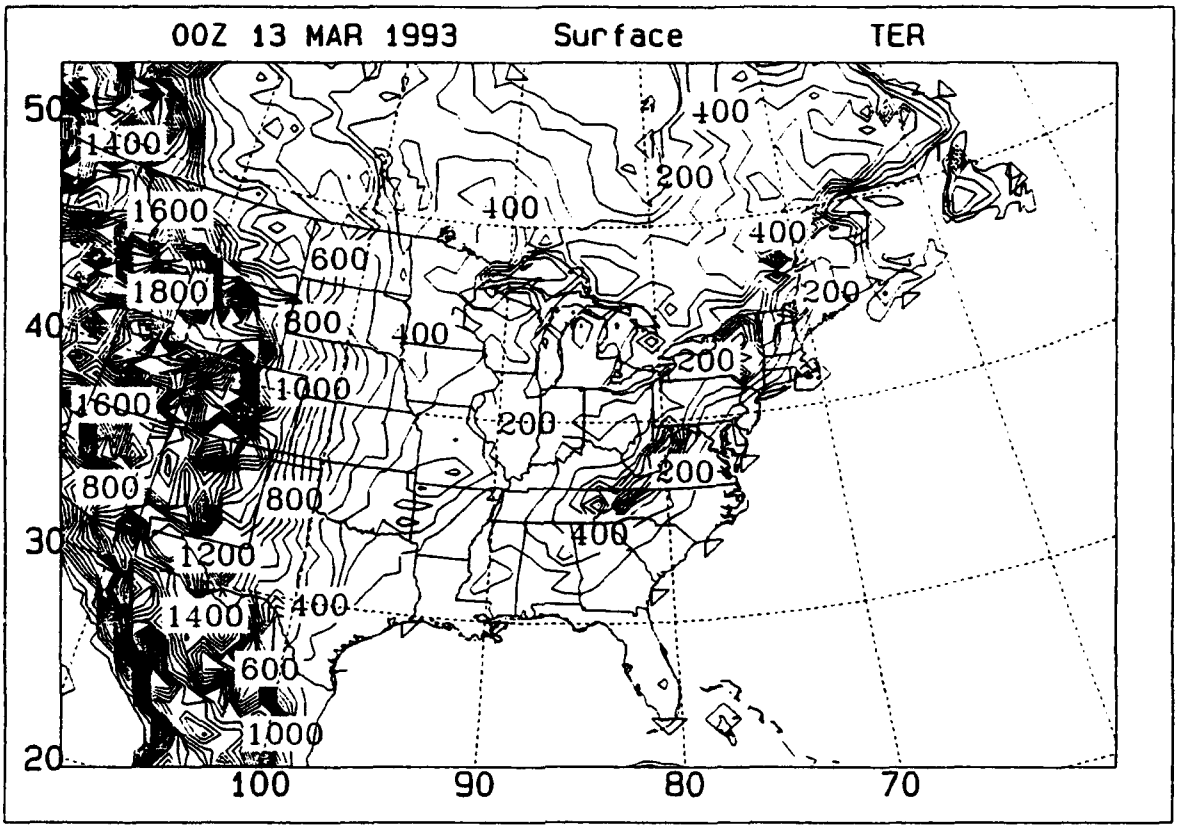

Figure 4. Terrain heights (100 m increment) on the Lambert conformal grid used in the VISUAL calculations.

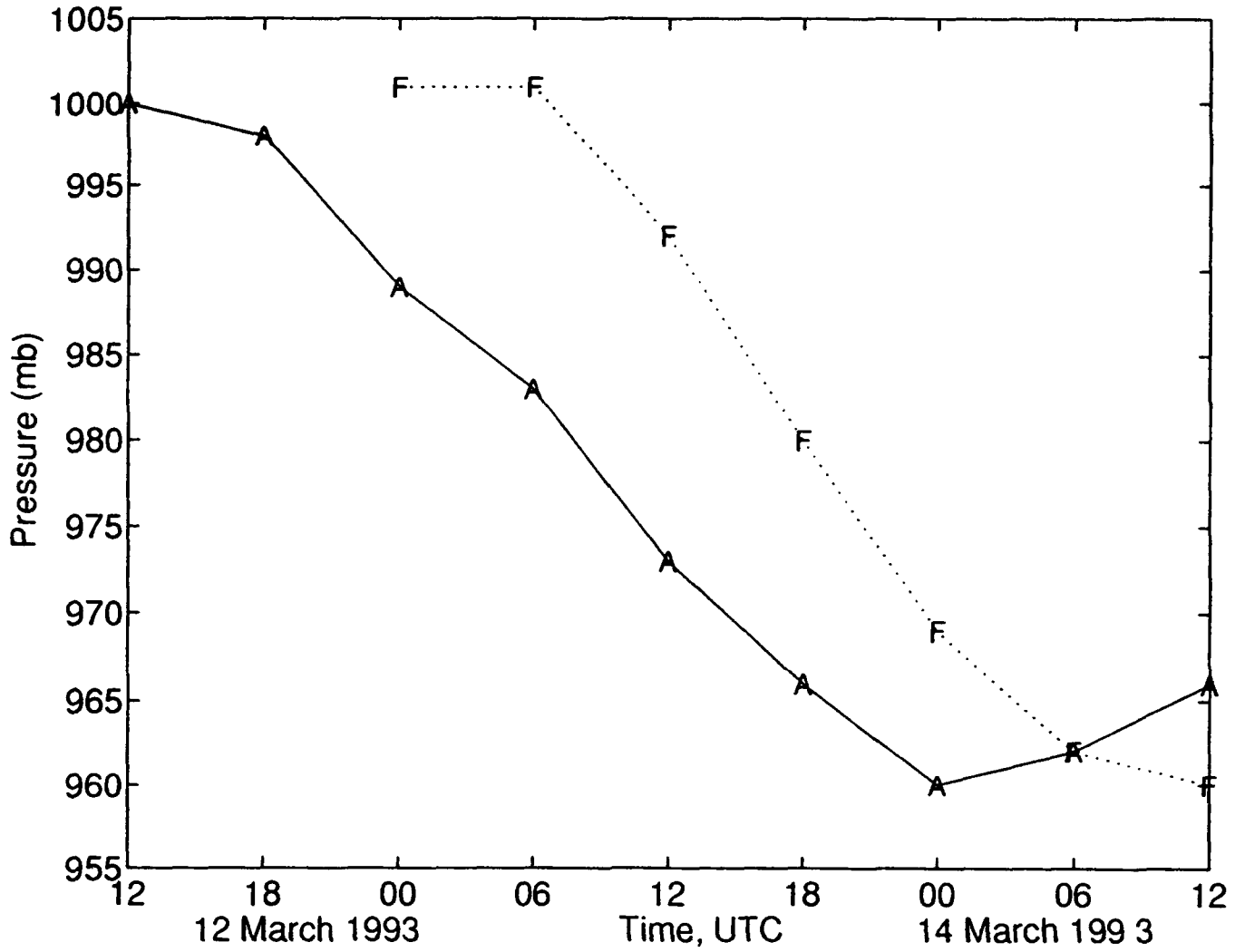

Figure 5. Time series of central sea-level pressure (mb) during the life cycle of the 12-14 March 1993 cyclone. **A** indicates the 6-hourly sea-level pressure from the NMC analysis; **F** indicates NMC 12-48 h aviation forecast of central sea-level pressure (mb) in 6 h increments.

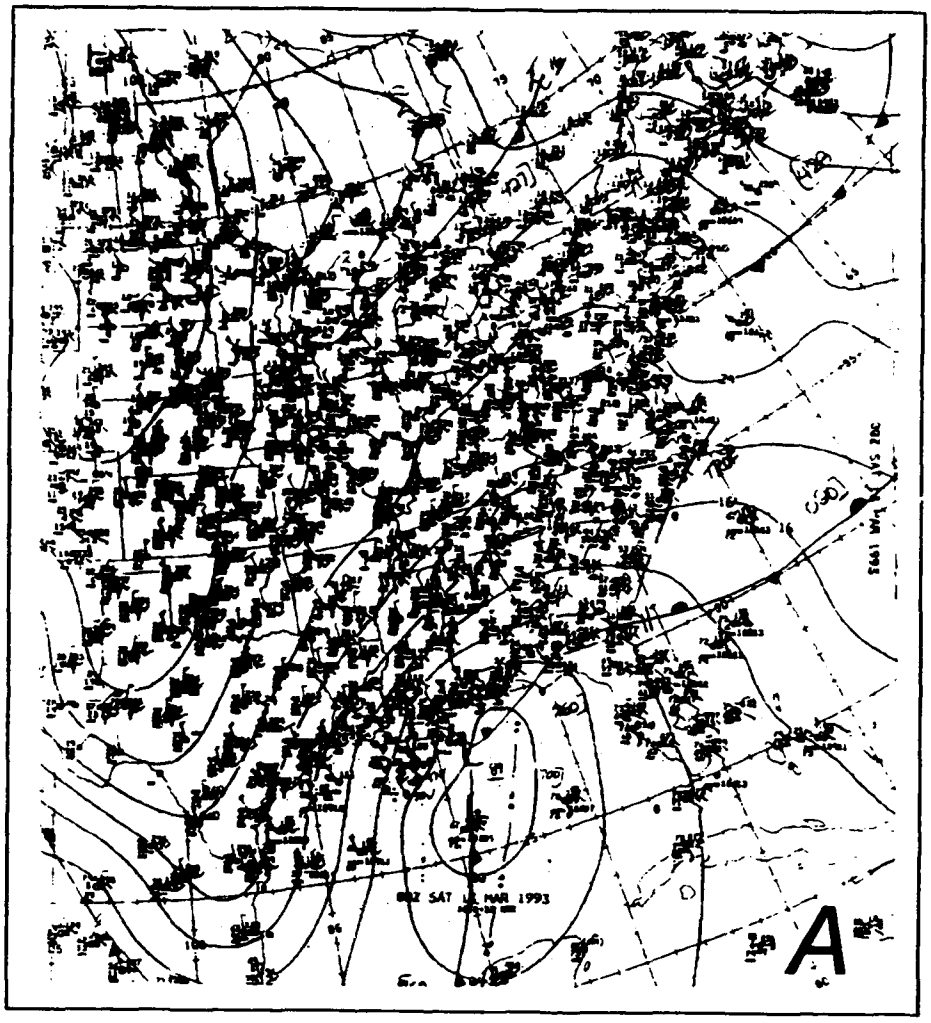

Figure 6. NMC analyses for 0000 UTC 13 March 1993. (**A**) Sea-level pressure (4 mb increment); (**B**) 500 mb height (solid; 6 dm increment) and temperature (dashed; 5°C increment); (**C**) 300 mb height (solid; 12 dm increment) and windspeed (dashed; 20 kt increment).

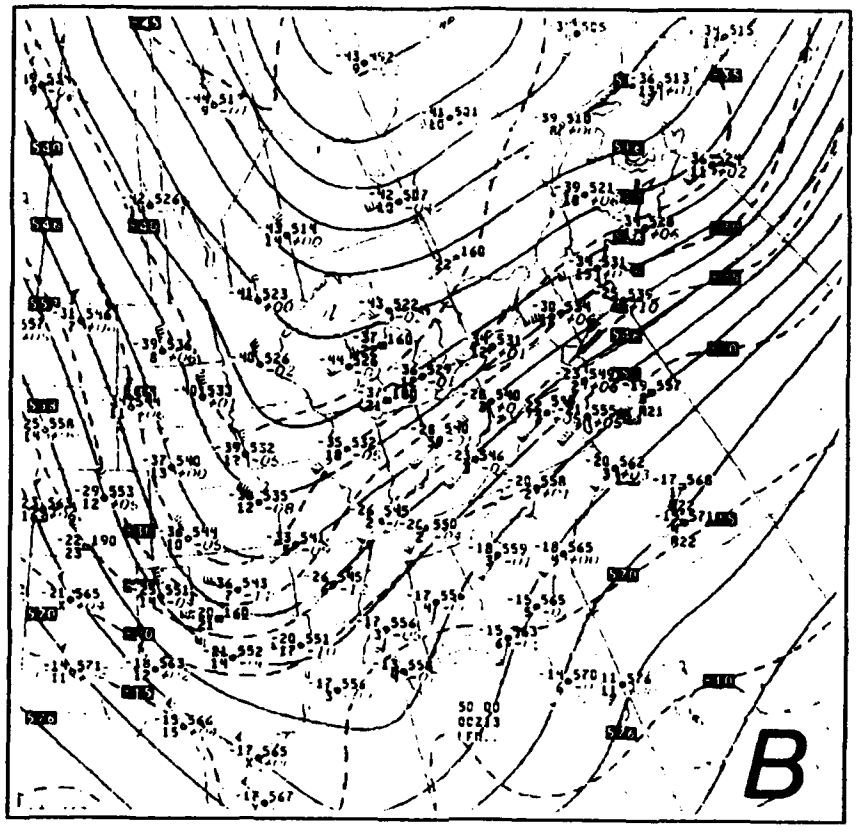
B

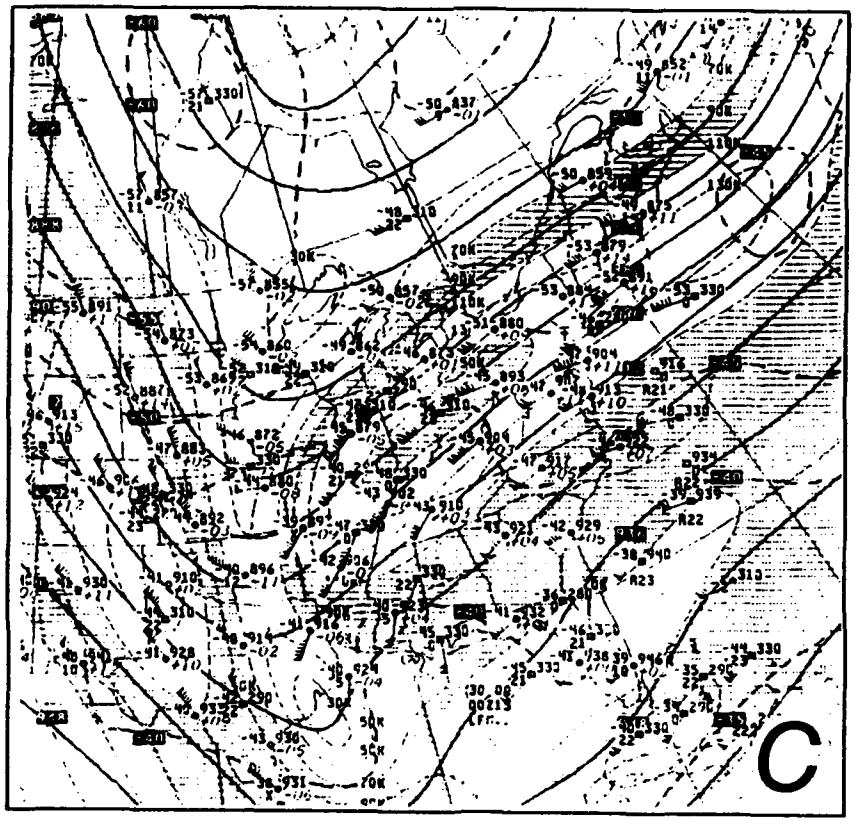
C

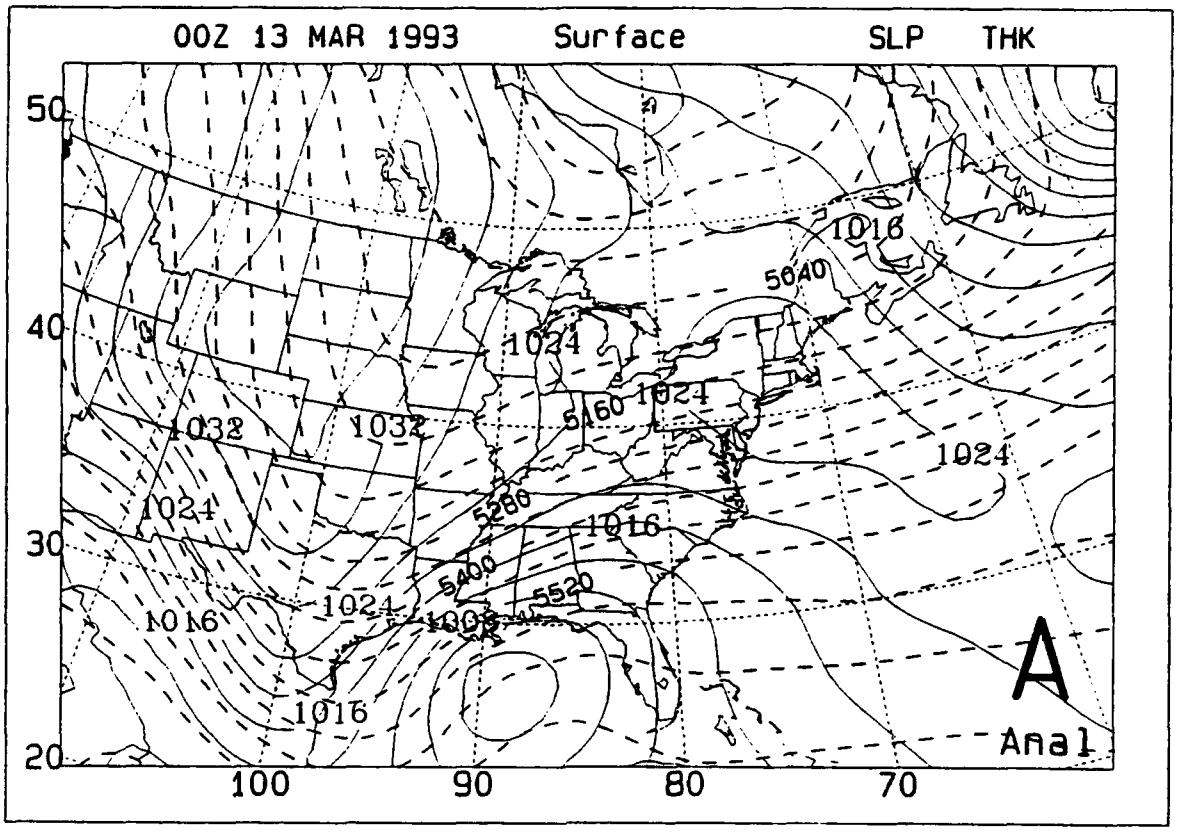

Figure 7. NMC AVN analysis for 0000 UTC 13 March 1993. (**A**) Sea-level pressure (4 mb increment); (**B**) 500 mb height (solid; 6 dm increment) and temperature (dashed; 5°C increment); (**C**) 300 mb height (solid; 12 dm increment) and windspeed (dashed; 20 kt increment).

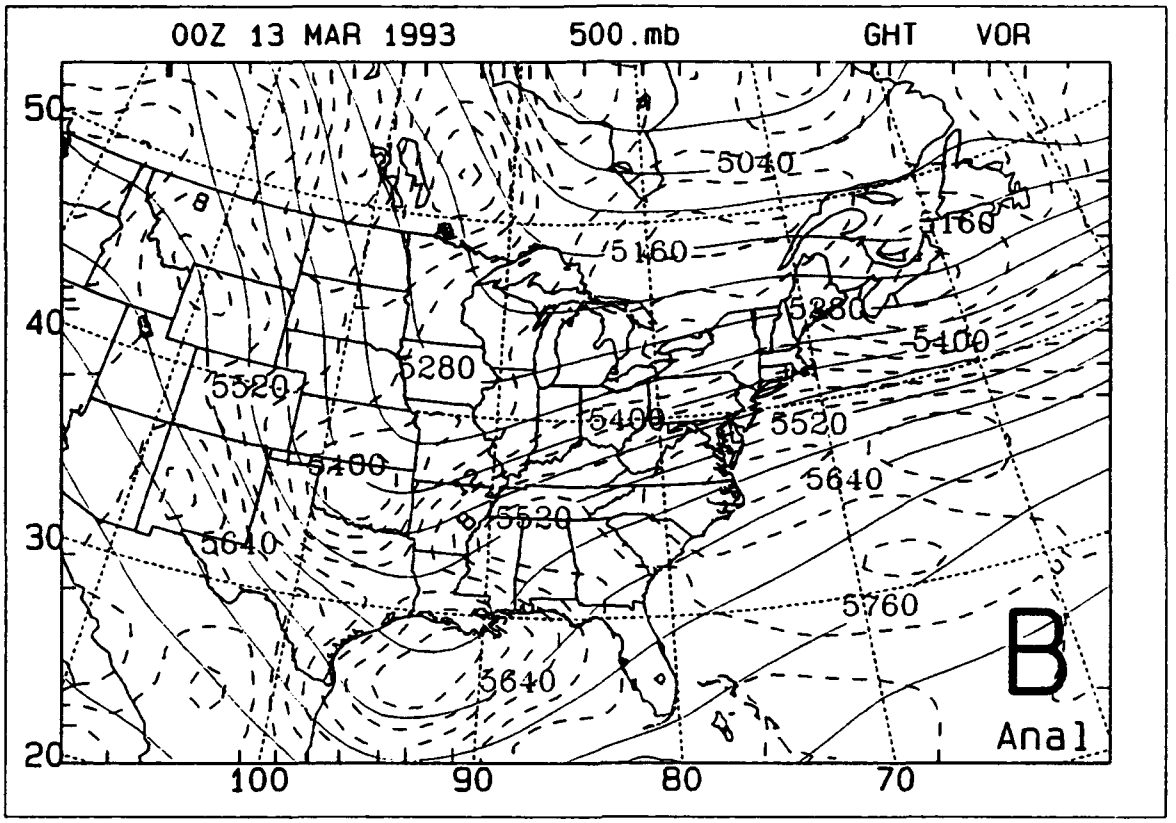
00Z 13 MAR 1993
500.mb
GHT
VOR
5040
5160
5280
5400
5520
5640
5760
B
Anal
50
40
30
20
100
90
80
70

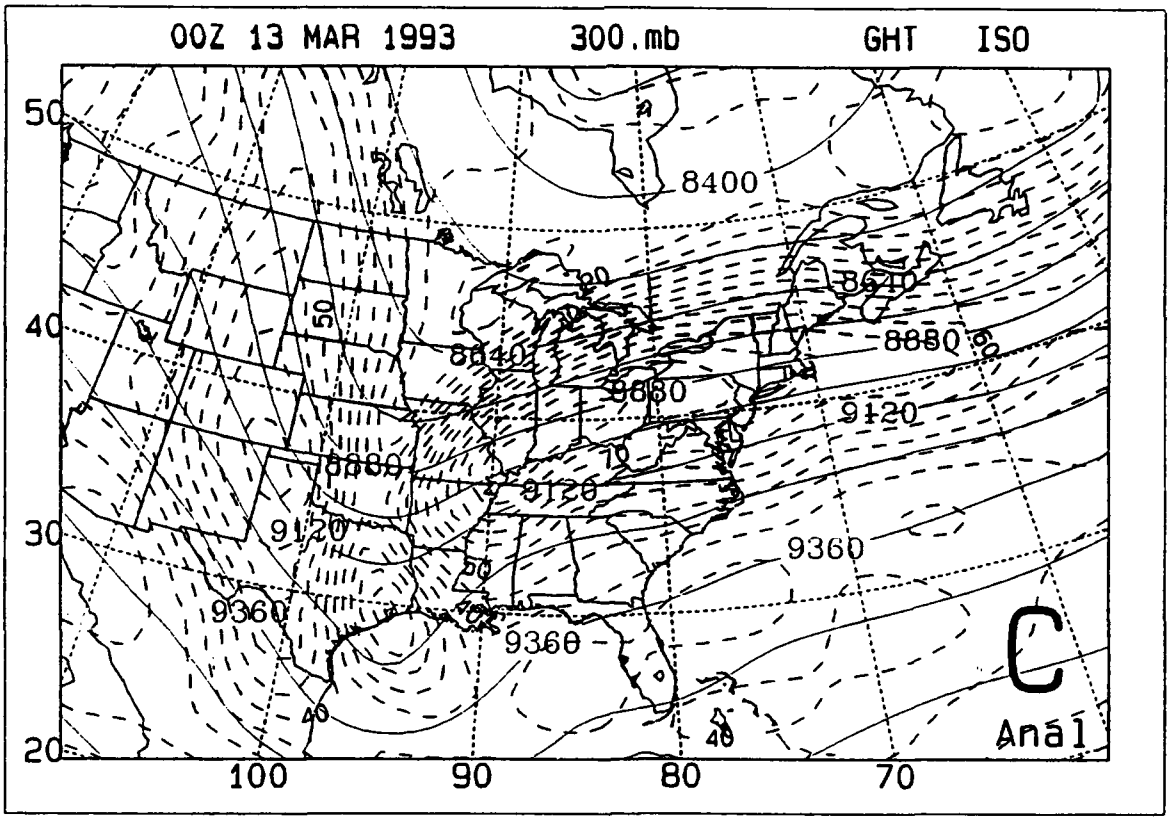
00Z 13 MAR 1993
300.mb
GHT
ISO
8400
8640
8880
9120
9360
C
Anal
50
40
30
20
100
90
80
70

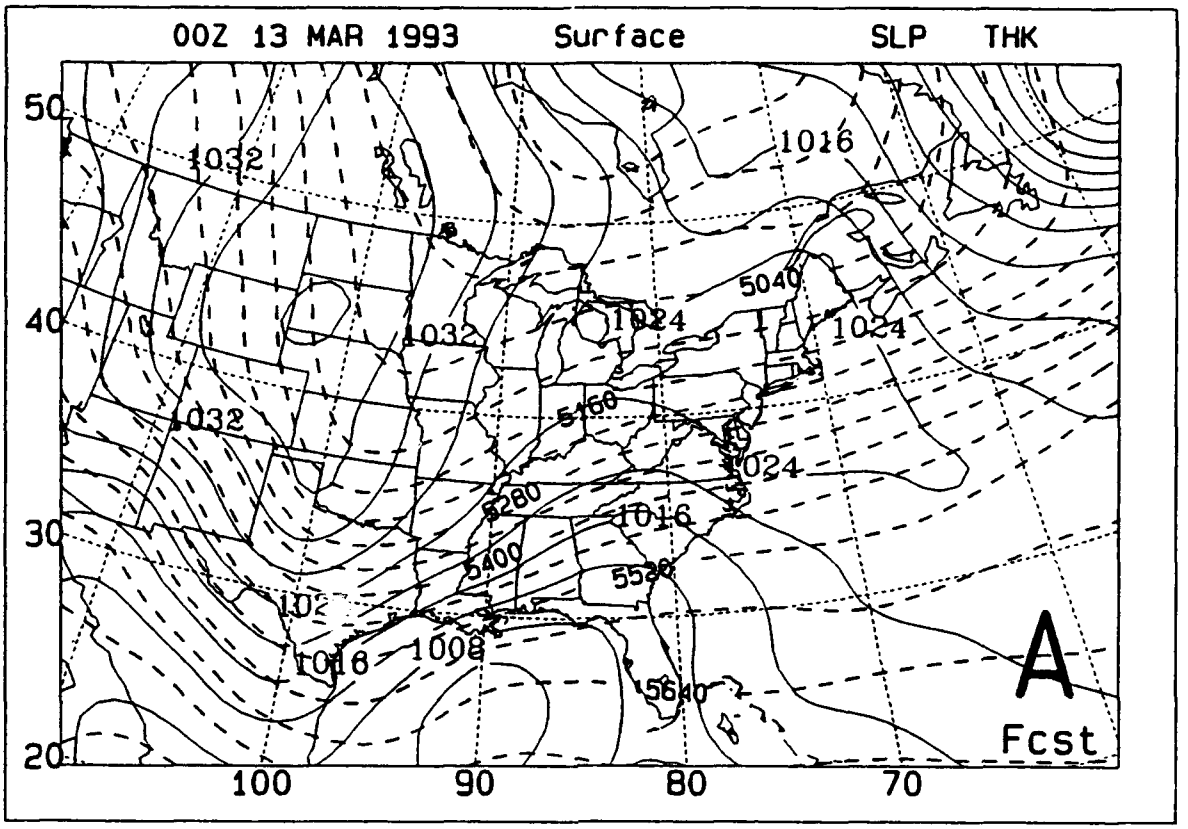

Figure 8. NMC 12 h Global Spectral Model forecast verifying at 0000 UTC 13 March 1993. (**A**) Sea-level pressure (solid; 4 mb increment) and 1000-500 mb thickness (dashed; 6 dm increment); (**B**) 500 mb height (solid; 6 dm increment) and absolute vorticity (dashed; 2 x 10^{-5} s^{-1} increment); (**C**) 300 mb height (solid; 12 dm increment) and windspeed (dashed; 5 m/s increment).

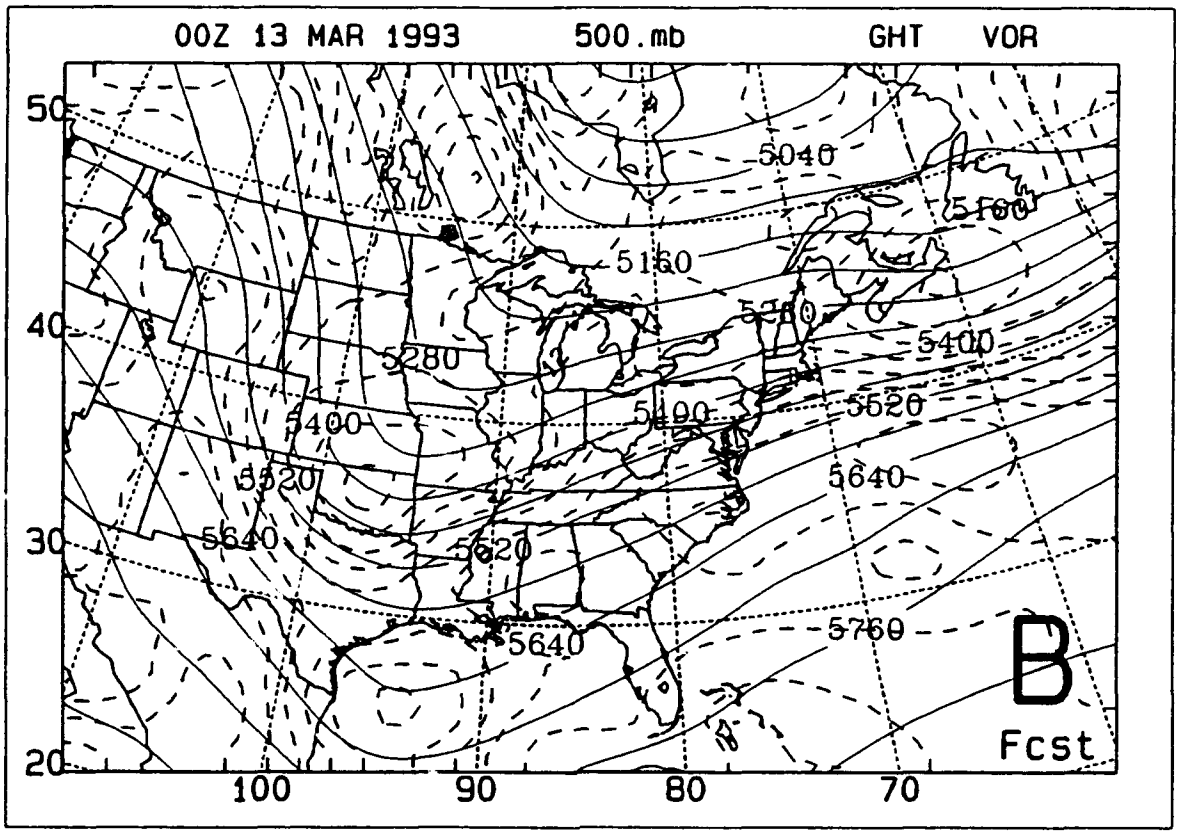
00Z 13 MAR 1993
500.mb
GHT
VOR
5040
5160
5280
5400
5520
5640
5760
B
Fcst
50
40
30
20
100
90
80
70

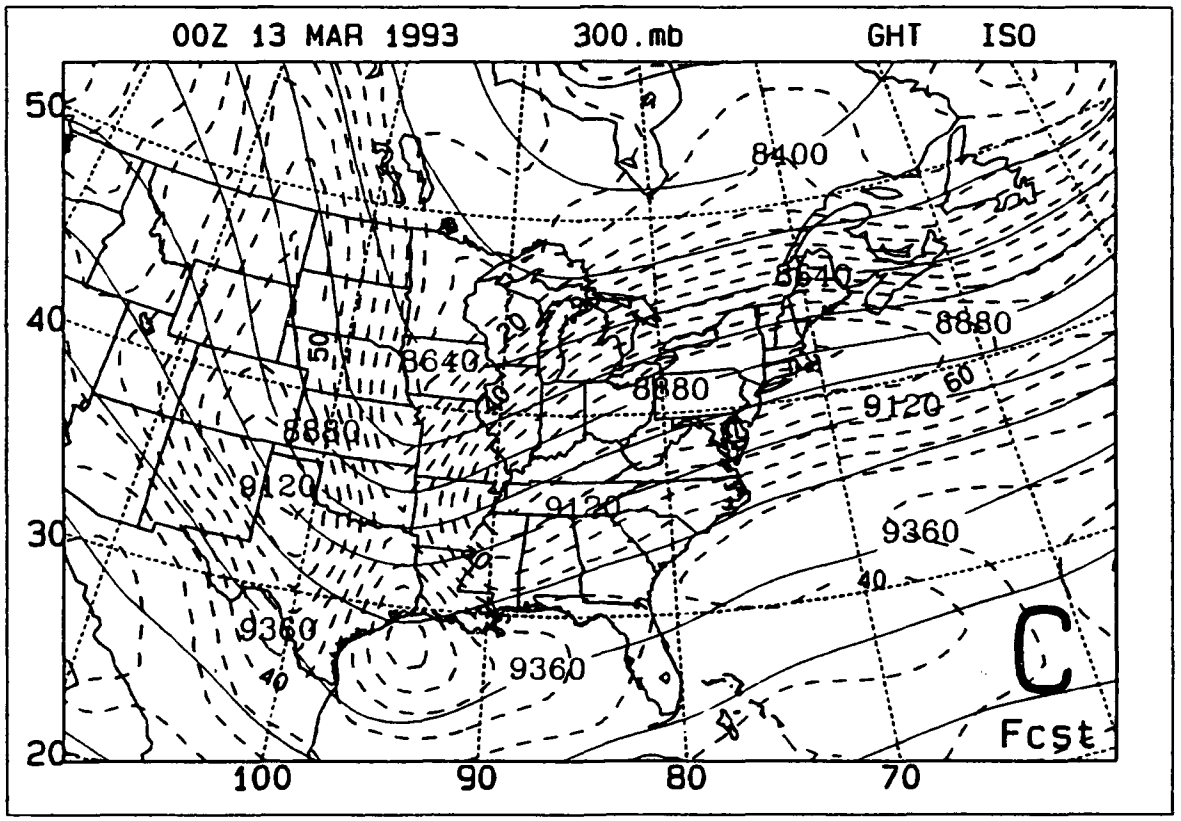
00Z 13 MAR 1993
300.mb
GHT
ISO
8400
8640
8880
9120
9360
C
Fcst
50
40
30
20
100
90
80
70

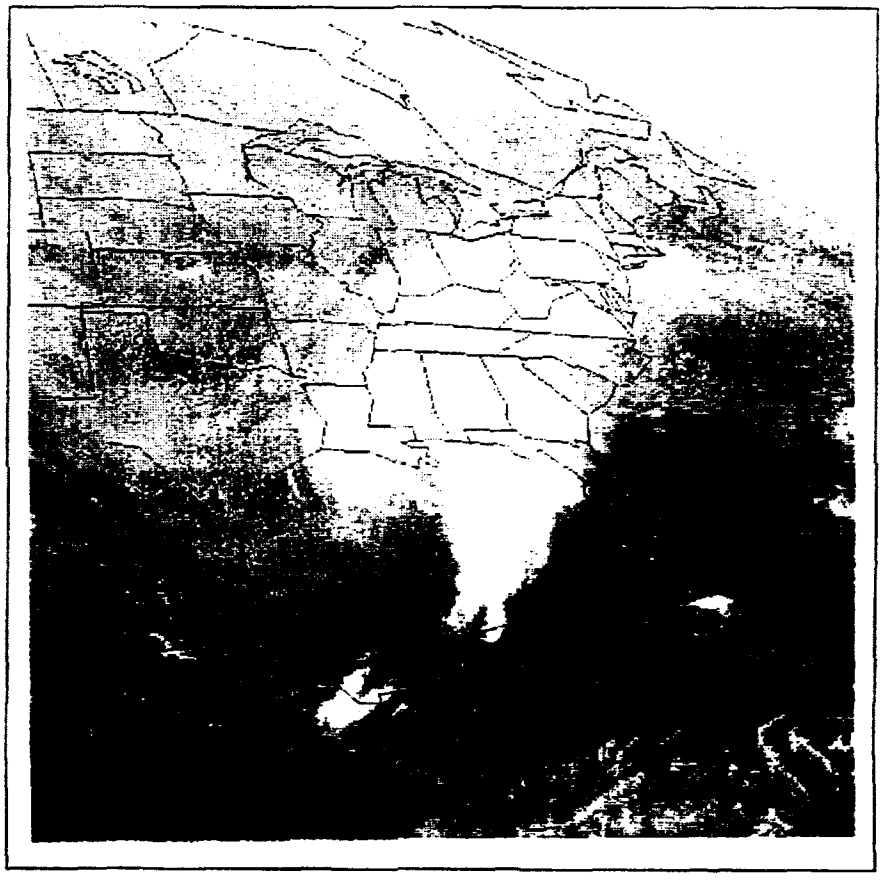

Figure 9. GOES infrared imagery for 0001 UTC 13 March 1993.

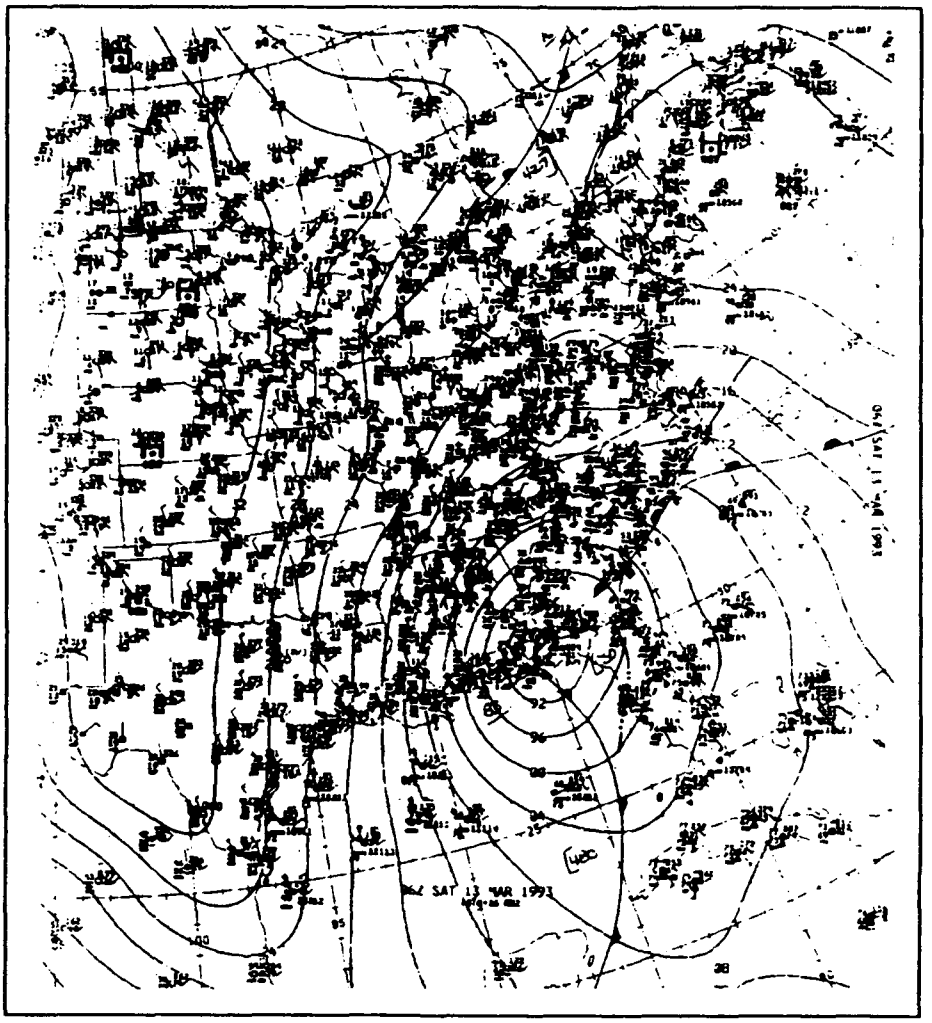

Figure 10. As in Figure 6, except for 0600 UTC 13 March 1993.

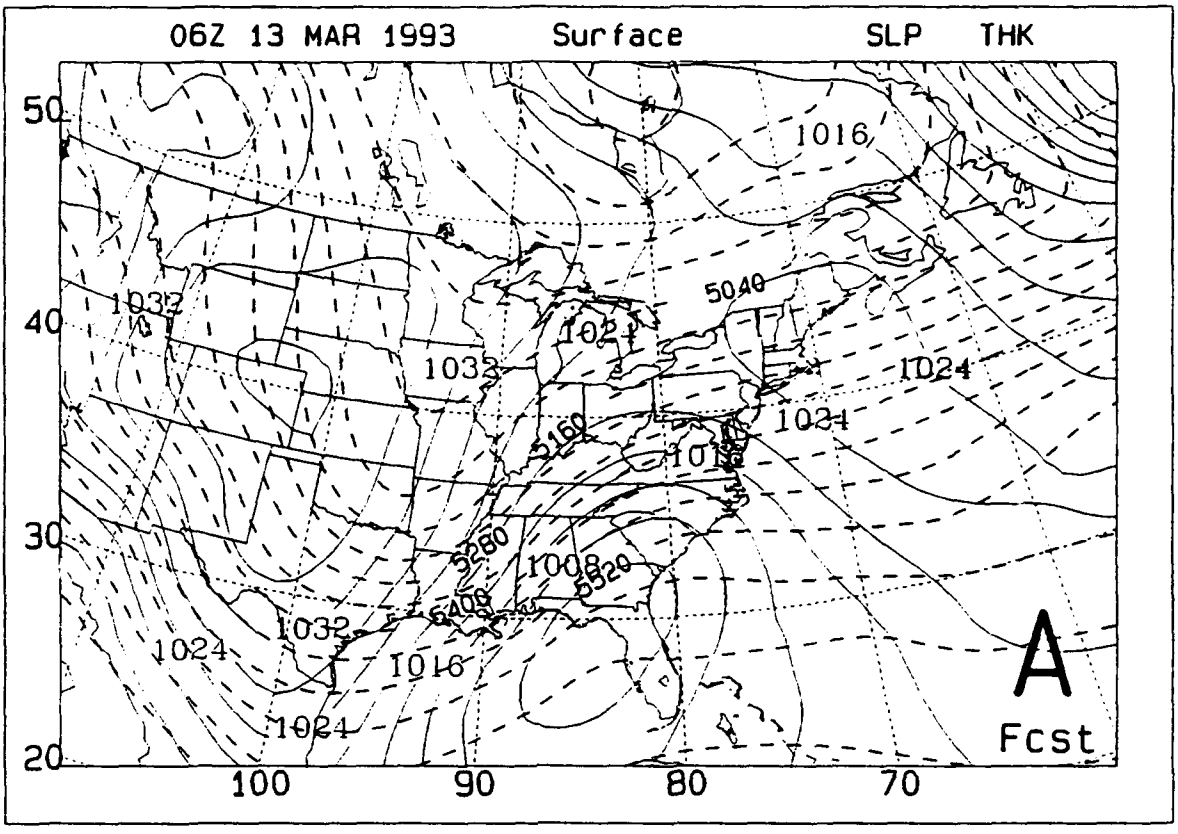

Figure 11. As in Figure 8, except for 18 h forecast verifying at 0600 UTC 13 March 1993.

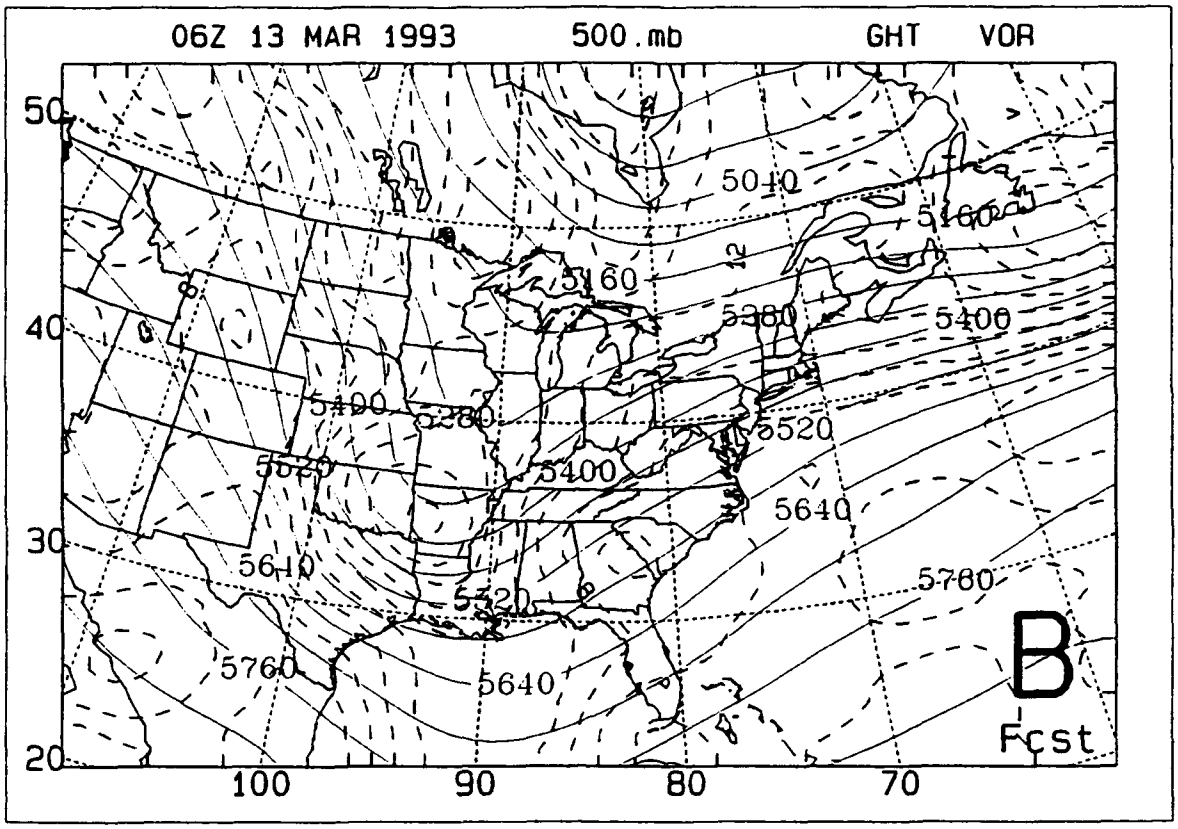
06Z 13 MAR 1993
500.mb
GHT
VOR
50
40
30
20
100
90
80
70
5040
5160
5280
5400
5520
5640
5760
B
Fcst

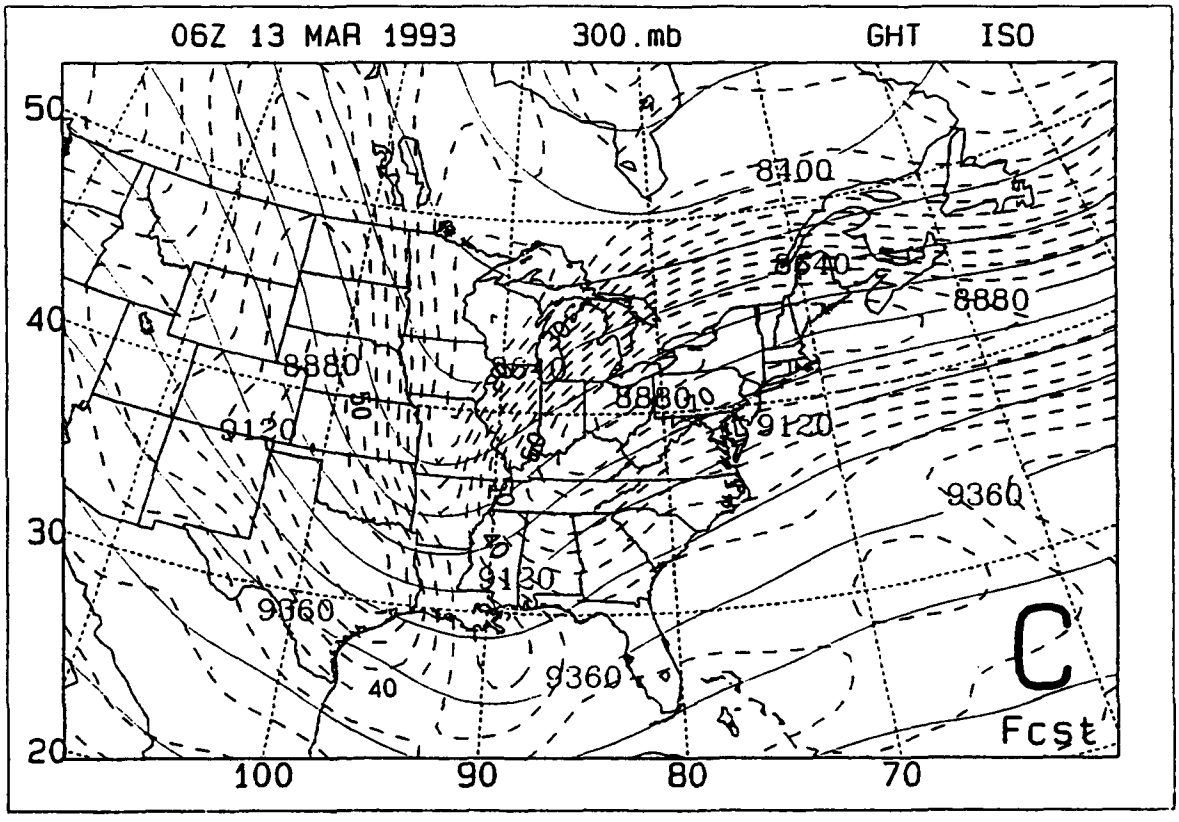
06Z 13 MAR 1993
300.mb
GHT
ISO
50
40
30
20
100
90
80
70
8400
8640
8880
9120
9360
C
Fcst

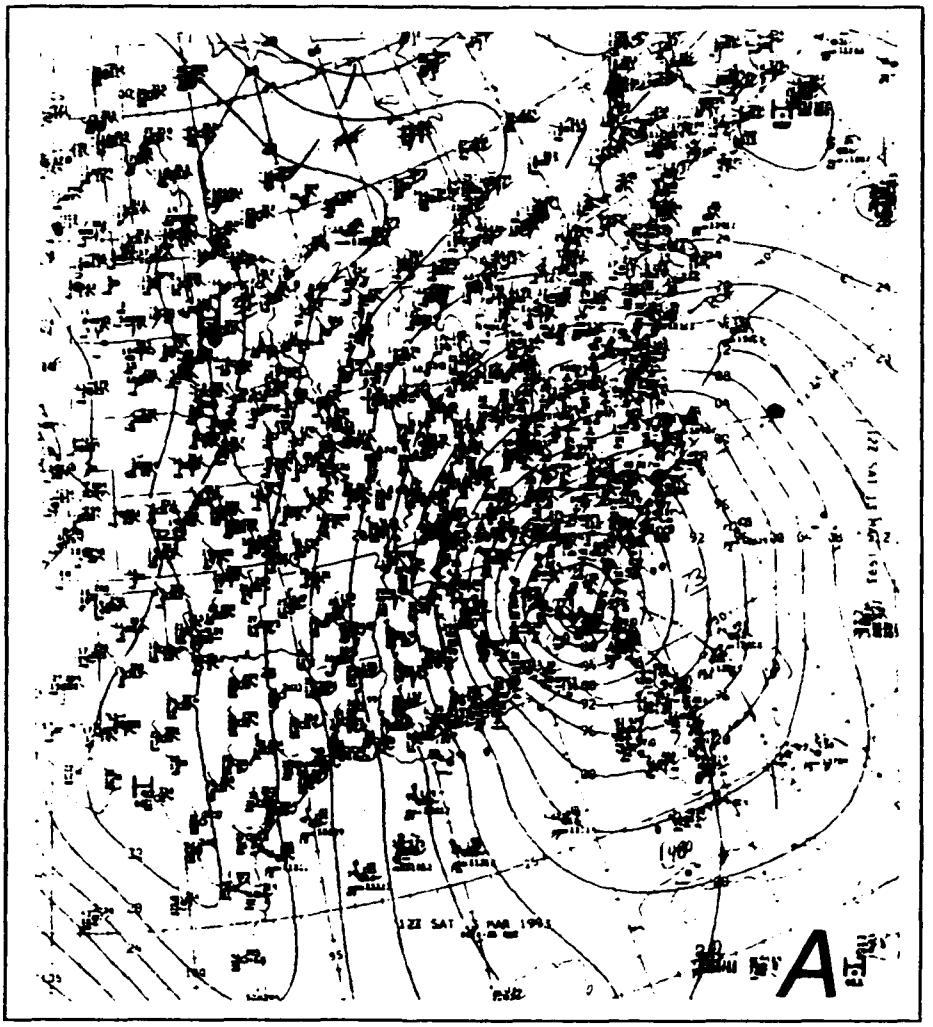

Figure 12. As in Figure 6, except for 1200 UTC 13 March 1993.

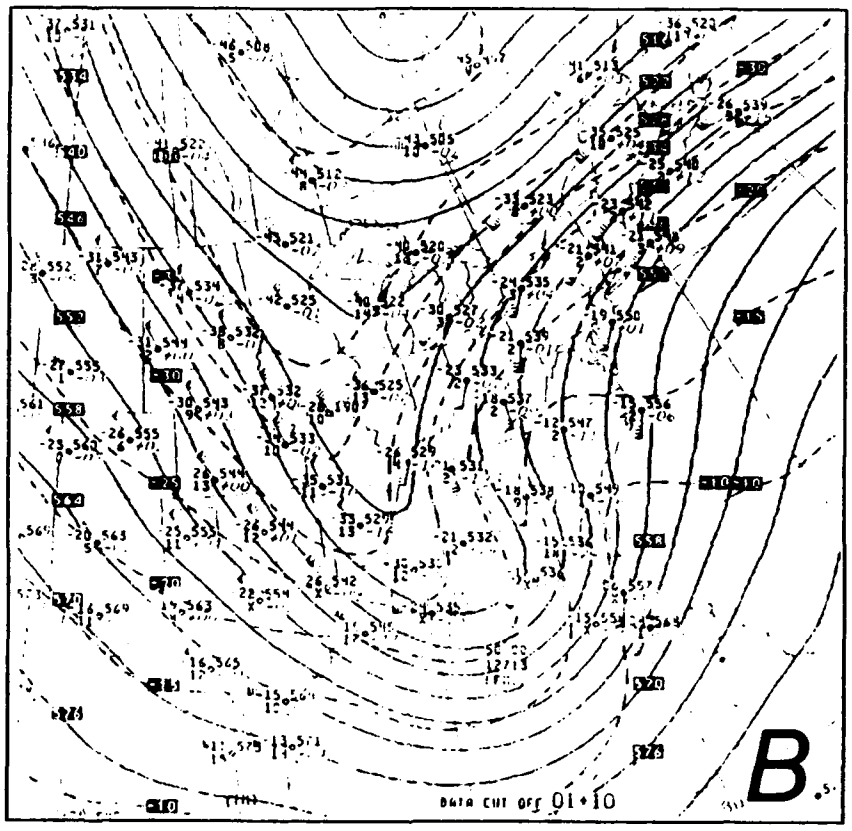
B
DATA CUT OFF 01+10

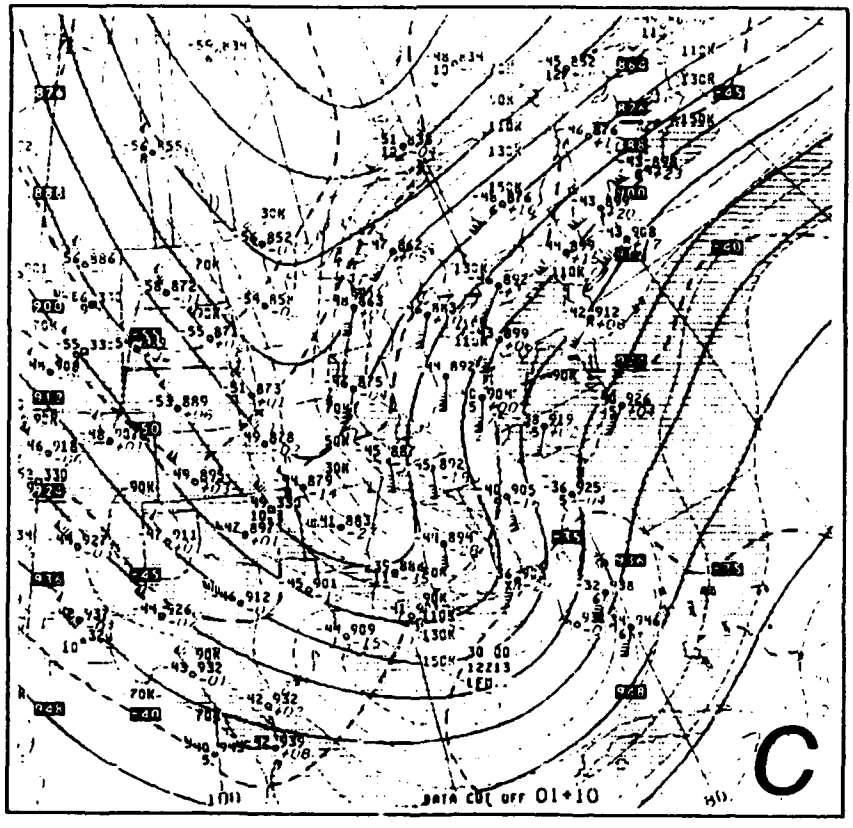
C
DATA CUT OFF 01+10

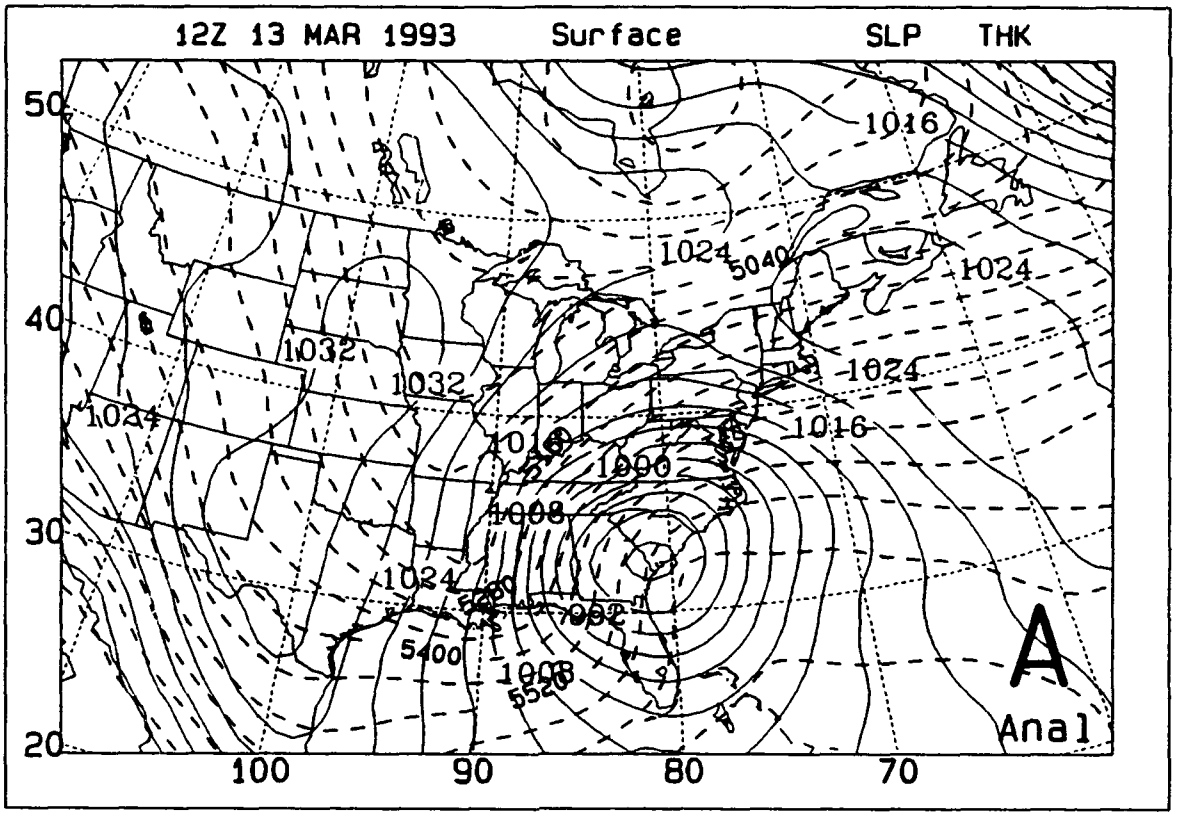

Figure 13. As in Figure 7, except for 1200 UTC 13 March 1993.

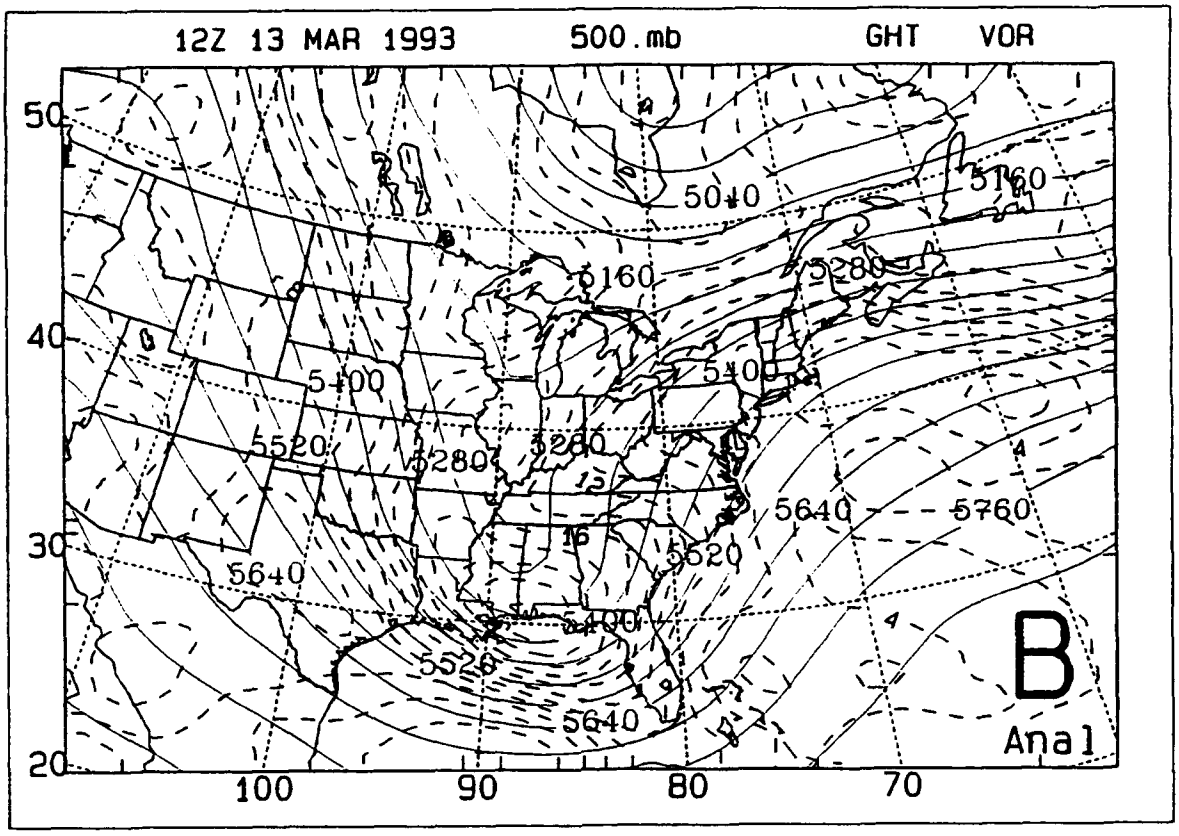
12Z 13 MAR 1993
500.mb
GHT
VOR
50
40
30
20
100
90
80
70
5040
5160
5160
5280
5400
5400
5520
5280
5280
5640
5760
5520
5640
5400
5520
5640
B
Anal

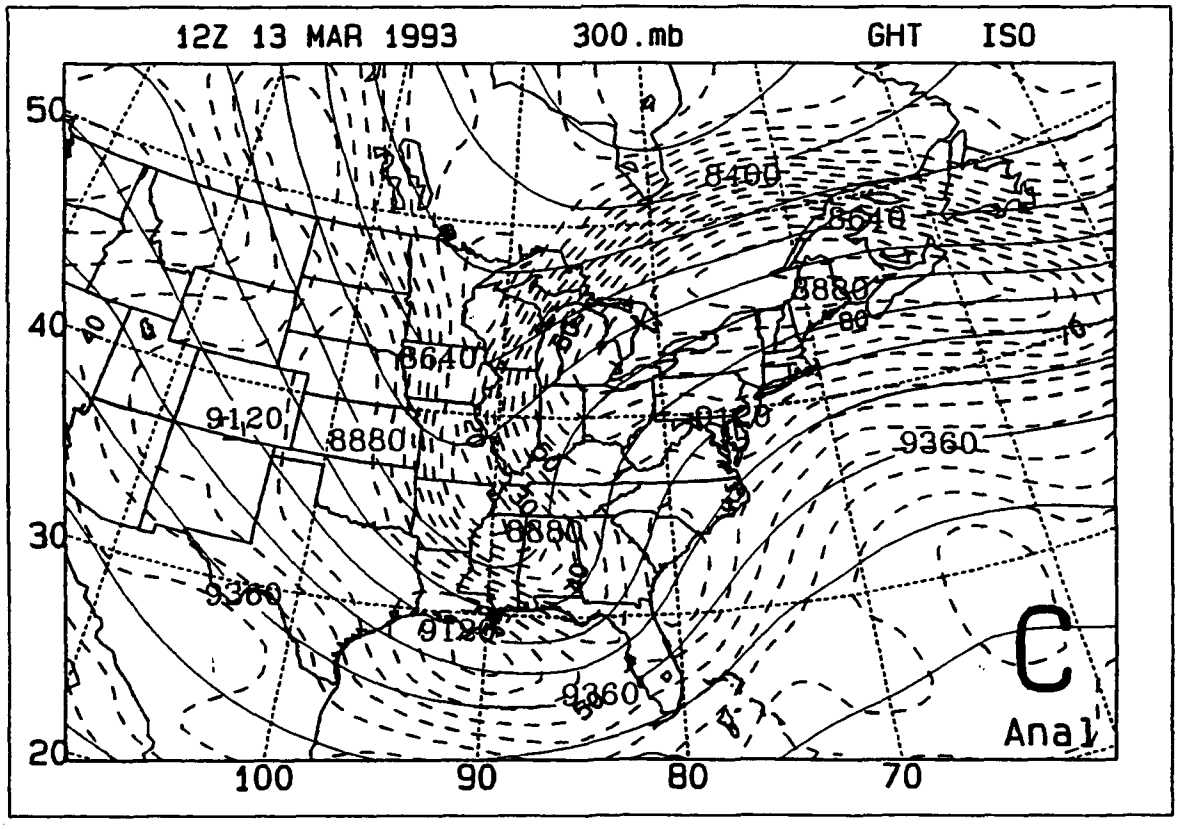
12Z 13 MAR 1993
300.mb
GHT
ISO
50
40
30
20
100
90
80
70
8400
8640
8880
9120
8880
9120
9360
8880
9360
9120
9360
C
Anal

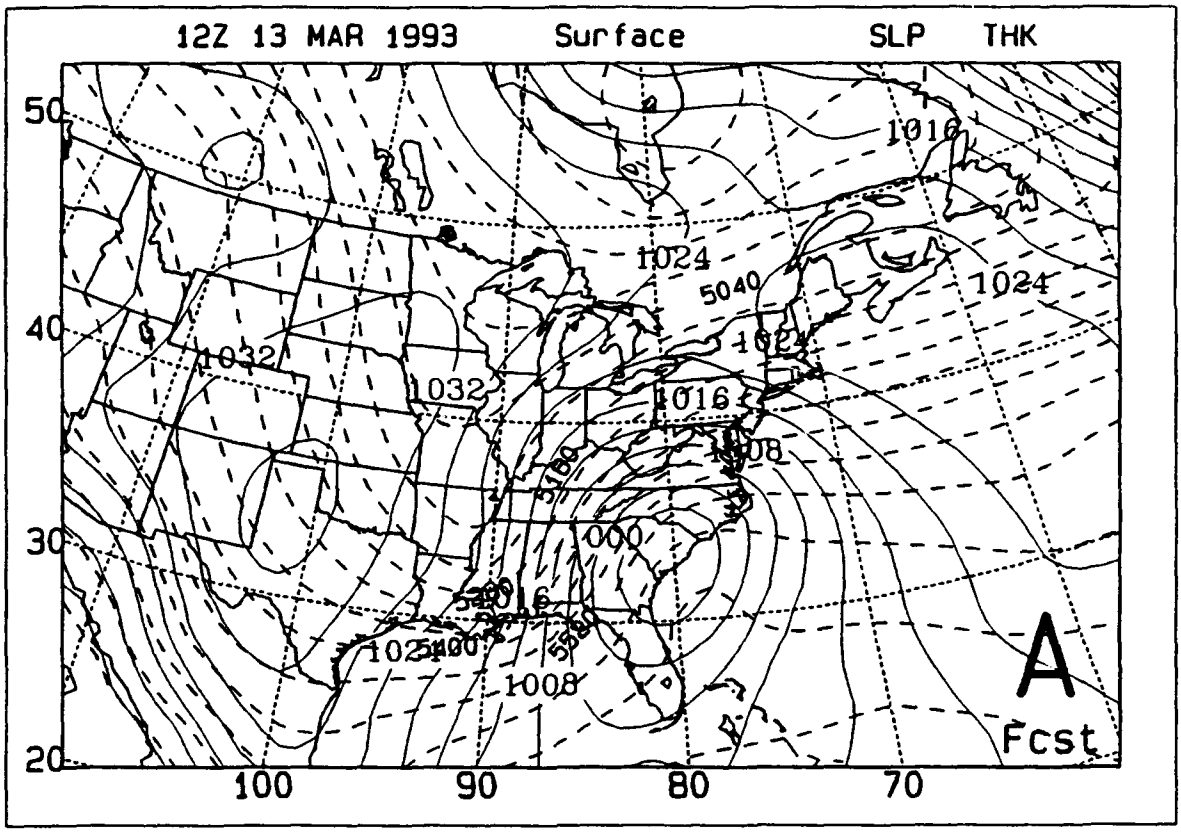

Figure 14. As in Figure 8, except for 24 h forecast verifying at 1200 UTC 13 March 1993.

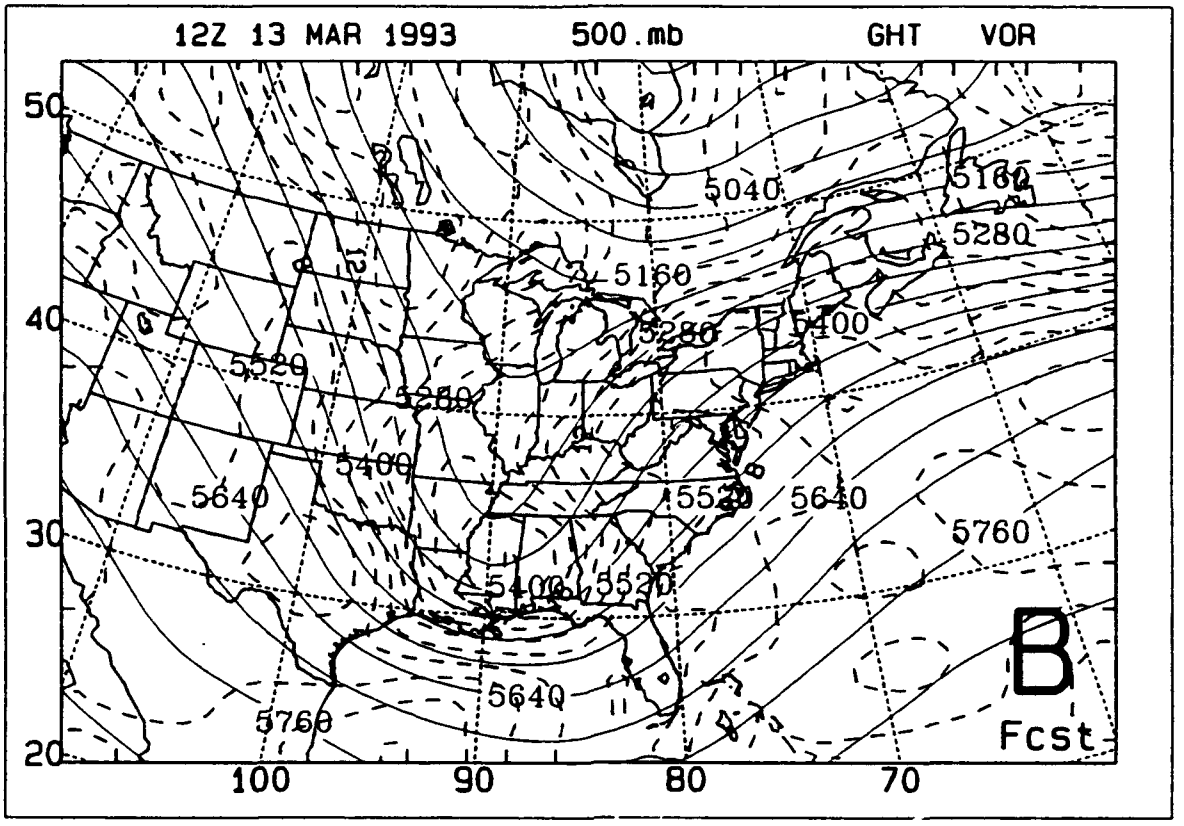
12Z 13 MAR 1993
500.mb
GHT
VOR
5040
5160
5280
5400
5520
5640
5760
B
Fcst
50
40
30
20
100
90
80
70

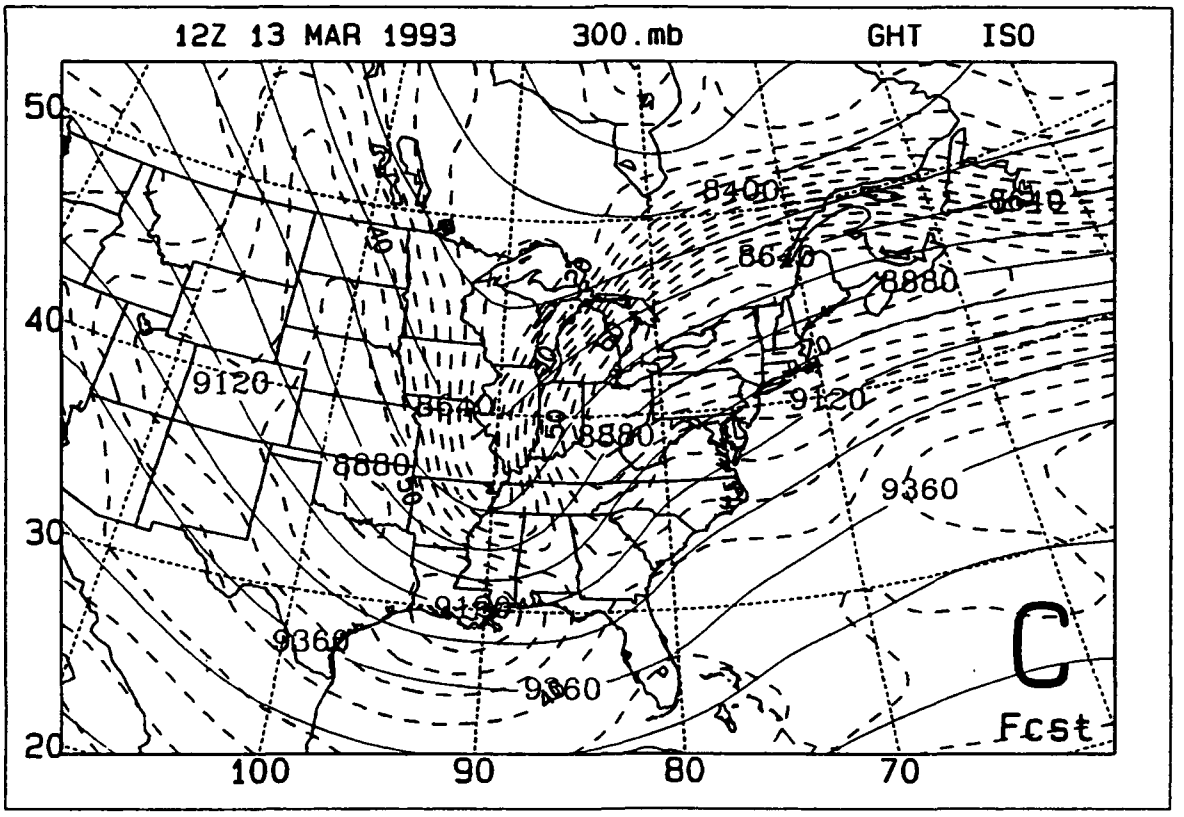
12Z 13 MAR 1993
300.mb
GHT
ISO
8400
8640
8880
9120
9360
C
Fcst
50
40
30
20
100
90
80
70

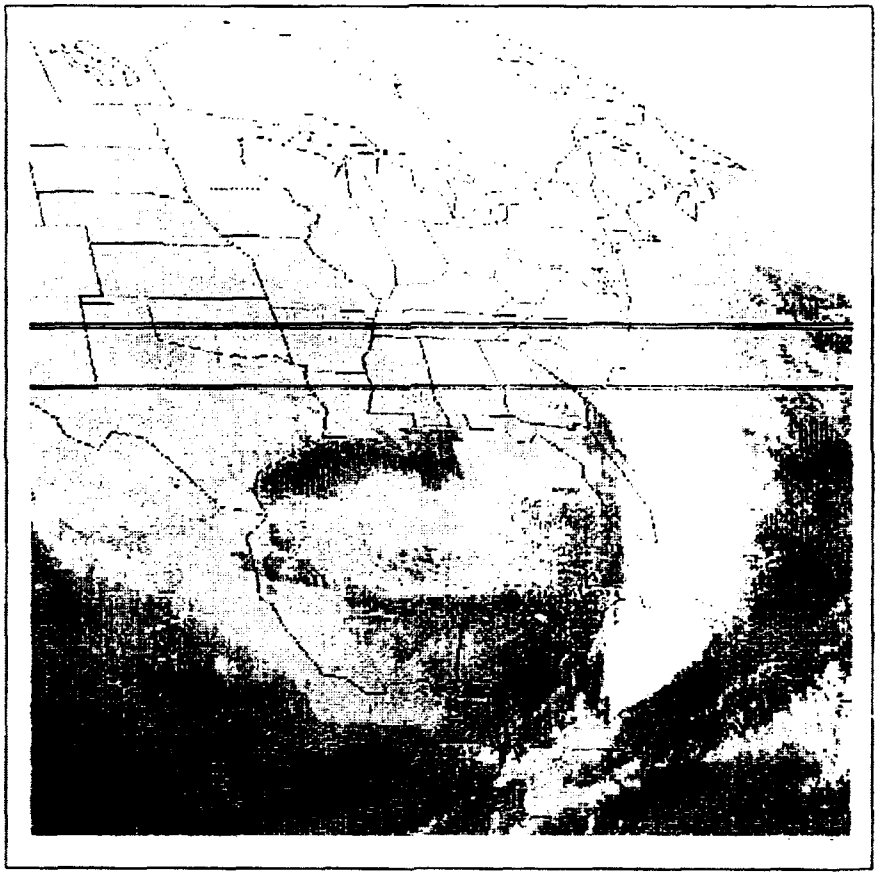

Figure 15. GOES infrared imagery for 1201Z 13 March 1993.

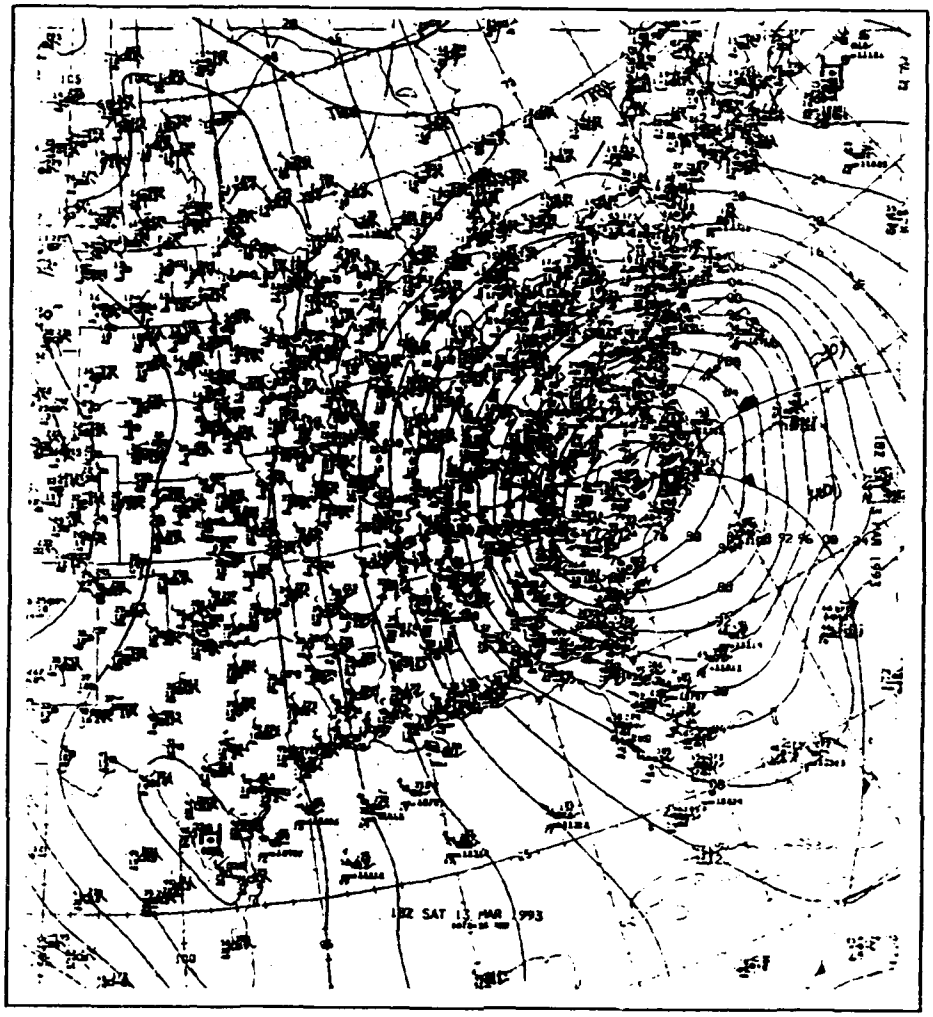

Figure 16. As in Figure 6, except for 1800 UTC 13 March 1993.

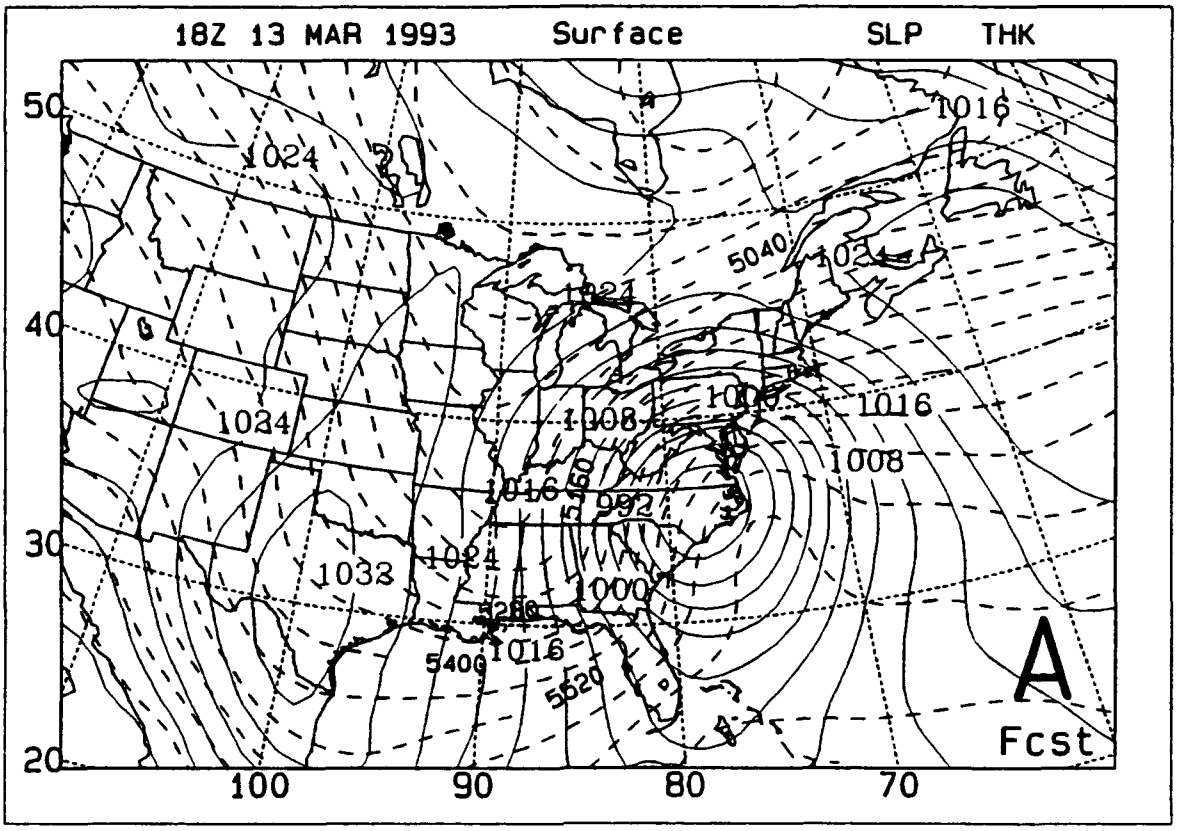

Figure 17. As in Figure 8, except for 30 h forecast verifying at 1800 UTC 13 March 1993.

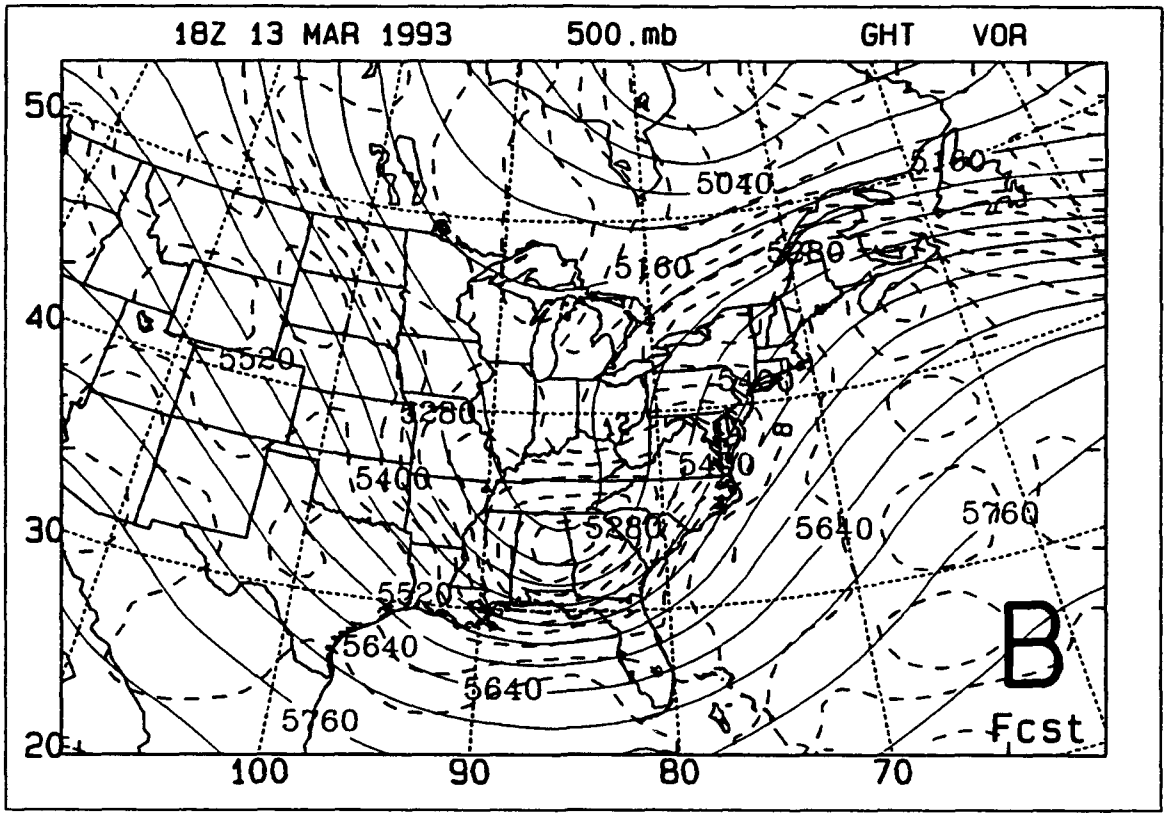
18Z 13 MAR 1993
500.mb
GHT
VOR
5040
5160
5160
5520
5280
5400
5400
5280
5640
5760
5520
5640
5640
5760
B
Fcst
50
40
30
20
100
90
80
70

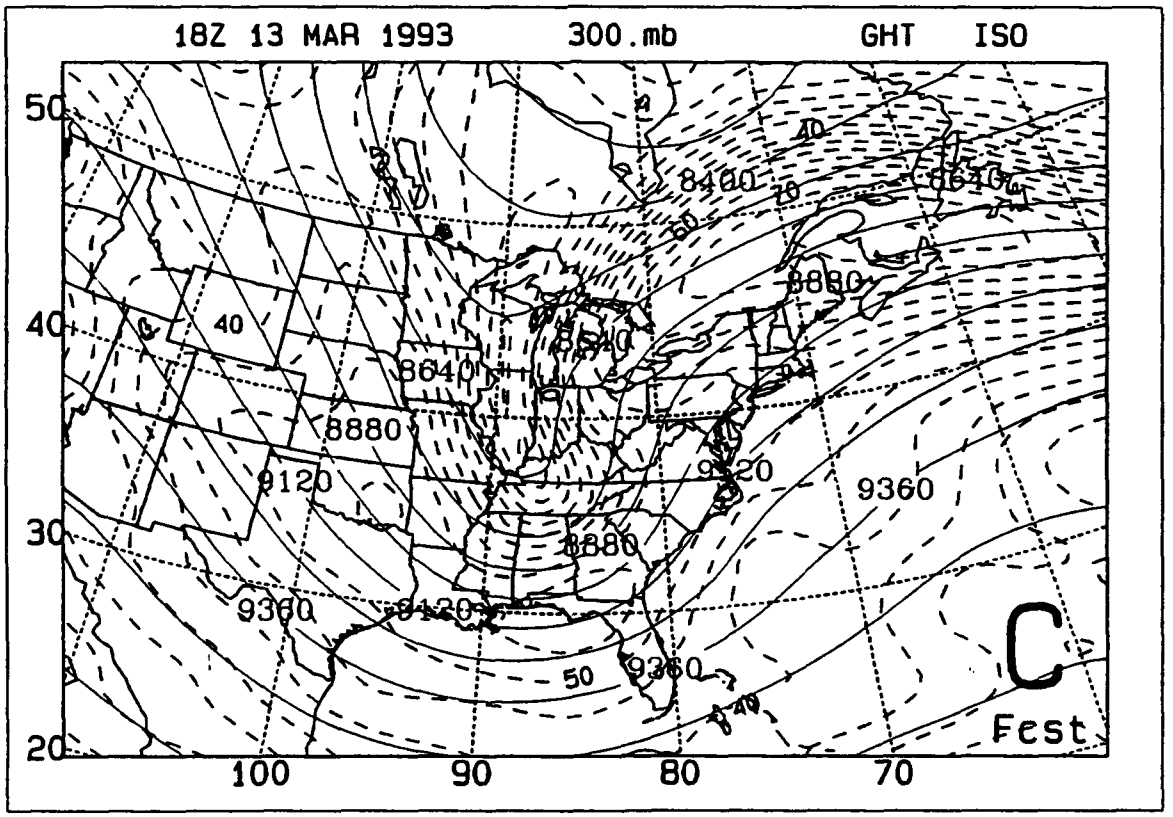
18Z 13 MAR 1993
300.mb
GHT
ISO
8400
8640
8880
8640
8880
9120
9120
9360
8880
9360
9120
9360
C
Fcst
50
40
30
20
100
90
80
70

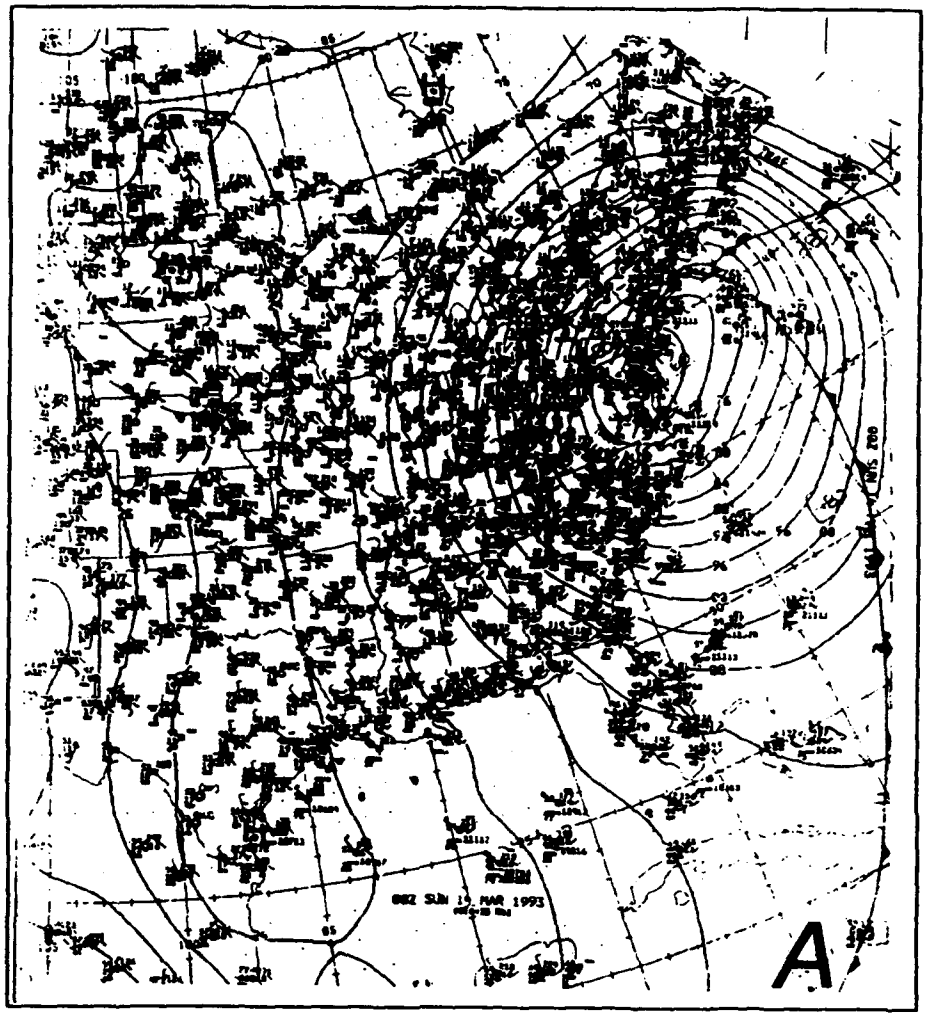

Figure 18. As in Figure 6, except for 0000 UTC 14 March 1993.

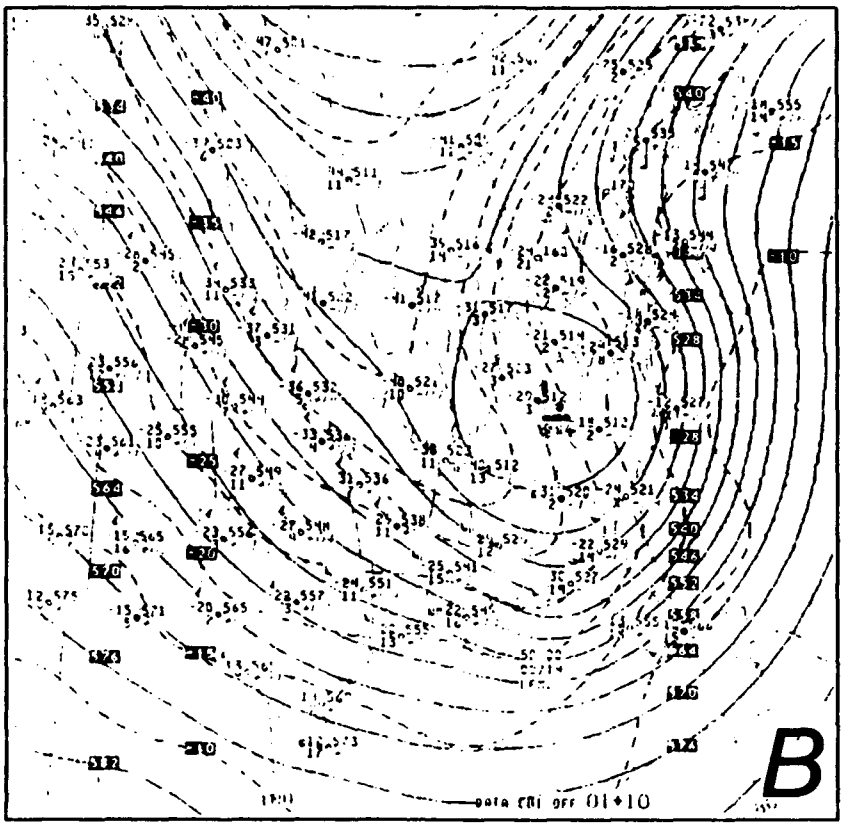
B

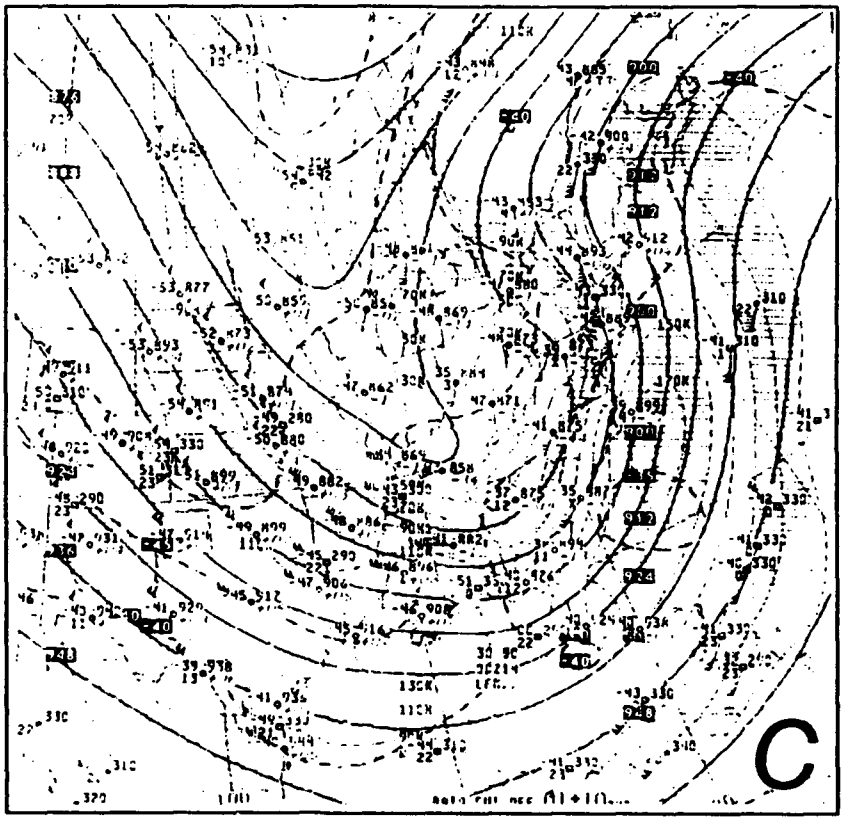
C

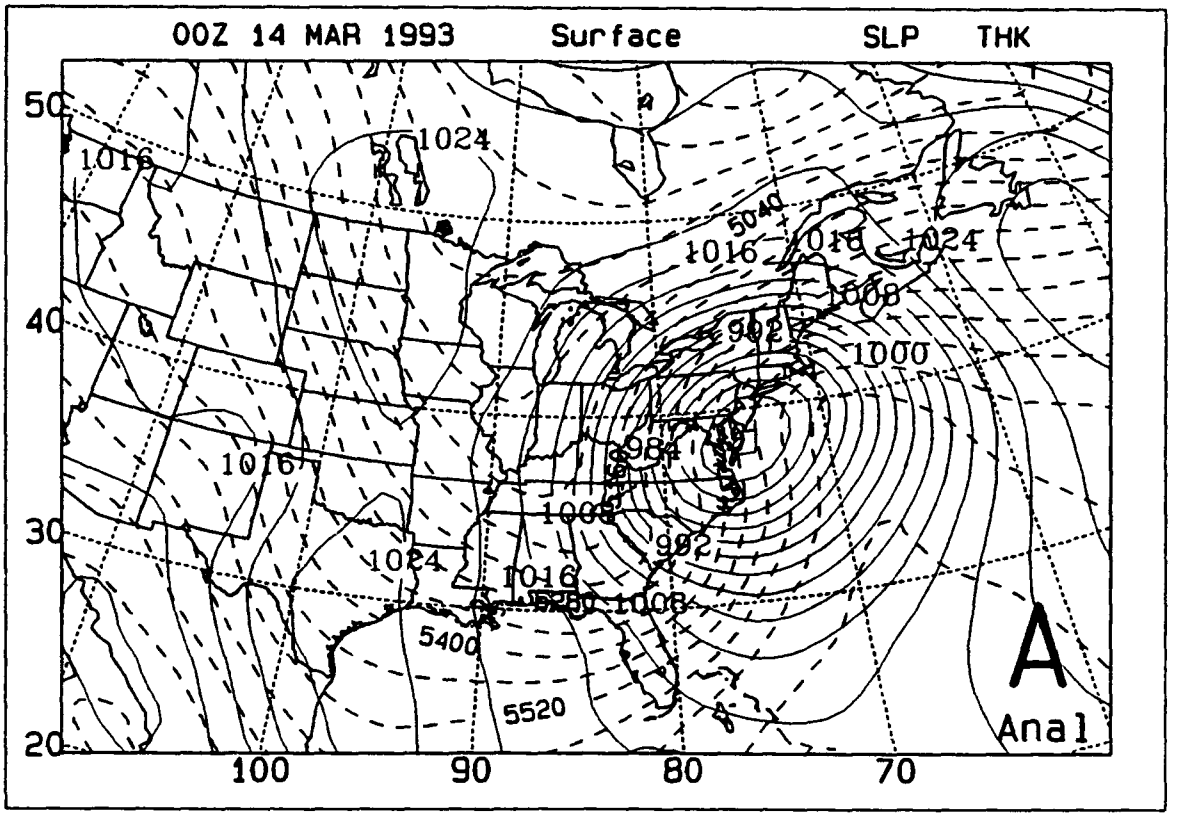

Figure 19. As in Figure 7, except for 0000 UTC 14 March 1993.

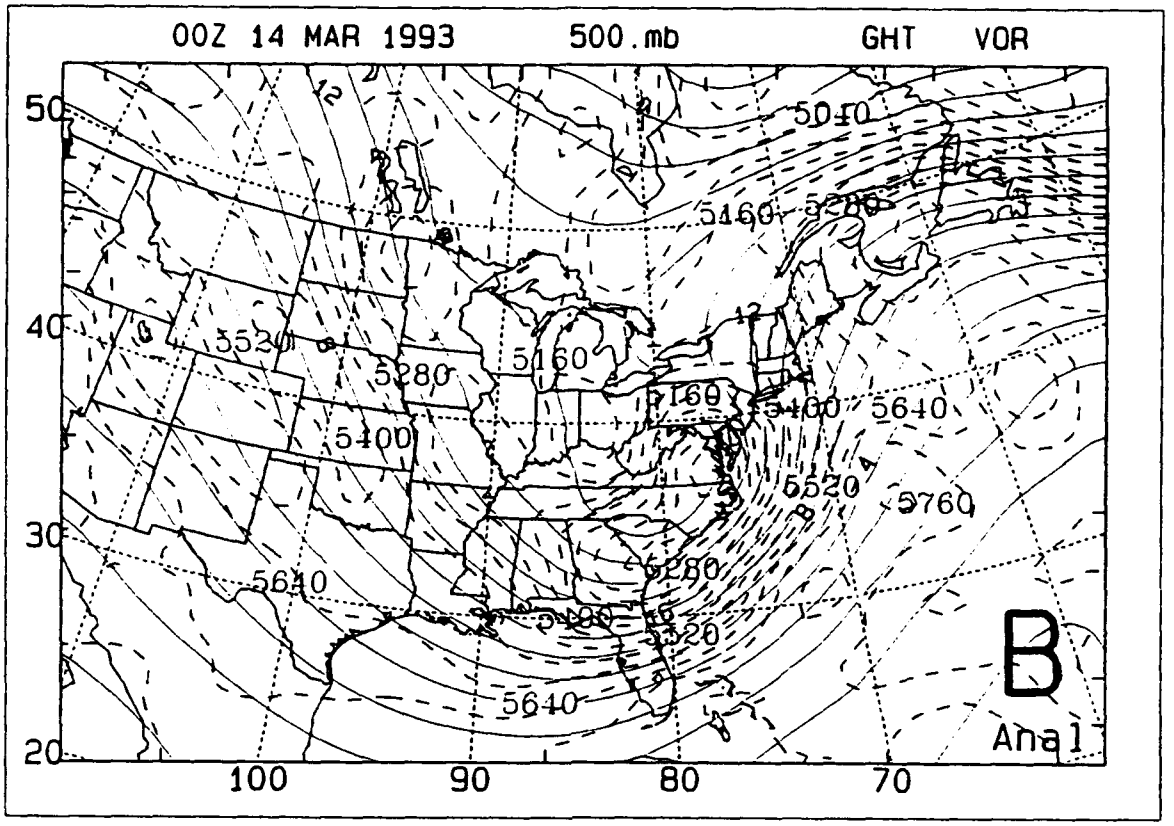
00Z 14 MAR 1993
500.mb
GHT
VOR
5040
5160
5280
5400
5520
5640
5760
50
40
30
20
100
90
80
70
B
Anal

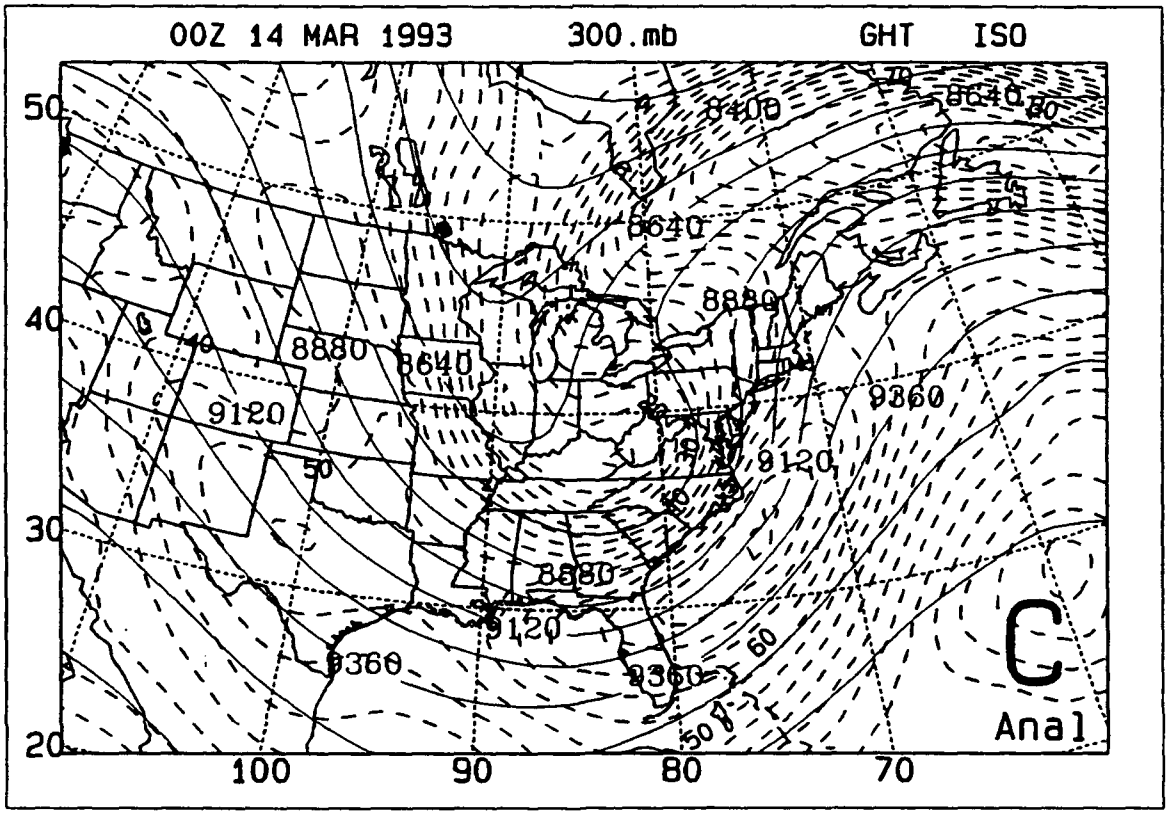
00Z 14 MAR 1993
300.mb
GHT
ISO
8400
8640
8880
9120
9360
50
40
30
20
100
90
80
70
C
Anal

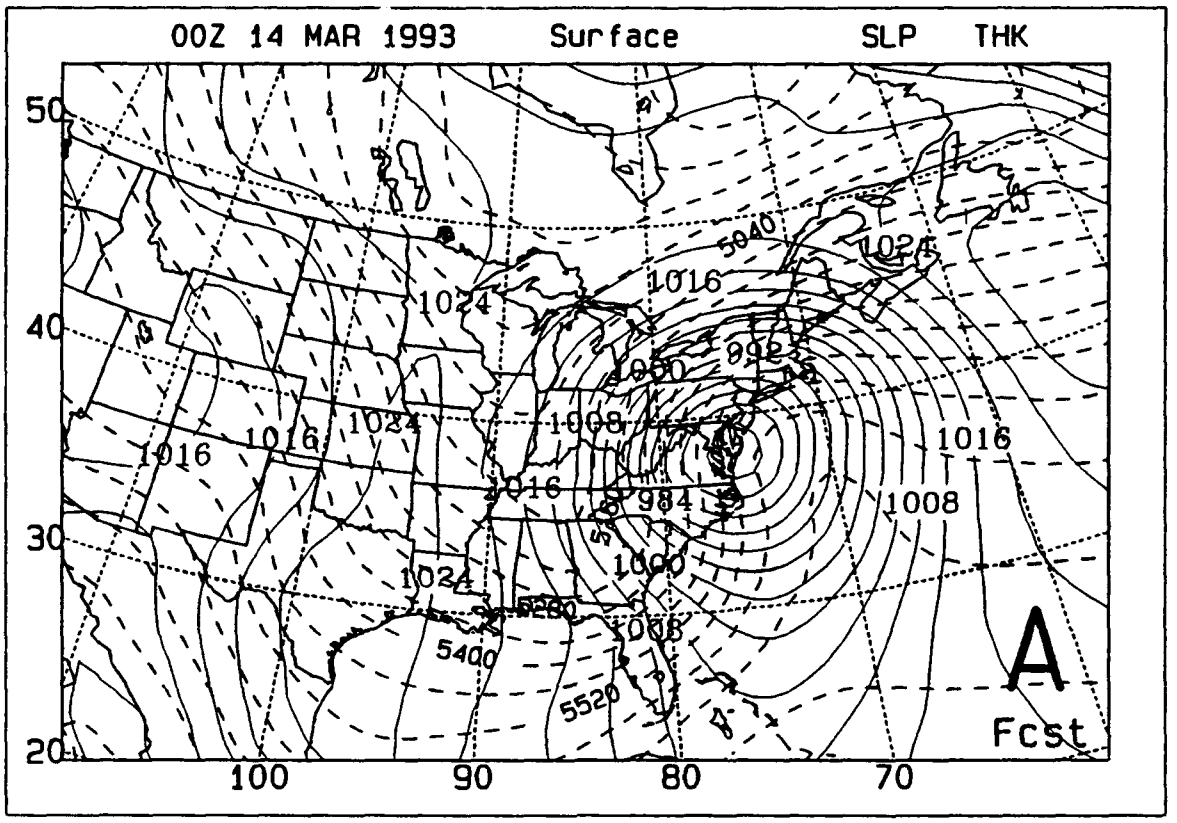

Figure 20. As in Figure 8, except for 36 h forecast verifying at 0000 UTC 14 March 1993.

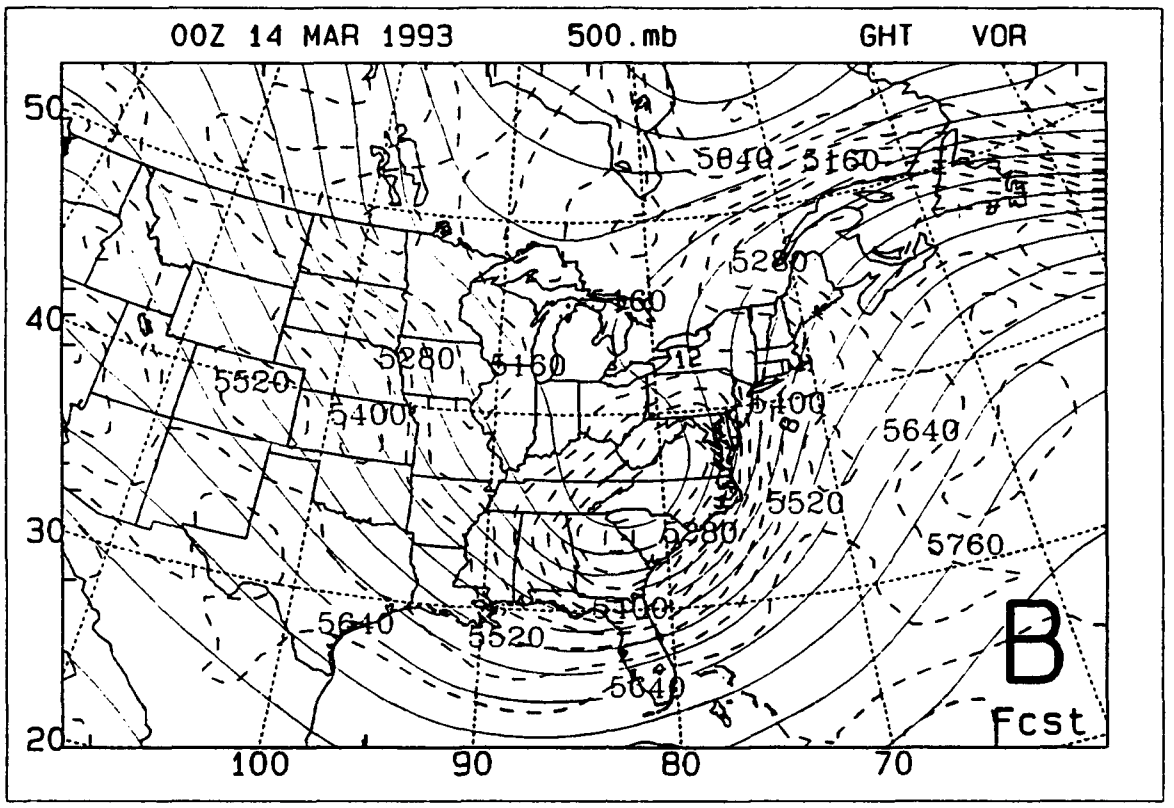
00Z 14 MAR 1993
500.mb
GHT
VOR
5040
5160
5280
5400
5520
5640
5760
5880
B
Fcst
50
40
30
20
100
90
80
70

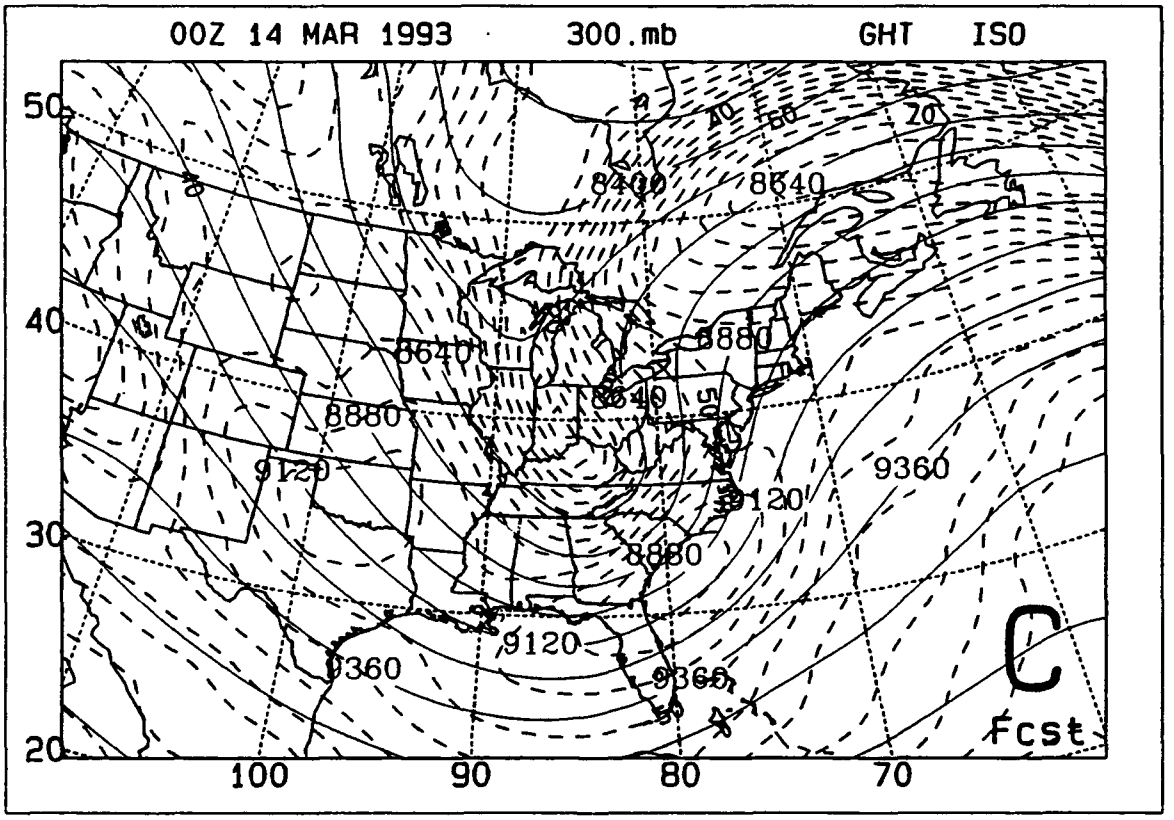
00Z 14 MAR 1993
300.mb
GHT
ISO
8400
8640
8880
9120
9360
C
Fcst
50
40
30
20
100
90
80
70

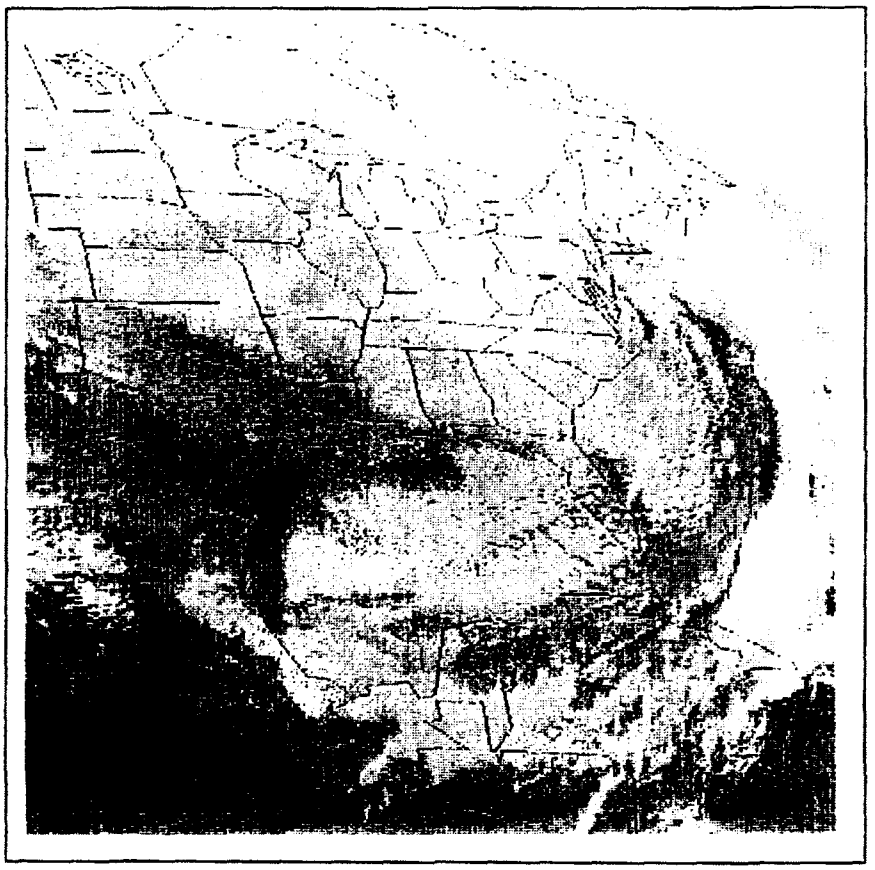

Figure 21. GOES infrared imagery for 0001 UTC 14 March 1993.

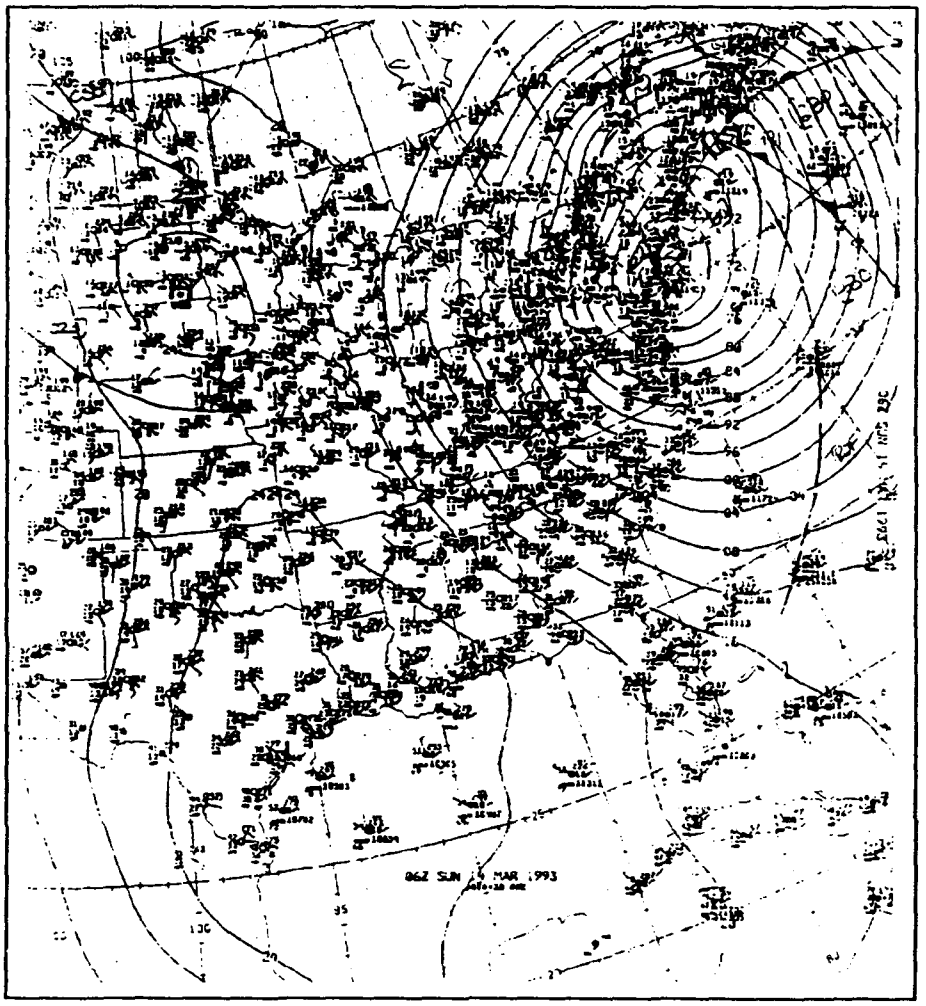

Figure 22. As in Figure 6, except for 0600 UTC 14 March 1993.

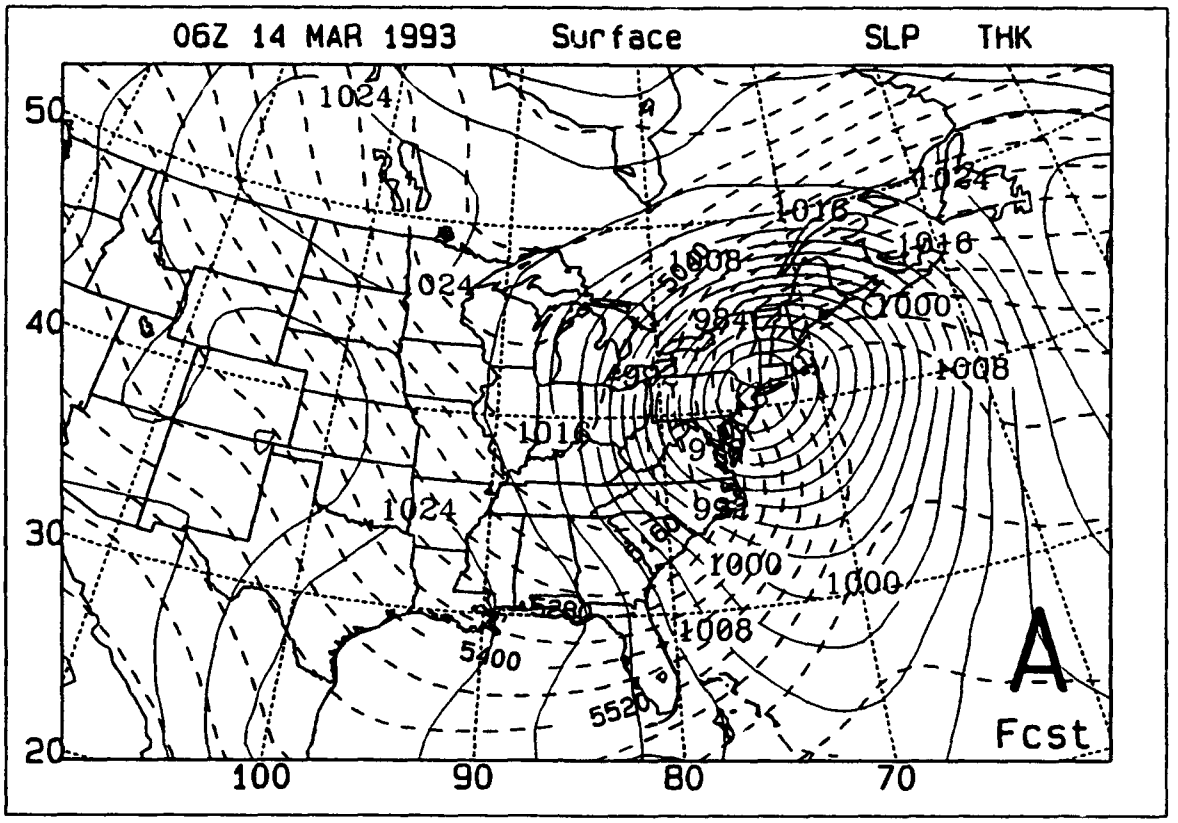

Figure 23. As in Figure 8, except for 42 h forecast verifying at 0600 UTC 14 March 1993.

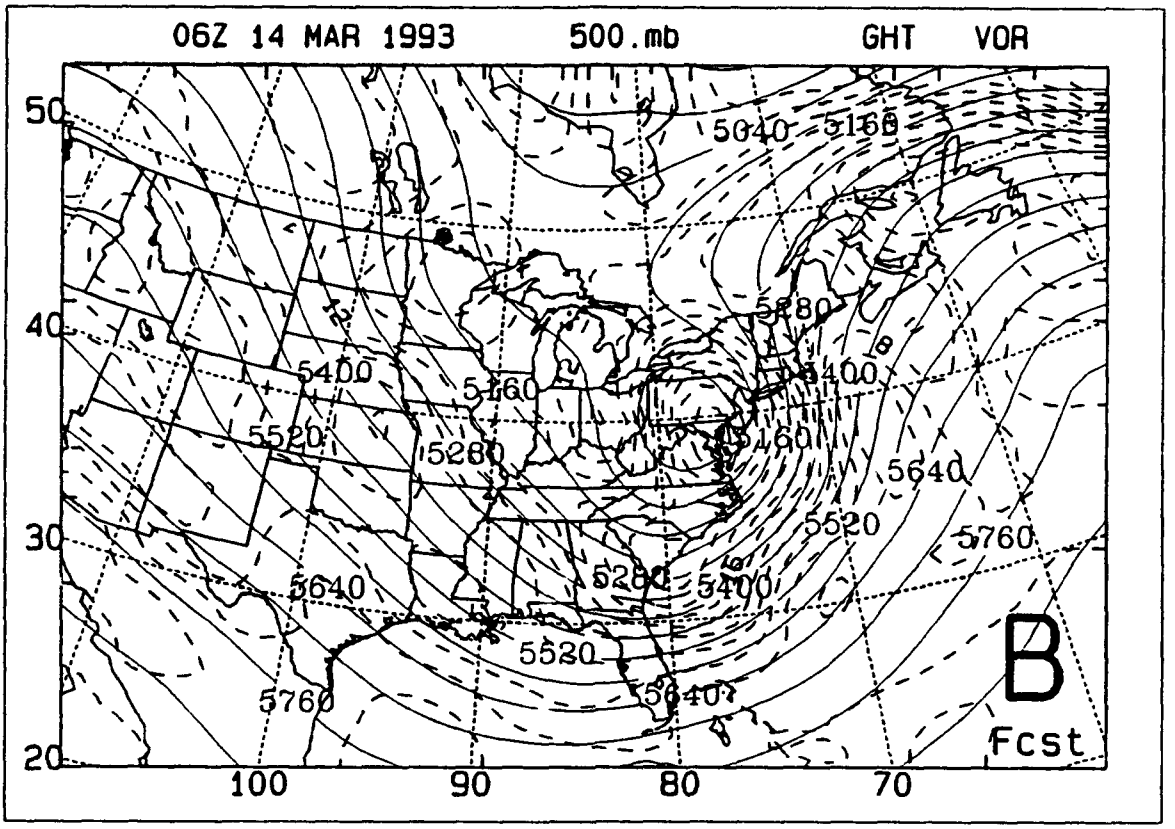
06Z 14 MAR 1993
500.mb
GHT
VOR
5040
5160
5280
5400
5520
5640
5760
B
Fcst
50
40
30
20
100
90
80
70

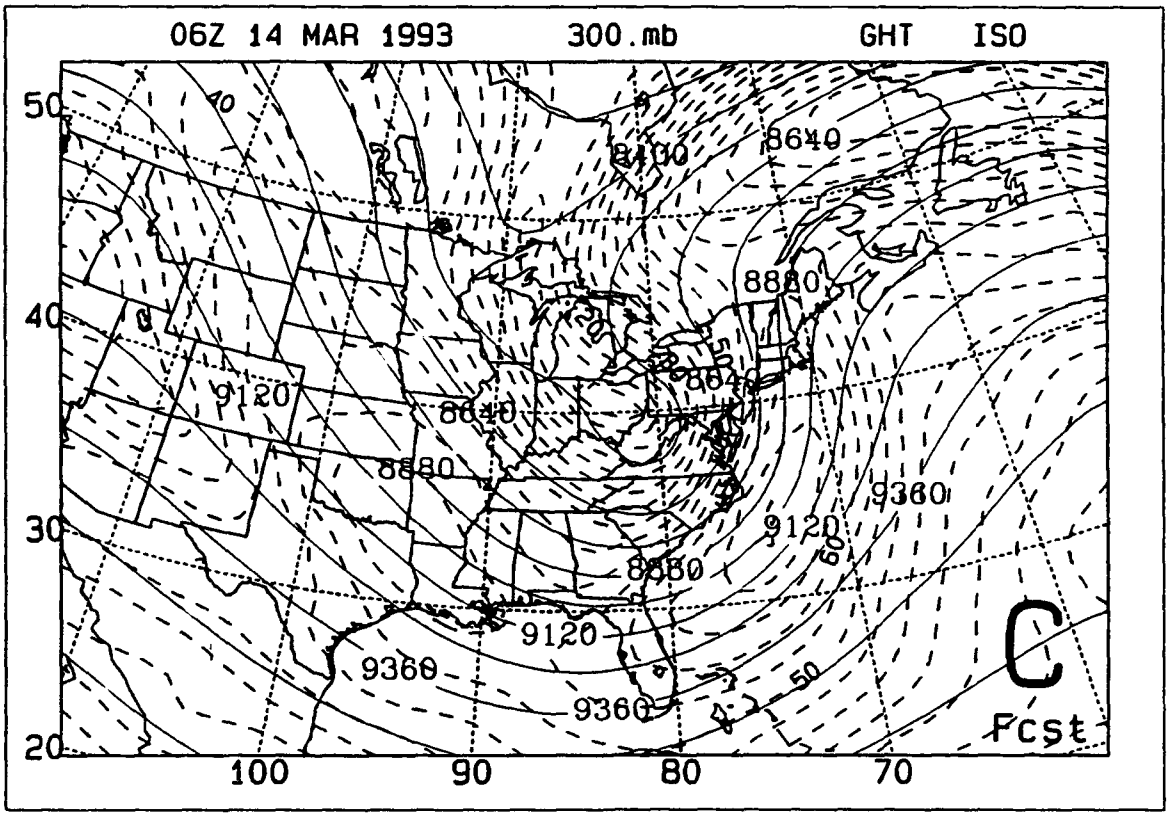
06Z 14 MAR 1993
300.mb
GHT
ISO
8400
8640
8880
9120
9360
C
Fcst
50
40
30
20
100
90
80
70

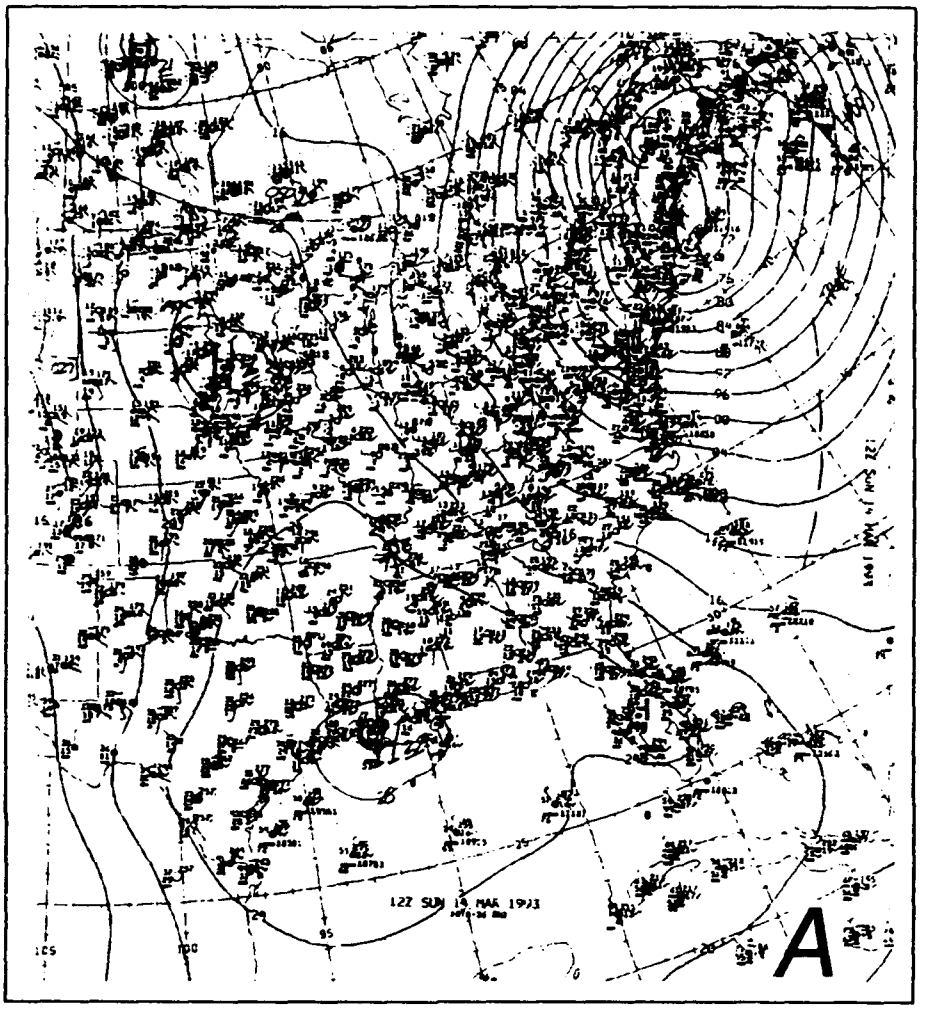

Figure 24. As in Figure 6, except for 1200 UTC 14 March 1993.

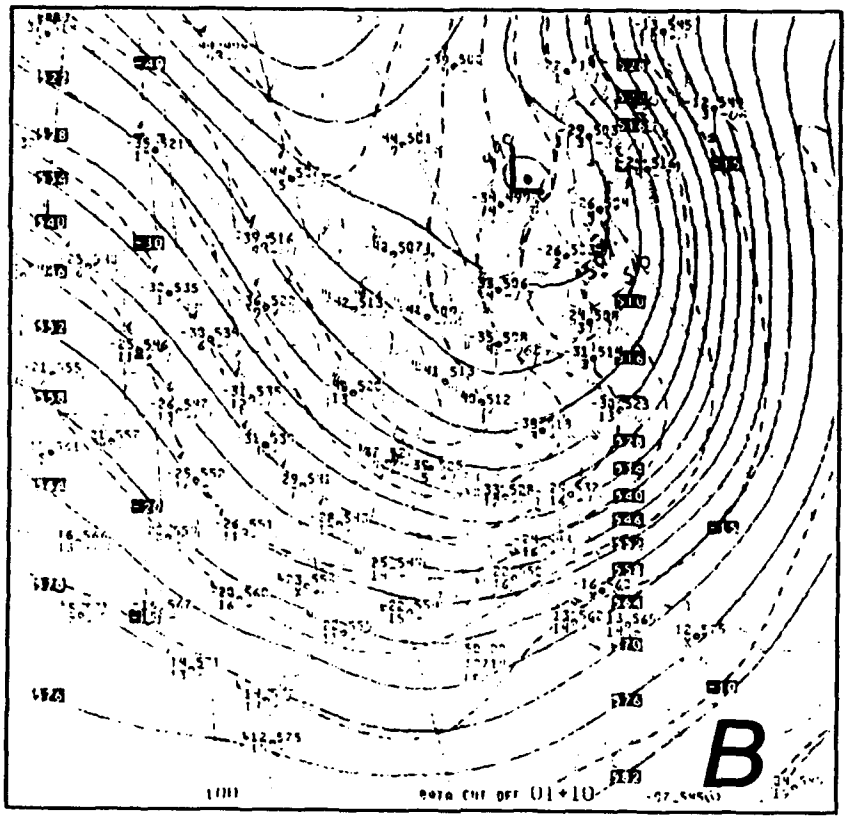
B
DATA CUT OFF 01+10

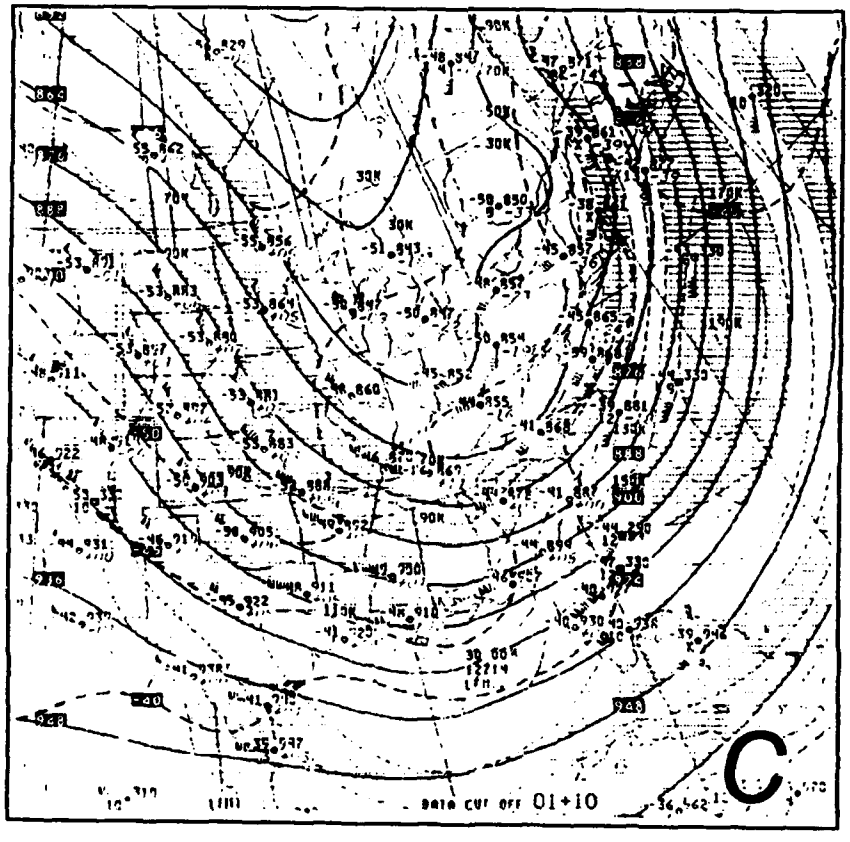
C
DATA CUT OFF 01+10

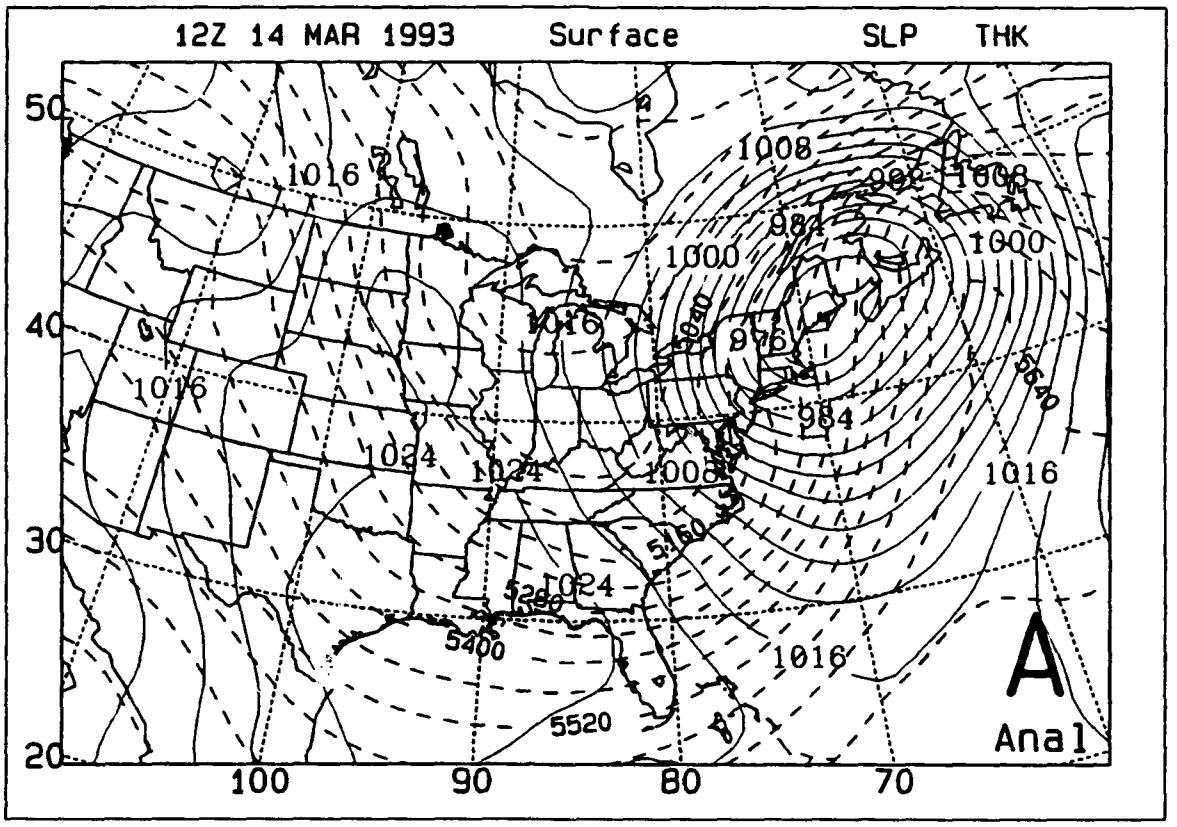

Figure 25. As in Figure 7, except for 1200 UTC 14 March 1993.

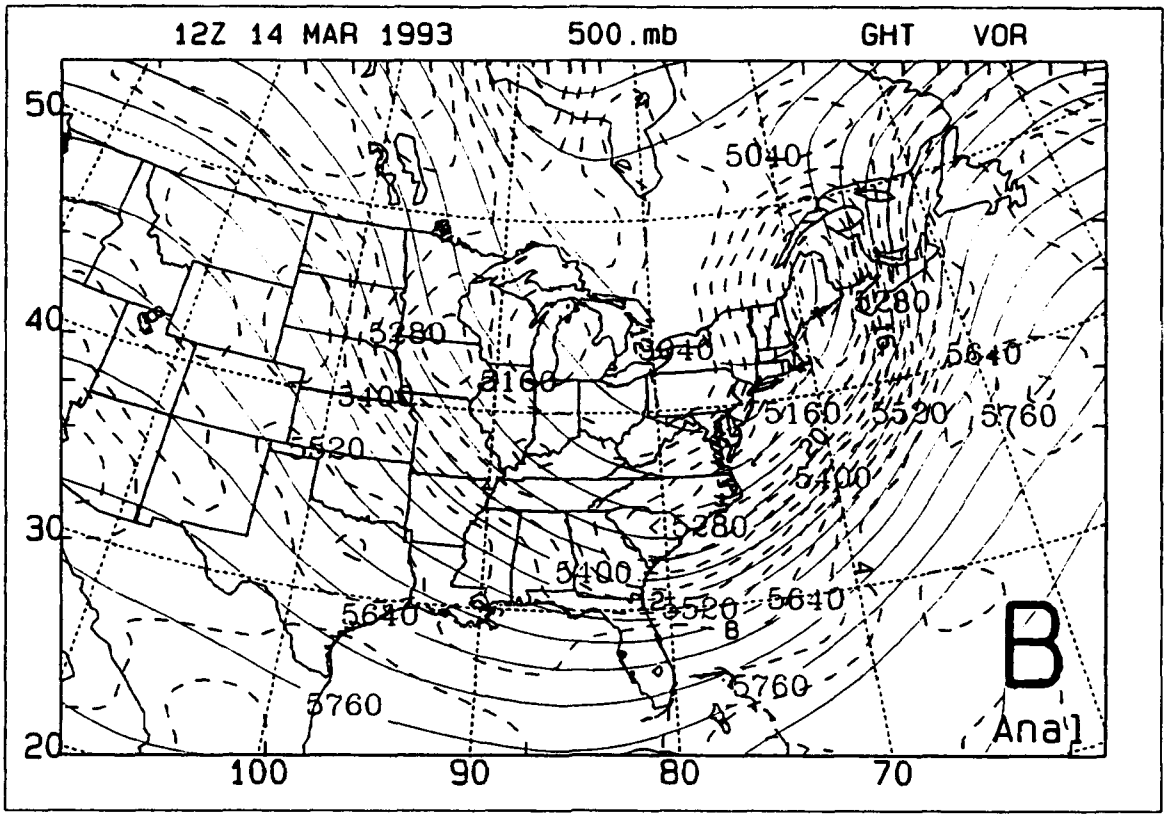
12Z 14 MAR 1993
500.mb
GHT
VOR
50
40
30
20
100
90
80
70
5040
5280
5640
5160
5520
5760
5400
5280
5400
5520
5640
5760
B
Anal

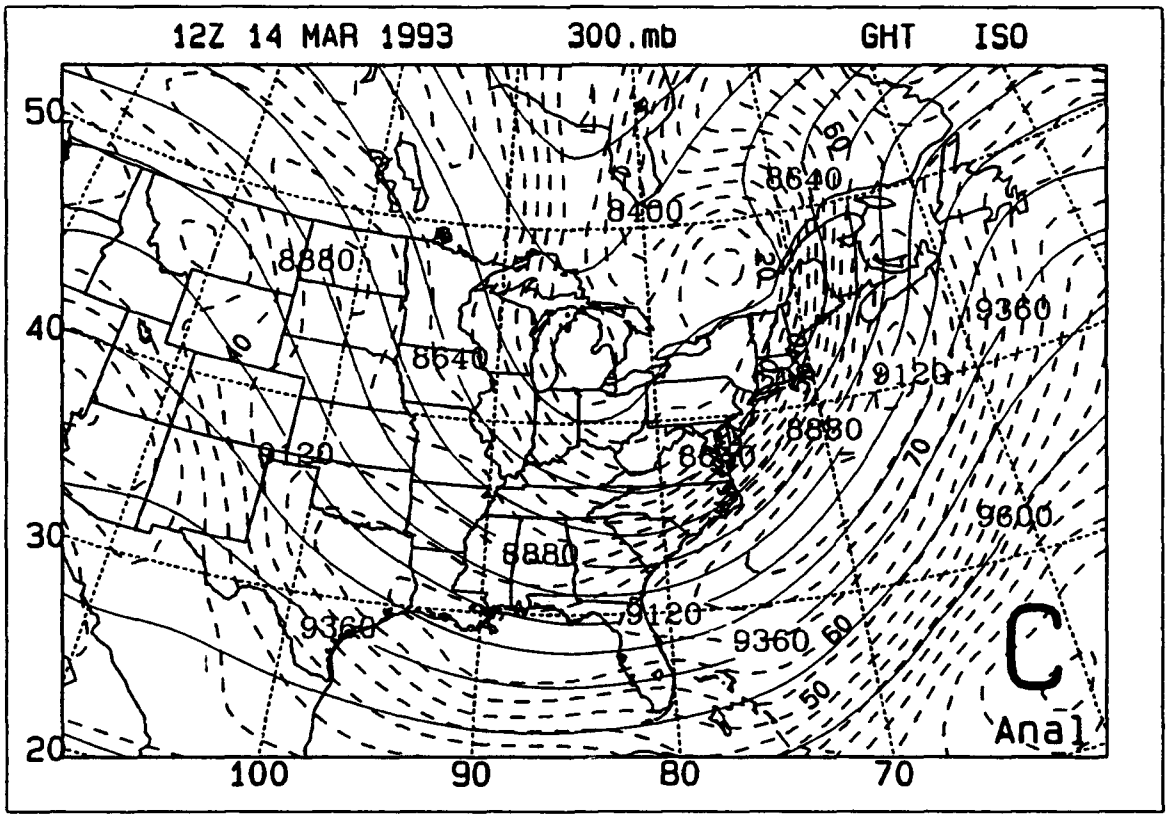
12Z 14 MAR 1993
300.mb
GHT
ISO
50
40
30
20
100
90
80
70
8400
8640
8880
9120
9360
9600
C
Anal

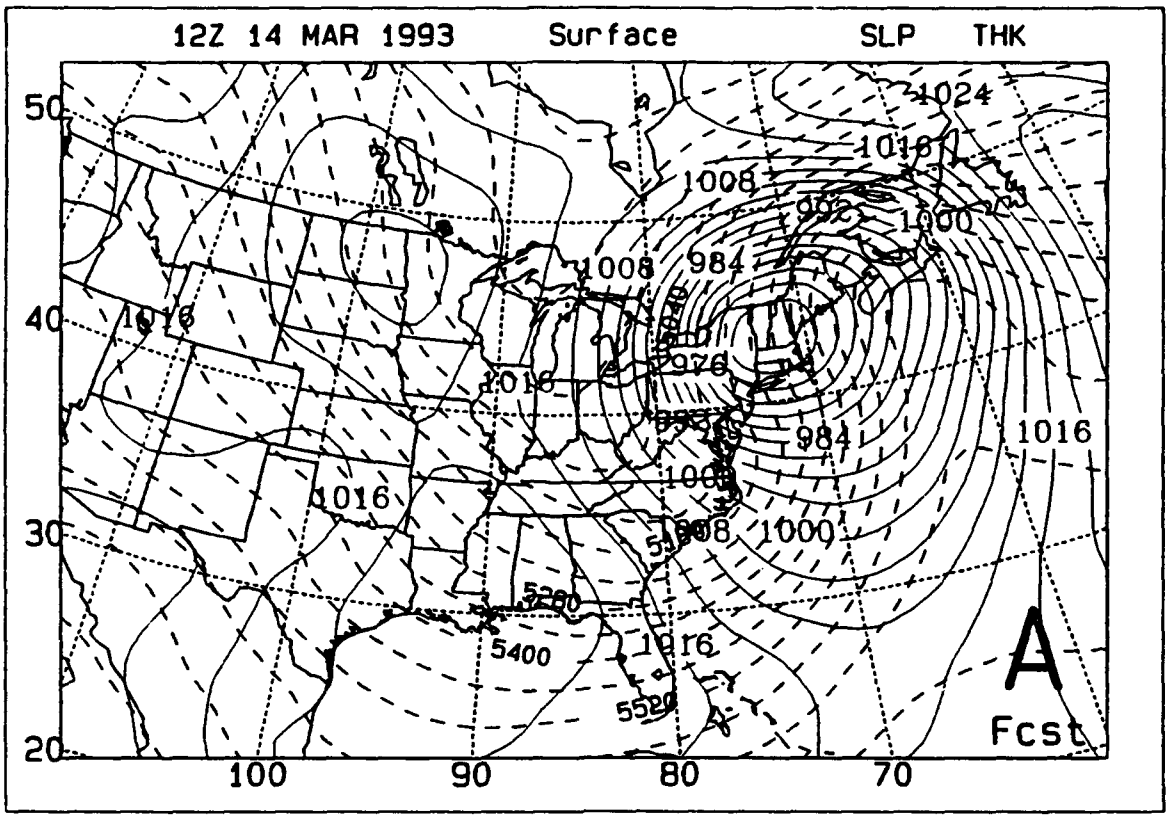

Figure 26. As in Figure 8, except for 48 h forecast verifying at 1200 UTC 14 March 1993.

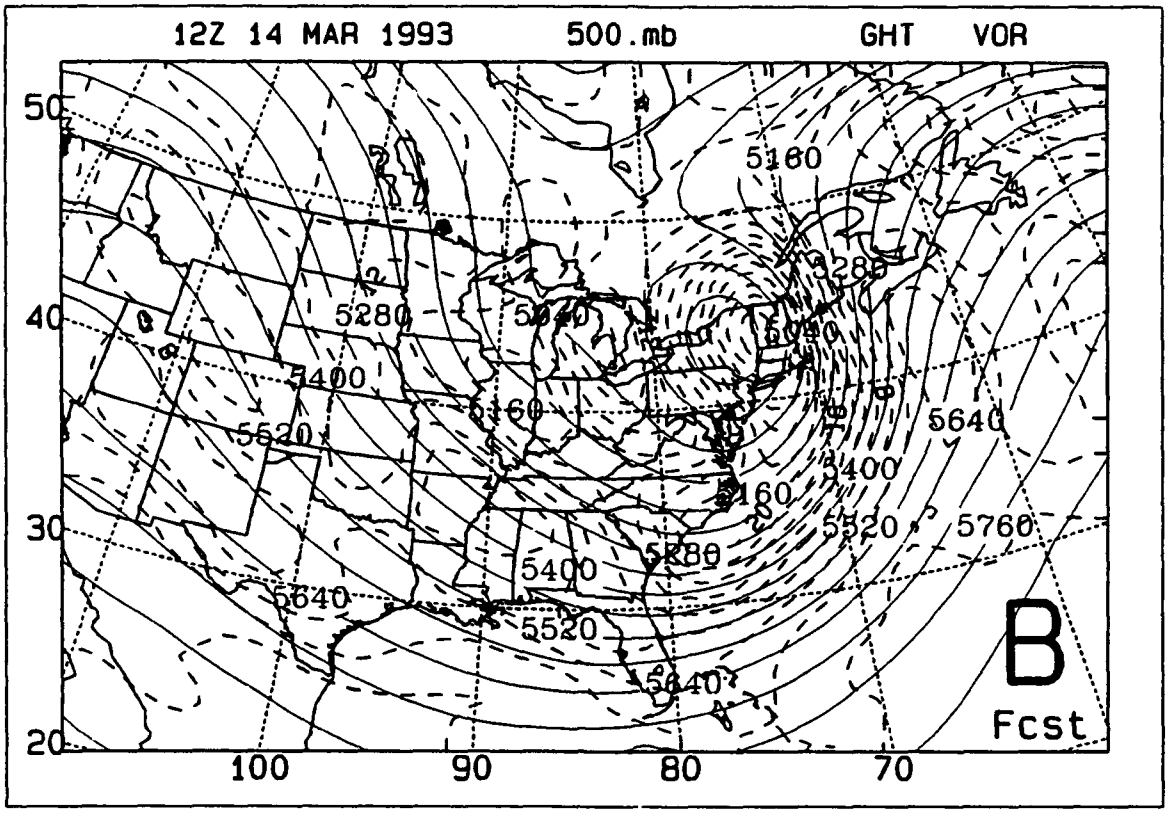
12Z 14 MAR 1993
500.mb
GHT
VOR
5160
5280
5400
5520
5640
5760
5880
B
Fcst
50
40
30
20
100
90
80
70

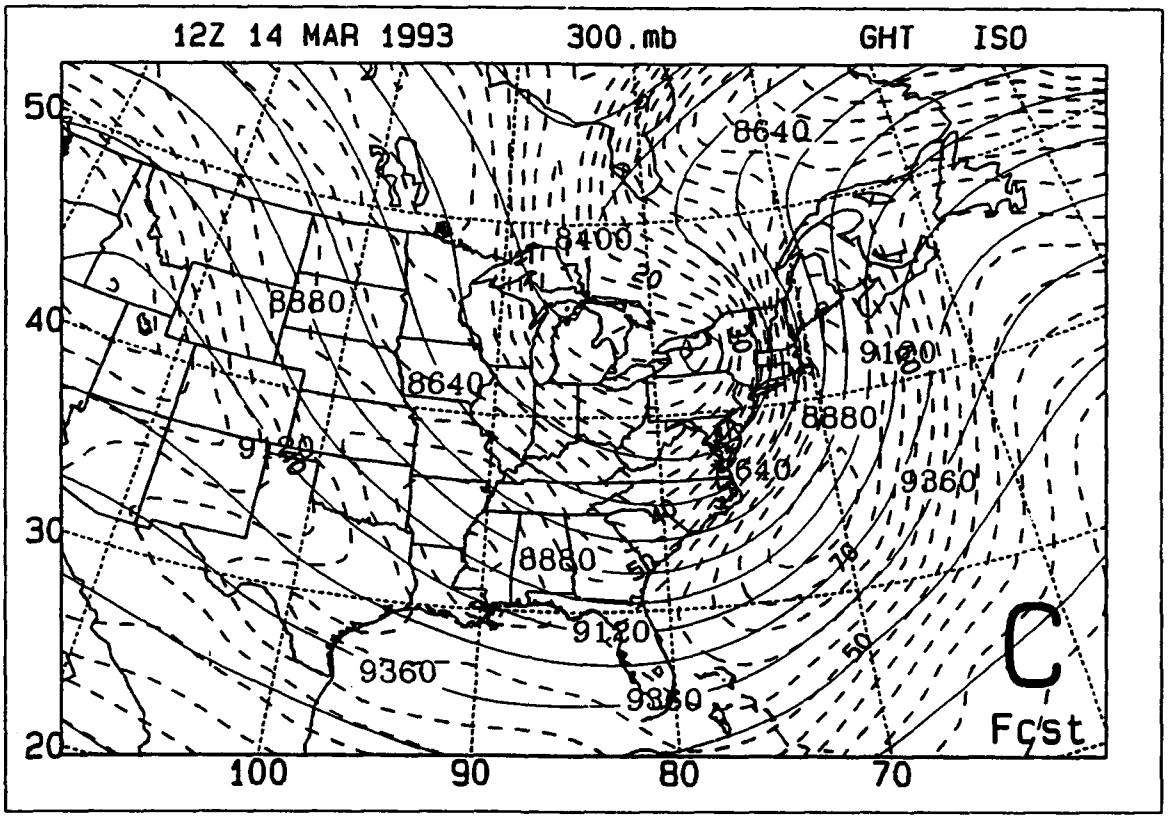
12Z 14 MAR 1993
300.mb
GHT
ISO
8400
8640
8880
9120
9360
C
Fcst
50
40
30
20
100
90
80
70

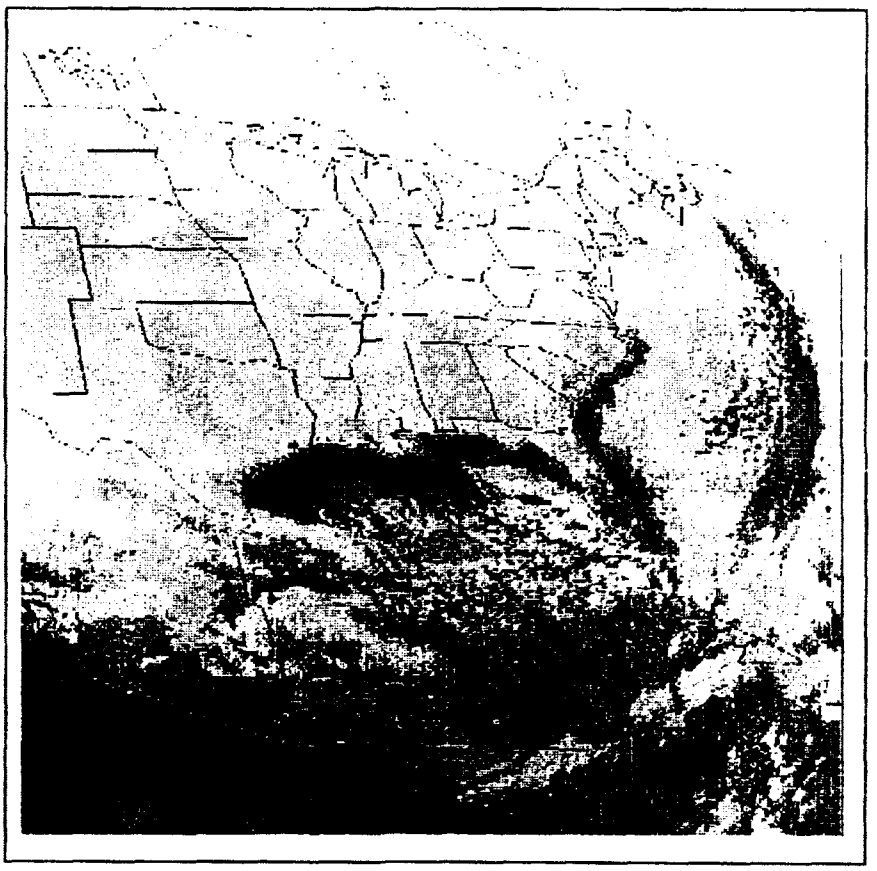

Figure 27. GOES infrared imagery for 1201 UTC 14 March 1993.

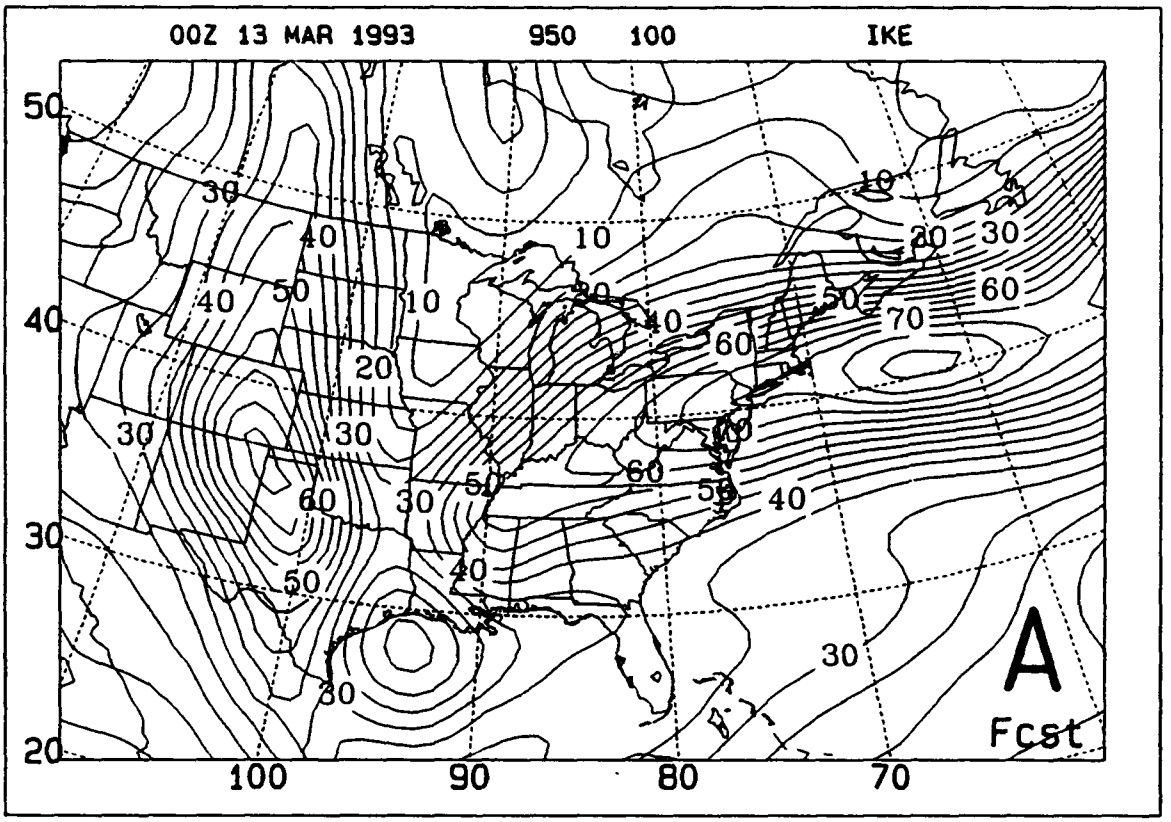

Figure 28. Vertically-integrated kinetic energy content (IKE) based on the NMC Global Spectral Model Forecast for 0000 UTC 13 March 1993 (5×10^5 J m^{-2} increment). (**A**) Integration from 950 mb to 100 mb; (**B**) integration from 950 mb to 700 mb; (**C**) integration from 700 mb to 100 mb.

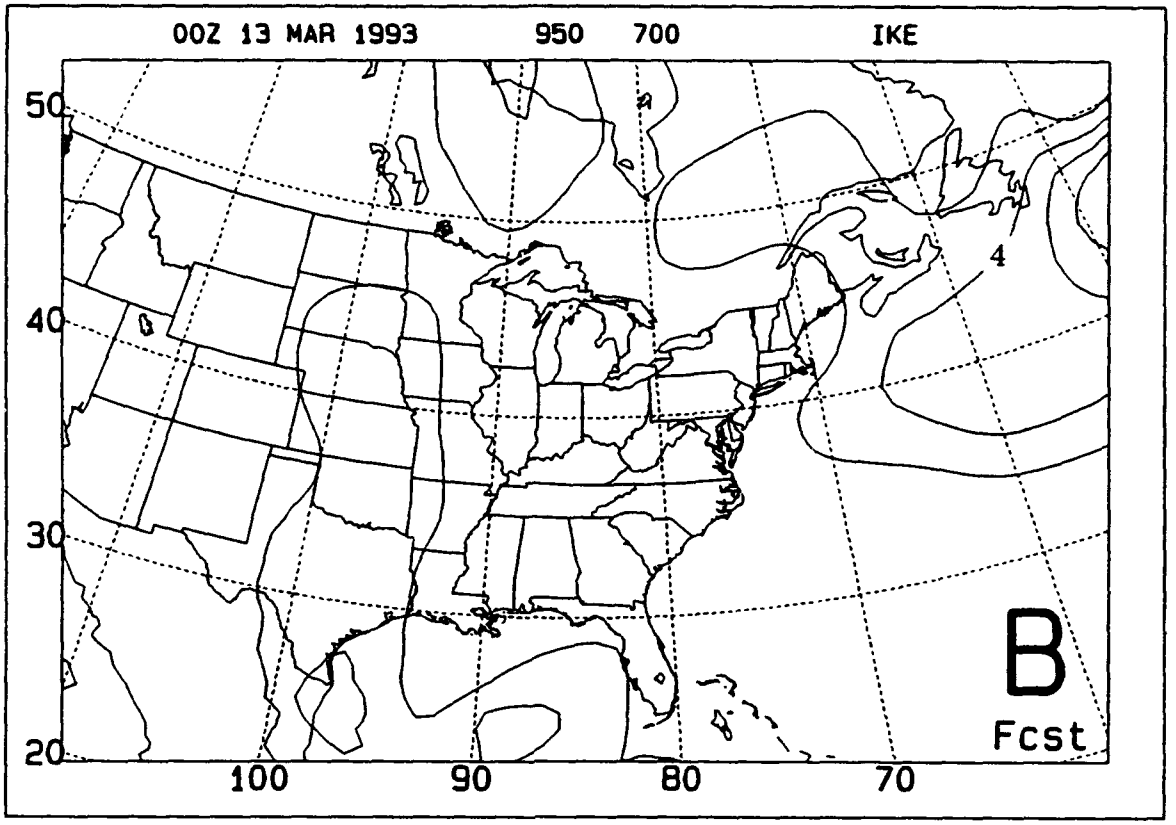
00Z 13 MAR 1993
950 700
IKE
50
40
30
20
100
90
80
70
4
B
Fcst

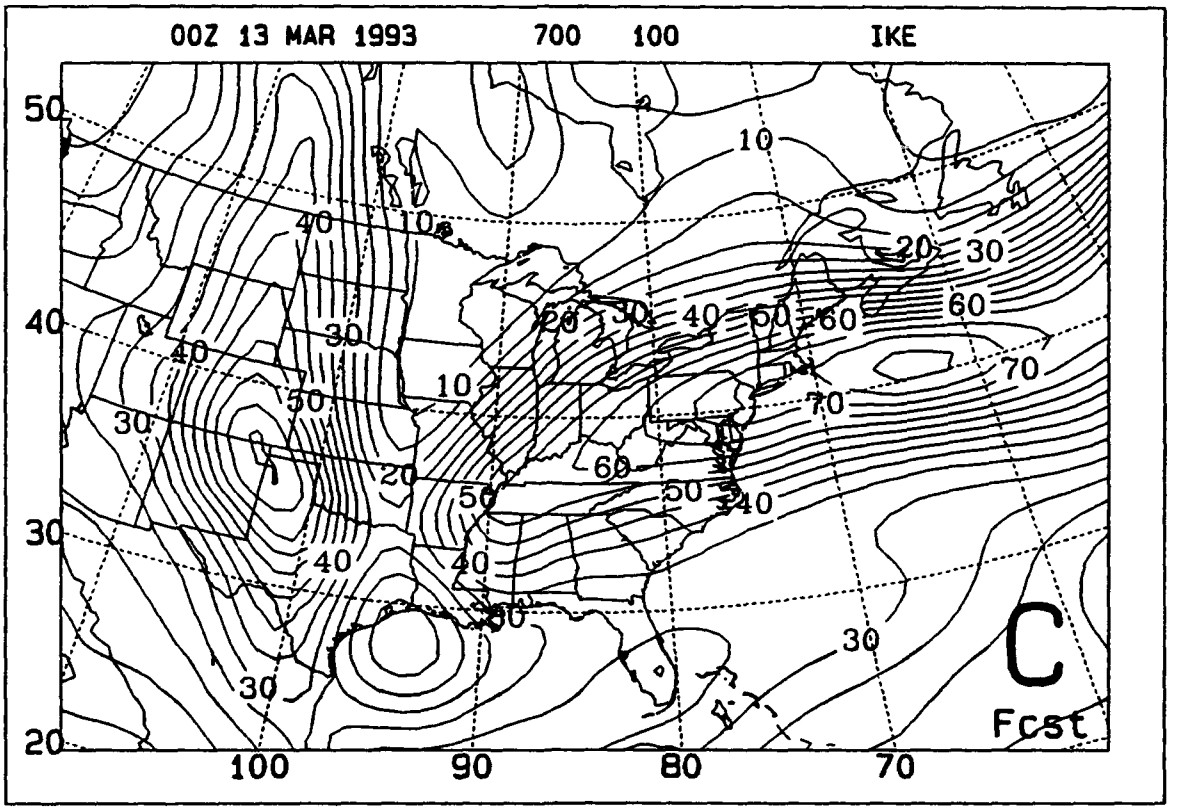
00Z 13 MAR 1993
700 100
IKE
50
40
30
20
100
90
80
70
10
20
30
40
50
60
70
C
Fcst

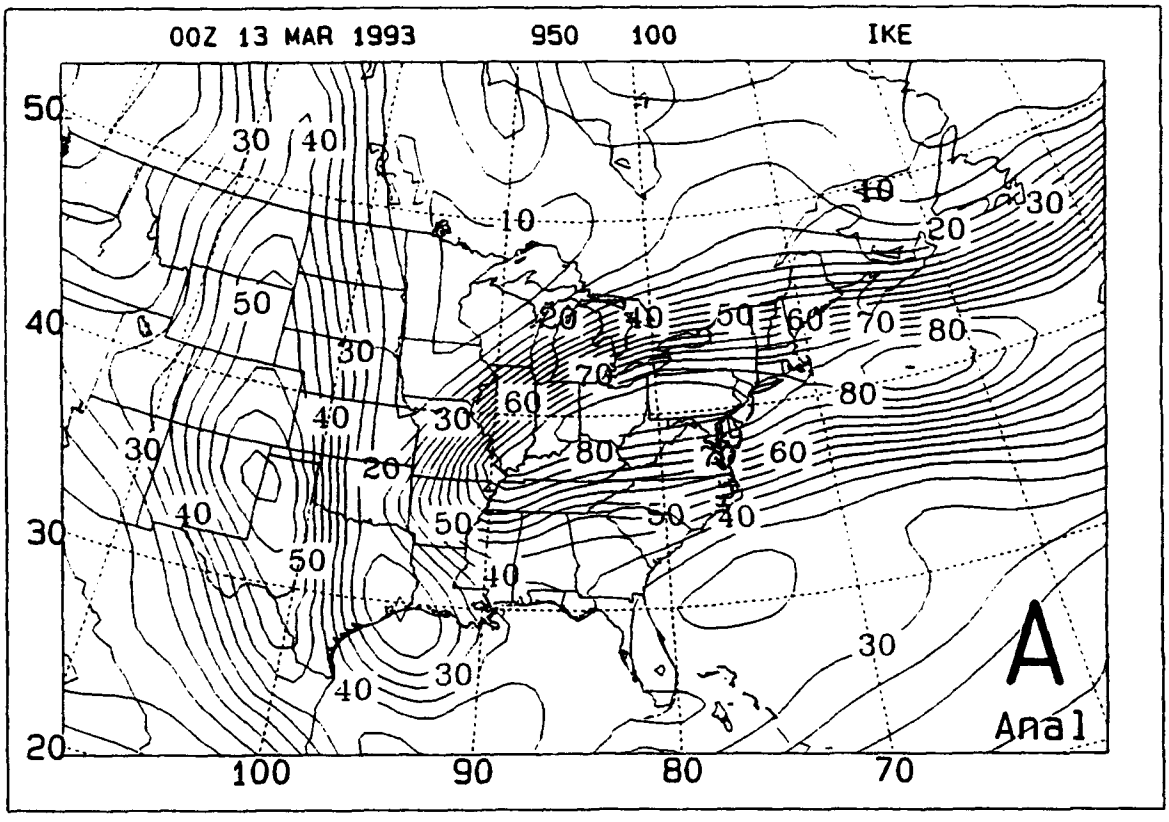

Figure 29. Vertically-integrated kinetic energy content (IKE) based on the NMC AVN Analysis for 0000 UTC 13 March 1993 ($5x10^5$ J m^{-2} increment). (**A**) Integration from 950 mb to 100 mb; (**B**) integration from 950 mb to 700 mb; (**C**) integration from 700 mb to 100 mb.

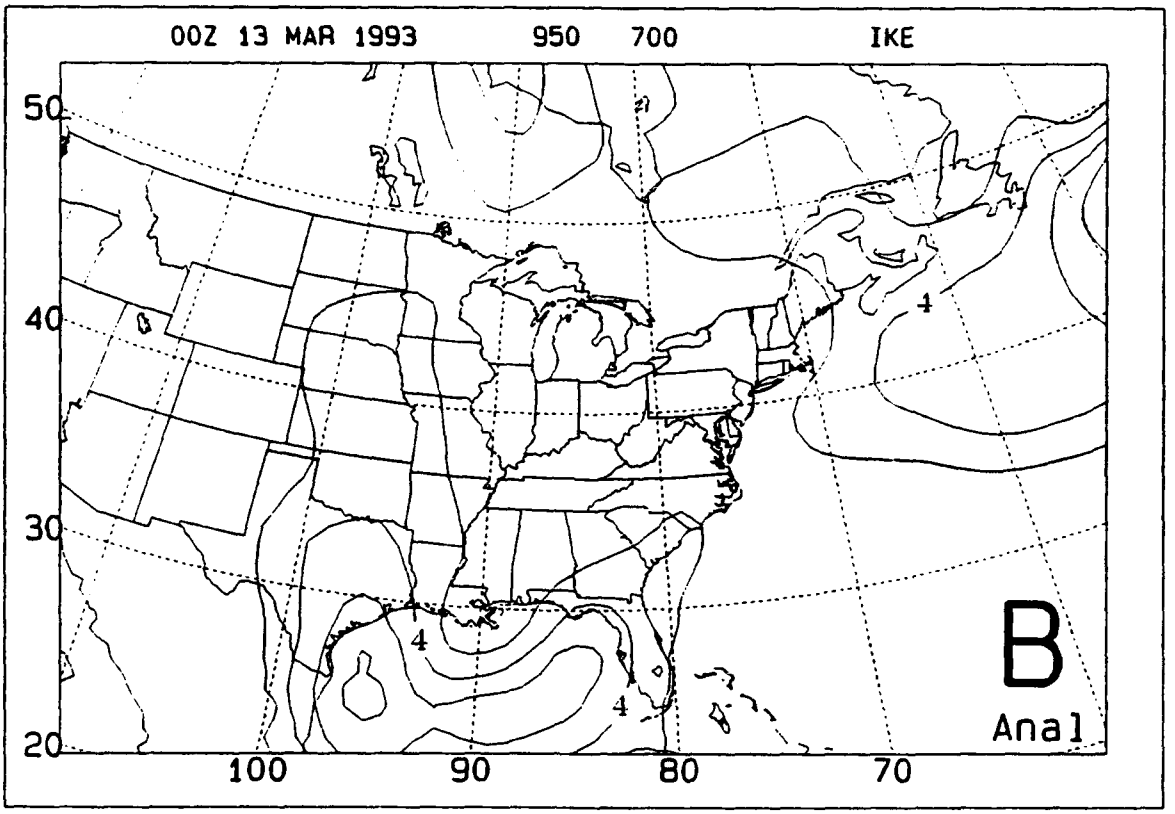
00Z 13 MAR 1993
950
700
IKE
50
40
30
20
100
90
80
70
4
4
4
B
Anal

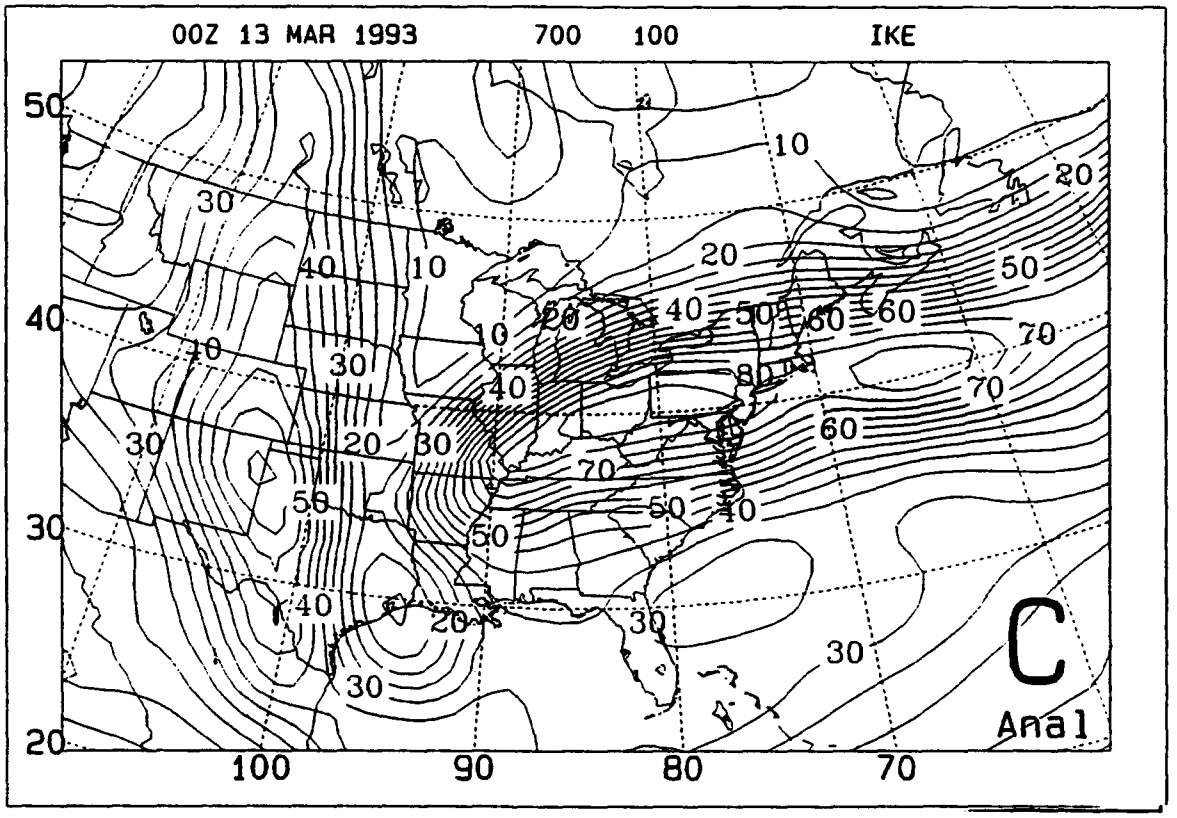
00Z 13 MAR 1993
700
100
IKE
50
40
30
20
100
90
80
70
10
20
30
40
50
60
70
80
C
Anal

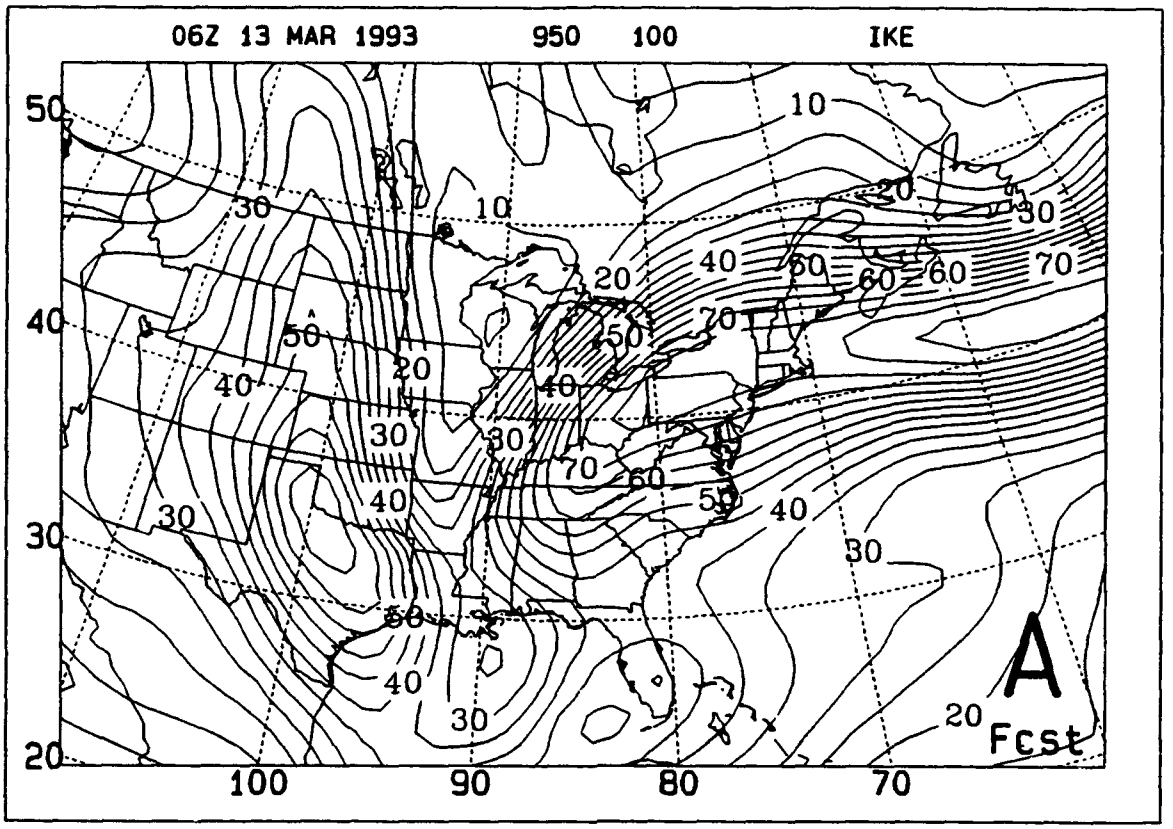

Figure 30. As in Figure 28, except for 0600 UTC 13 March 1993.

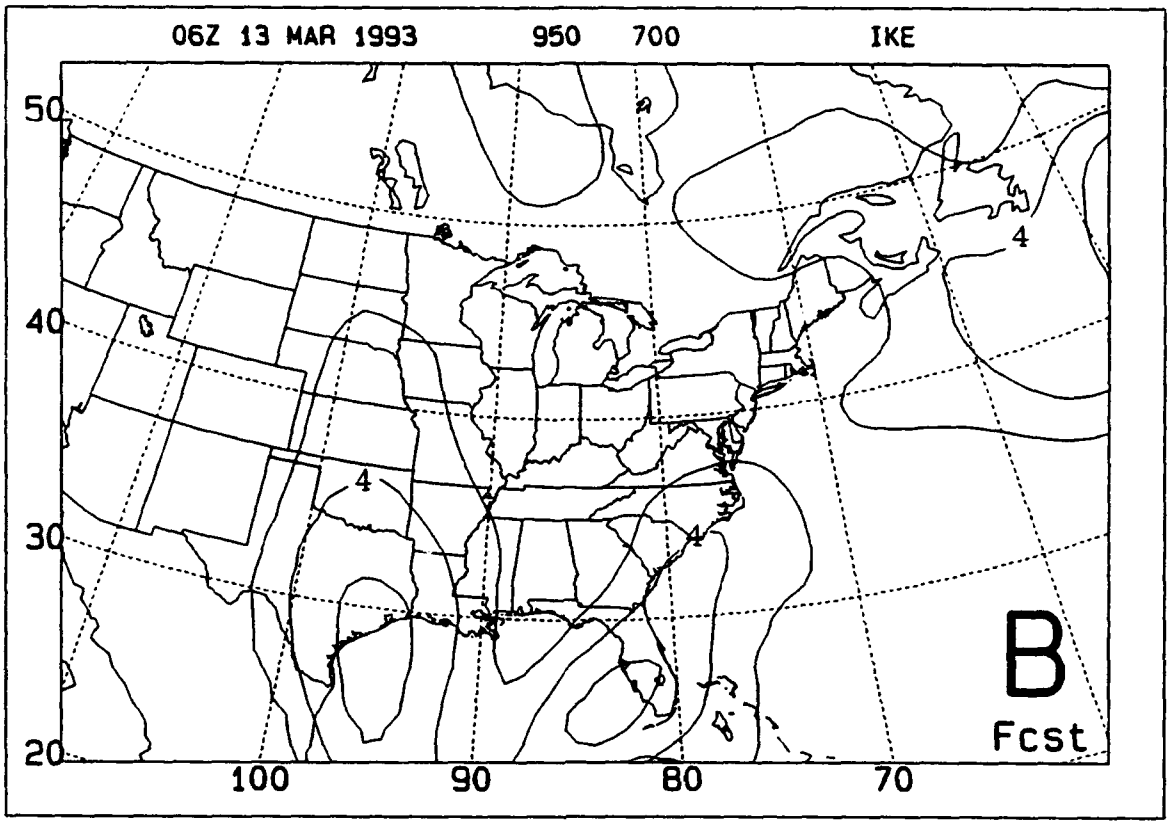
06Z 13 MAR 1993
950
700
IKE
50
40
30
20
100
90
80
70
4
4
4
B
Fcst

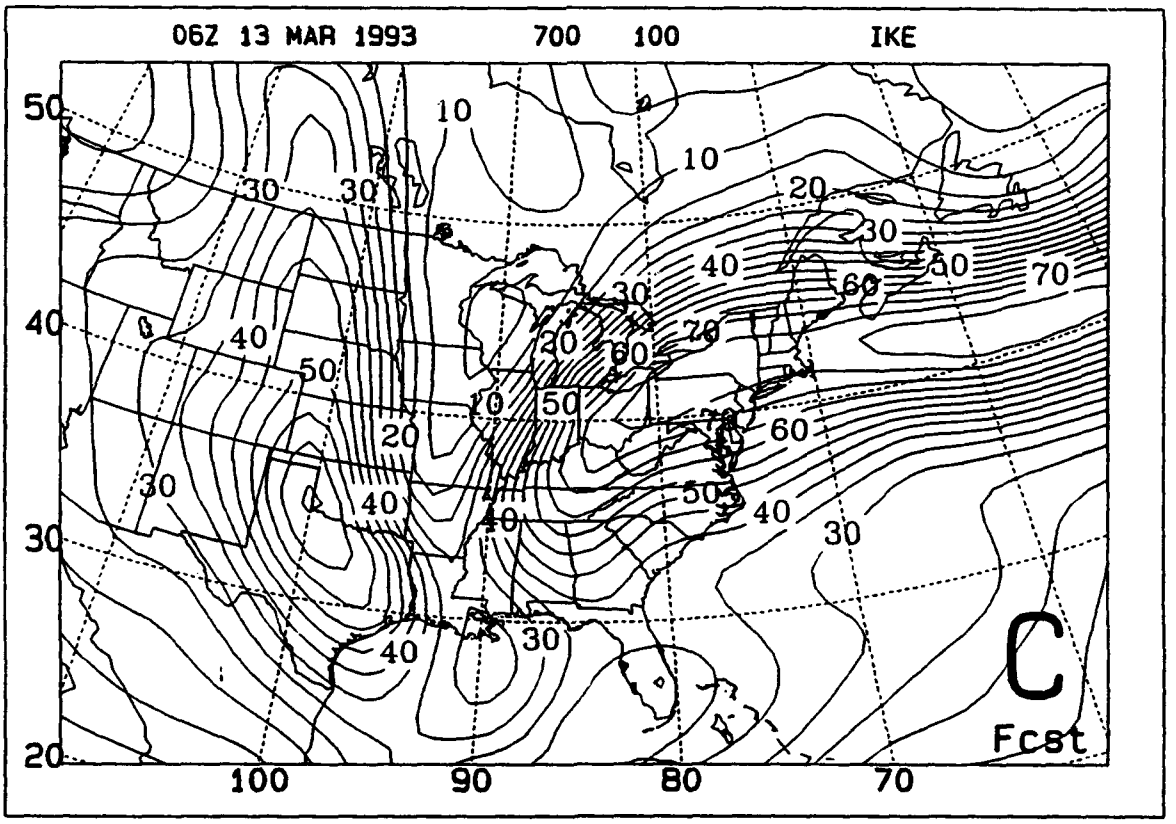
06Z 13 MAR 1993
700
100
IKE
50
40
30
20
100
90
80
70
10
10
20
30
40
50
60
70
C
Fcst

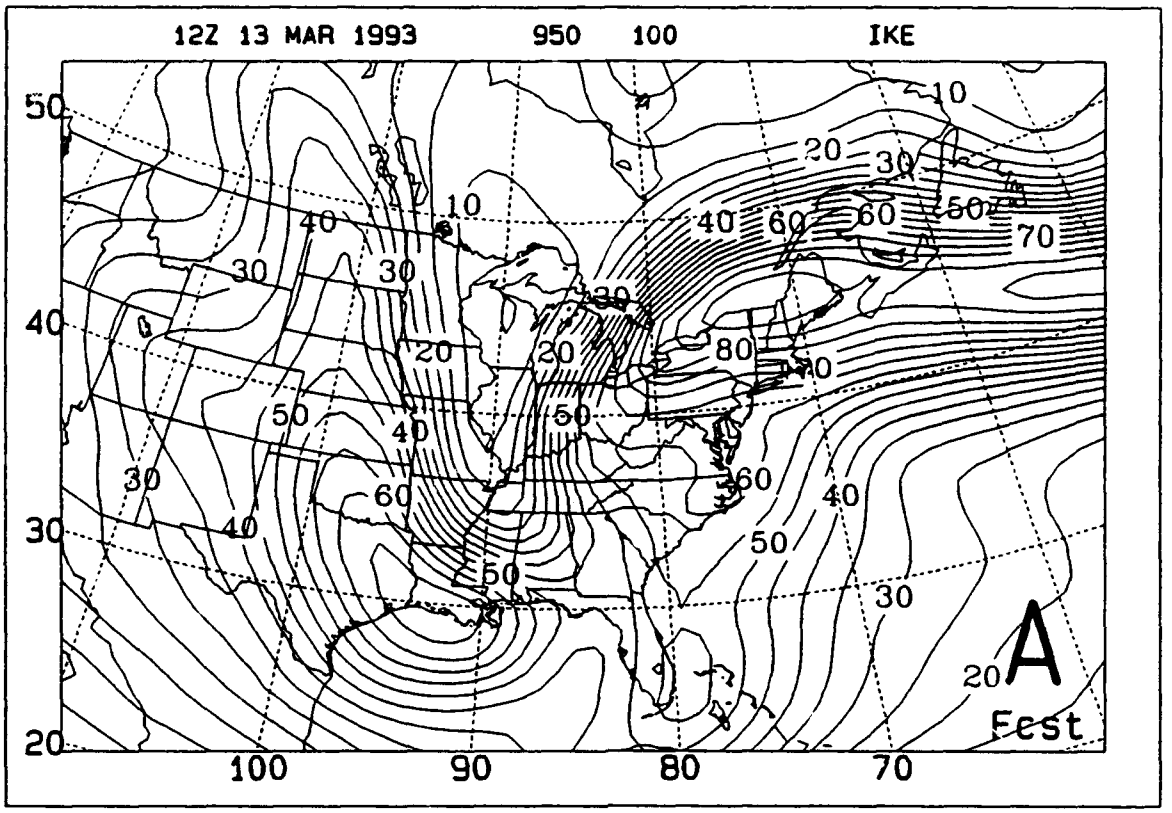

Figure 31. As in Figure 28, except for 1200 UTC 13 March 1993.

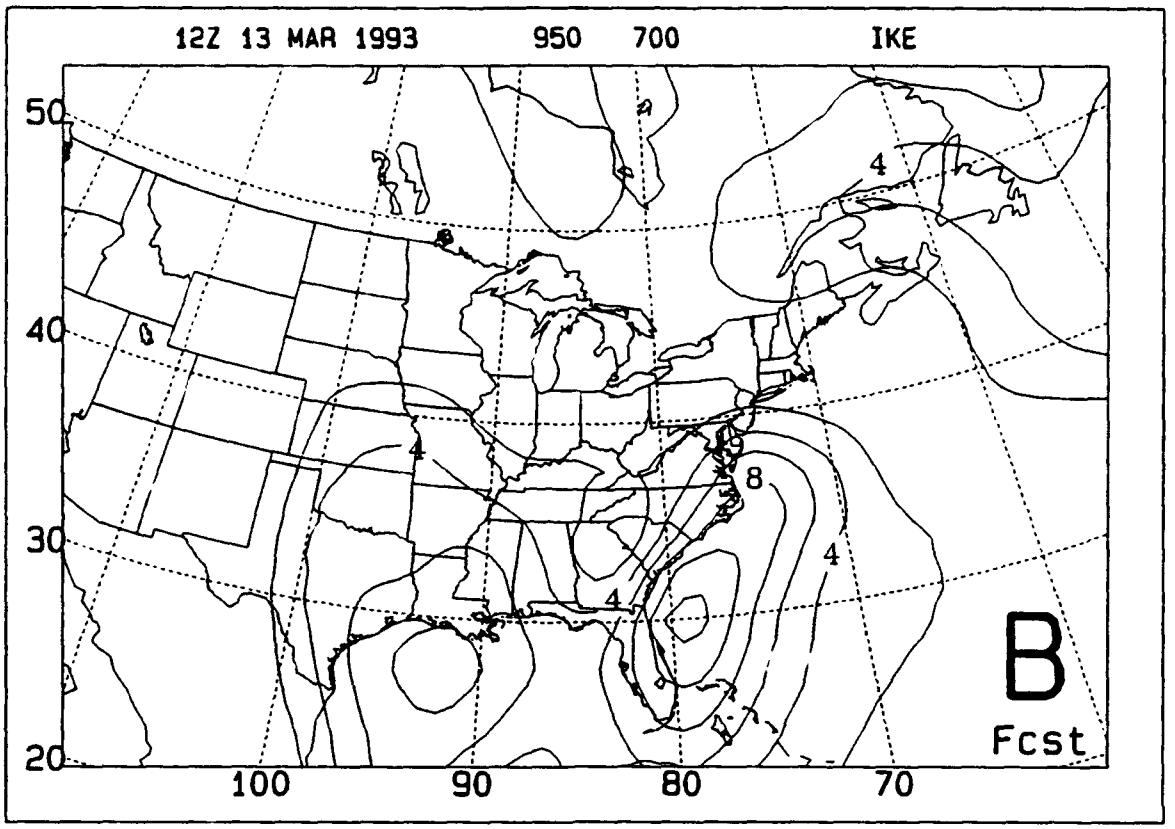
12Z 13 MAR 1993
950 700
IKE
50
40
30
20
100
90
80
70
4
8
B
Fcst

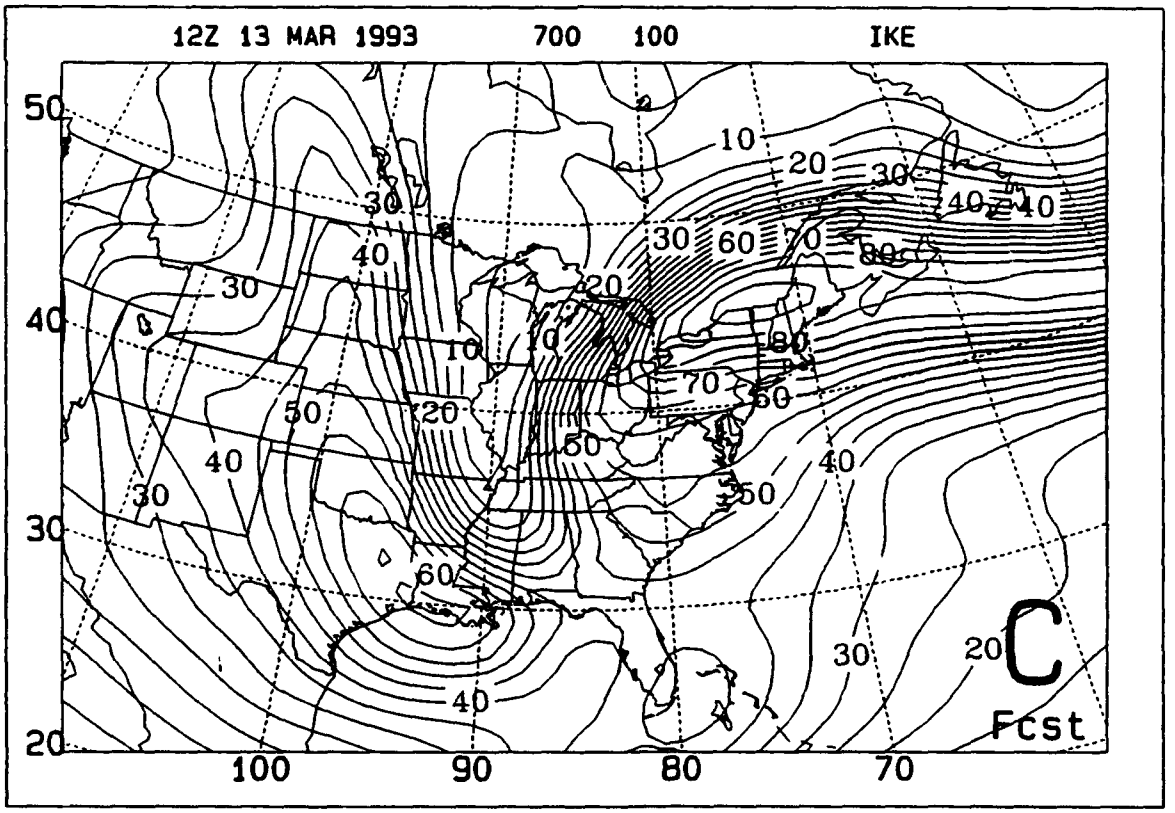
12Z 13 MAR 1993
700 100
IKE
50
40
30
20
100
90
80
70
10
20
30
40
50
60
70
80
C
Fcst

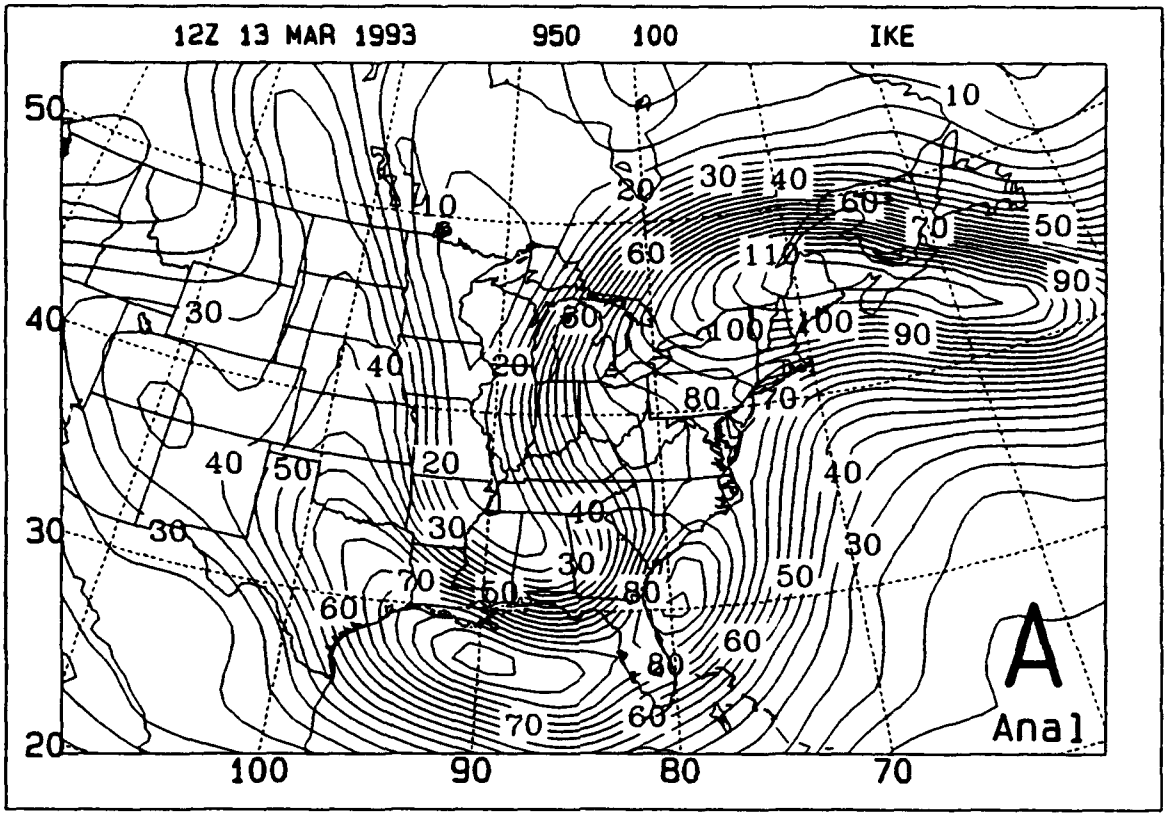

Figure 32. As in Figure 29, except for 1200 UTC 13 March 1993.

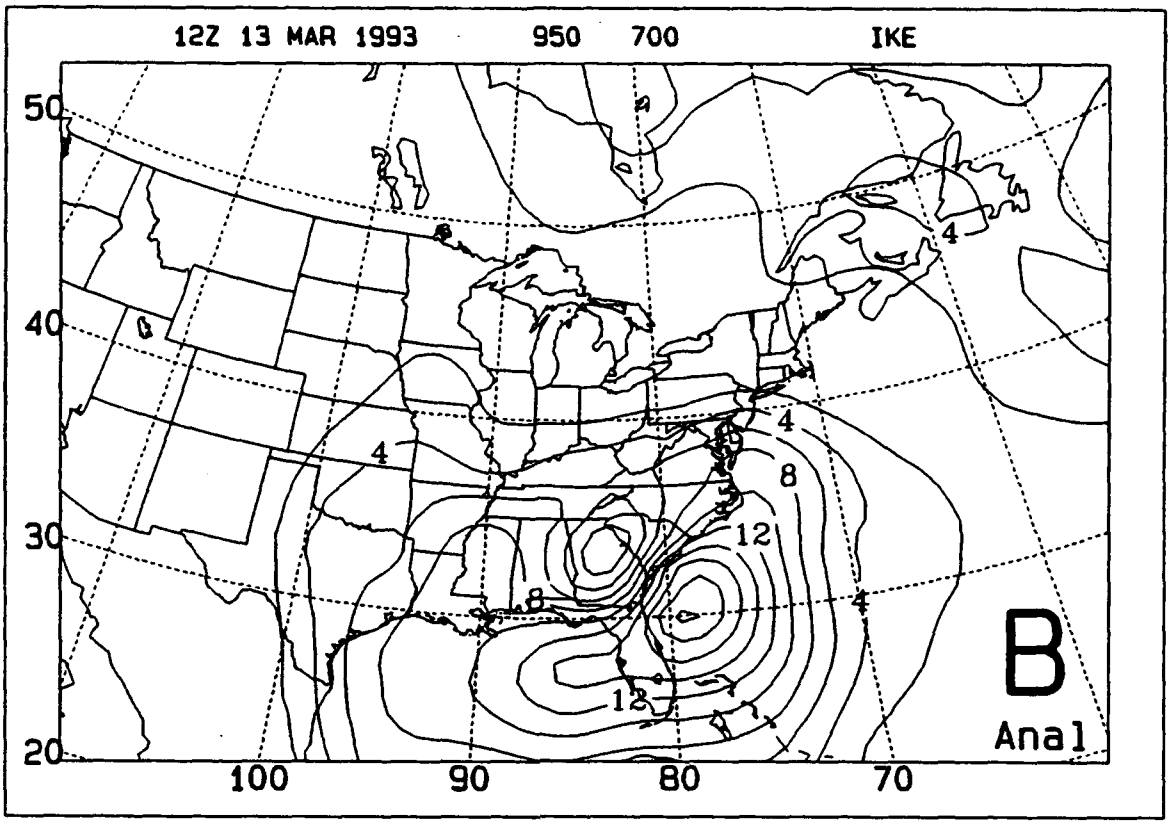
12Z 13 MAR 1993
950 700
IKE
50
40
30
20
100
90
80
70
4
8
12
B
Anal

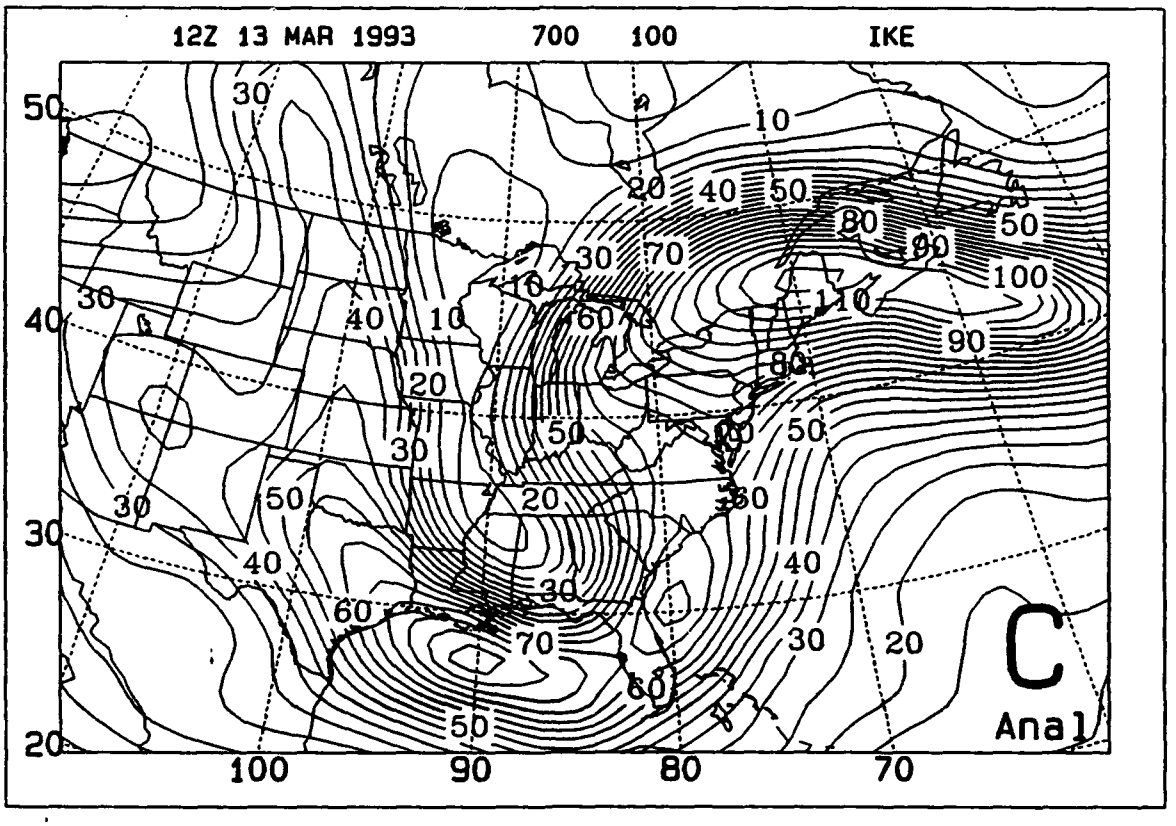
12Z 13 MAR 1993
700 100
IKE
50
40
30
20
100
90
80
70
10
20
30
40
50
60
70
80
90
100
C
Anal

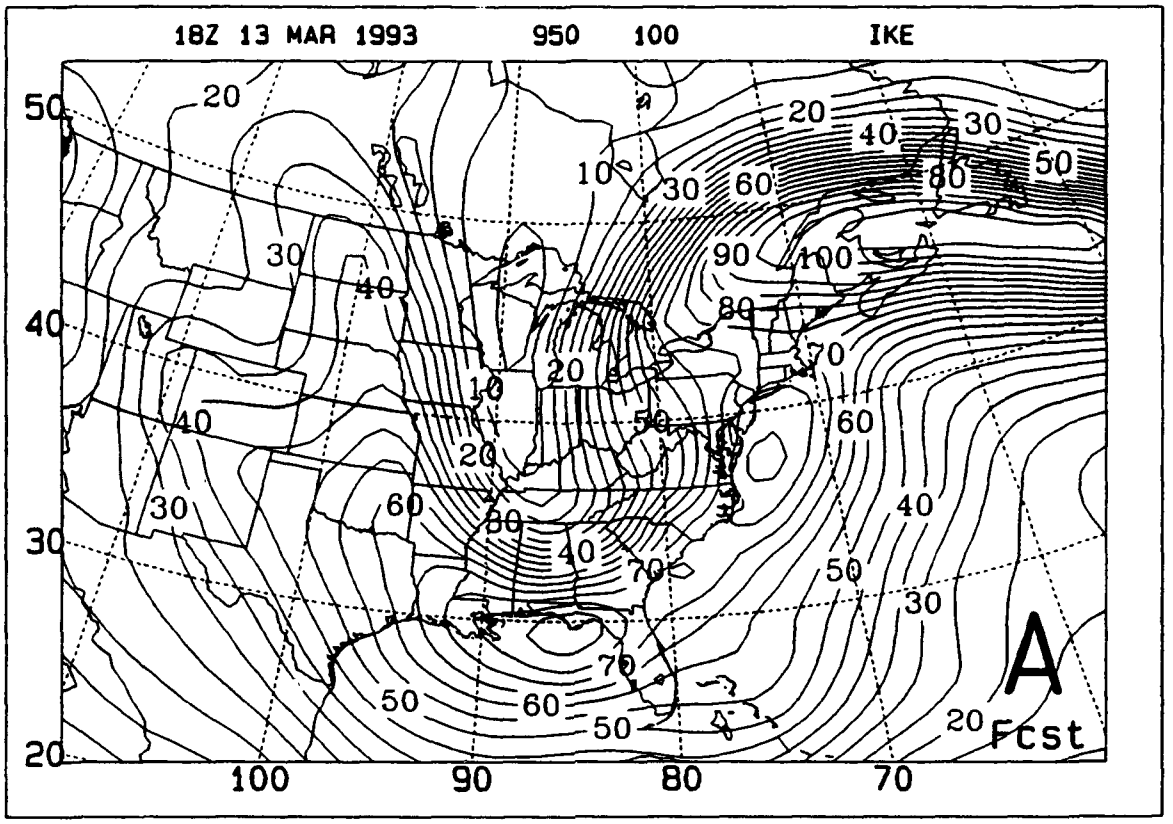

Figure 33. As in Figure 28, except for 1800 UTC 13 March 1993.

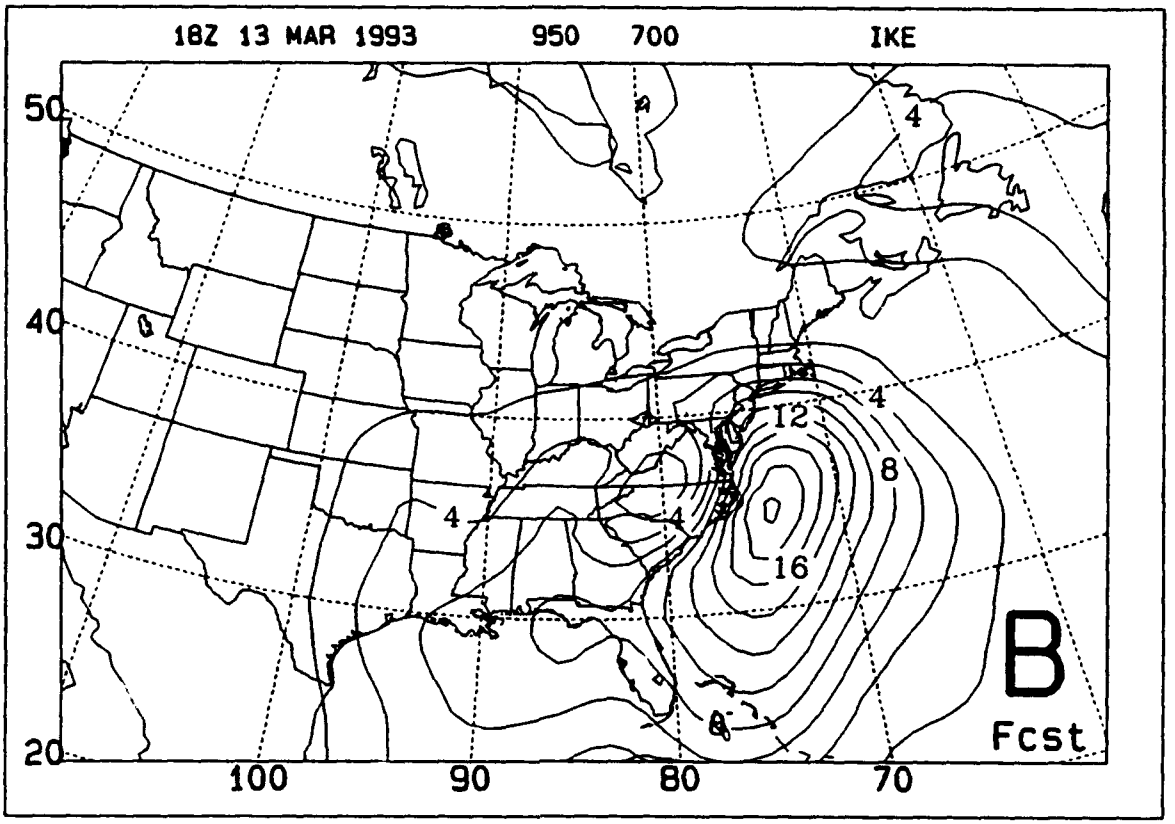
18Z 13 MAR 1993
950 700
IKE
50
40
30
20
100
90
80
70
4
4
12
4
8
4
4
16
B
Fcst

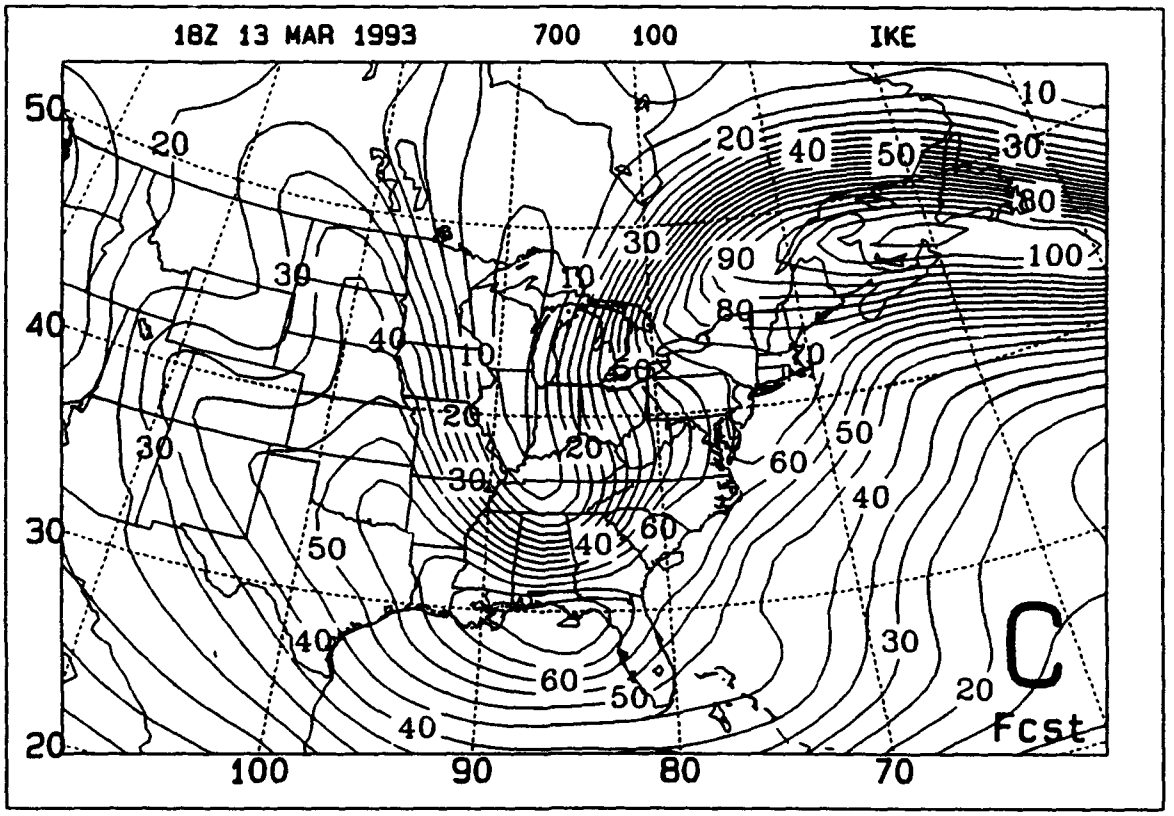
18Z 13 MAR 1993
700 100
IKE
50
40
30
20
100
90
80
70
10
20
40
50
30
80
100
90
30
10
80
40
10
50
20
20
30
30
50
60
40
60
40
50
30
40
60
50
40
20
C
Fcst

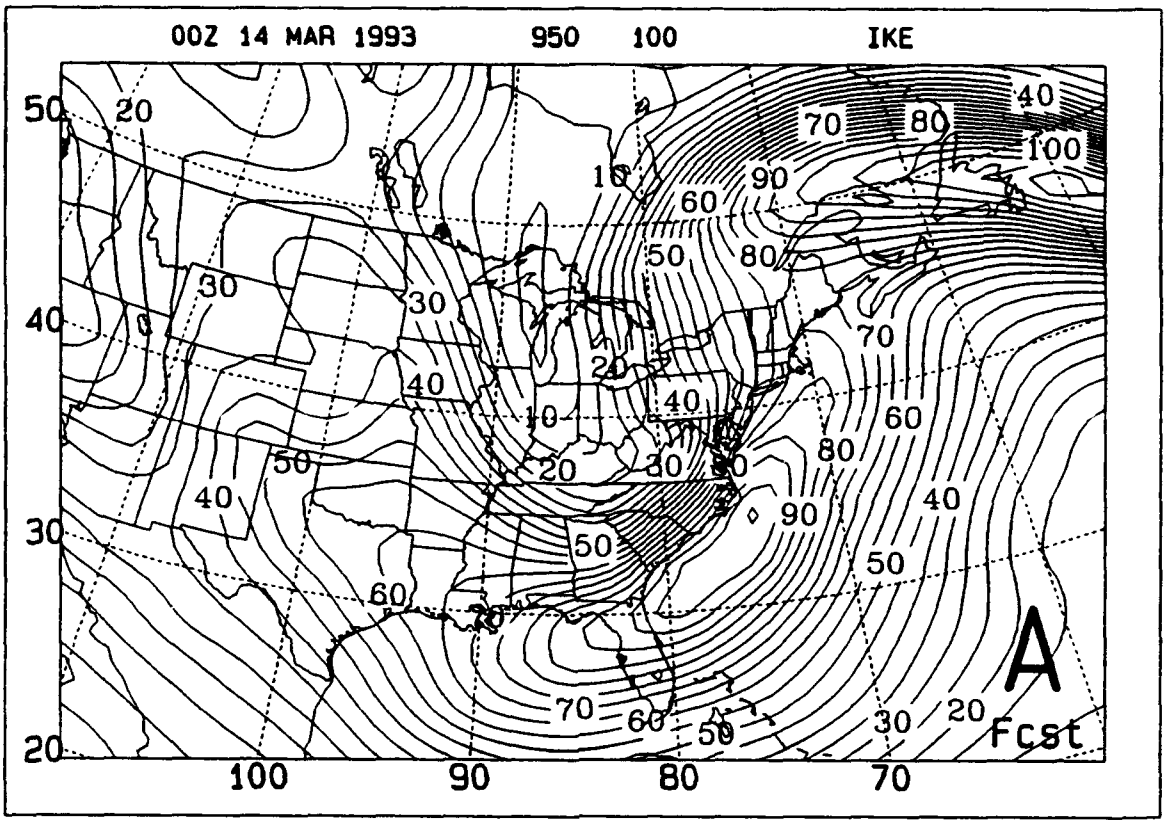

Figure 34. As in Figure 28, except for 0000 UTC 14 March 1993.

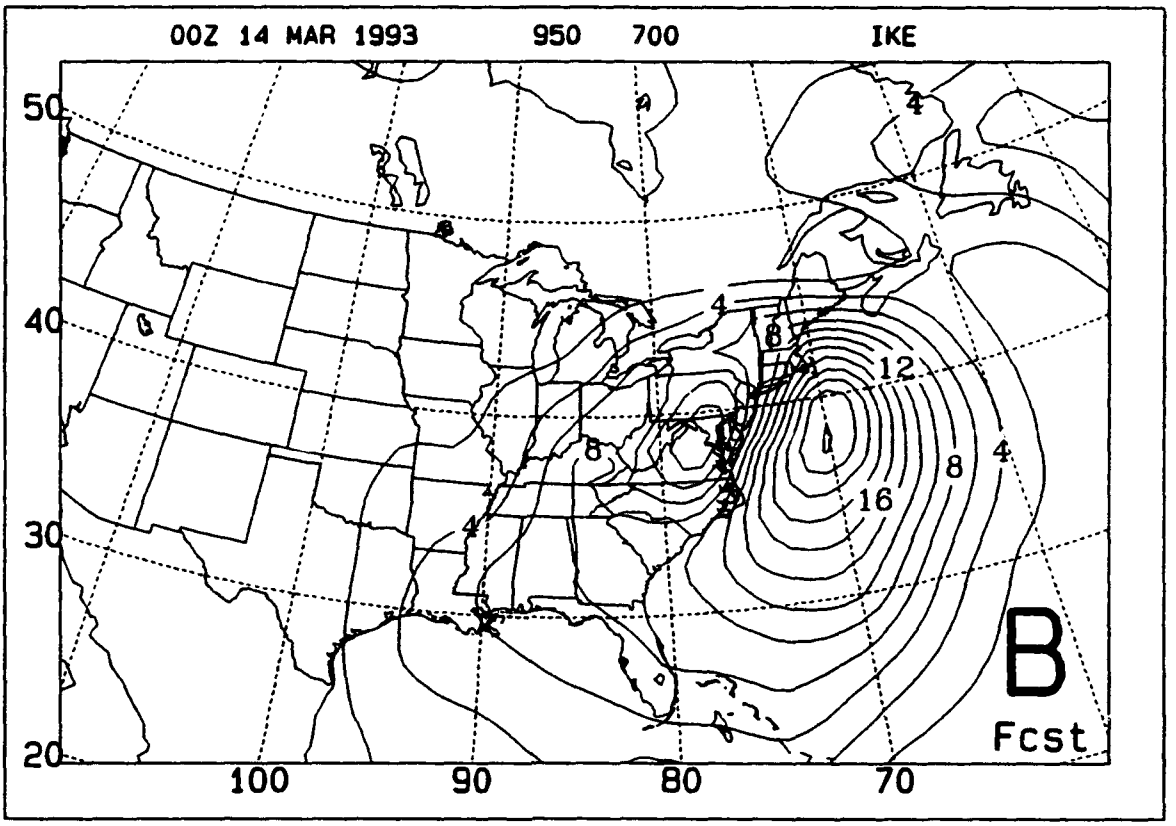
00Z 14 MAR 1993
950
700
IKE
50
40
30
20
100
90
80
70
4
8
12
16
B
Fcst

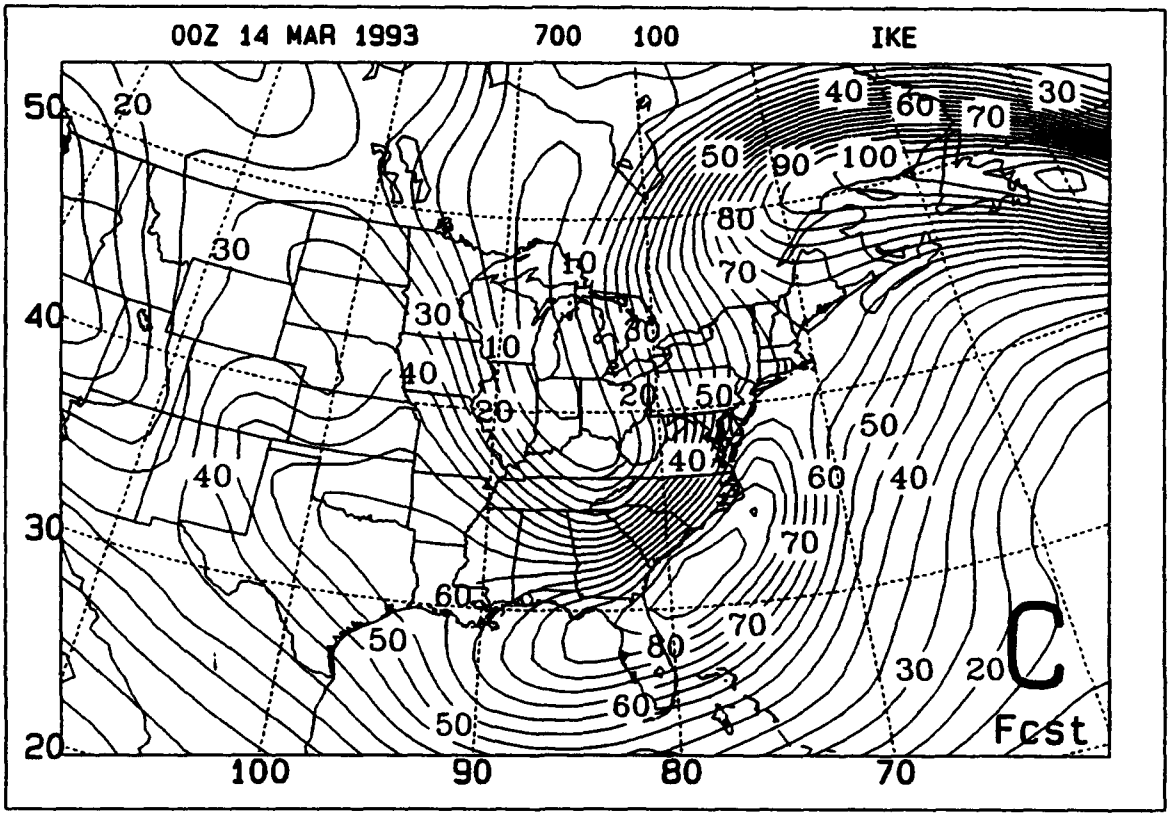
00Z 14 MAR 1993
700
100
IKE
50
40
30
20
100
90
80
70
10
20
30
40
50
60
70
80
90
100
C
Fcst

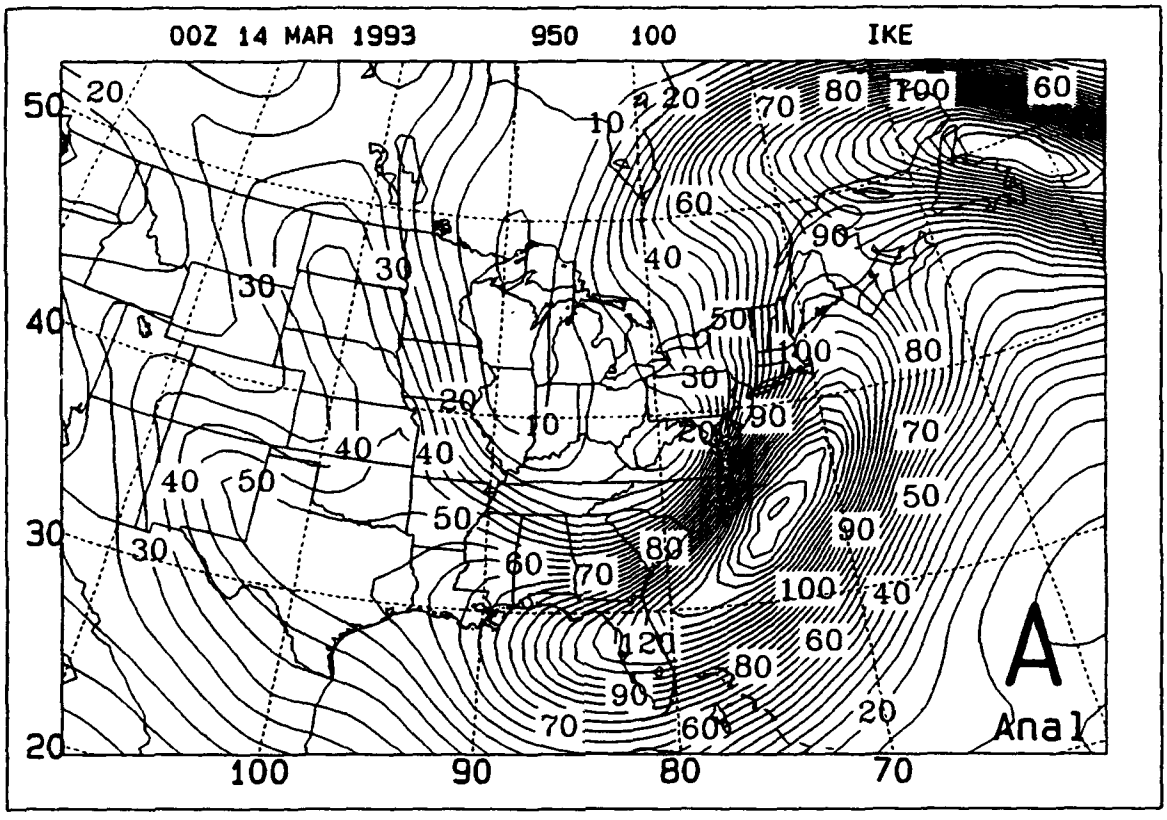

Figure 35. As in Figure 29, except for 0000 UTC March 1993.

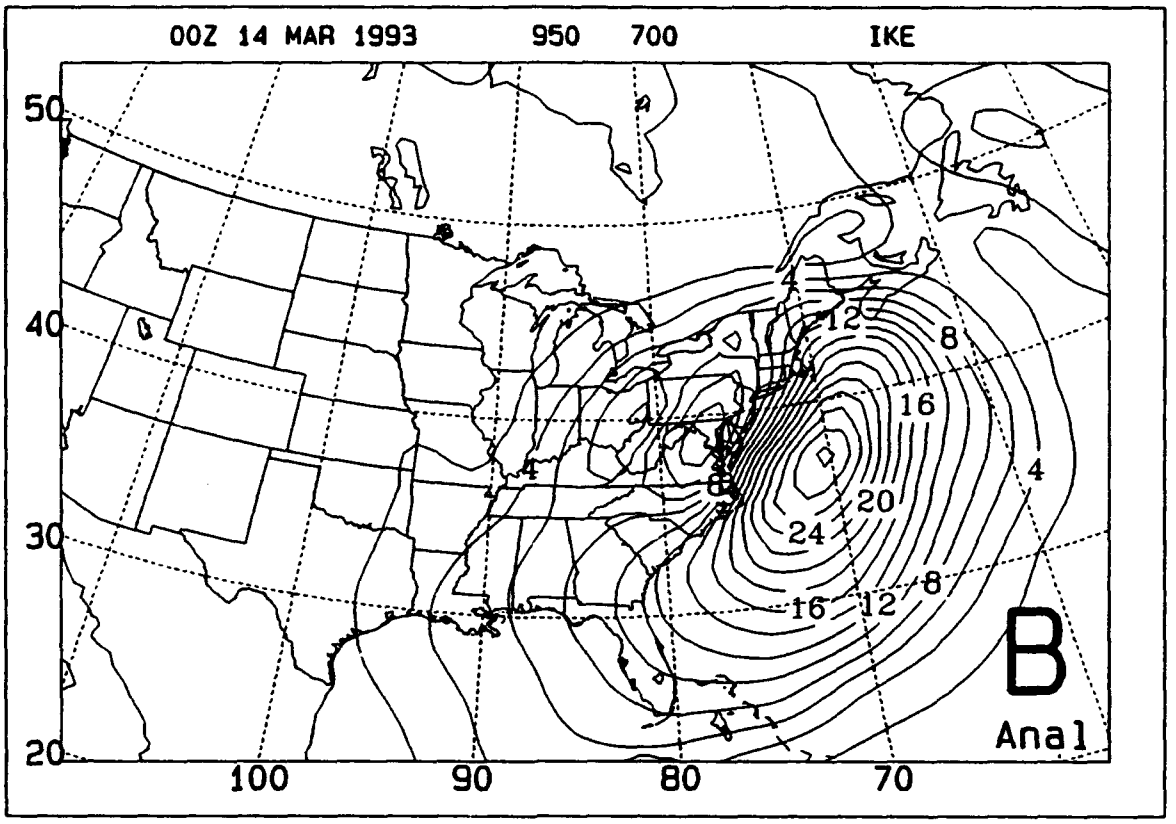
00Z 14 MAR 1993
950 700
IKE
50
40
30
20
100
90
80
70
B
Anal

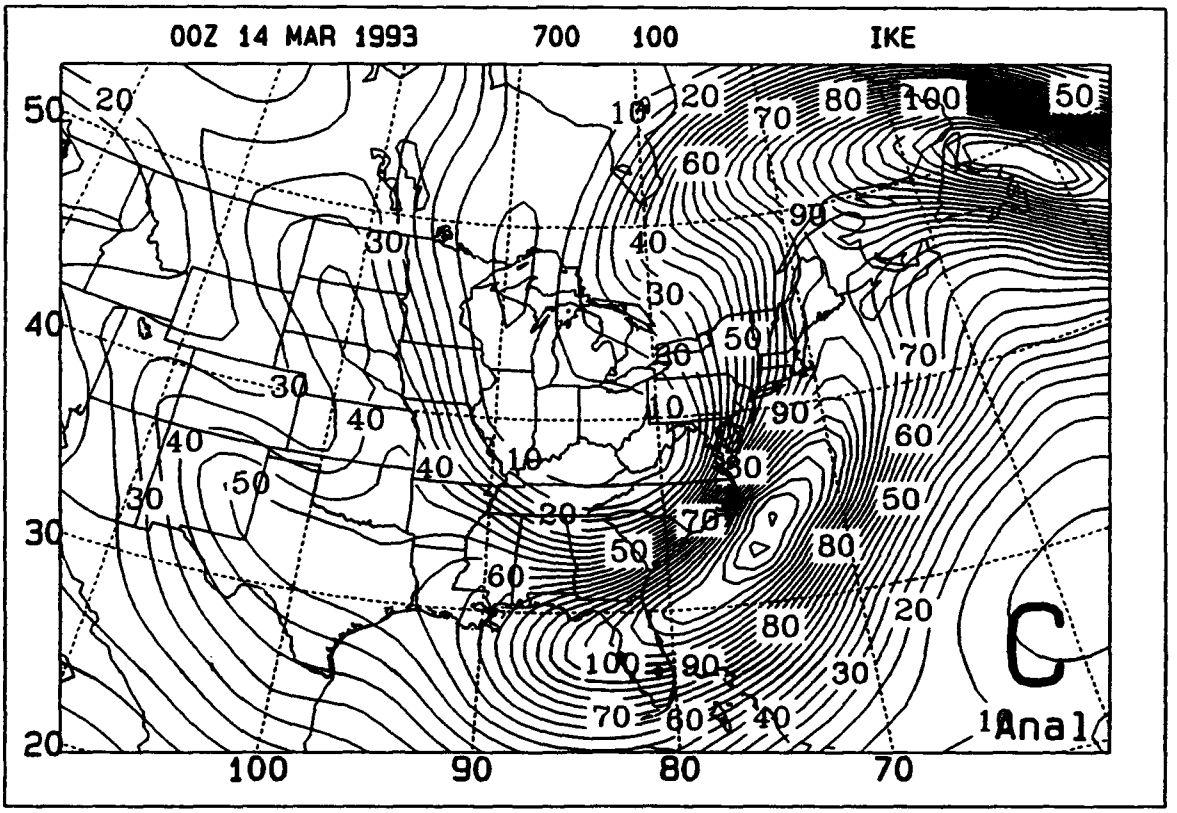
00Z 14 MAR 1993
700 100
IKE
50
40
30
20
100
90
80
70
C
Anal

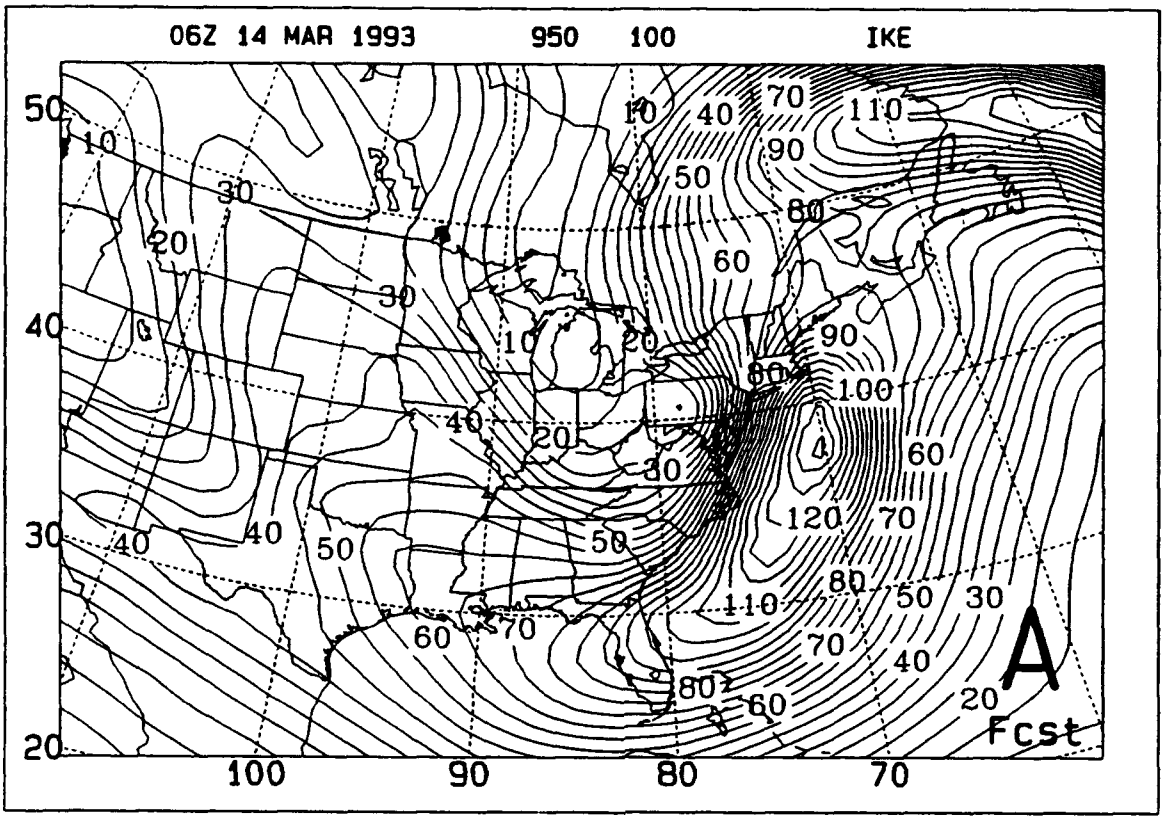

Figure 36. As in Figure 28, except for 0600 UTC 14 March 1993.

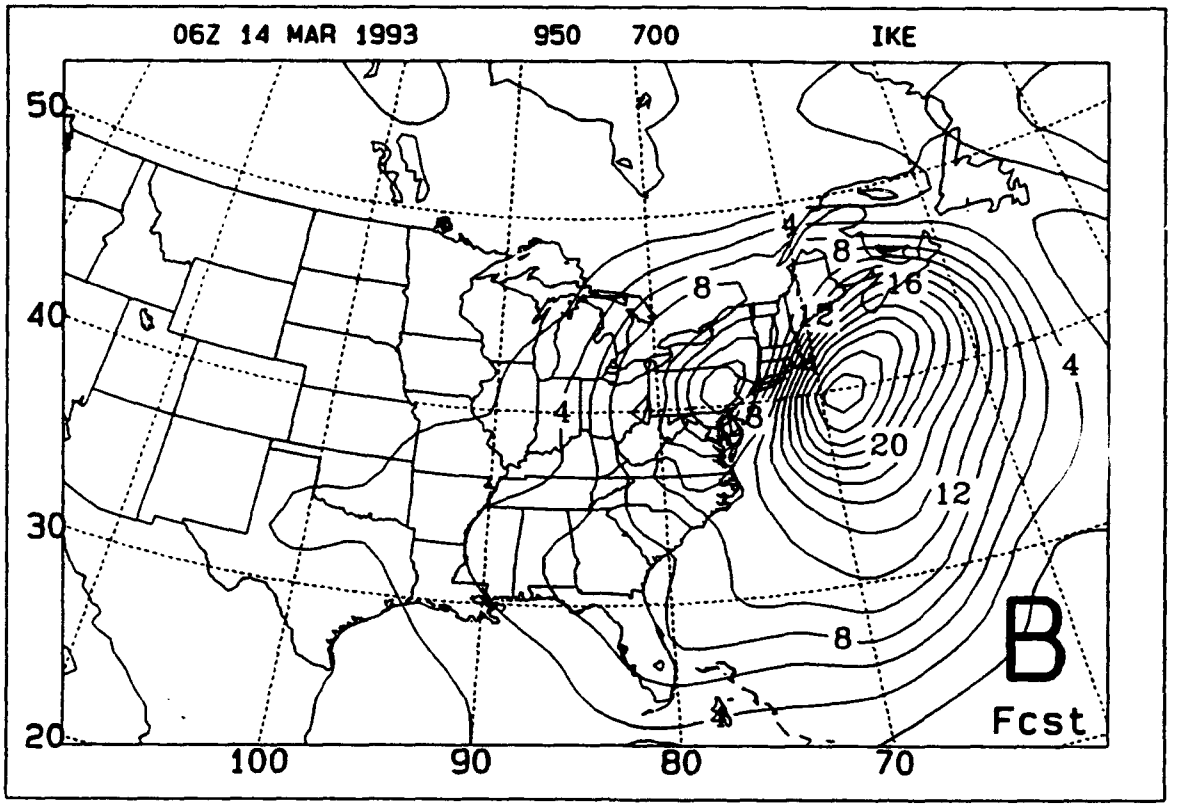
06Z 14 MAR 1993
950 700
IKE
50
40
30
20
100
90
80
70
8
16
12
4
20
B
Fcst

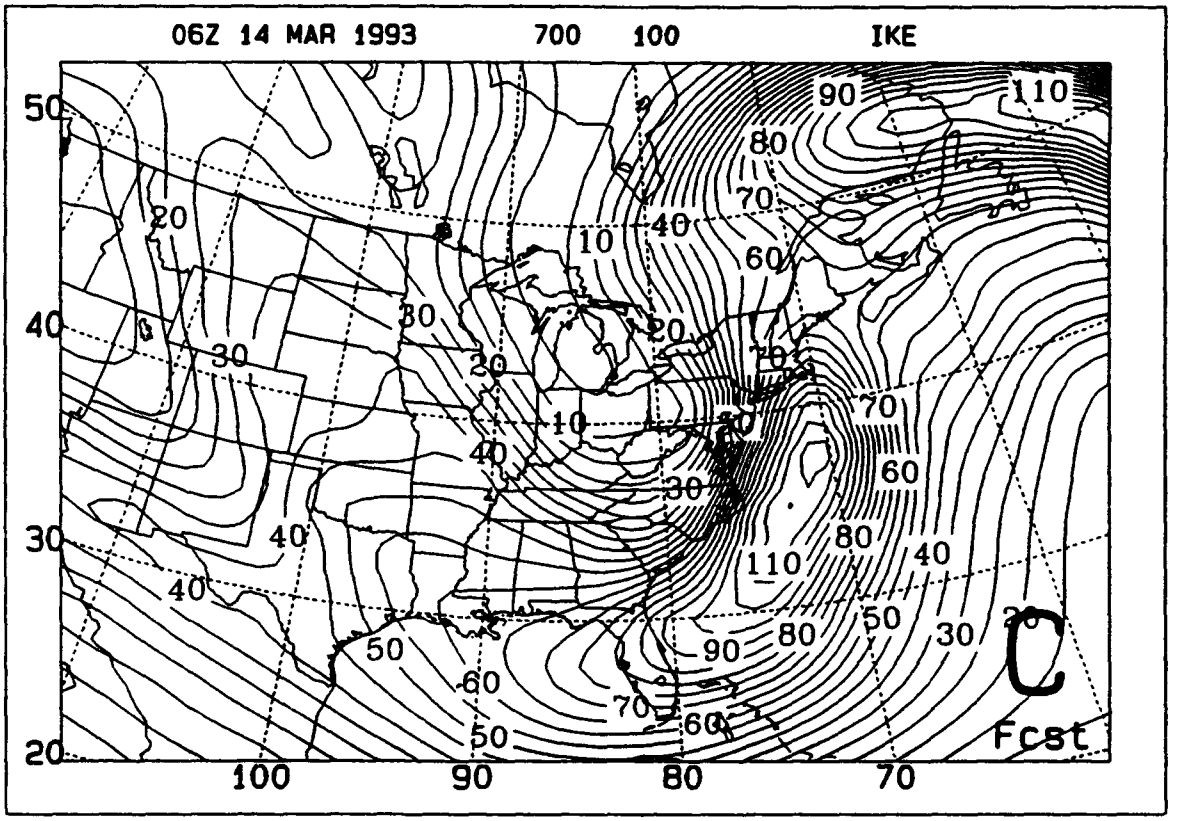
06Z 14 MAR 1993
700 100
IKE
50
40
30
20
100
90
80
70
90
110
80
70
60
40
30
20
10
C
Fcst

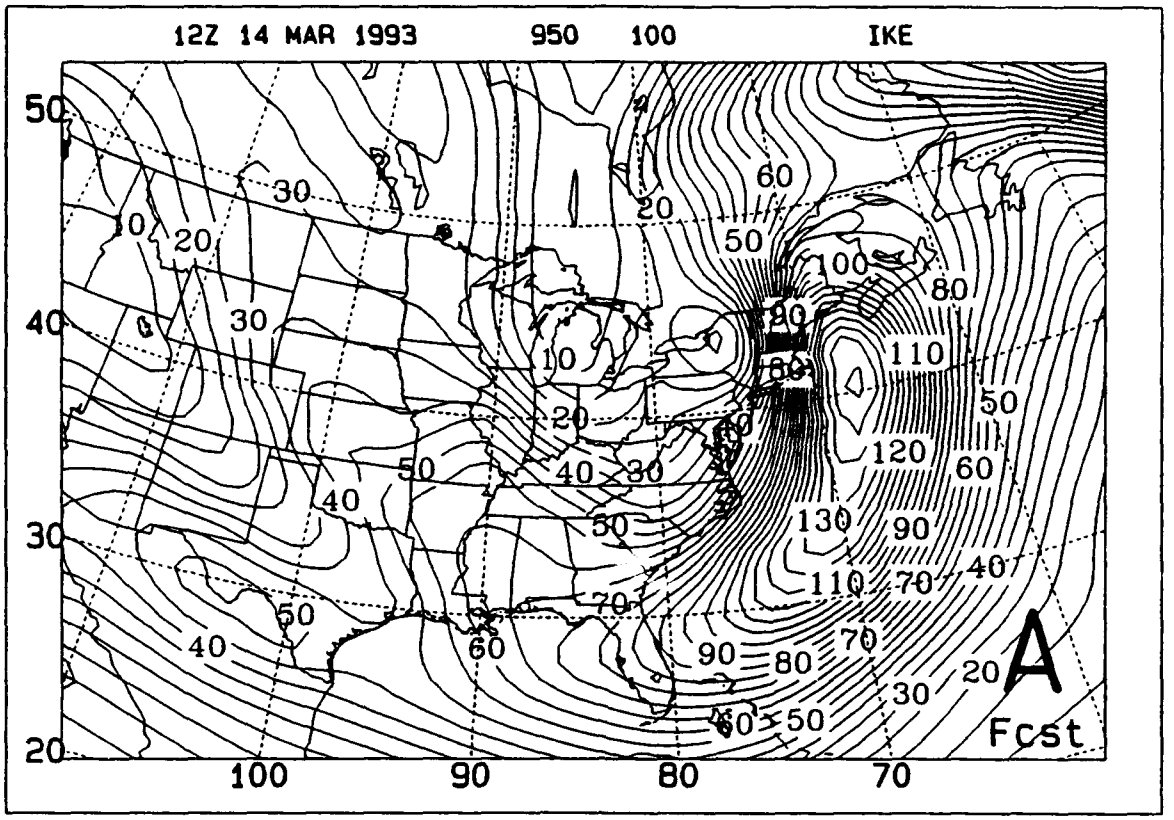

Figure 37. As in Figure 28, except for 1200 UTC 14 March 1993.

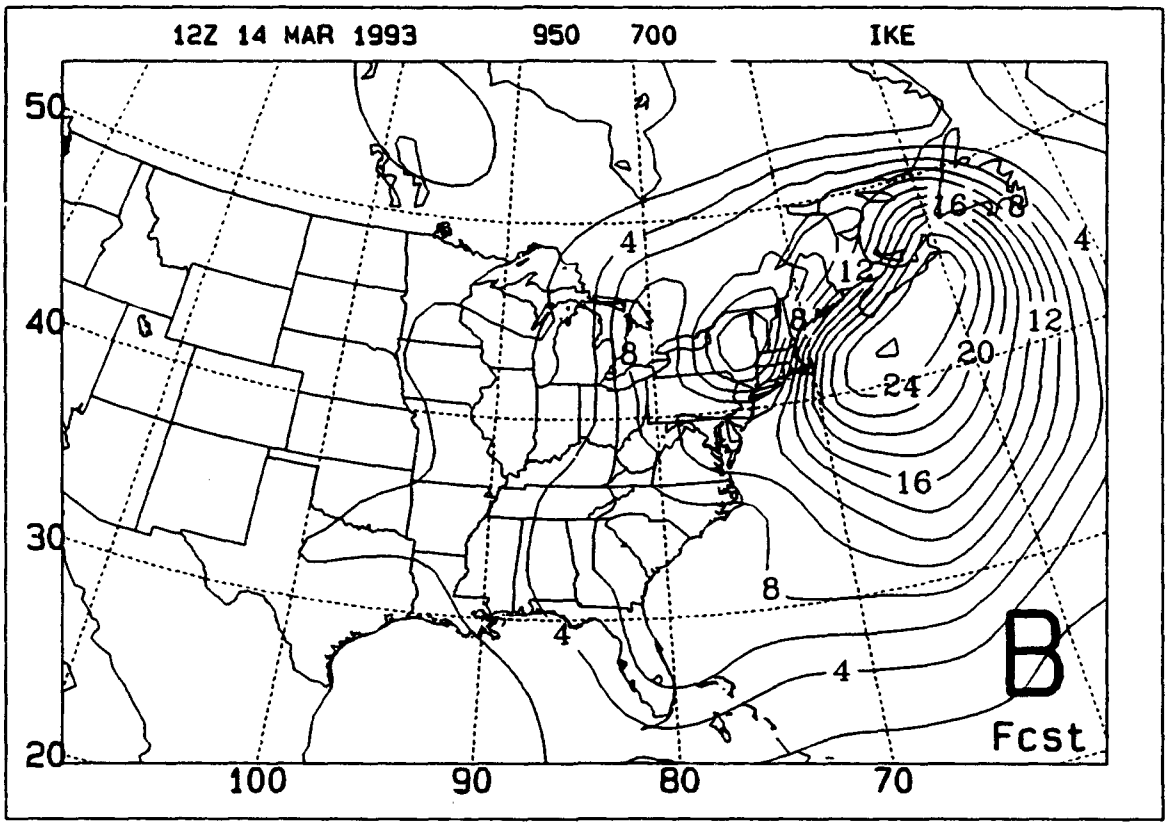
12Z 14 MAR 1993
950 700
IKE
50
40
30
20
100
90
80
70
4
8
12
16
20
24
B
Fcst

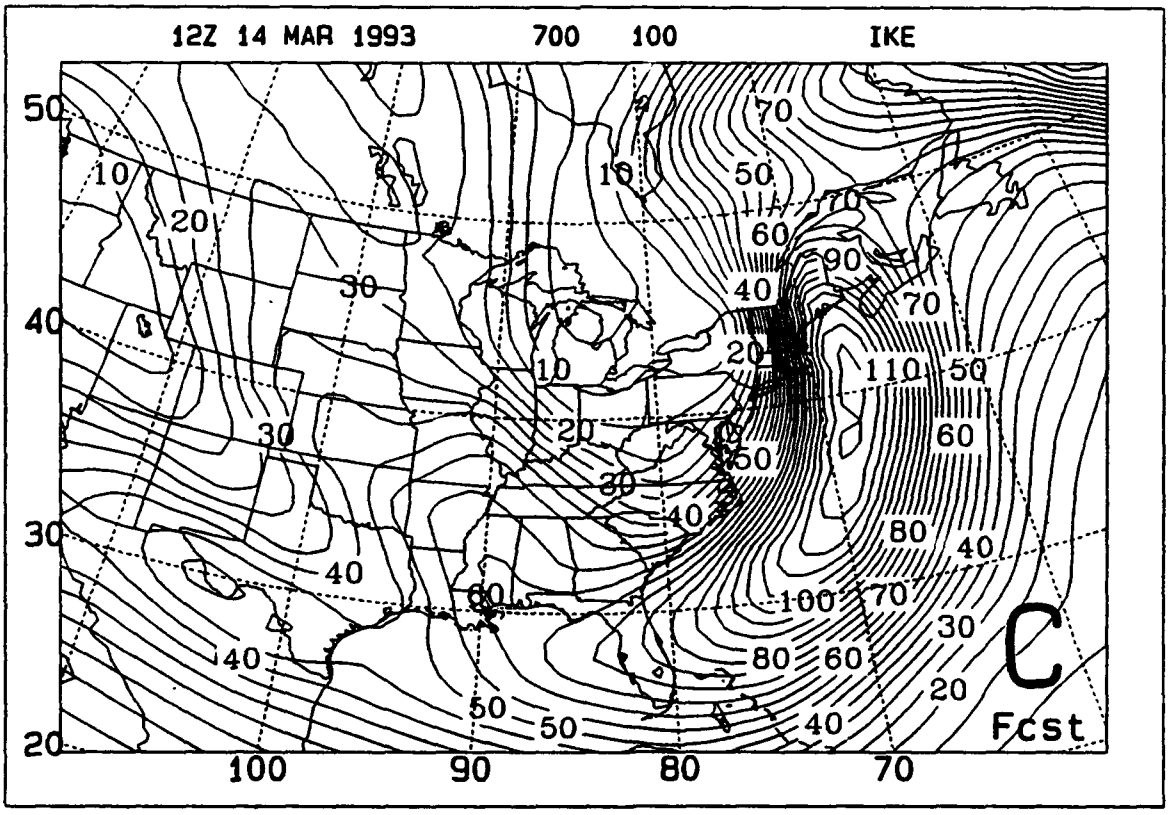
12Z 14 MAR 1993
700 100
IKE
50
40
30
20
100
90
80
70
10
20
30
40
50
60
70
80
90
100
110
C
Fcst

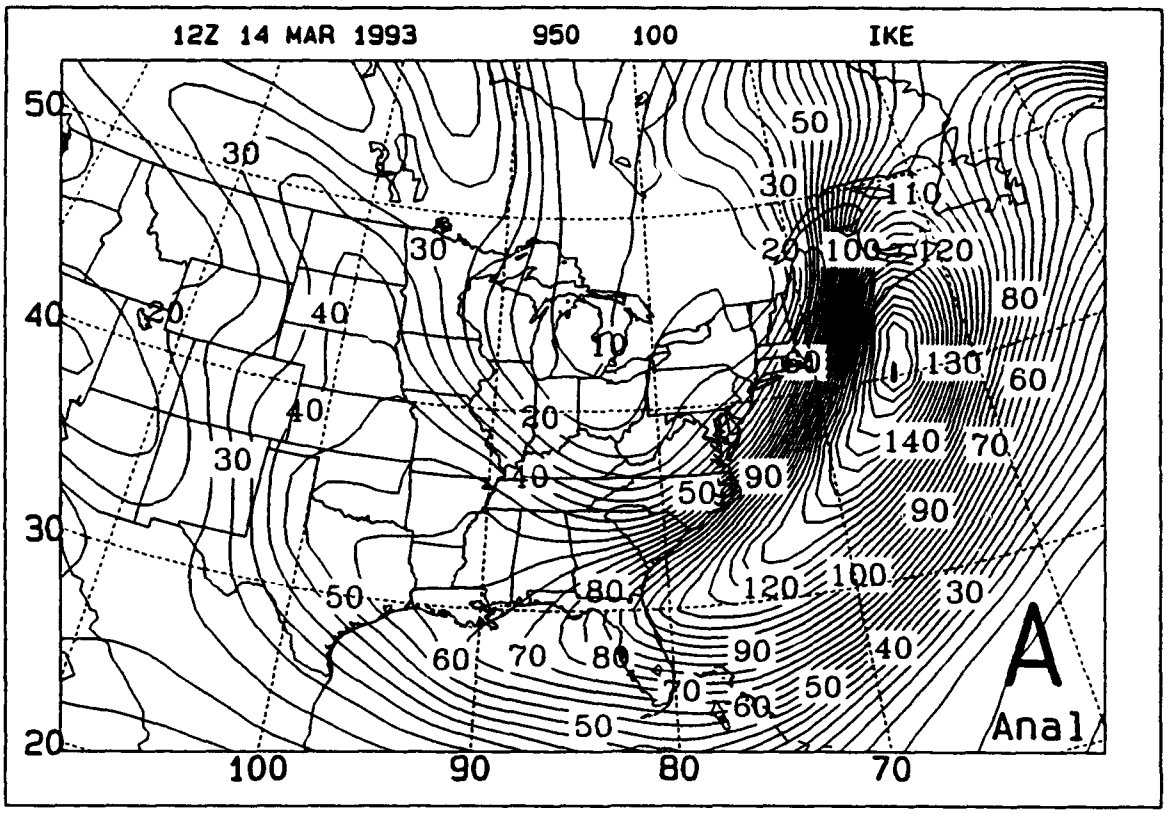

Figure 38. As in Figure 29, except for 1200 UTC 14 March 1993.

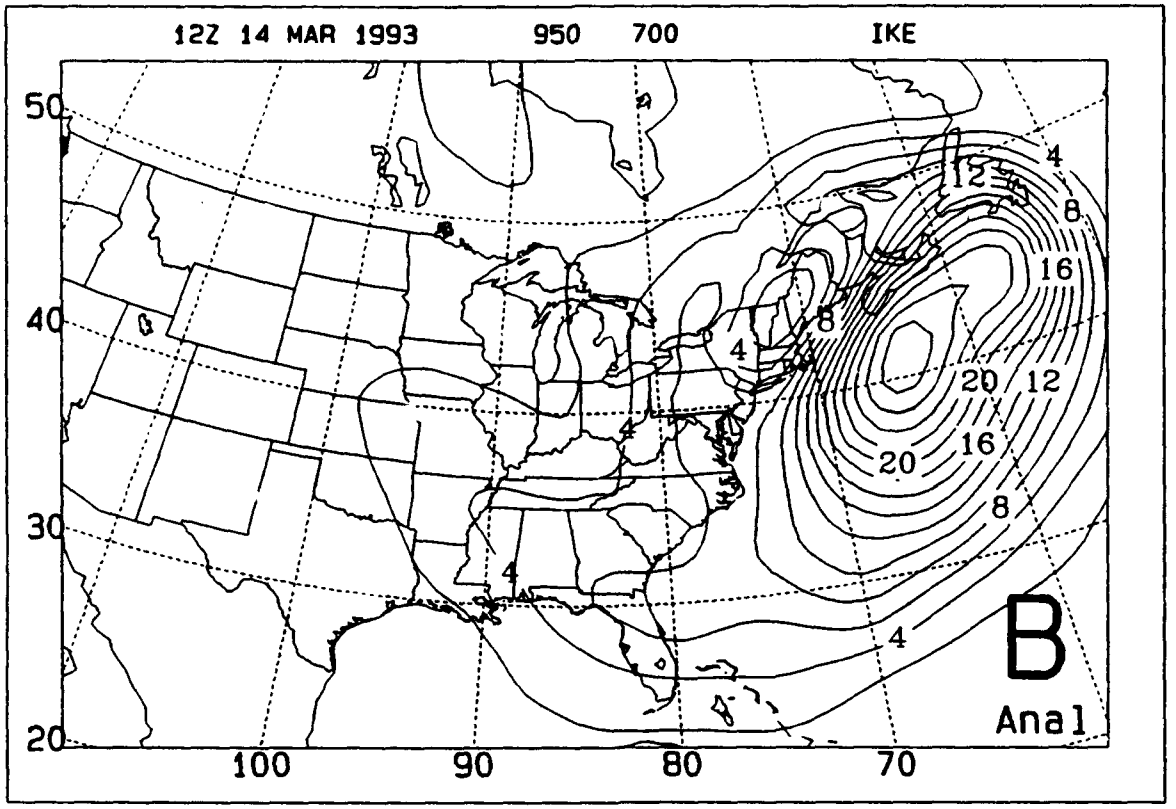
12Z 14 MAR 1993
950 700
IKE
50
40
30
20
100
90
80
70
4
8
12
16
20
B
Anal

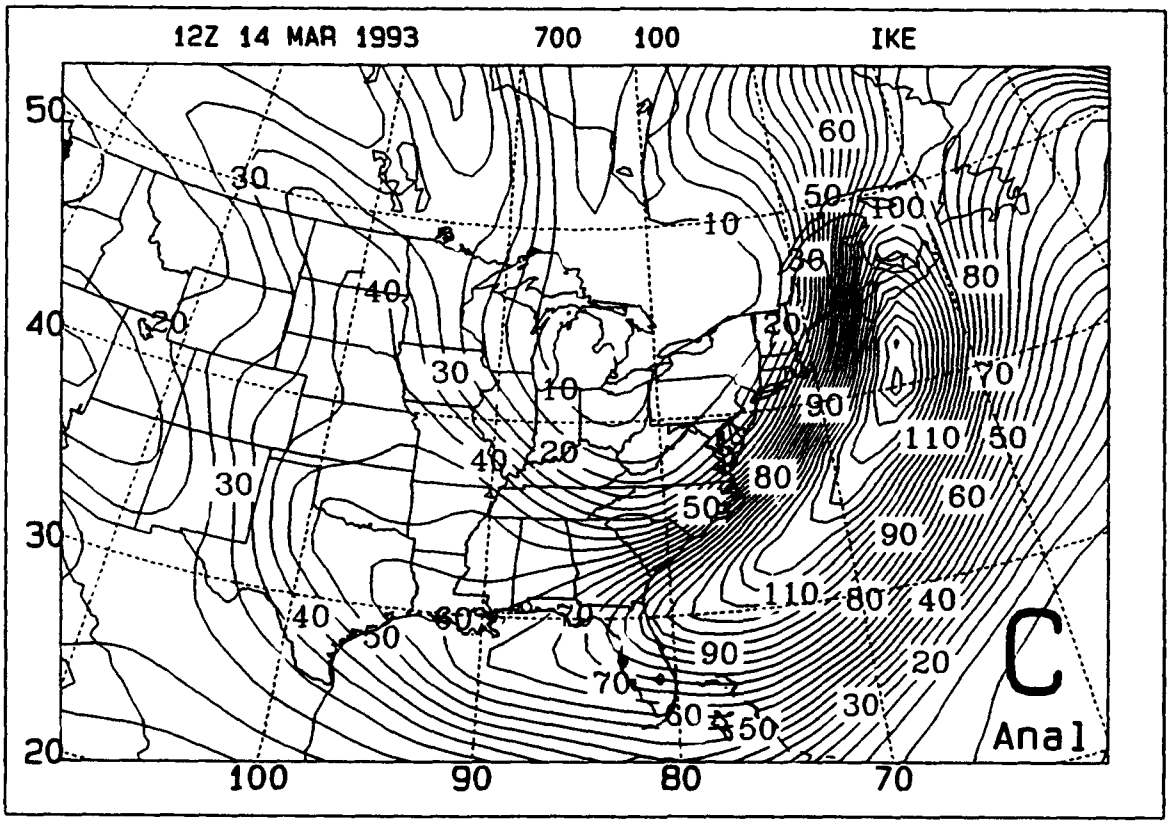
12Z 14 MAR 1993
700 100
IKE
50
40
30
20
100
90
80
70
10
20
30
40
50
60
70
80
90
100
110
C
Anal

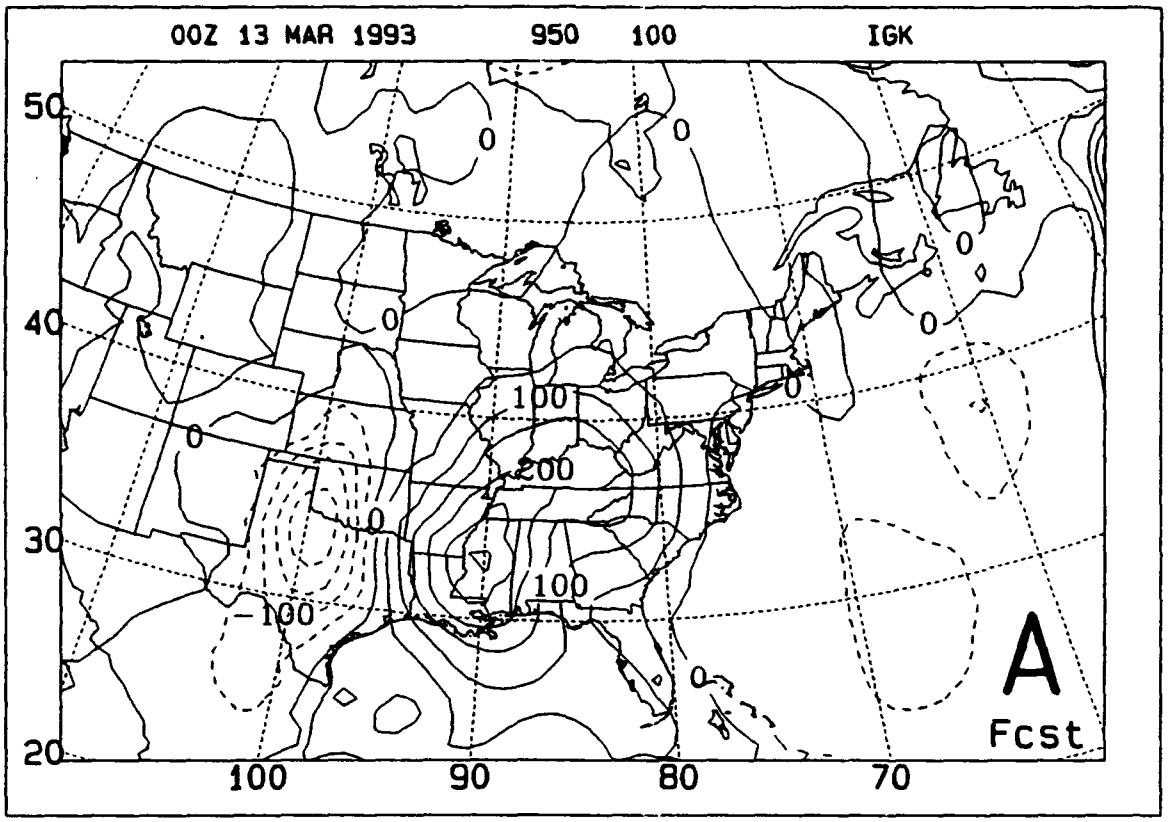

Figure 39. Vertically-integrated generation of kinetic energy (IGK) based on the NMC Global Spectral Model forecast for 0000 UTC 13 March 1993 ($5x10^5$ J m^{-2} increment). (**A**) Integration from 950 mb to 100 mb; (**B**) integration from 950 mb to 700 mb; (**C**) integration from 700 mb to 100 mb.

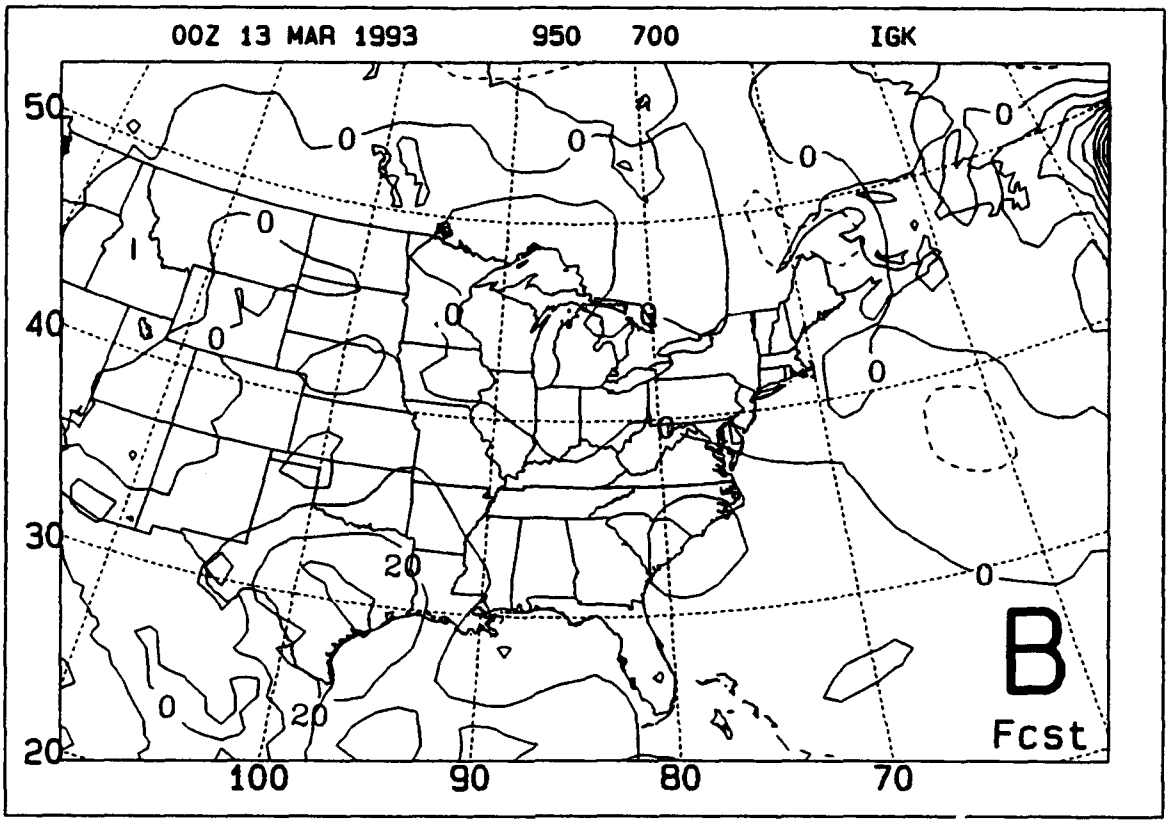
00Z 13 MAR 1993
950 700
IGK
50
40
30
20
100
90
80
70
B
Fcst

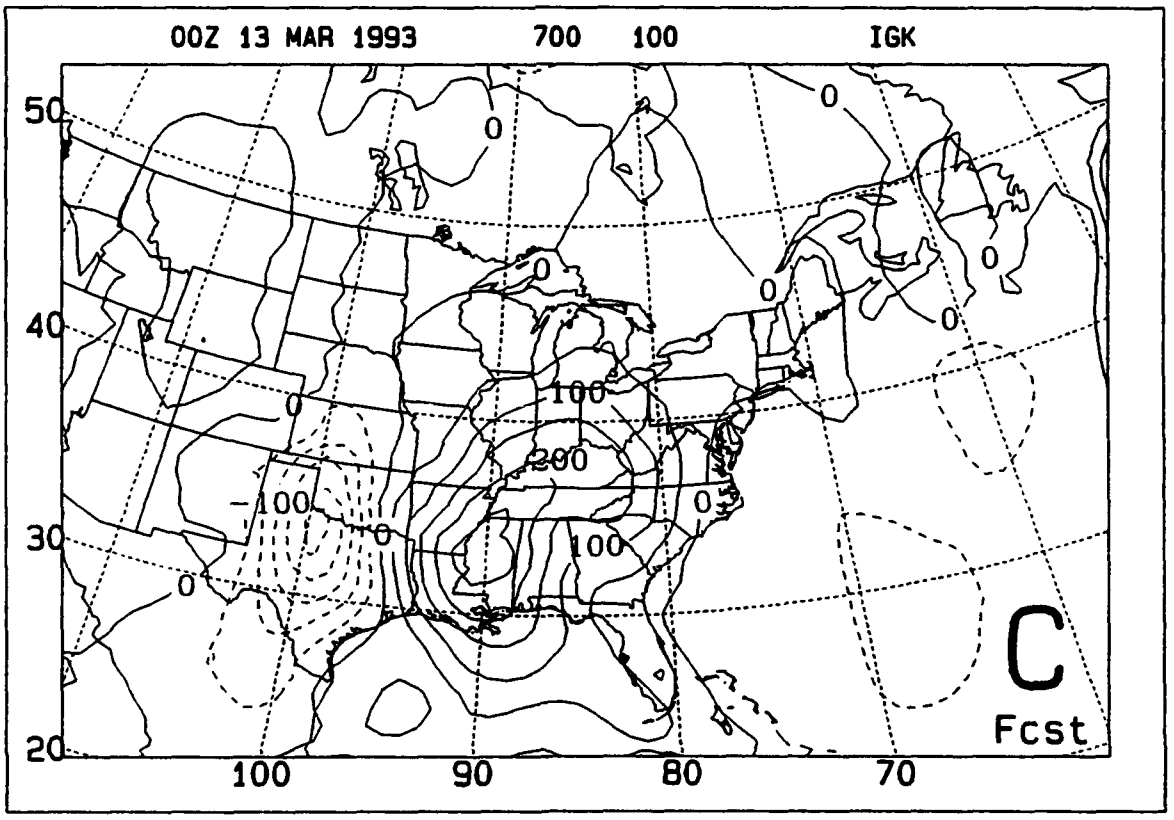
00Z 13 MAR 1993
700 100
IGK
50
40
30
20
100
90
80
70
C
Fcst

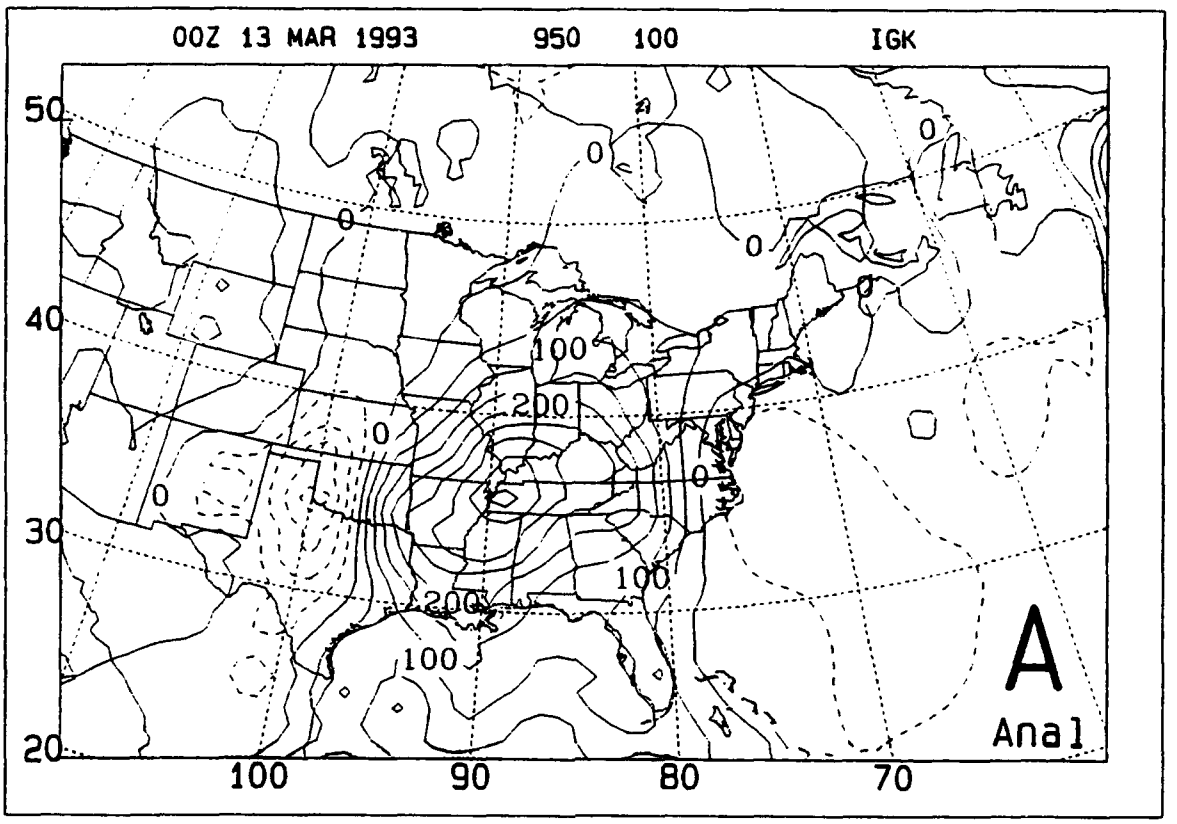

Figure 40. Vertically-integrated generation of kinetic energy (IGK) based on NMC AVN Analysis for 0000 UTC 13 March 1993 ($5x10^5$ J m^{-2} increment). (**A**) Integration from 950 mb to 100 mb; (**B**) integration from 950 mb to 700 mb; (**C**) integration from 700 mb to 100 mb.

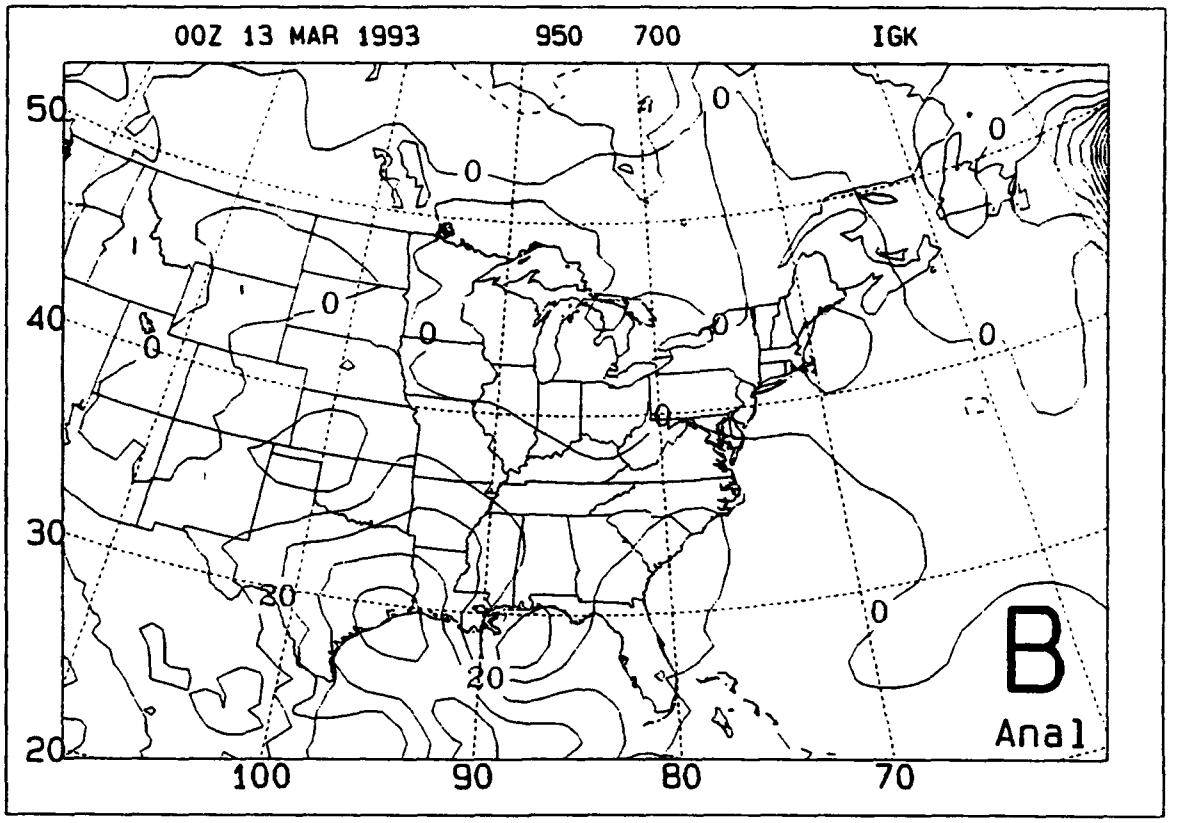
00Z 13 MAR 1993
950
700
IGK
50
40
30
20
100
90
80
70
0
20
B
Anal

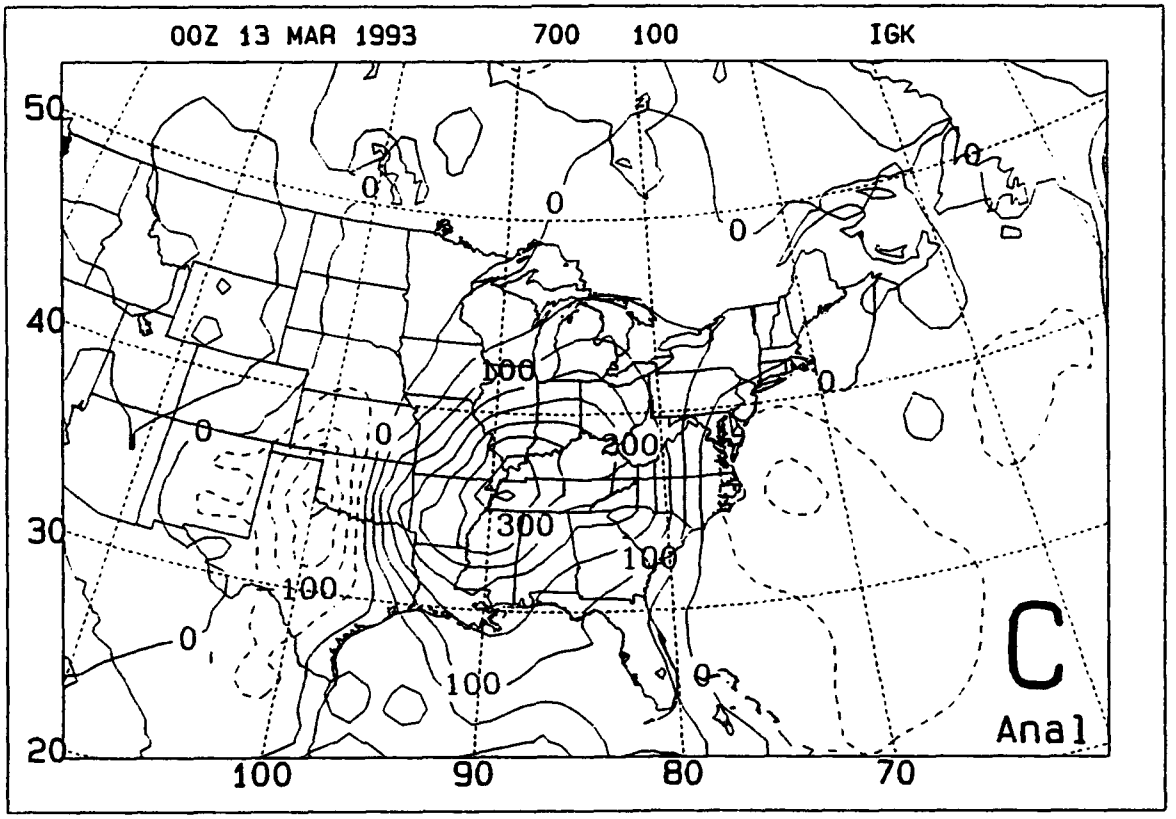
00Z 13 MAR 1993
700
100
IGK
50
40
30
20
100
90
80
70
0
100
200
300
-100
C
Anal

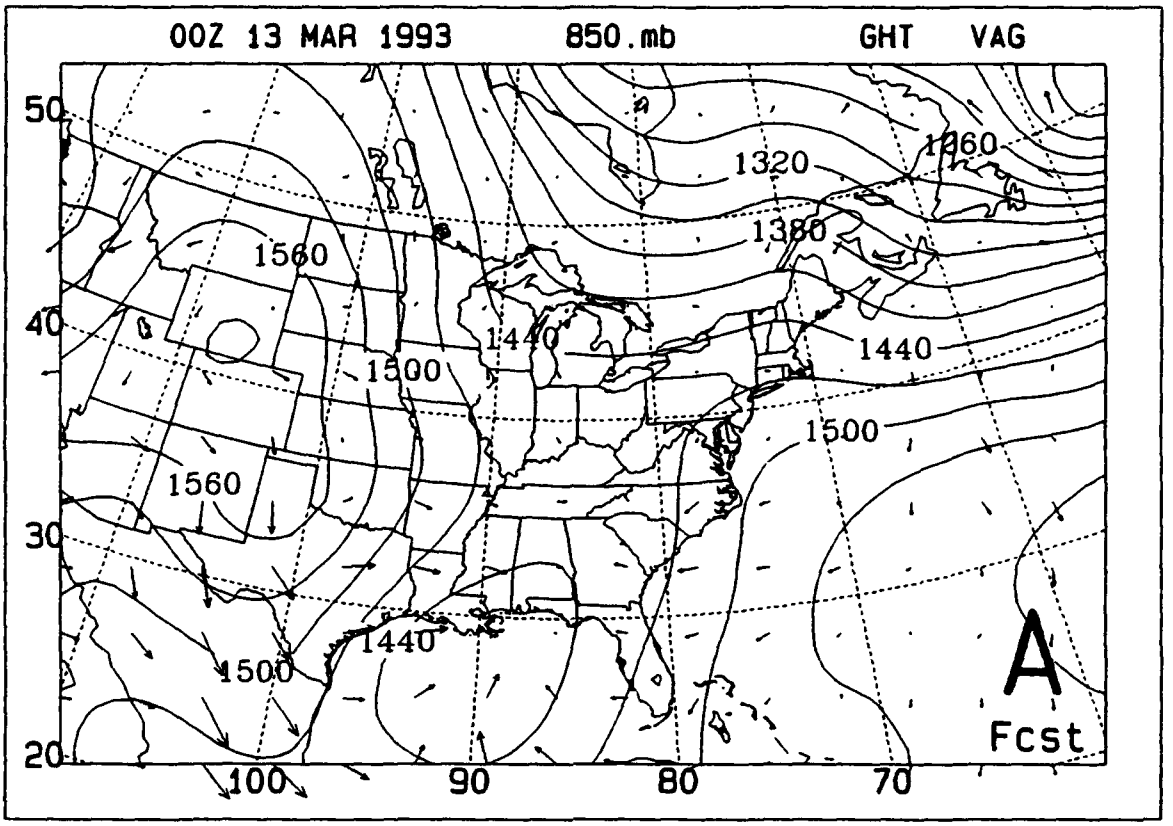

Figure 41. NMC Global Spectral Model forecast verifying at 0000 UTC 13 March 1993. (**A**) 850 mb height (solid; 3 dm increment) and ageostrophic wind (arrows); (**B**) 300 mb height (solid; 12 dm increment) and ageostrophic wind (arrows); (**C**) 300 mb windspeed (solid; 5 m/s increments).

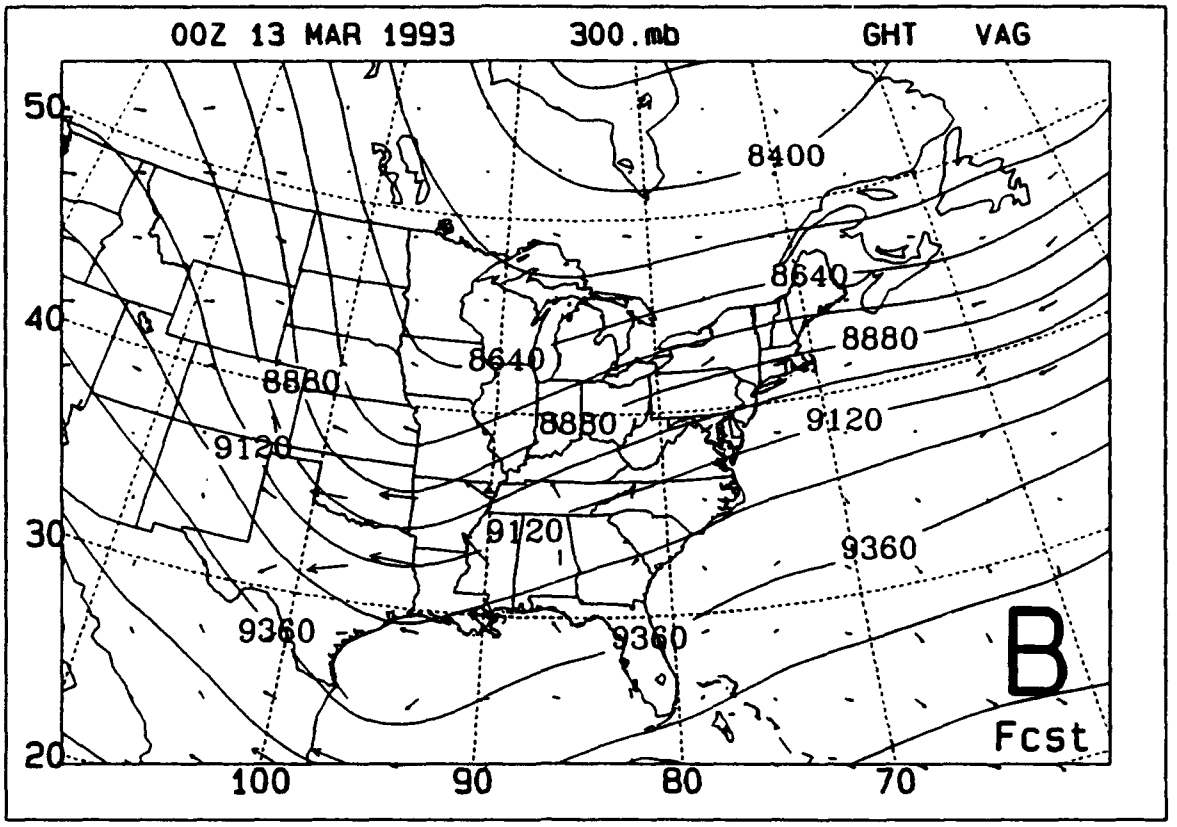
00Z 13 MAR 1993
300.mb
GHT
VAG
50
40
30
20
100
90
80
70
8400
8640
8880
9120
9360
B
Fcst

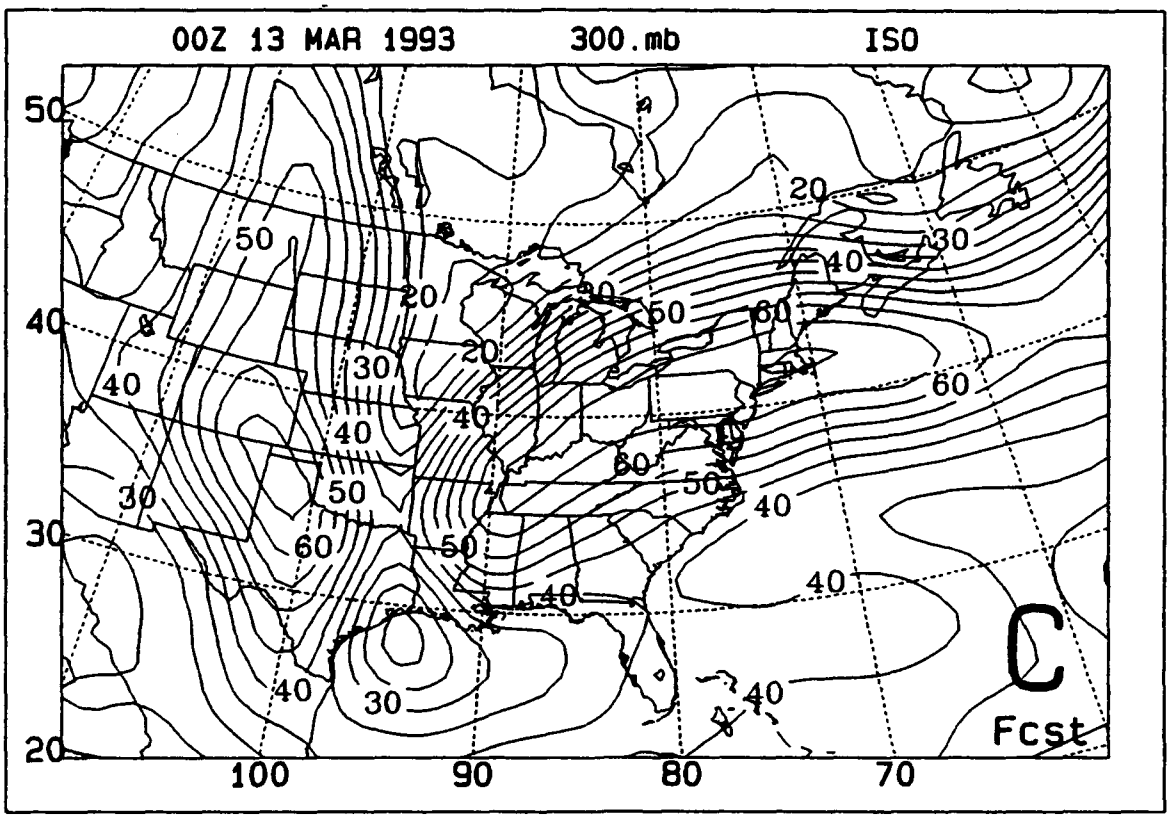
00Z 13 MAR 1993
300.mb
ISO
50
40
30
20
100
90
80
70
C
Fcst

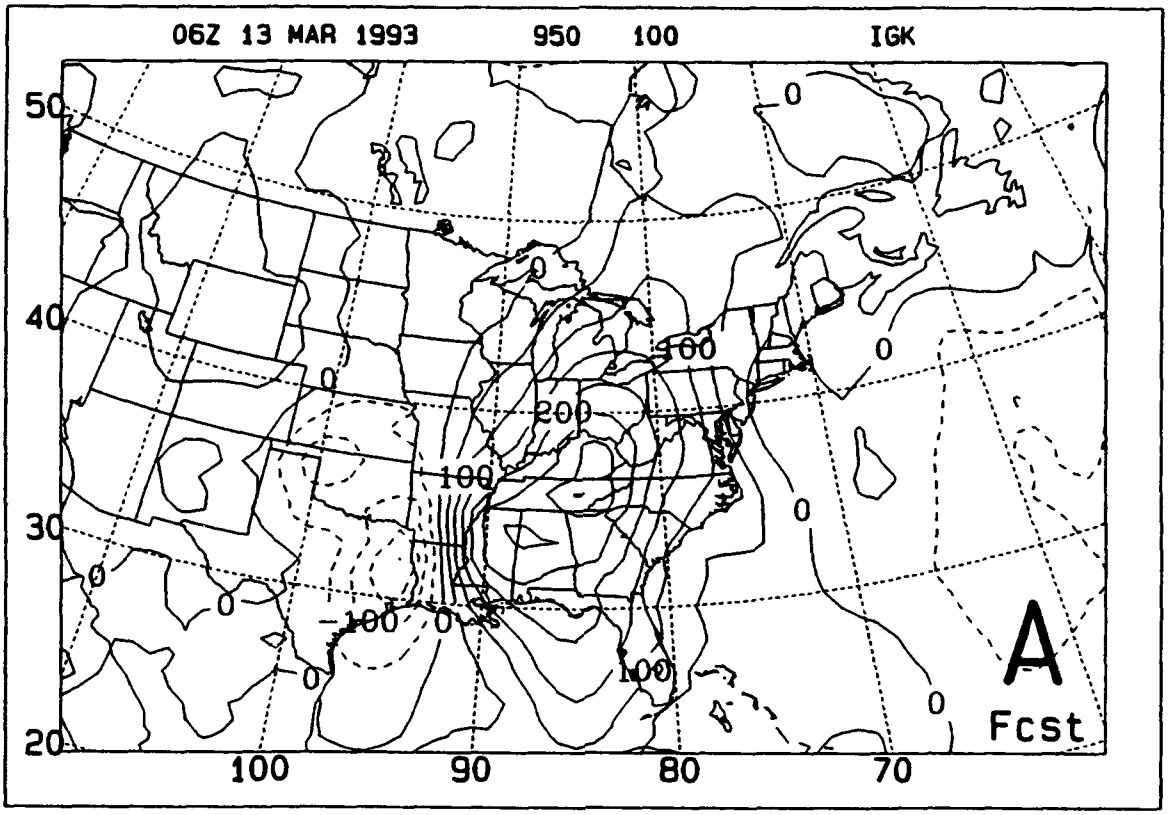

Figure 42. As in Figure 39, except for 0600 UTC 13 March 1993.

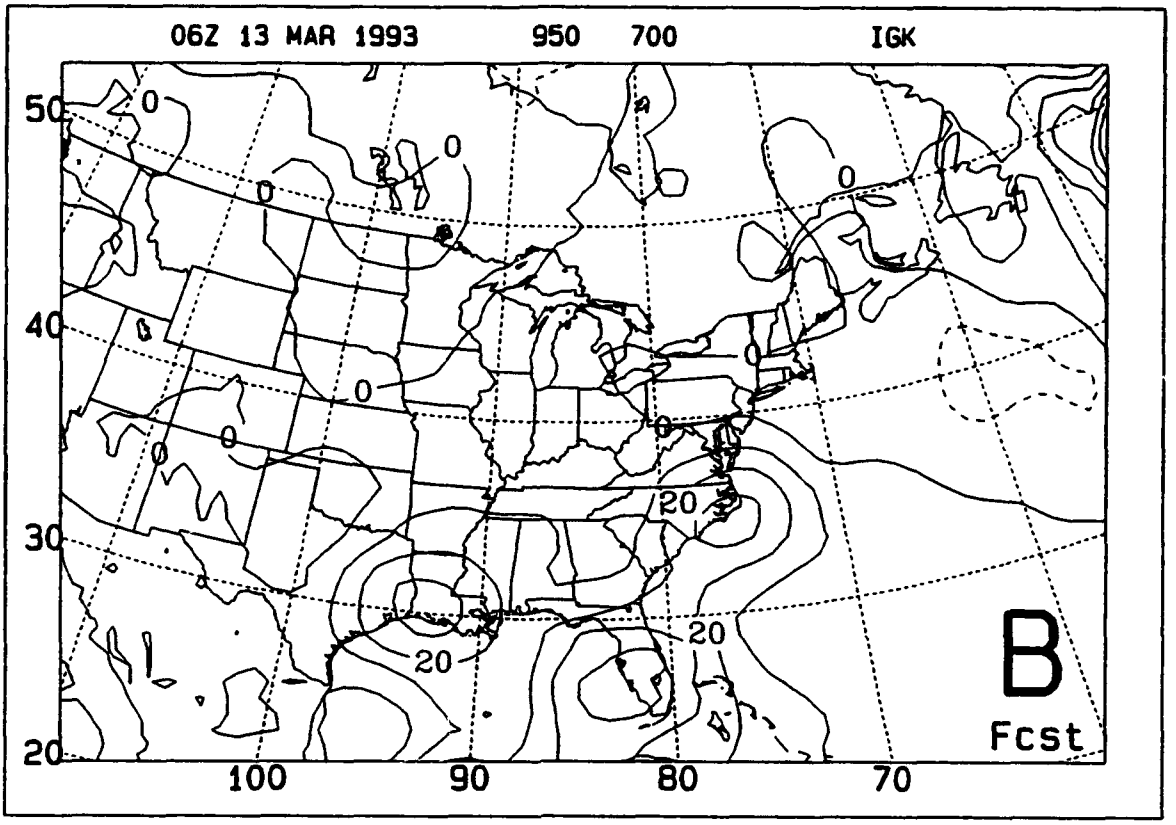
06Z 13 MAR 1993
950 700
IGK
50
40
30
20
100
90
80
70
0
20
B
Fcst

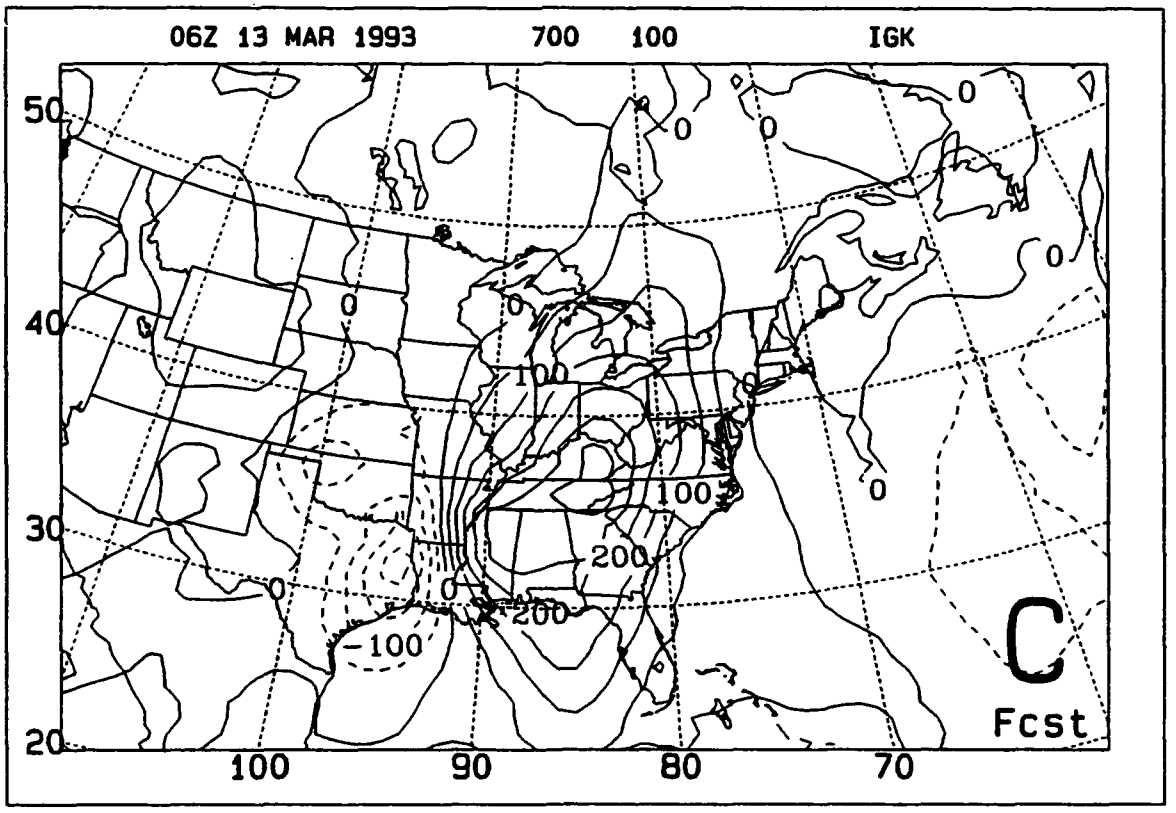
06Z 13 MAR 1993
700 100
IGK
50
40
30
20
100
90
80
70
0
100
200
-100
C
Fcst

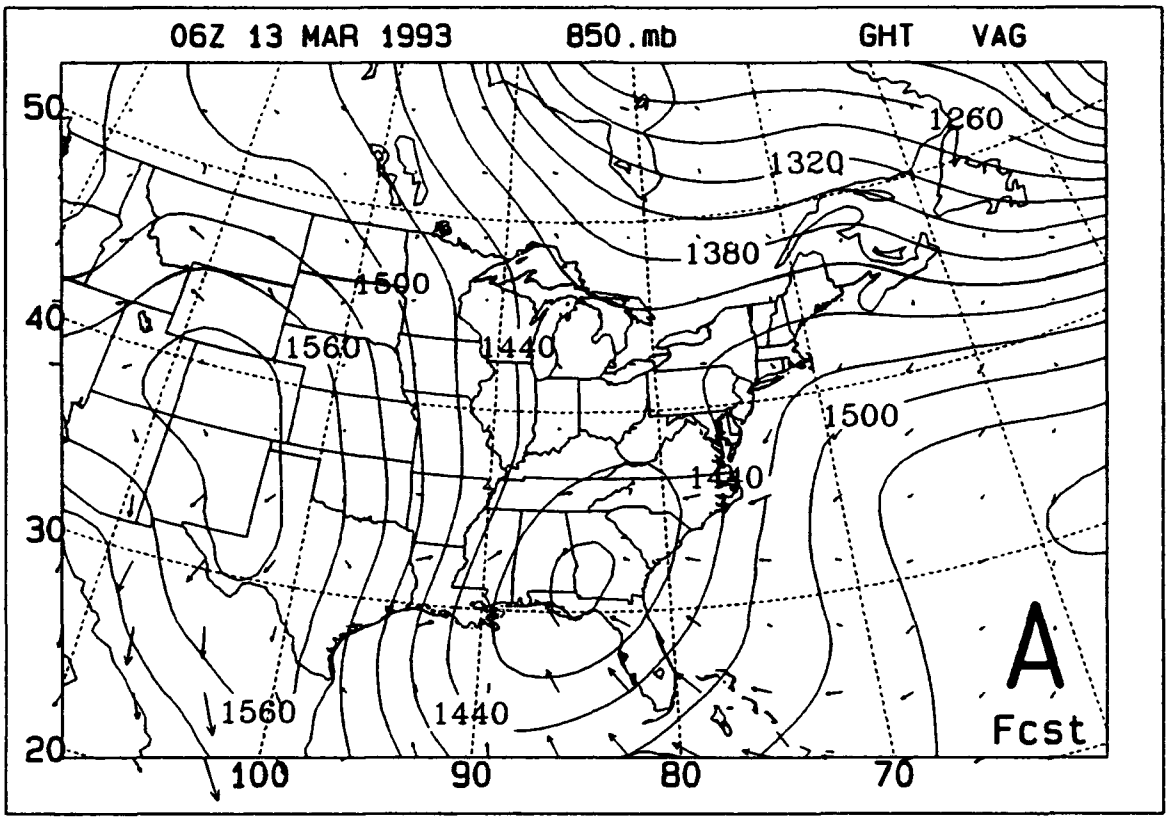

Figure 43. As in Figure 41, except for 0600 UTC 13 March 1993.

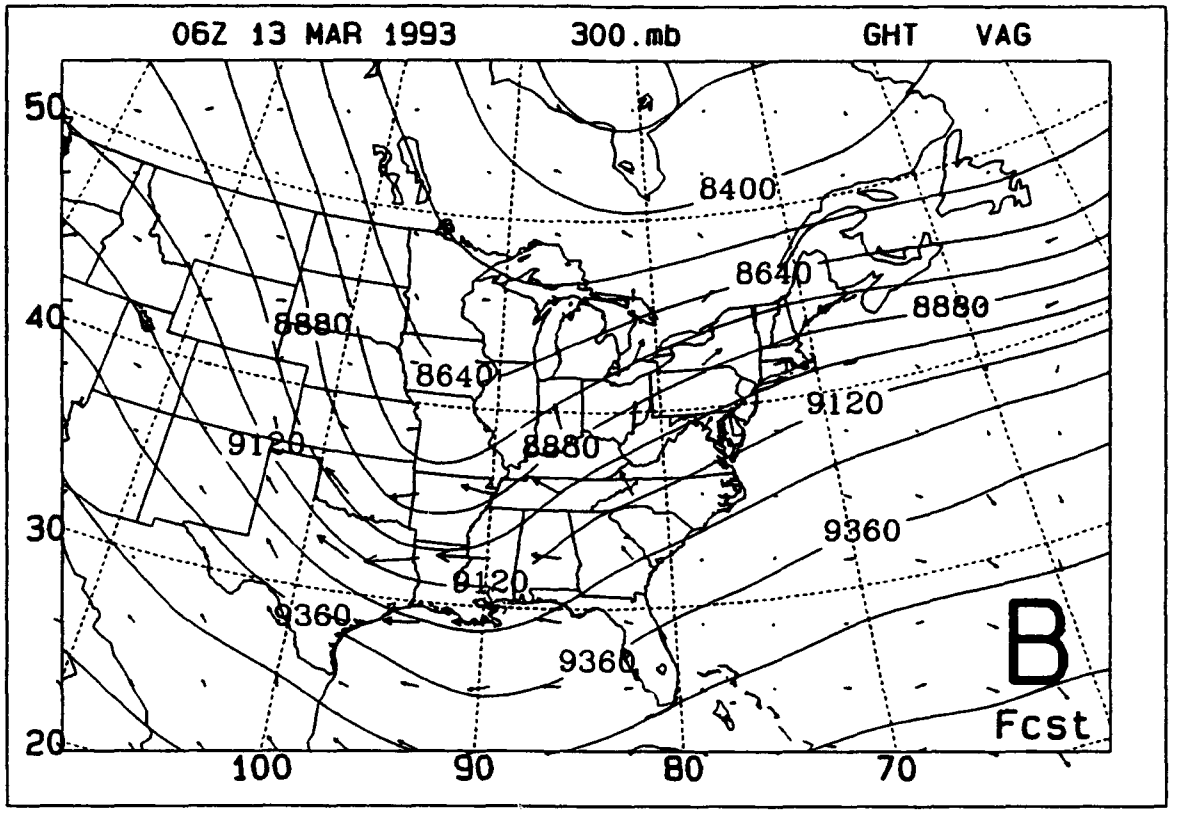
06Z 13 MAR 1993
300.mb
GHT
VAG
50
40
30
20
100
90
80
70
8400
8640
8880
9120
9360
B
Fcst

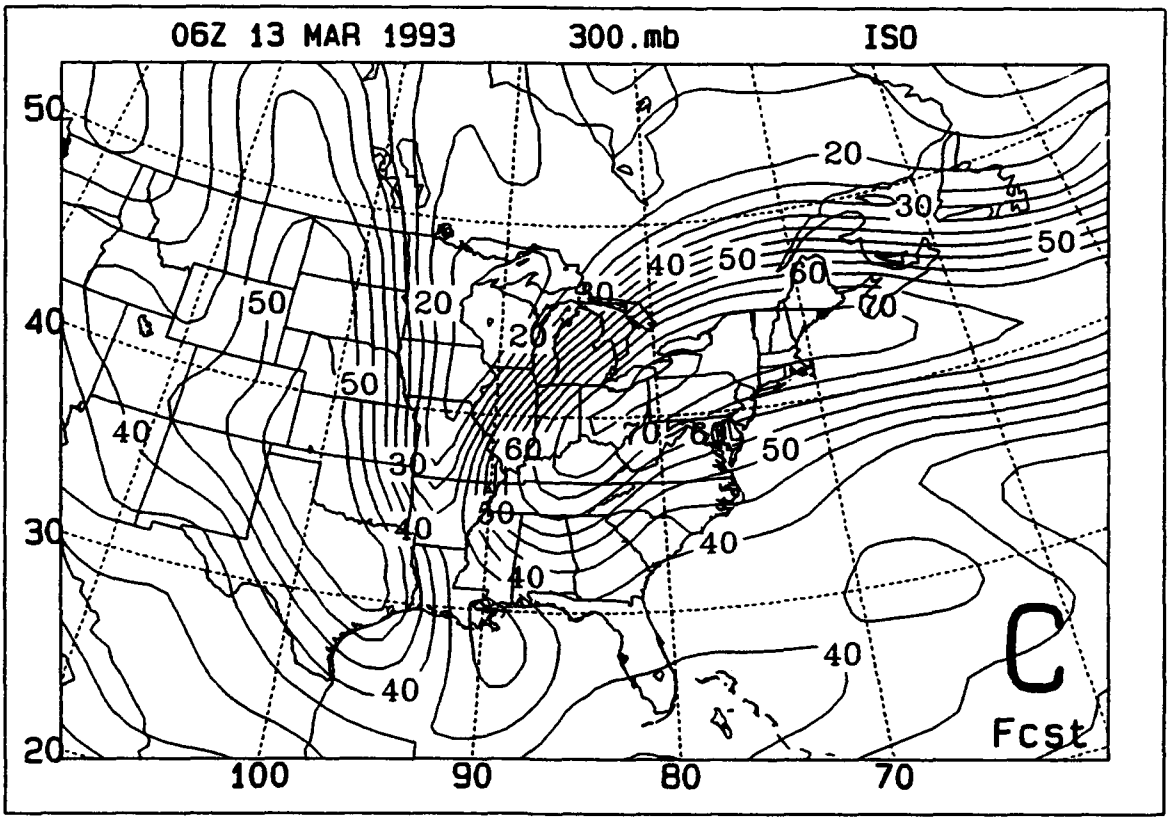
06Z 13 MAR 1993
300.mb
ISO
50
40
30
20
100
90
80
70
20
30
40
50
60
C
Fcst

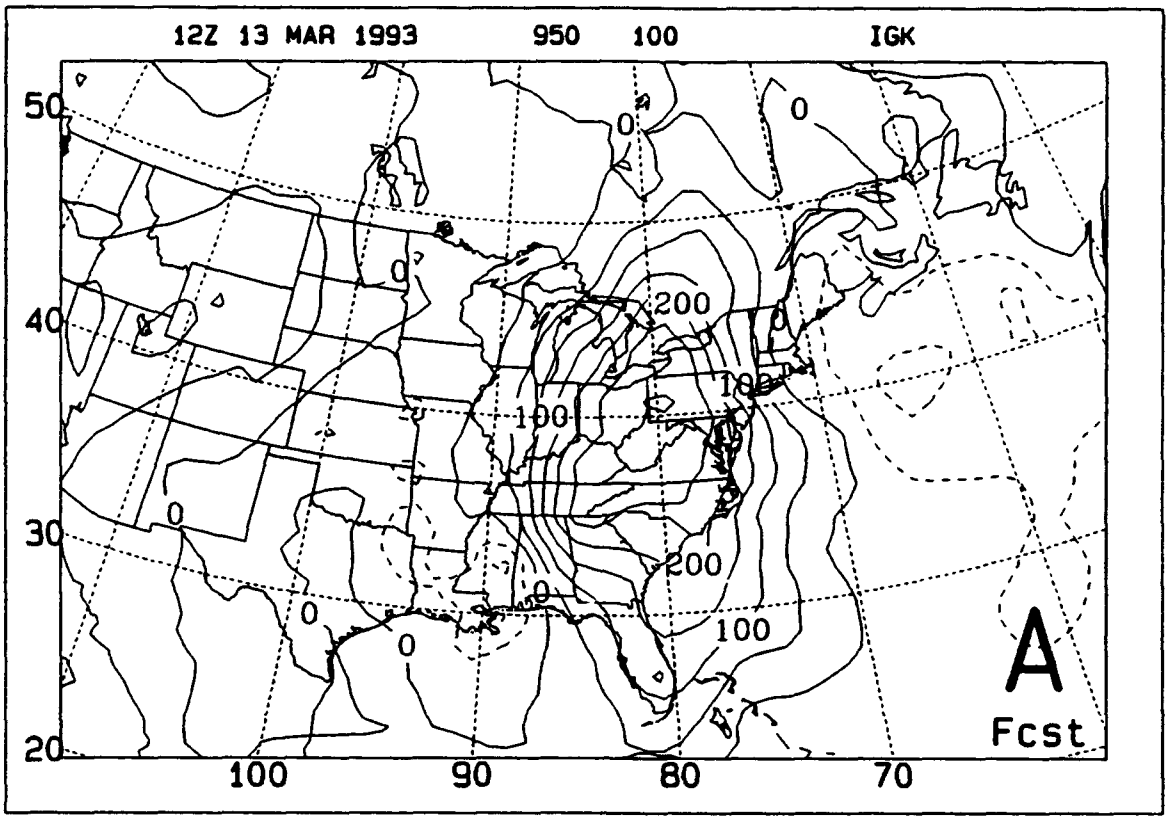

Figure 44. As in Figure 39, except for 1200 UTC 13 March 1993.

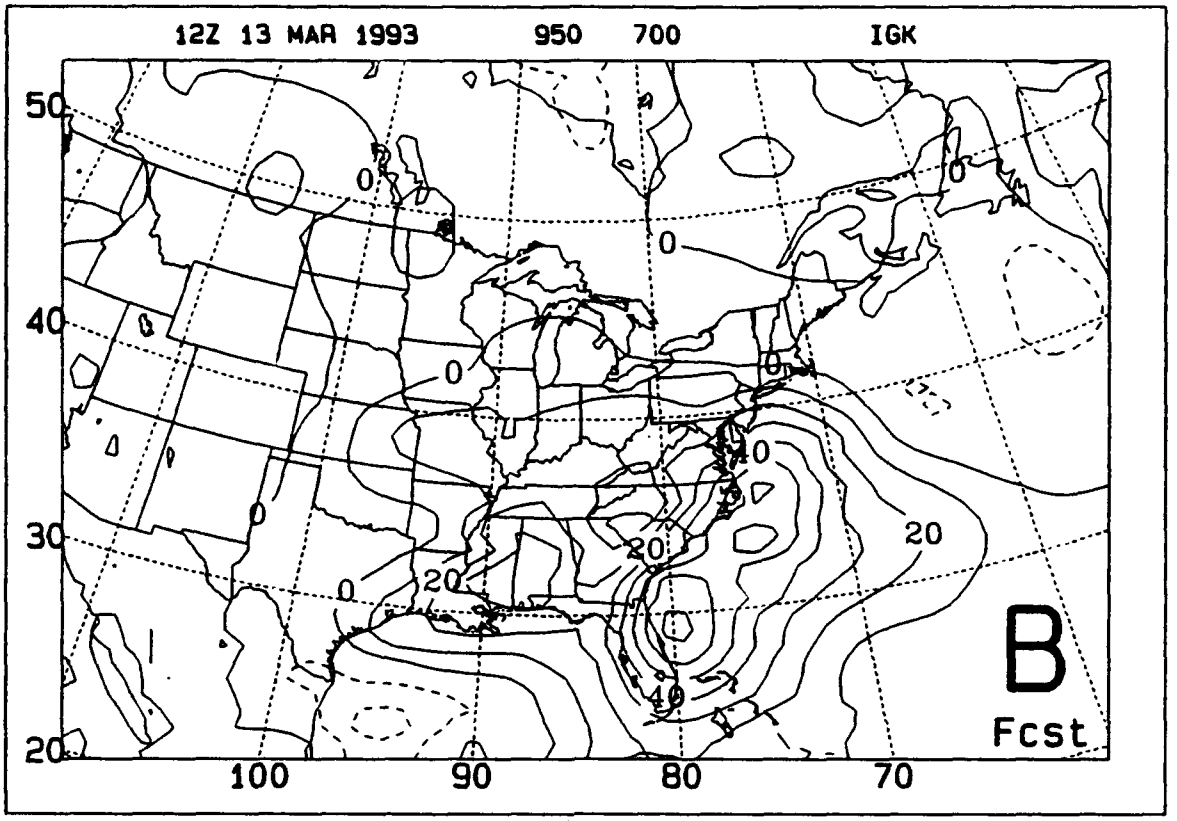
12Z 13 MAR 1993
950 700
IGK
50
40
30
20
100
90
80
70
0
20
40
B
Fcst

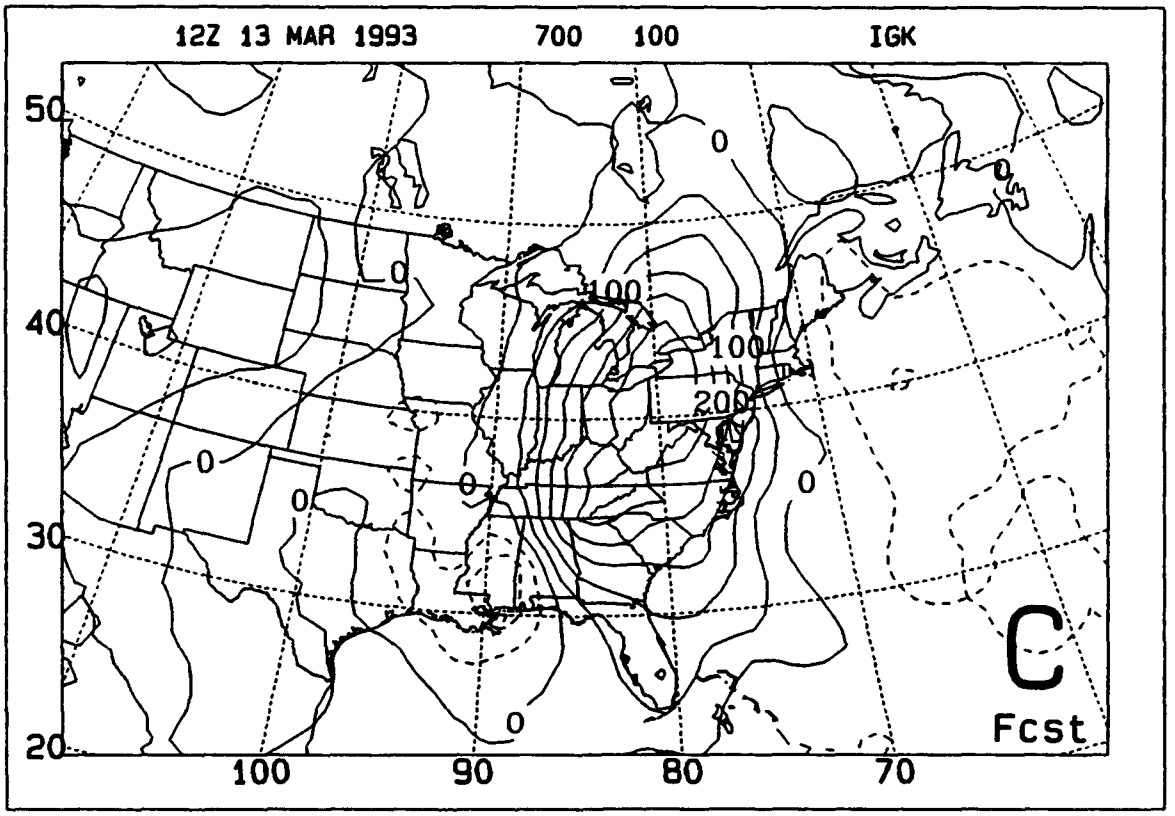
12Z 13 MAR 1993
700 100
IGK
50
40
30
20
100
90
80
70
0
100
200
C
Fcst

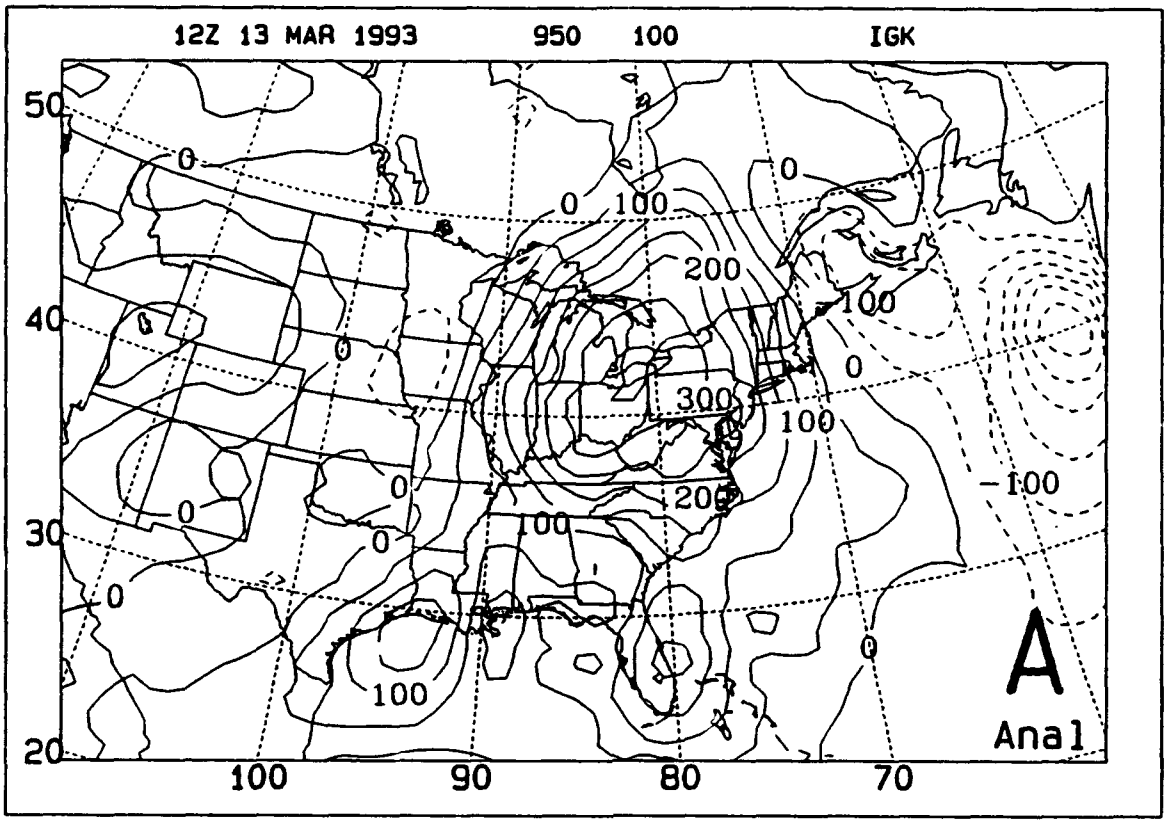

Figure 45. As in Figure 40, except for 1200 UTC 13 March 1993.

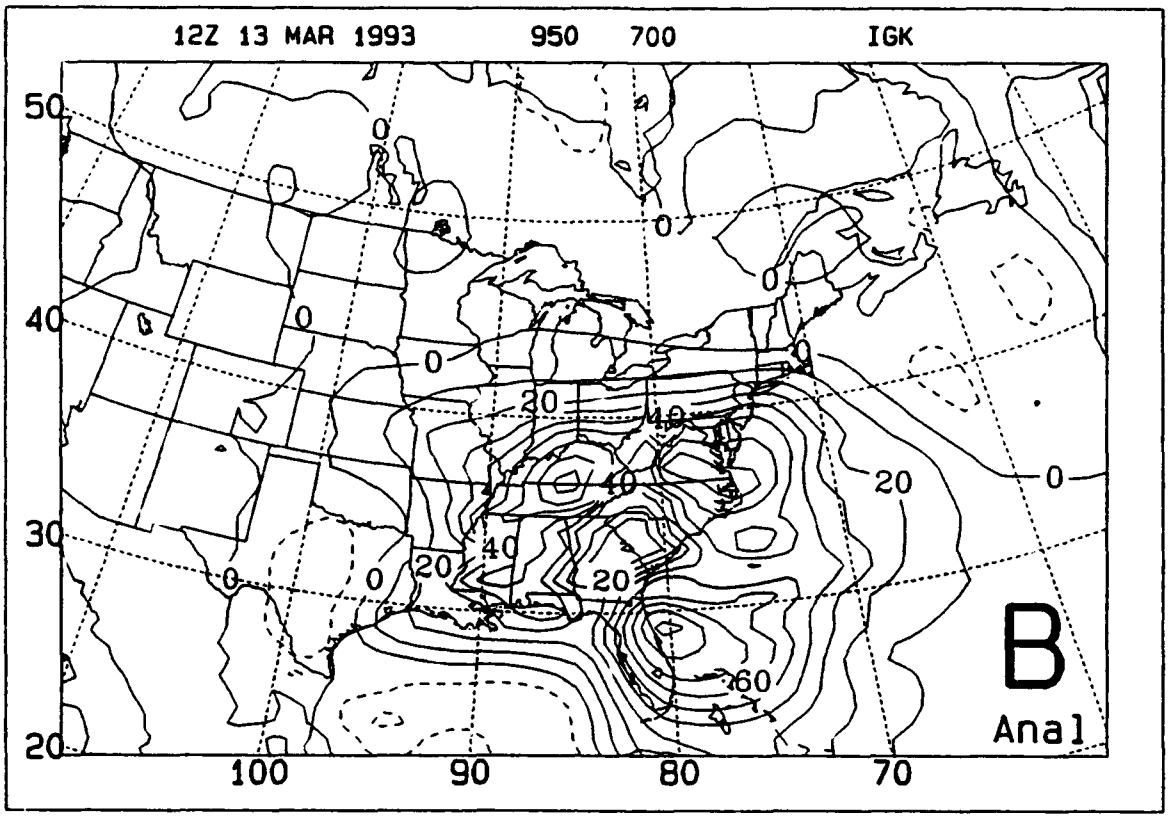
12Z 13 MAR 1993
950 700
IGK
50
40
30
20
100
90
80
70
0
20
40
60
B
Anal

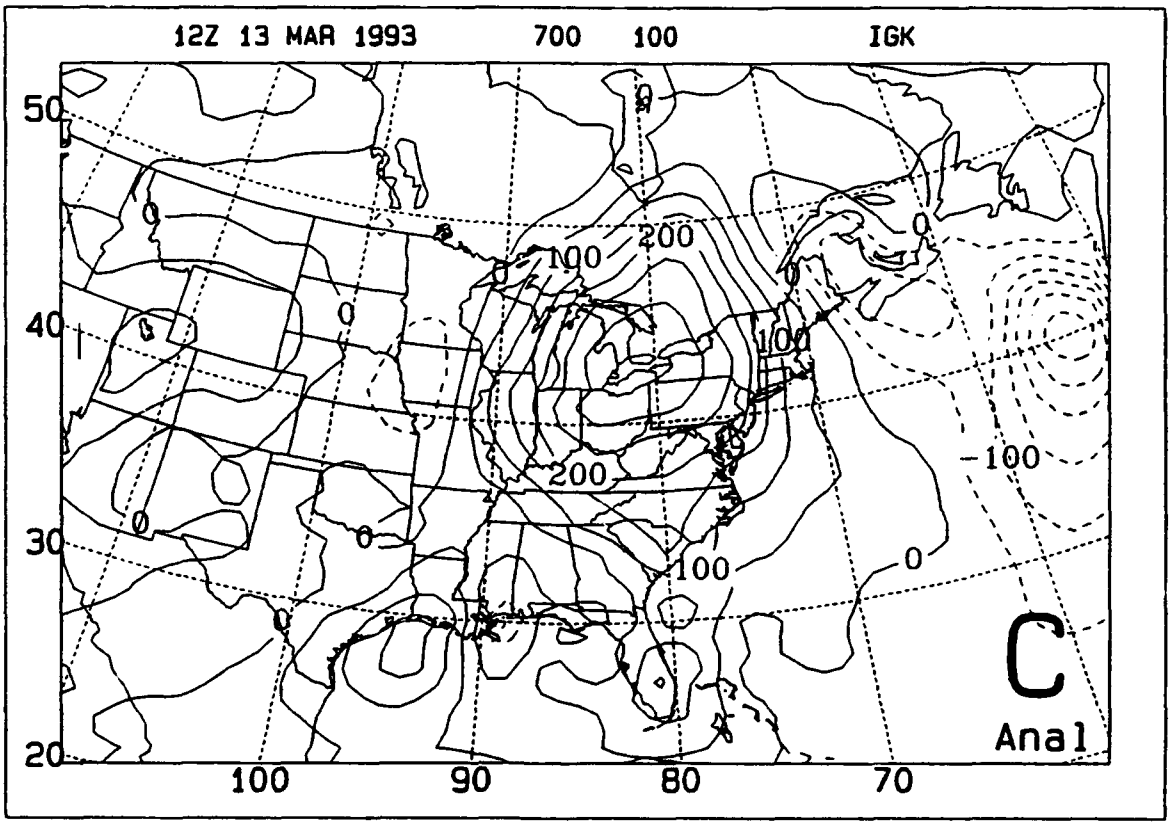
12Z 13 MAR 1993
700 100
IGK
50
40
30
20
100
90
80
70
0
100
200
-100
C
Anal

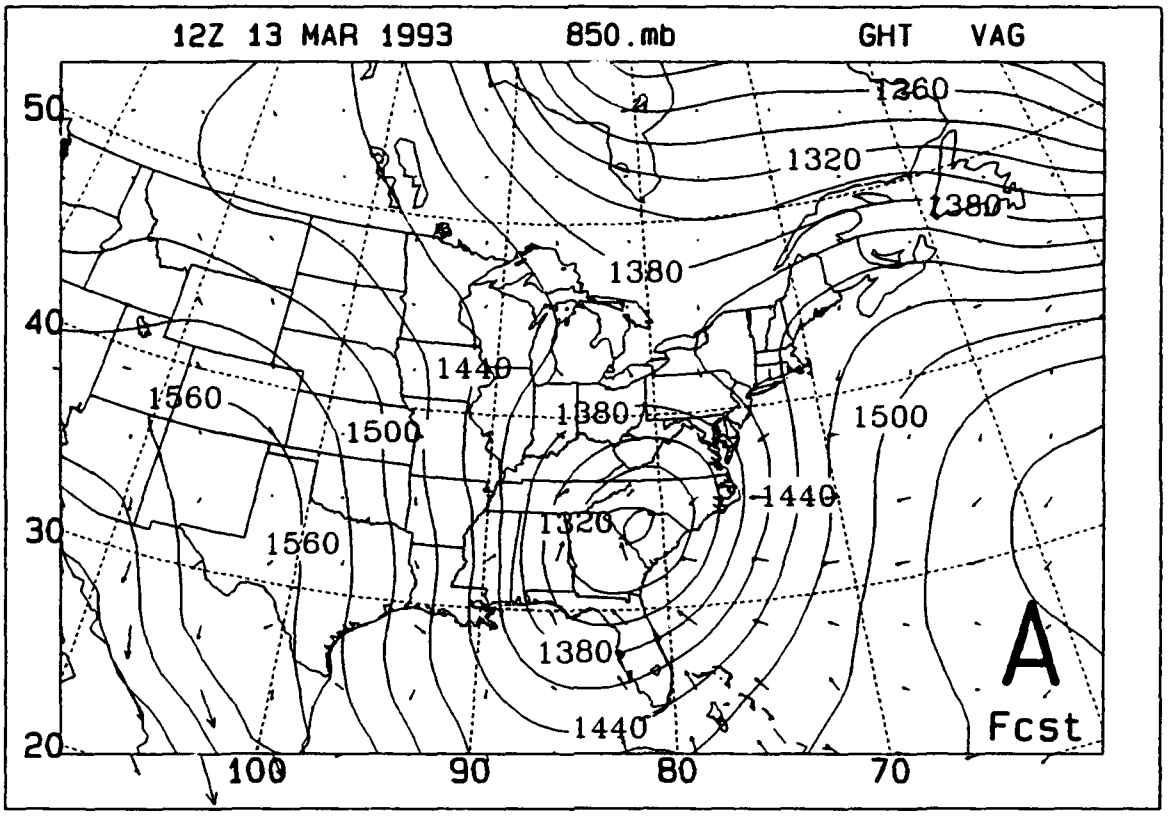

Figure 46. As in Figure 41, except for 1200 UTC 13 March 1993.

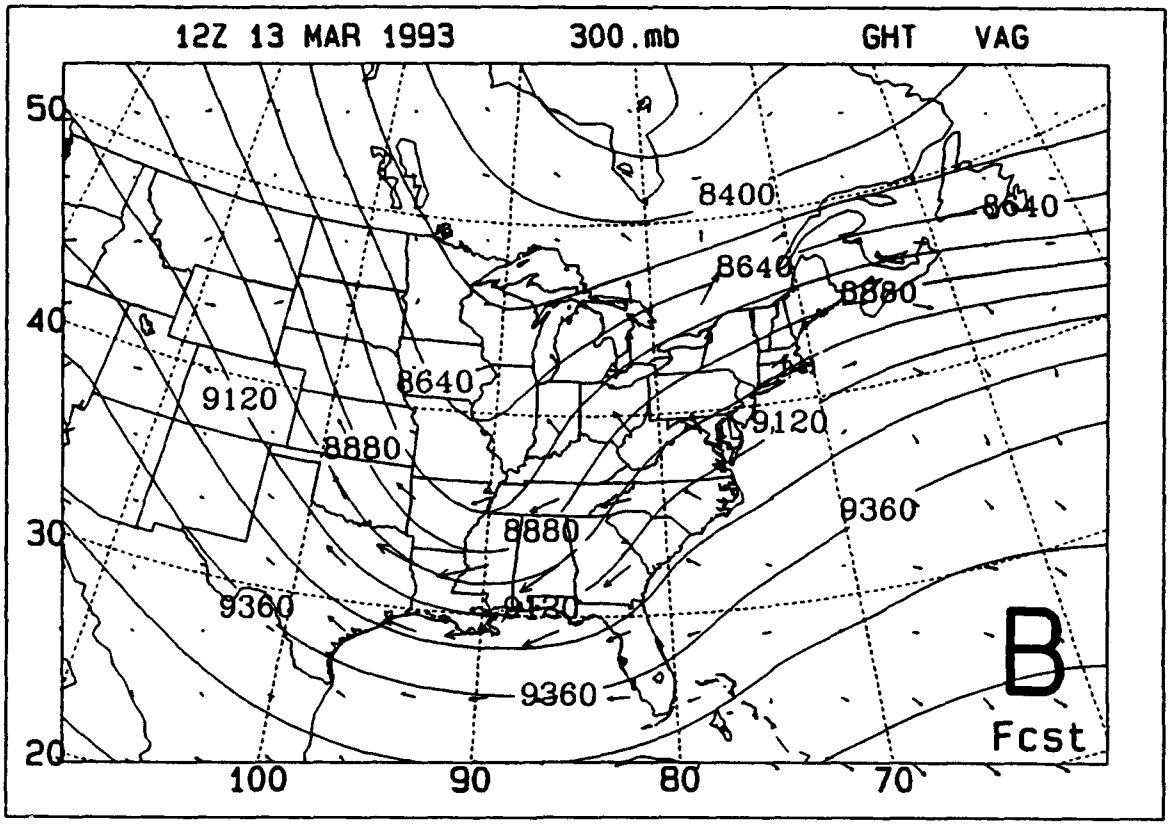
12Z 13 MAR 1993
300.mb
GHT
VAG
50
40
30
20
100
90
80
70
8400
8640
8880
9120
9360
B
Fcst

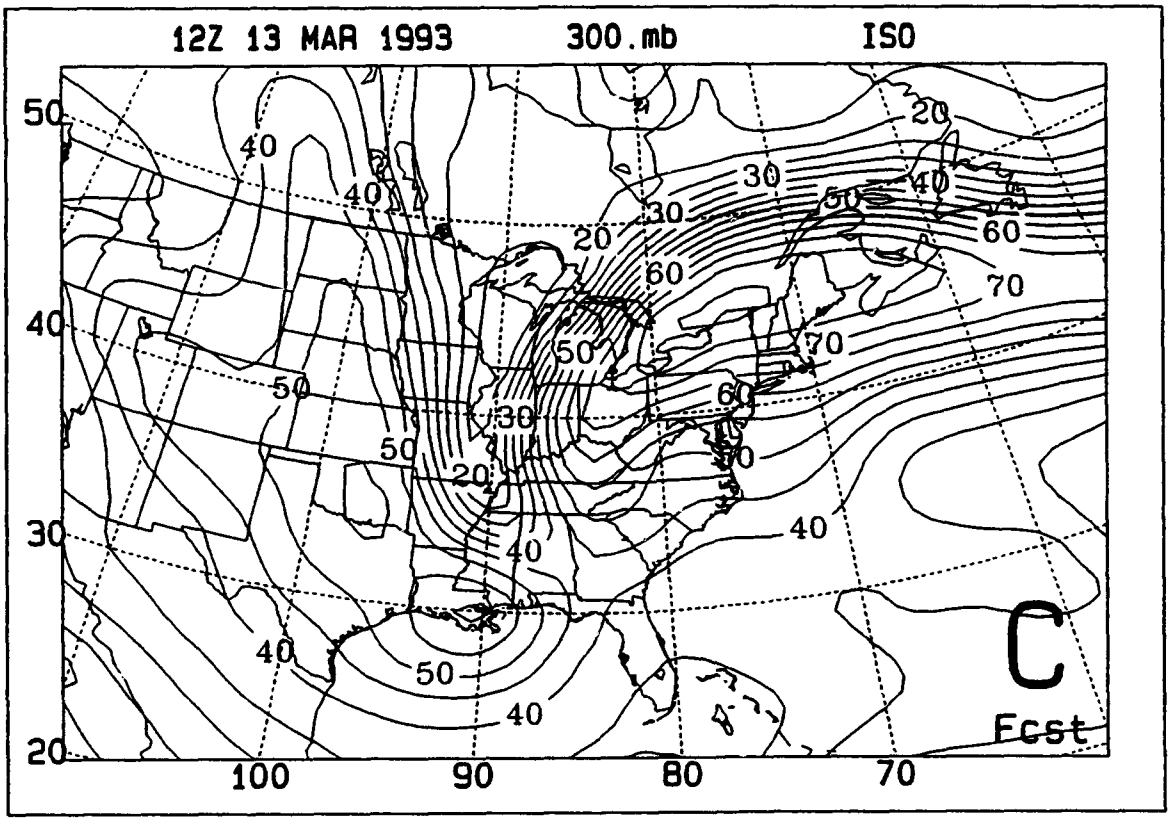
12Z 13 MAR 1993
300.mb
ISO
50
40
30
20
100
90
80
70
20
30
40
50
60
70
C
Fcst

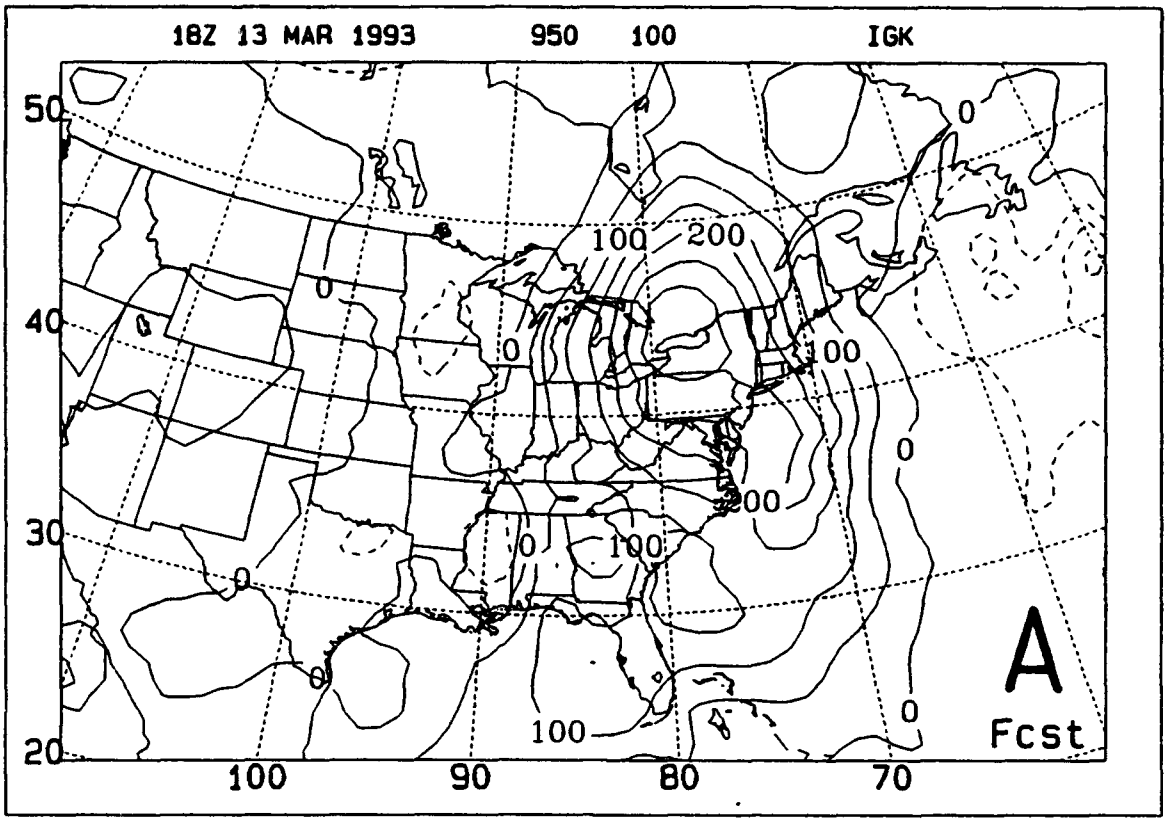

Figure 47. As in Figure 39, except for 1800 UTC 13 March 1993.

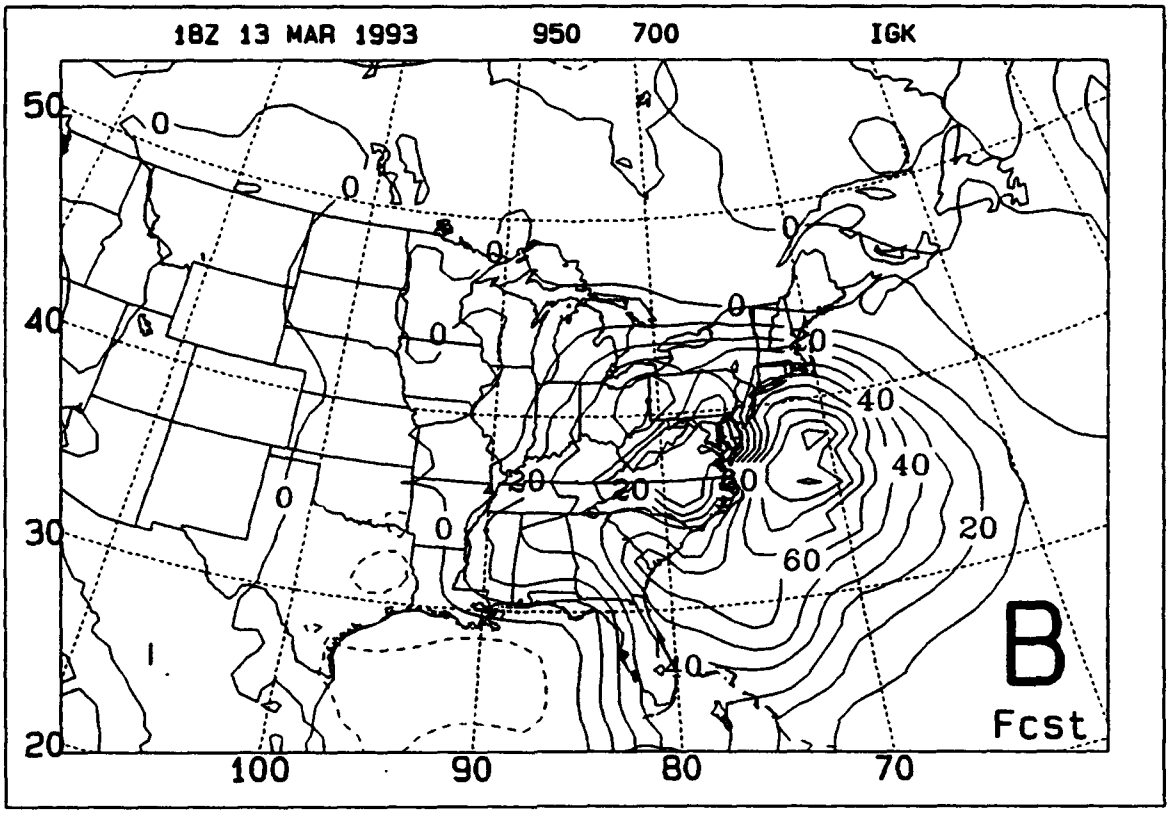
18Z 13 MAR 1993
950
700
IGK
50
40
30
20
100
90
80
70
B
Fcst

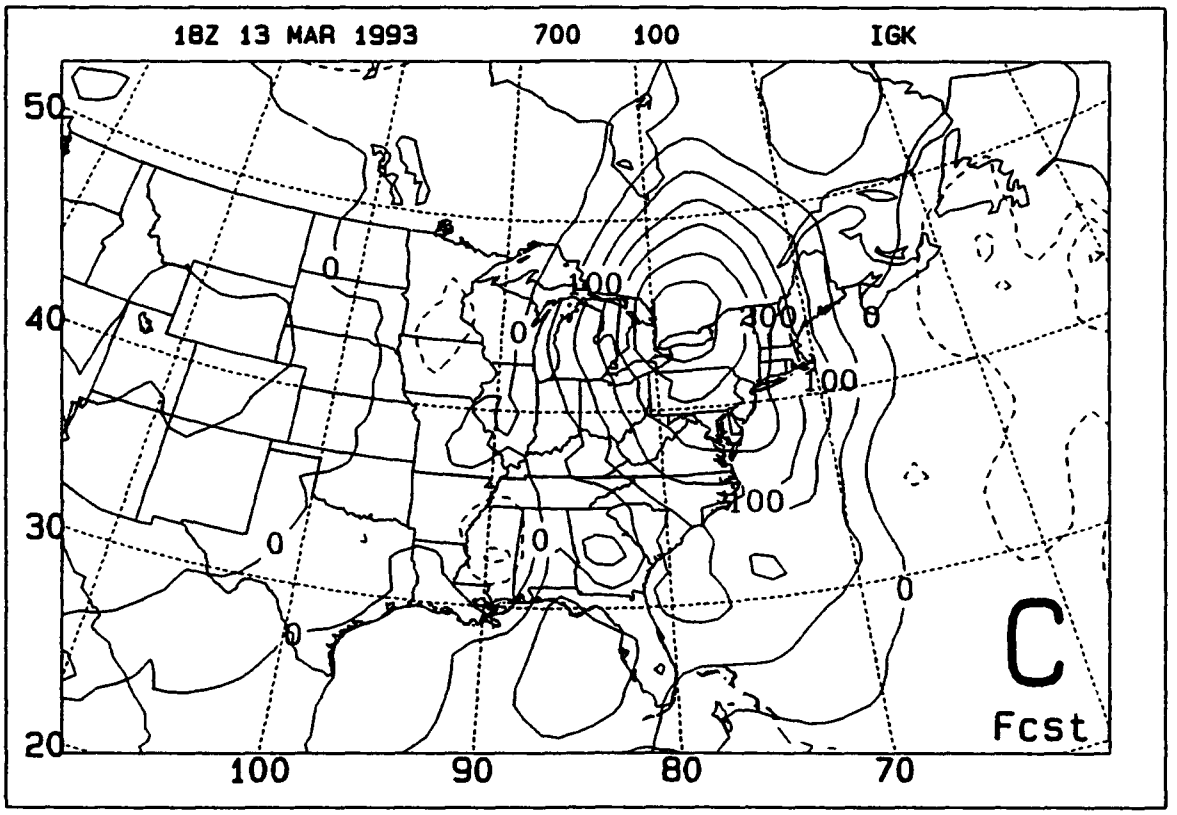
18Z 13 MAR 1993
700
100
IGK
50
40
30
20
100
90
80
70
C
Fcst

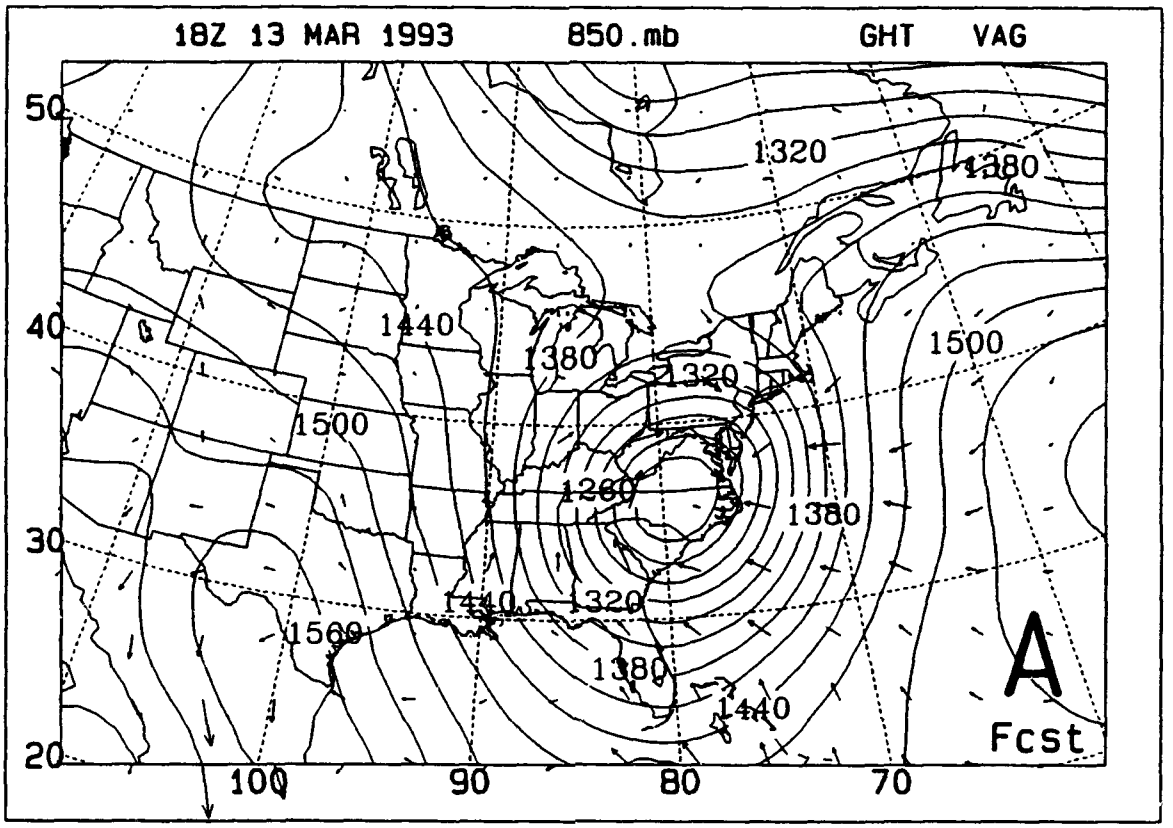

Figure 48. As in Figure 41, except for 1800 UTC 13 March 1993.

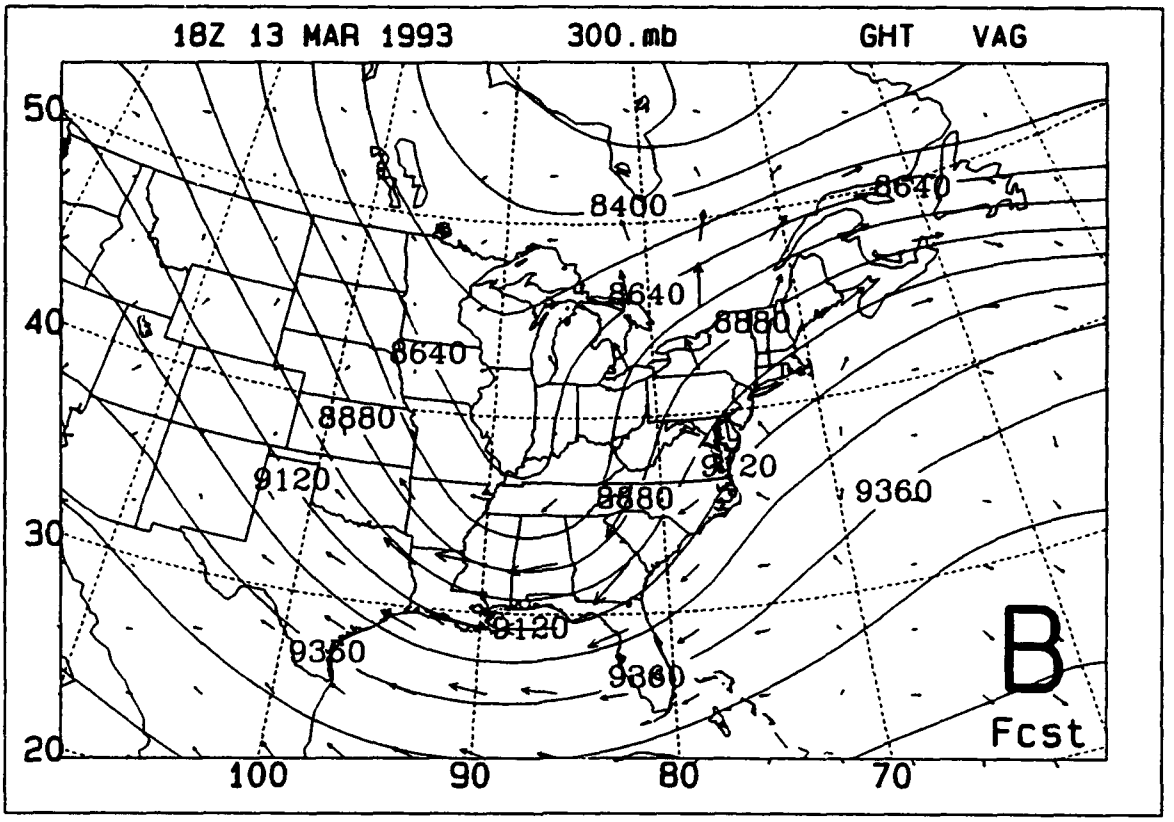
18Z 13 MAR 1993
300.mb
GHT
VAG
8400
8640
8880
9120
9360
B
Fcst
50
40
30
20
100
90
80
70

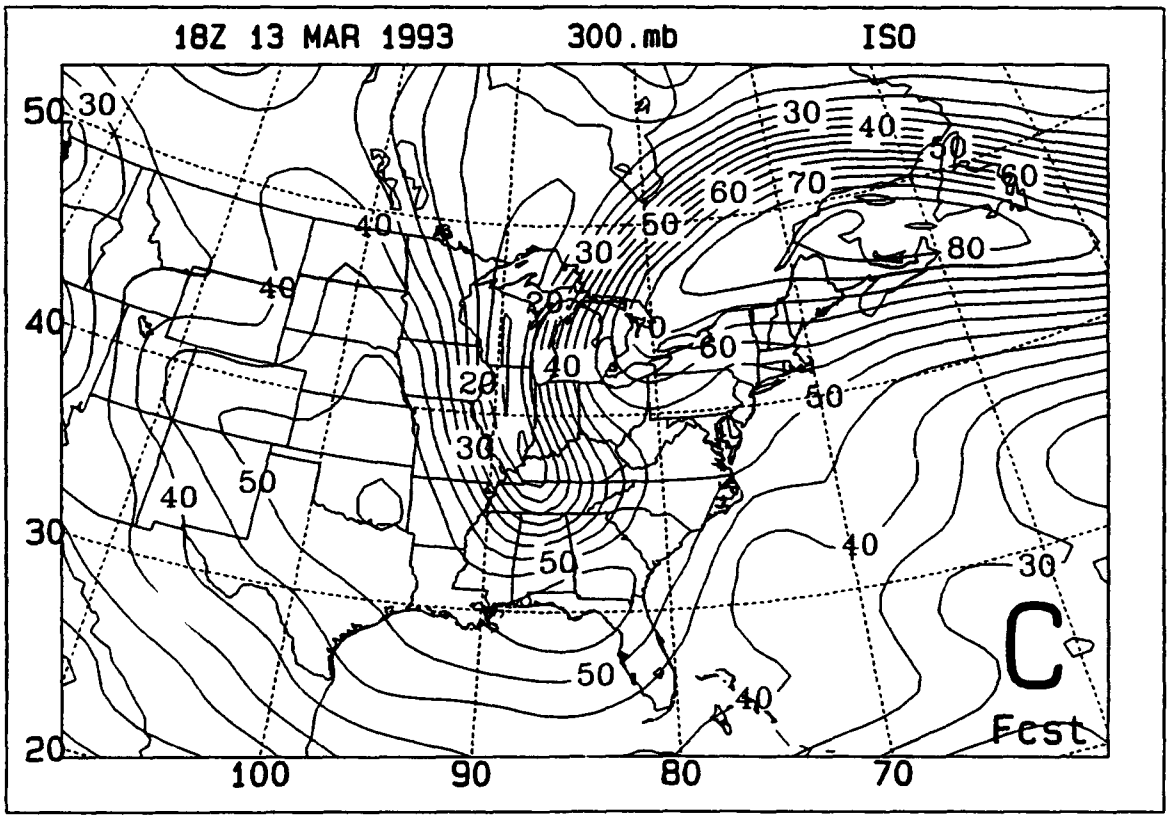
18Z 13 MAR 1993
300.mb
ISO
C
Fcst
50
40
30
20
100
90
80
70

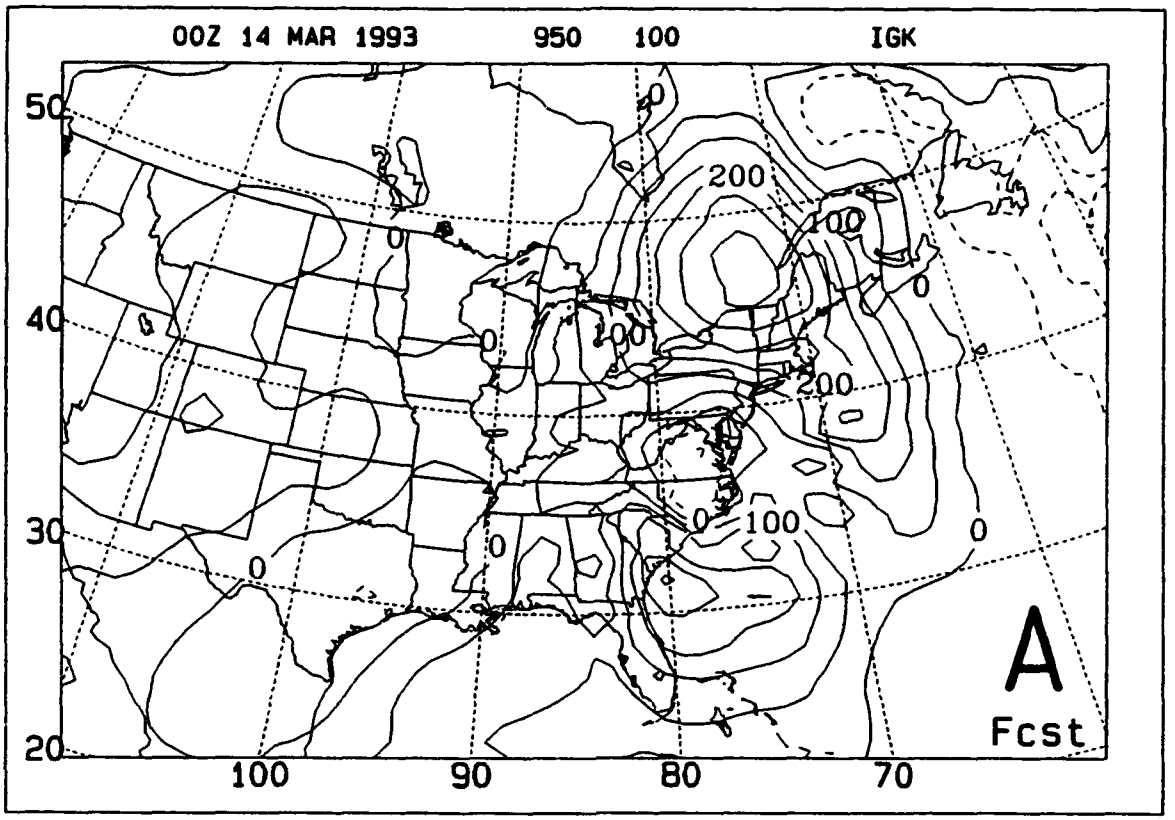

Figure 49. As in Figure 39, except for 0000 UTC 14 March 1993.

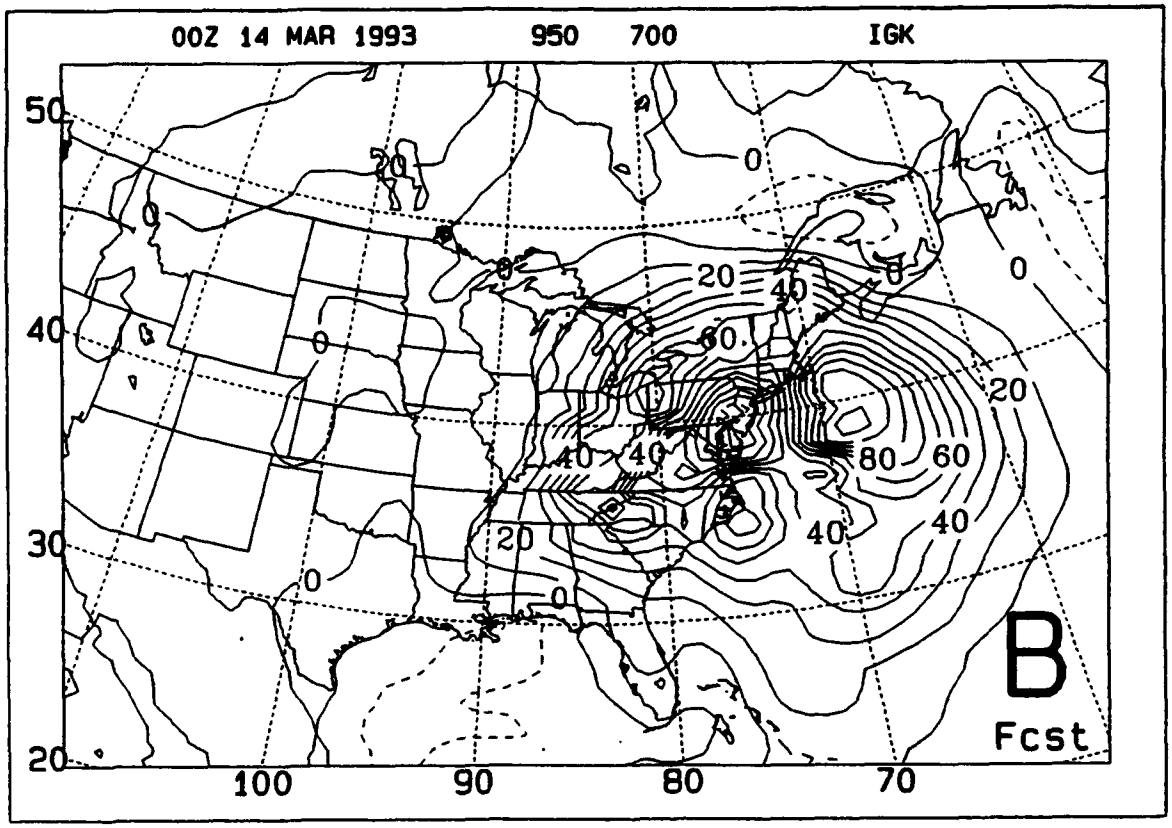
00Z 14 MAR 1993
950
700
IGK
50
40
30
20
100
90
80
70
B
Fcst

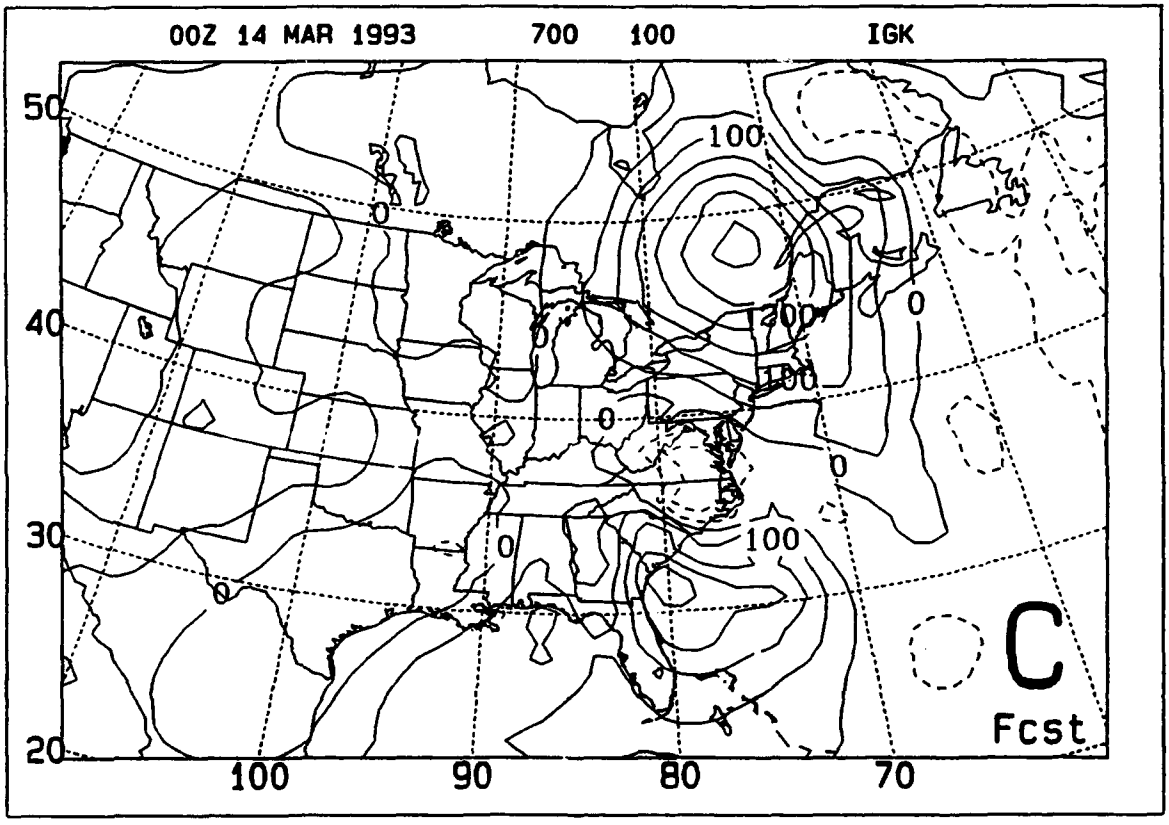
00Z 14 MAR 1993
700
100
IGK
50
40
30
20
100
90
80
70
C
Fcst

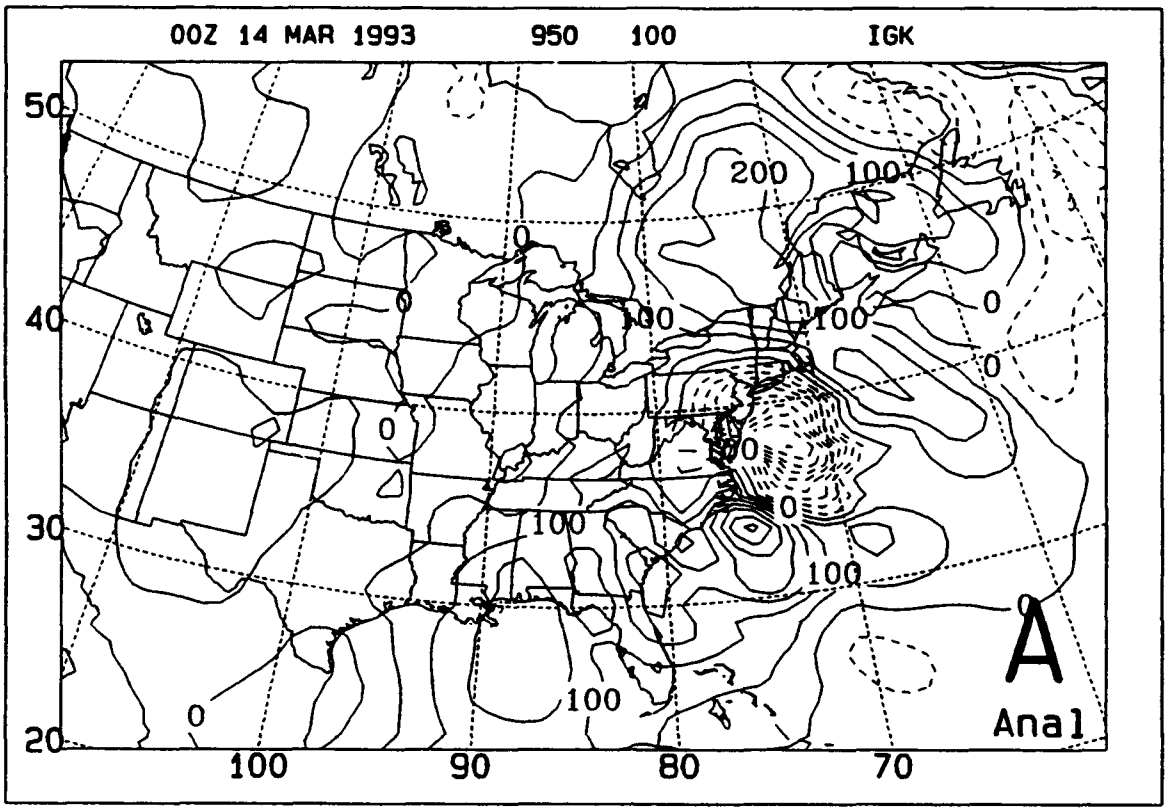

Figure 50. As in Figure 40, except for 0000 UTC 14 March 1993.

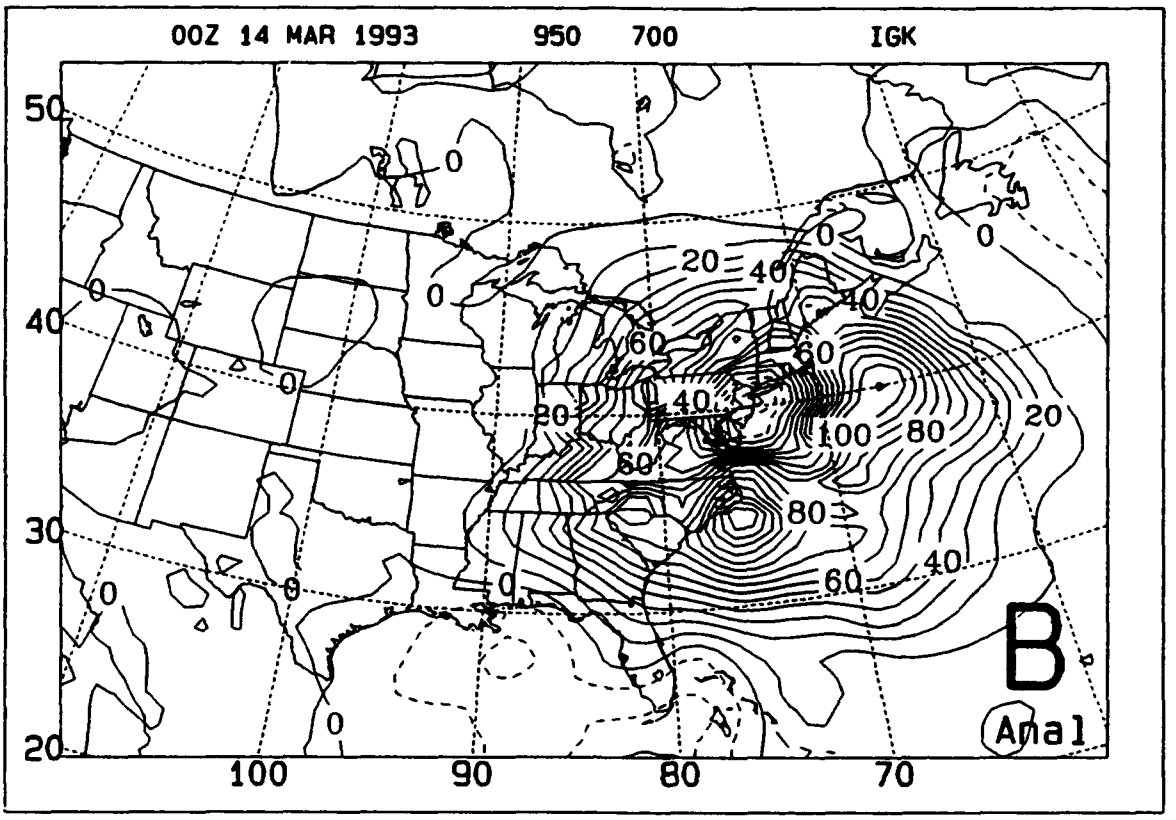
00Z 14 MAR 1993
950 700
IGK
50
40
30
20
100
90
80
70
B
Anal

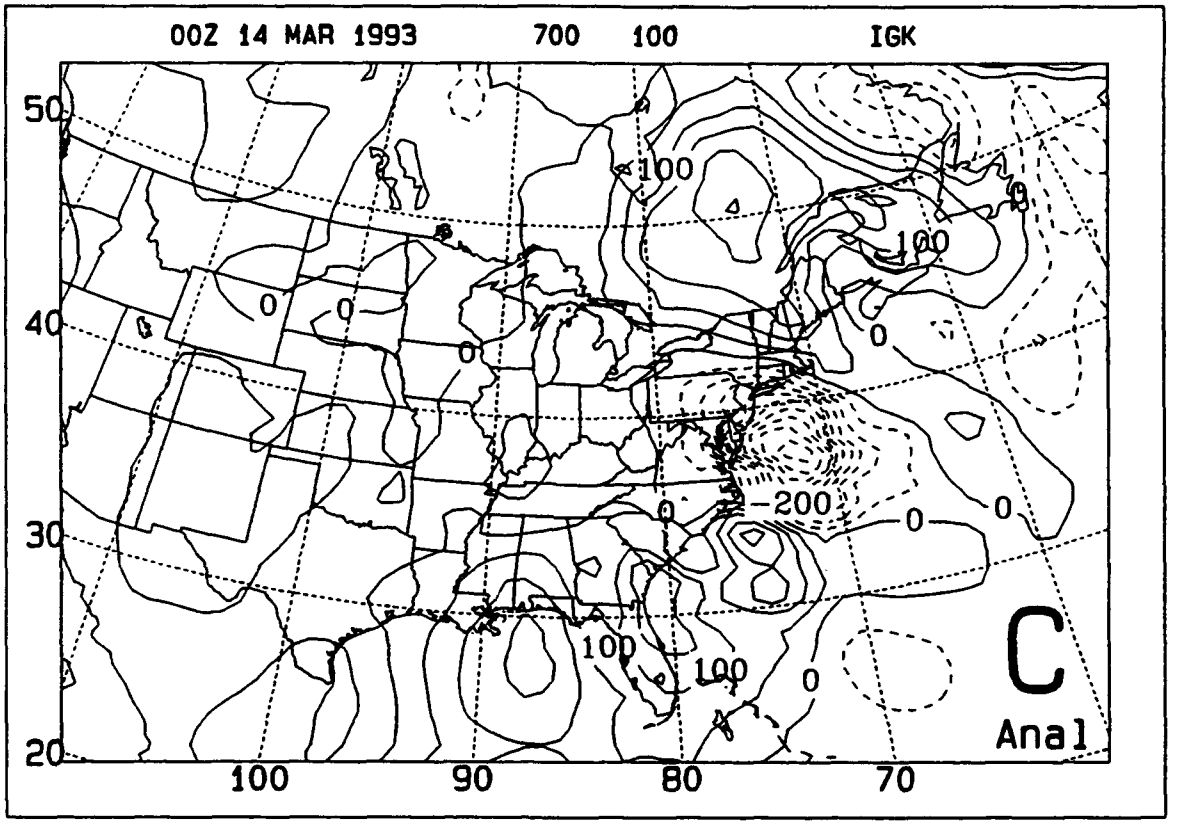
00Z 14 MAR 1993
700 100
IGK
50
40
30
20
100
90
80
70
C
Anal

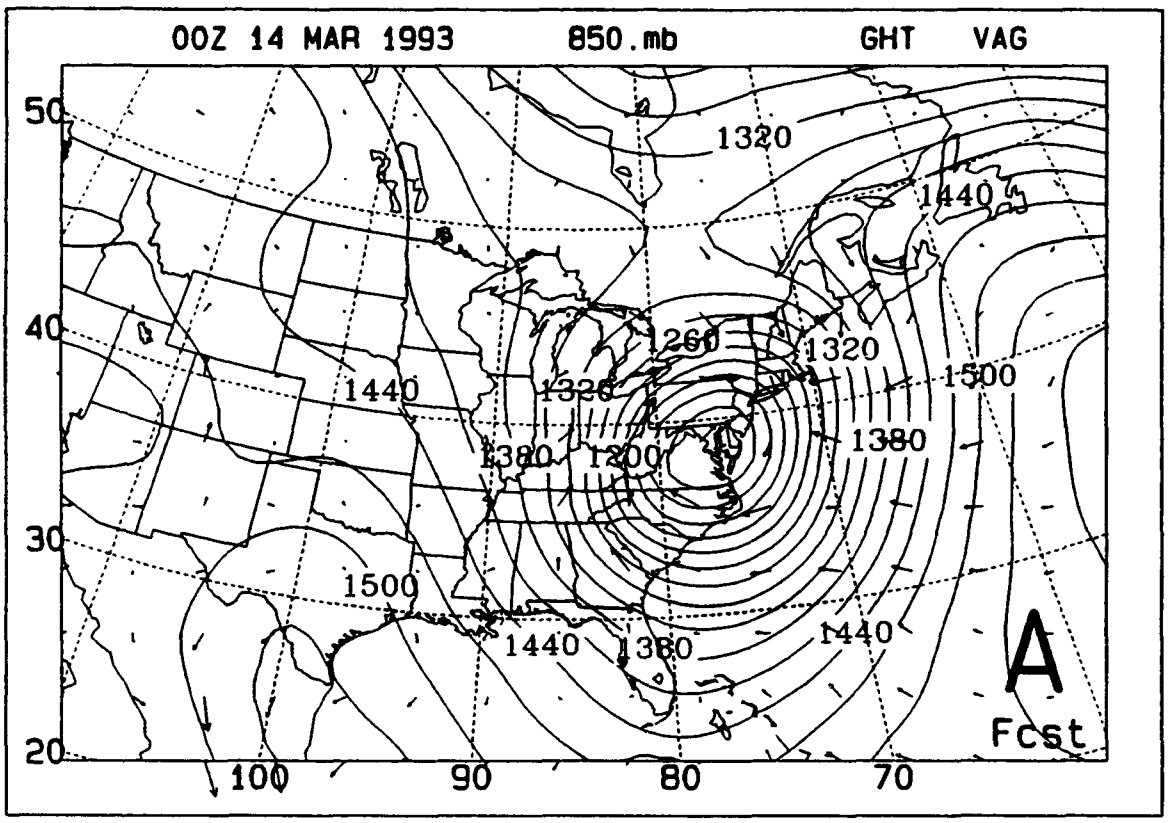

Figure 51. As in Figure 41, except for 0000 UTC 14 March 1993.

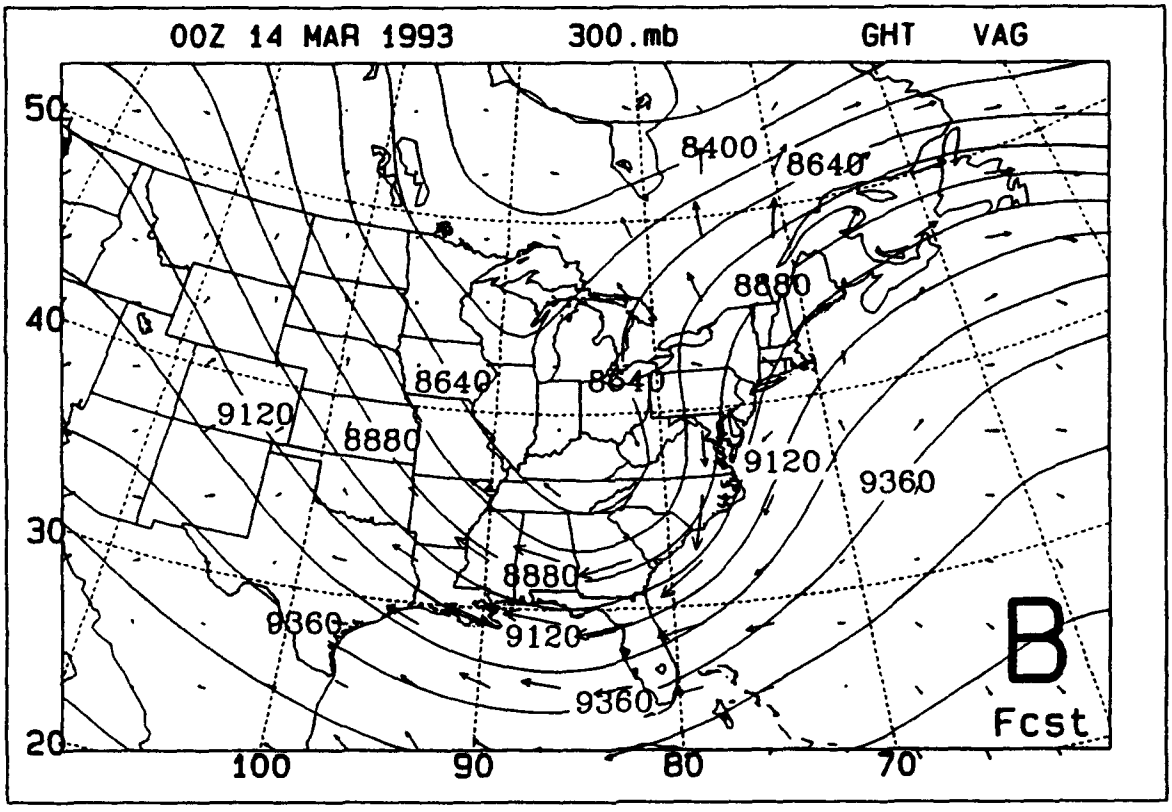
00Z 14 MAR 1993
300.mb
GHT
VAG
50
40
30
20
100
90
80
70
8400
8640
8880
8640
8640
9120
8880
9120
9360
8880
9360
9120
9360
B
Fcst

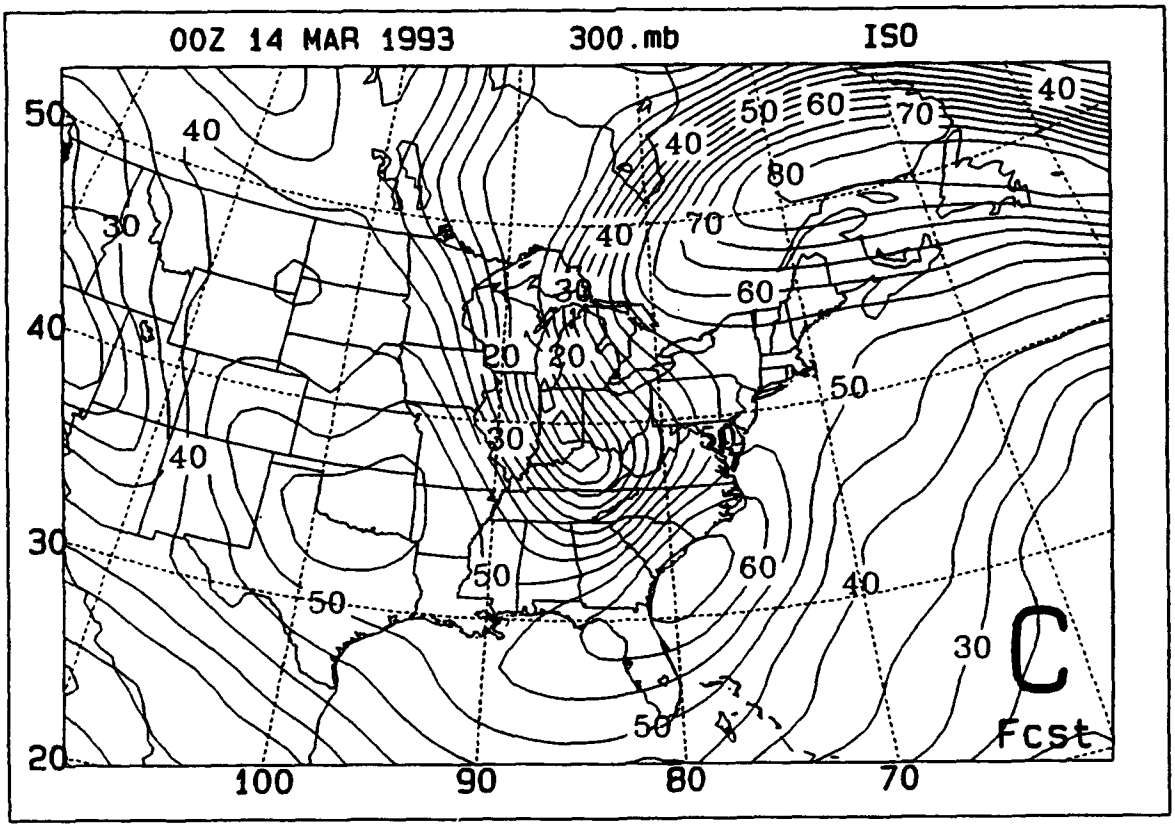
00Z 14 MAR 1993
300.mb
ISO
50
40
30
20
100
90
80
70
40
40
50
60
70
40
80
30
40
70
30
60
20
20
50
30
30
40
50
60
40
30
C
Fcst

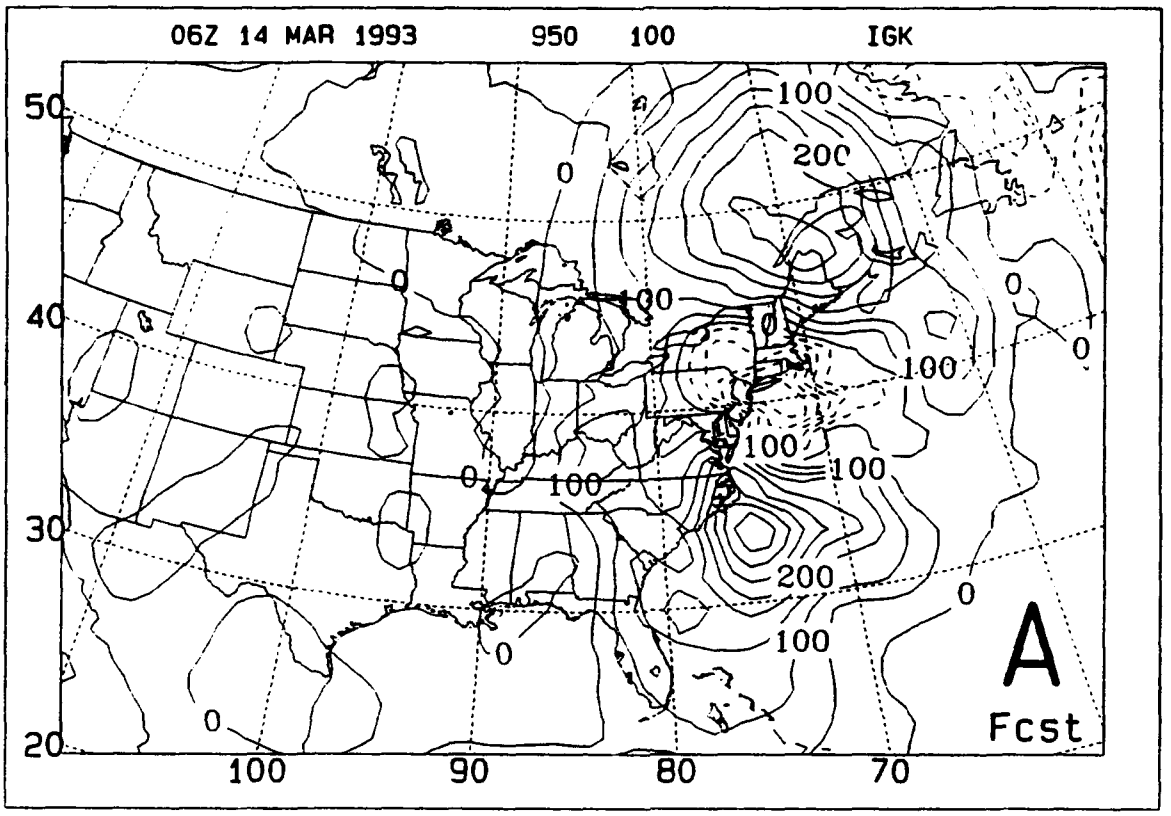

Figure 52. As in Figure 39, except for 0600 UTC 14 March 1993.

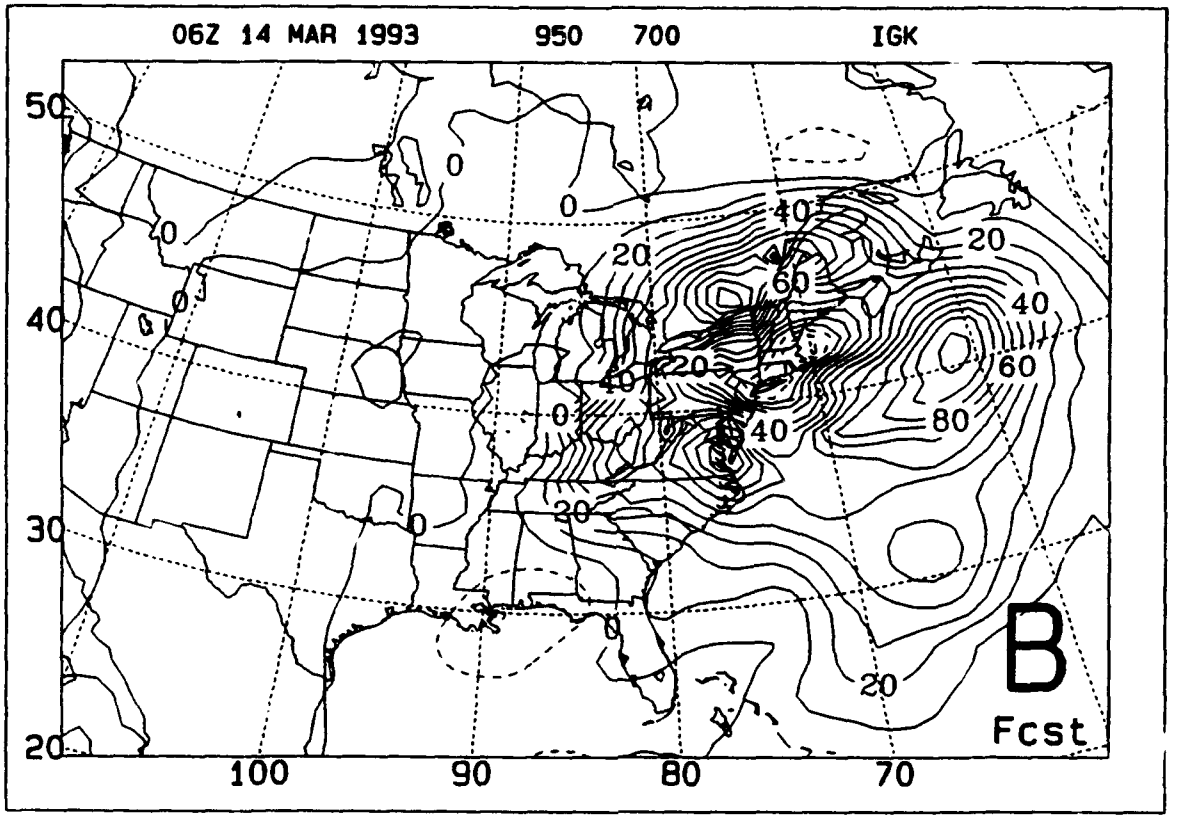
06Z 14 MAR 1993
950 700
IGK
50
40
30
20
100
90
80
70
B
Fcst

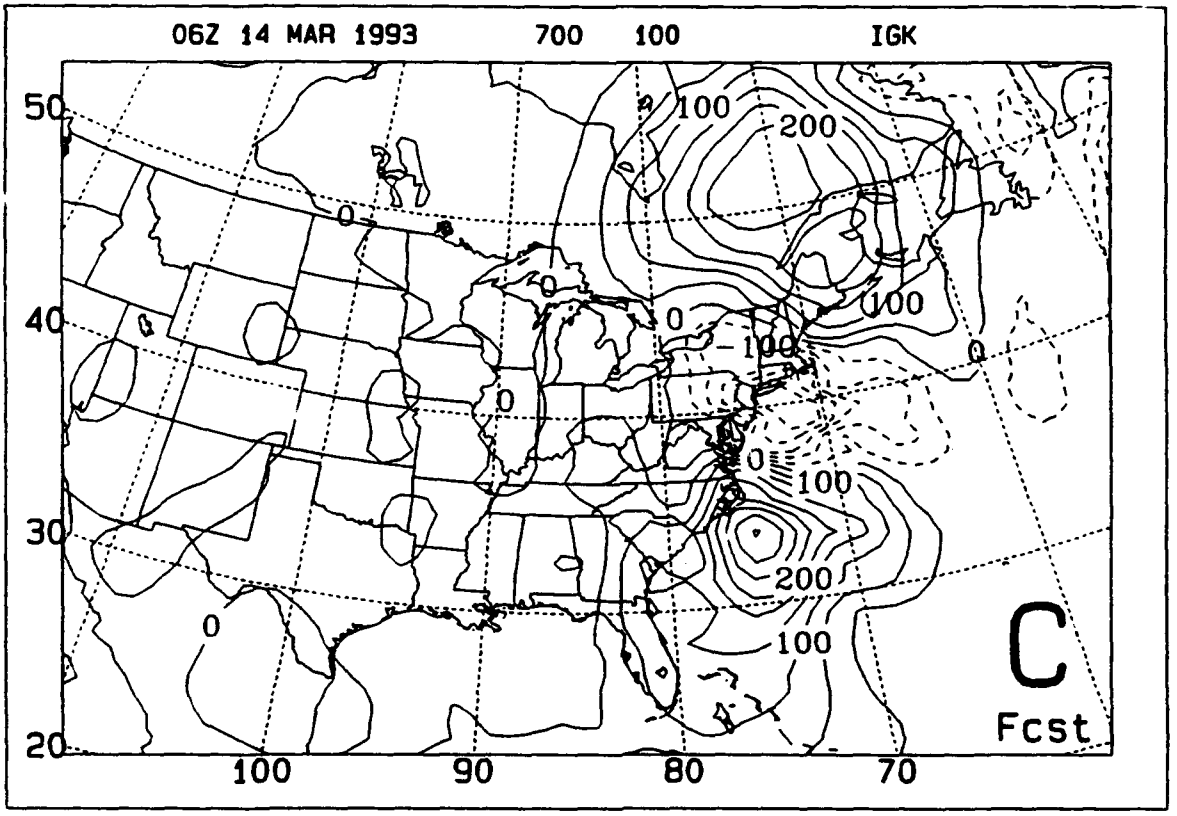
06Z 14 MAR 1993
700 100
IGK
50
40
30
20
100
90
80
70
C
Fcst

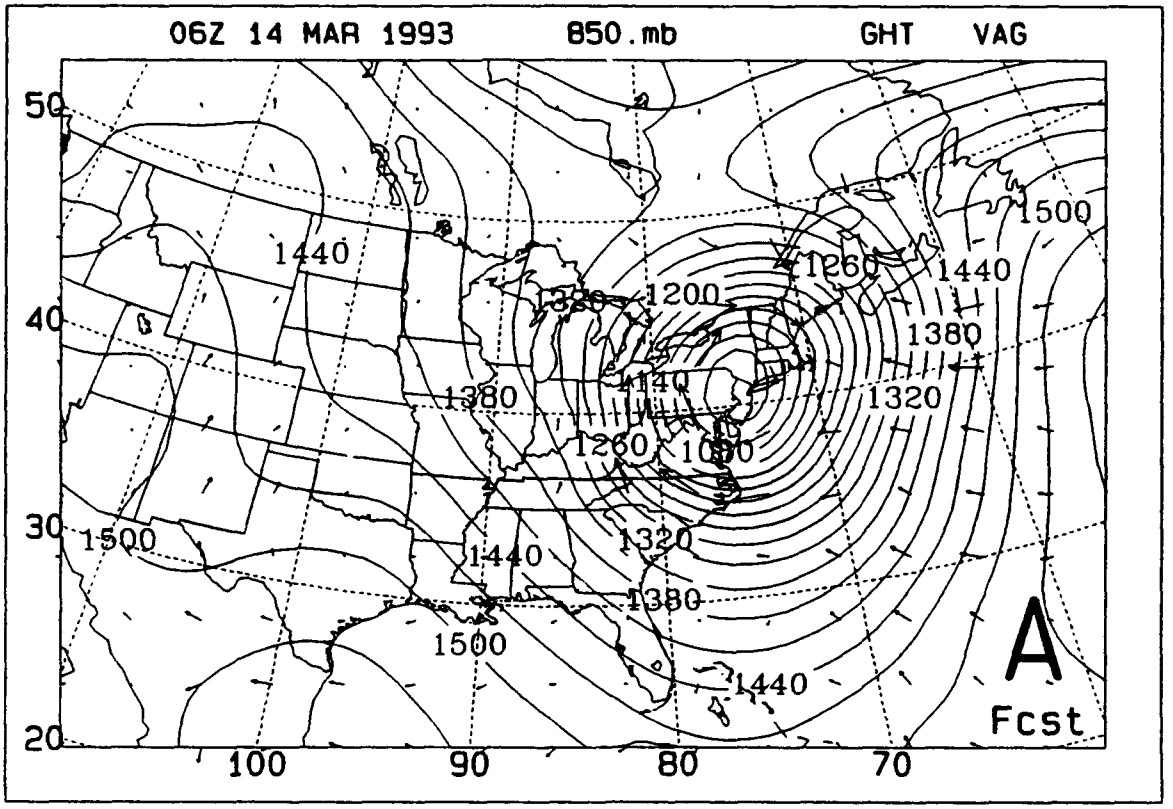

Figure 53. As in Figure 41, except for 0600 UTC 14 March 1993.

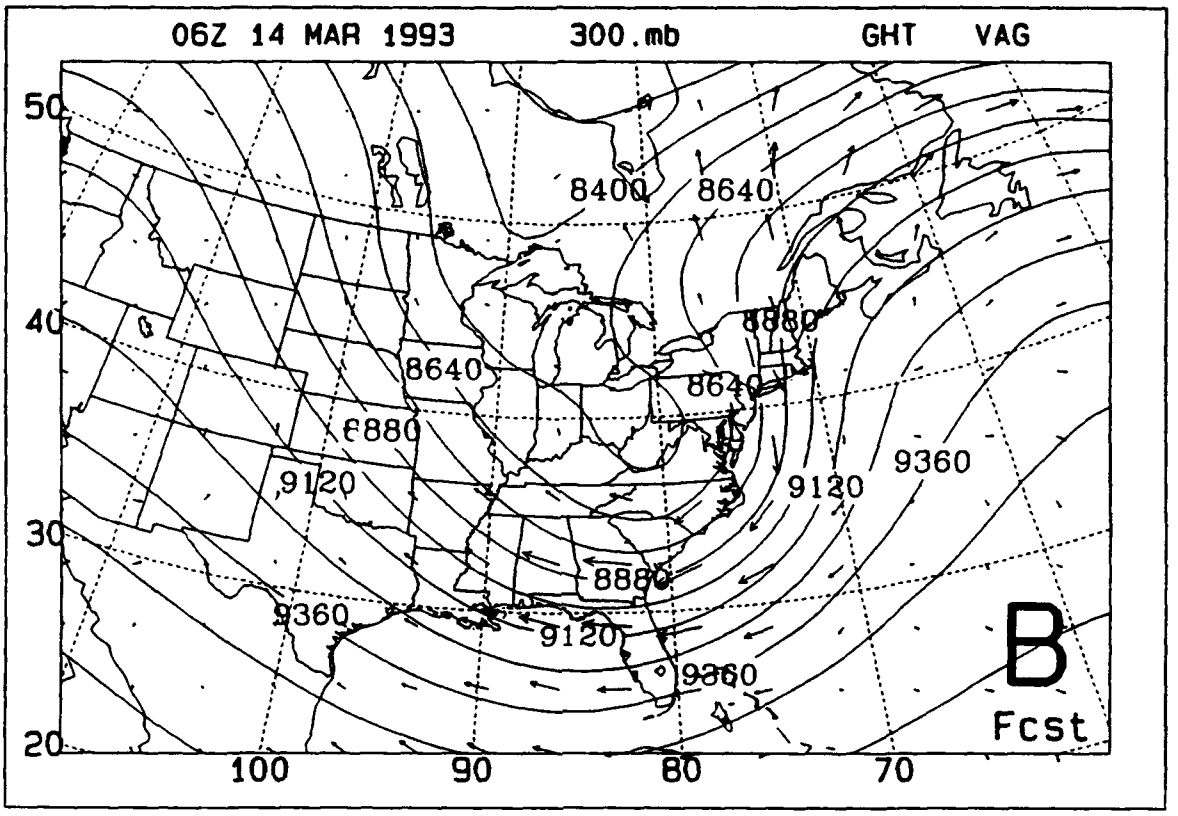
06Z 14 MAR 1993
300.mb
GHT
VAG
8400
8640
8880
9120
9360
B
Fcst
50
40
30
20
100
90
80
70

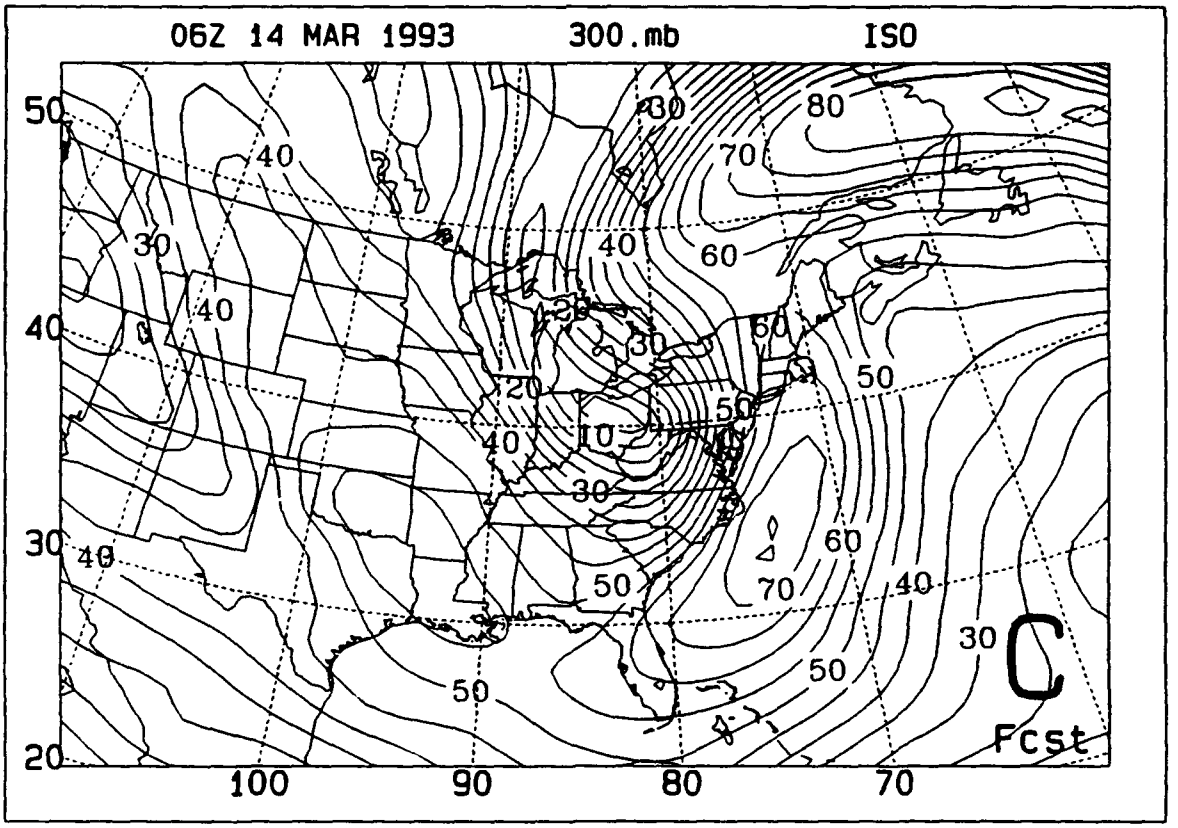
06Z 14 MAR 1993
300.mb
ISO
C
Fcst
50
40
30
20
100
90
80
70

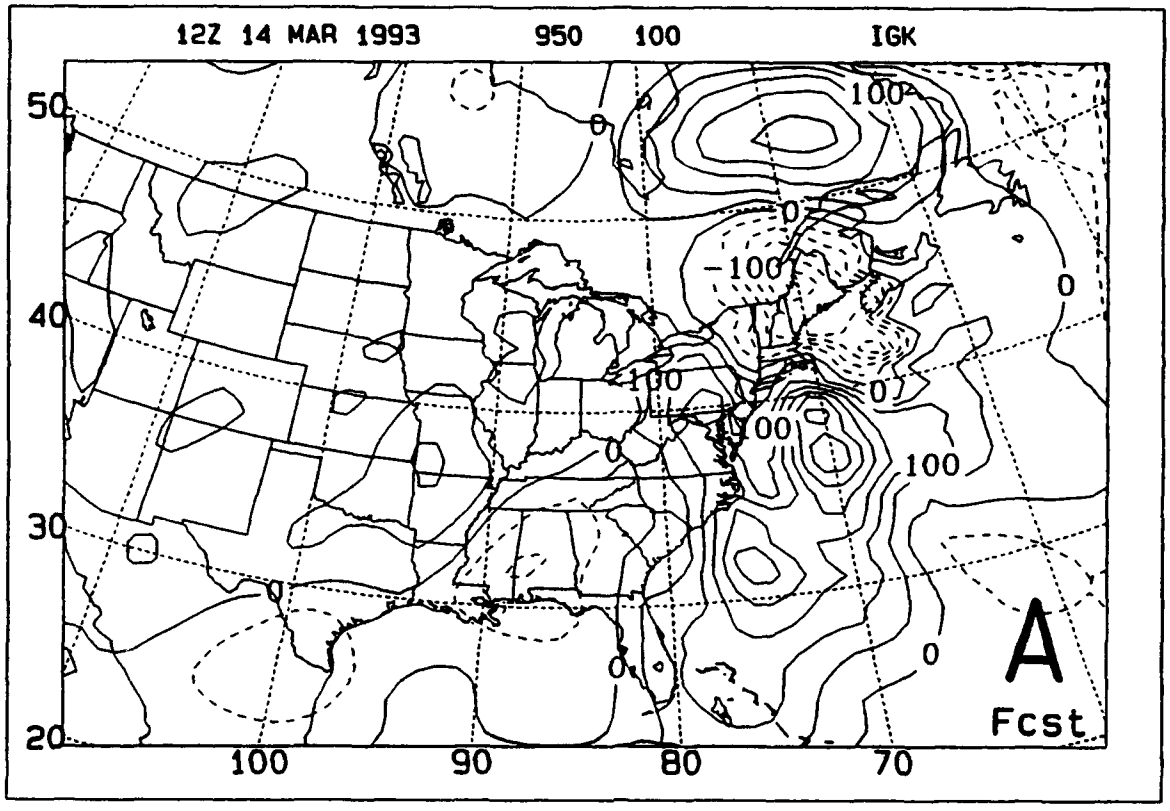

Figure 54. As in Figure 39, except for 1200 UTC 14 March 1993.

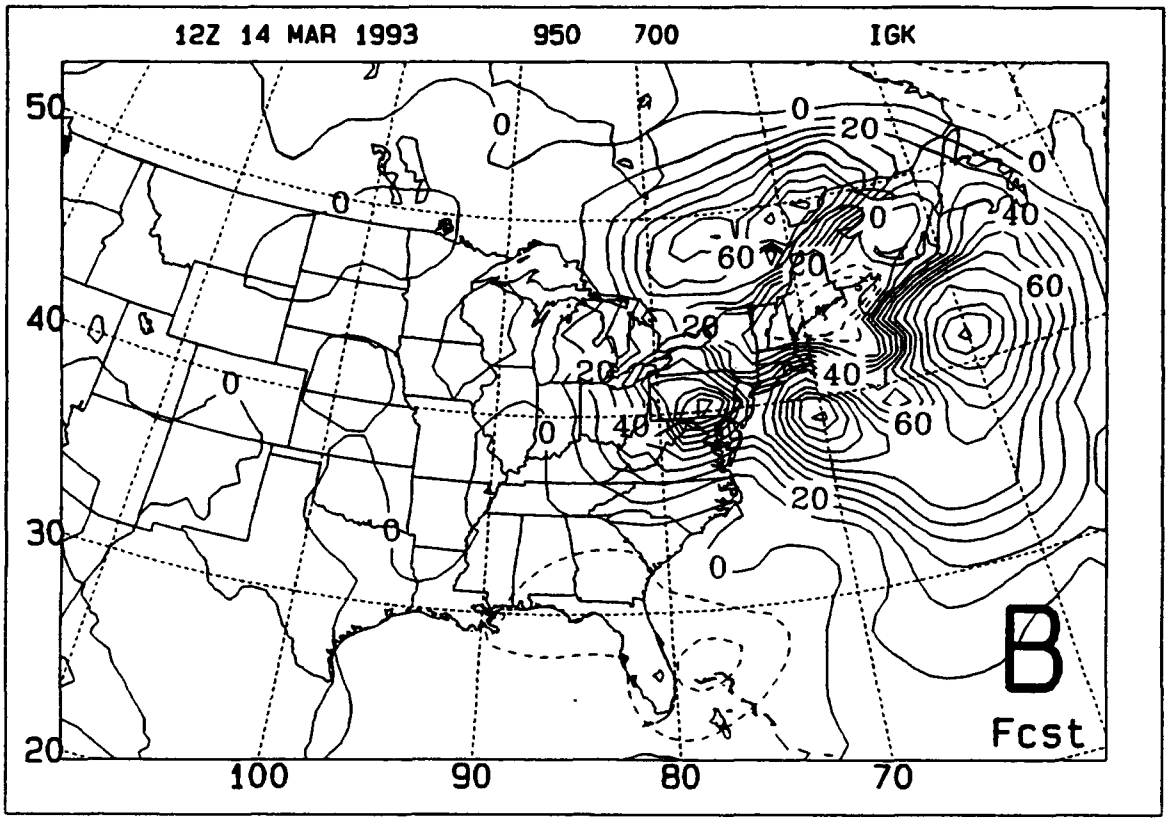
12Z 14 MAR 1993
950
700
IGK
50
40
30
20
100
90
80
70
B
Fcst

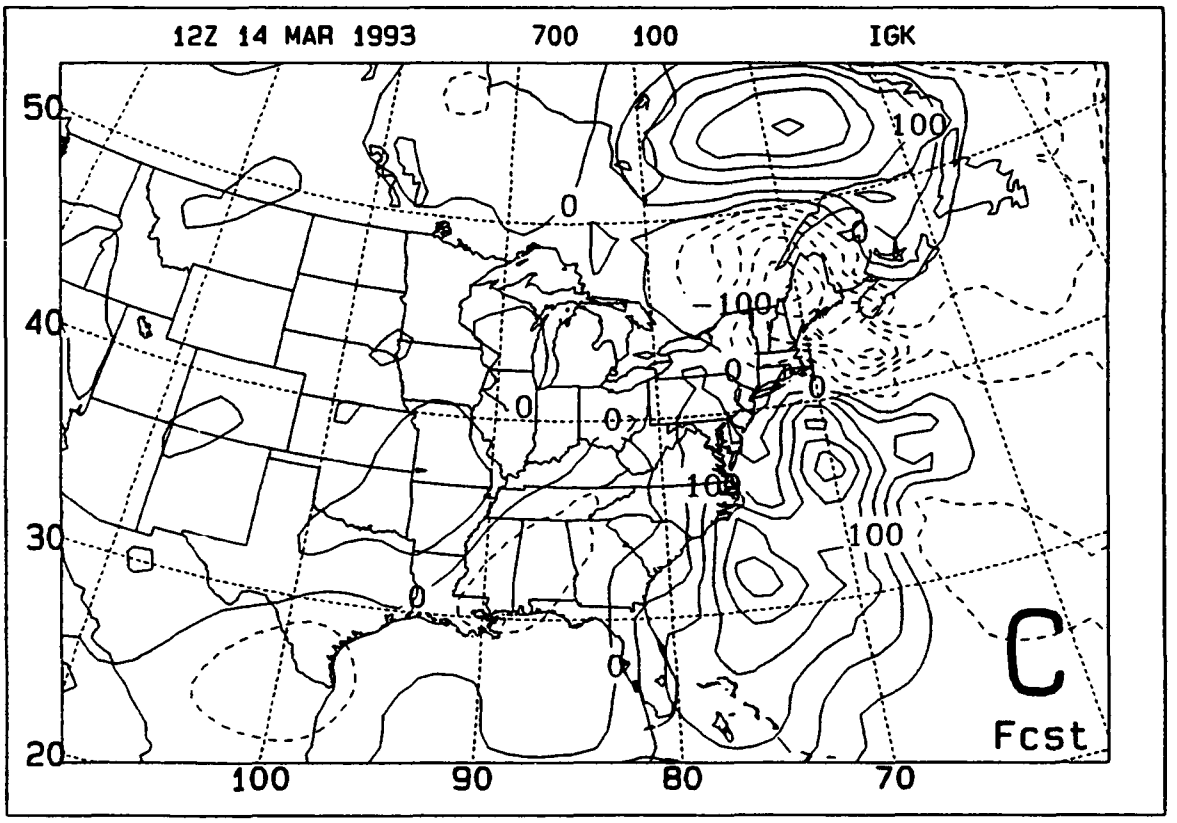
12Z 14 MAR 1993
700
100
IGK
50
40
30
20
100
90
80
70
C
Fcst

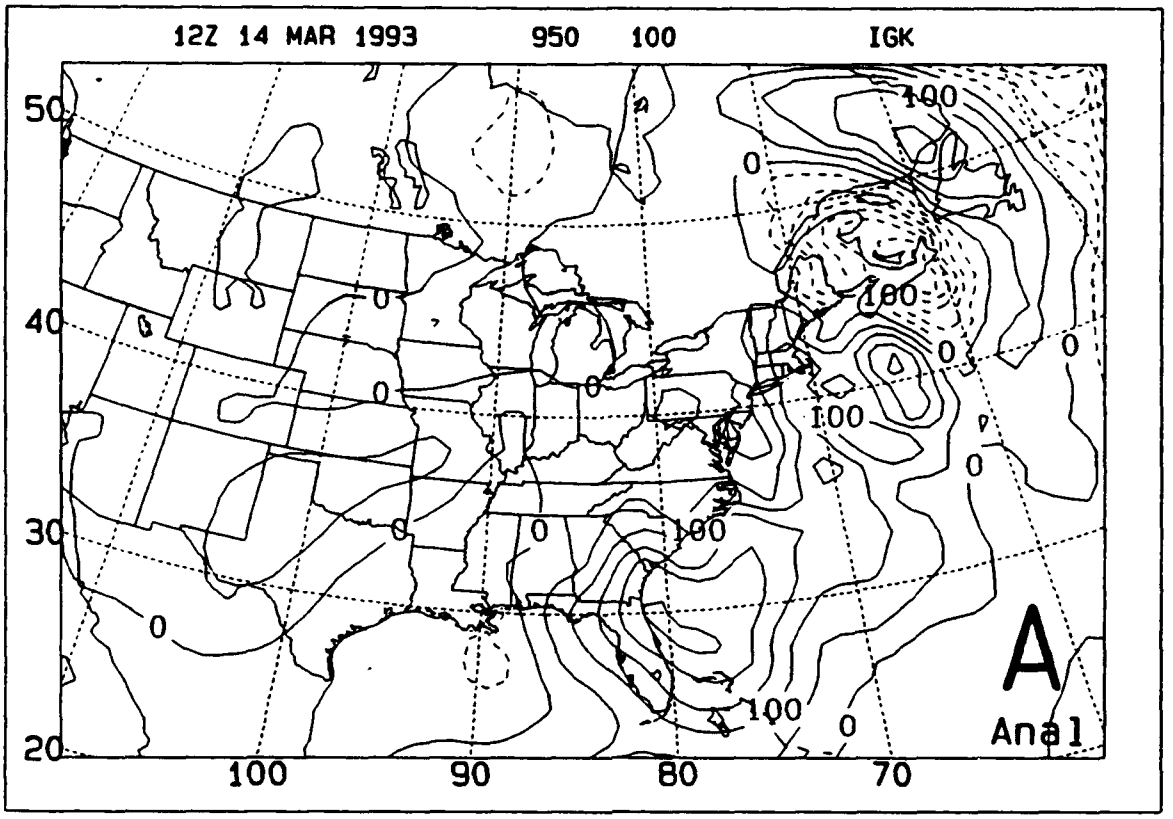

Figure 55. As in Figure 40, except for 1200 UTC 14 March 1993.

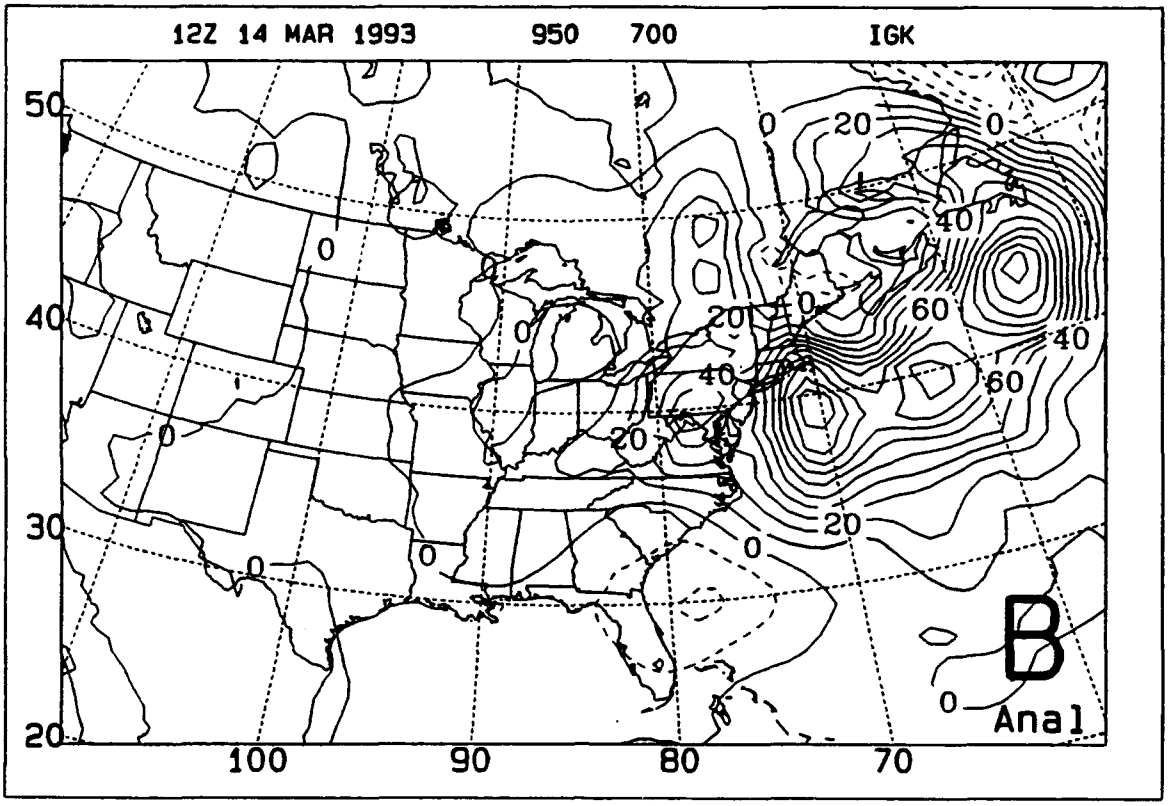
12Z 14 MAR 1993
950 700
IGK
50
40
30
20
100
90
80
70
B
Anal

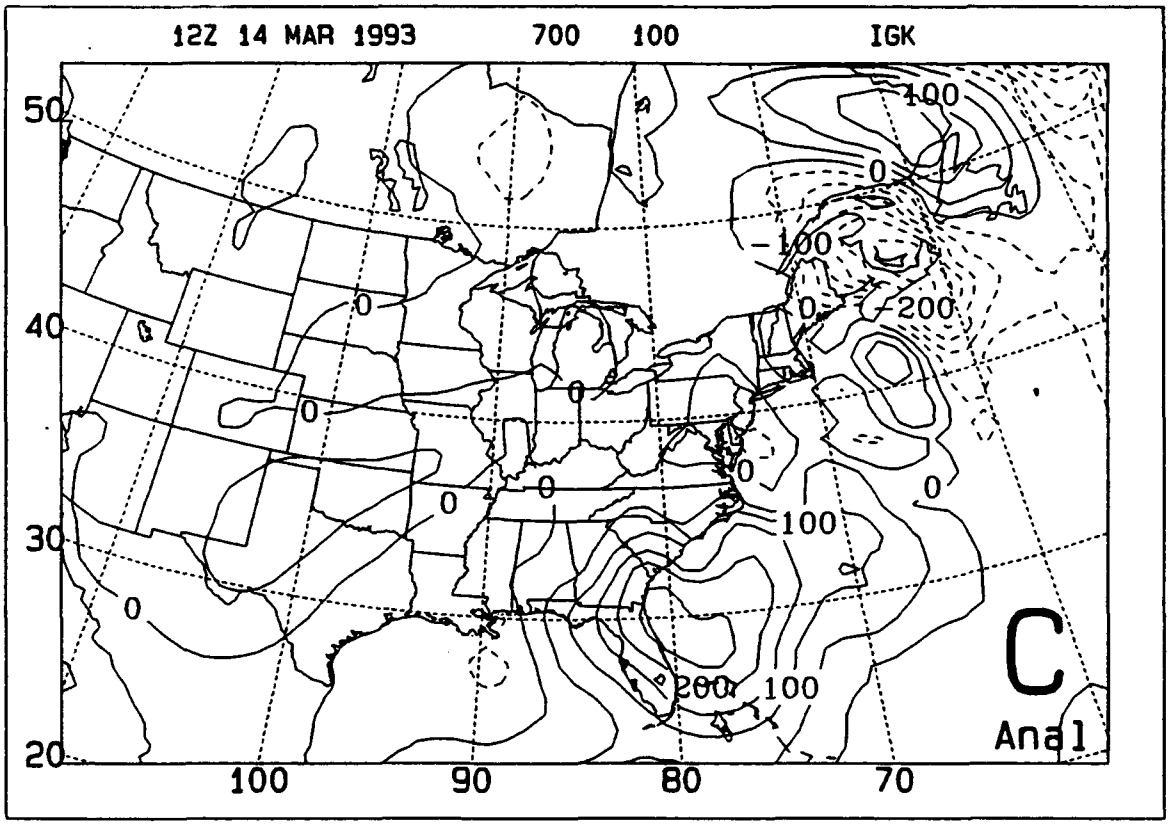
12Z 14 MAR 1993
700 100
IGK
50
40
30
20
100
90
80
70
C
Anal

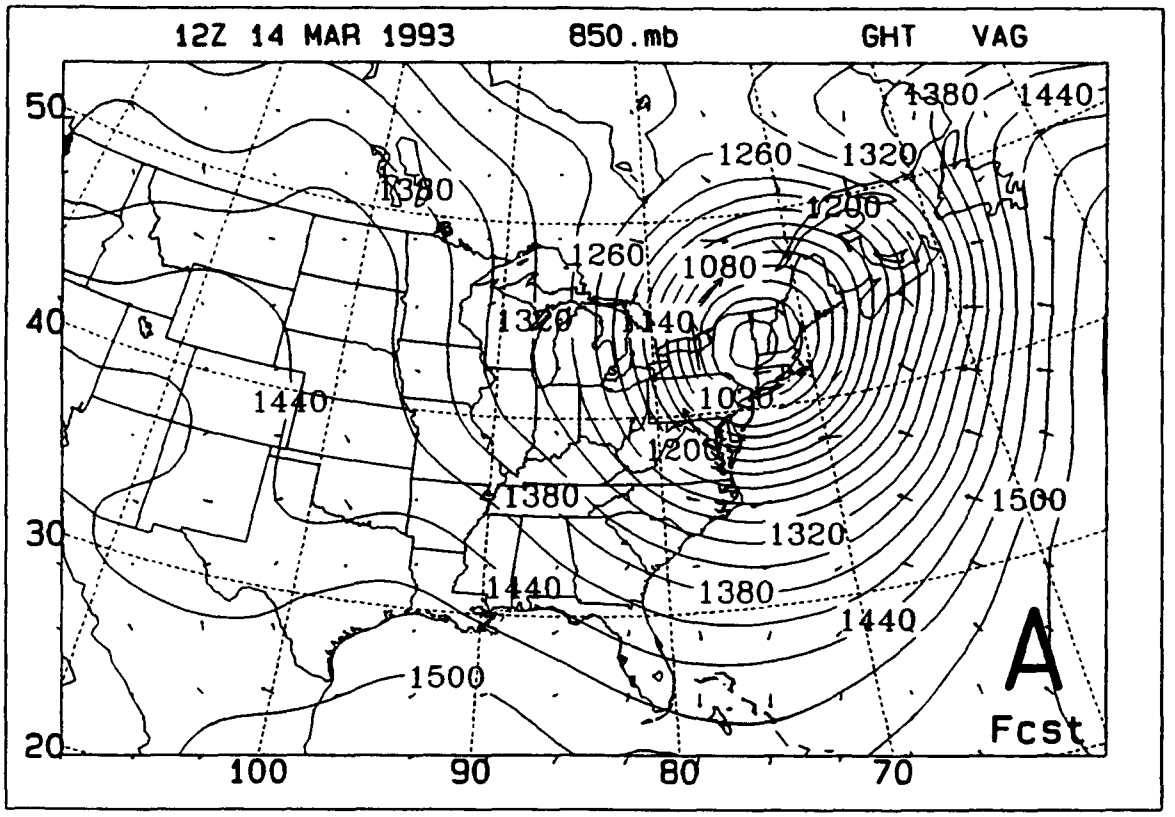

Figure 56. As in Figure 41, except for 1200 UTC 14 March 1993.

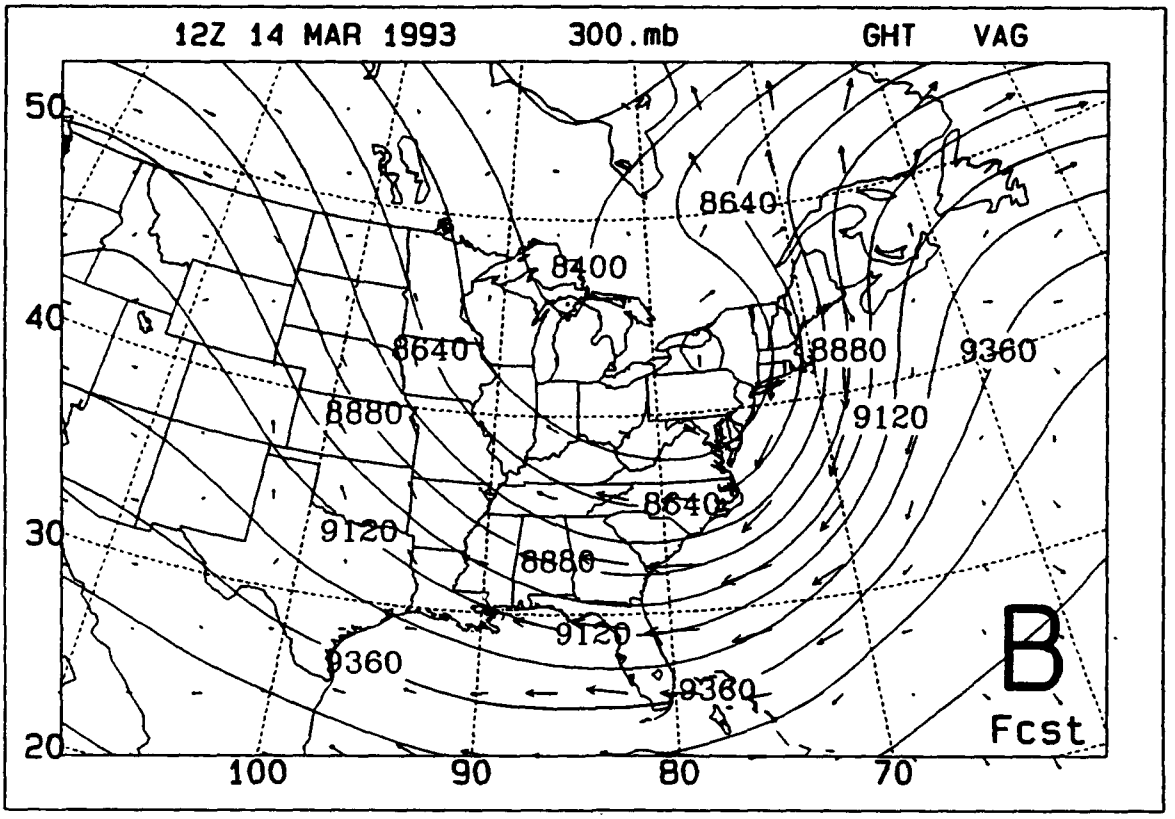
12Z 14 MAR 1993
300.mb
GHT
VAG
8640
8400
8640
8880
9360
8880
9120
8640
9120
8880
9120
9360
9360
B
Fcst
50
40
30
20
100
90
80
70

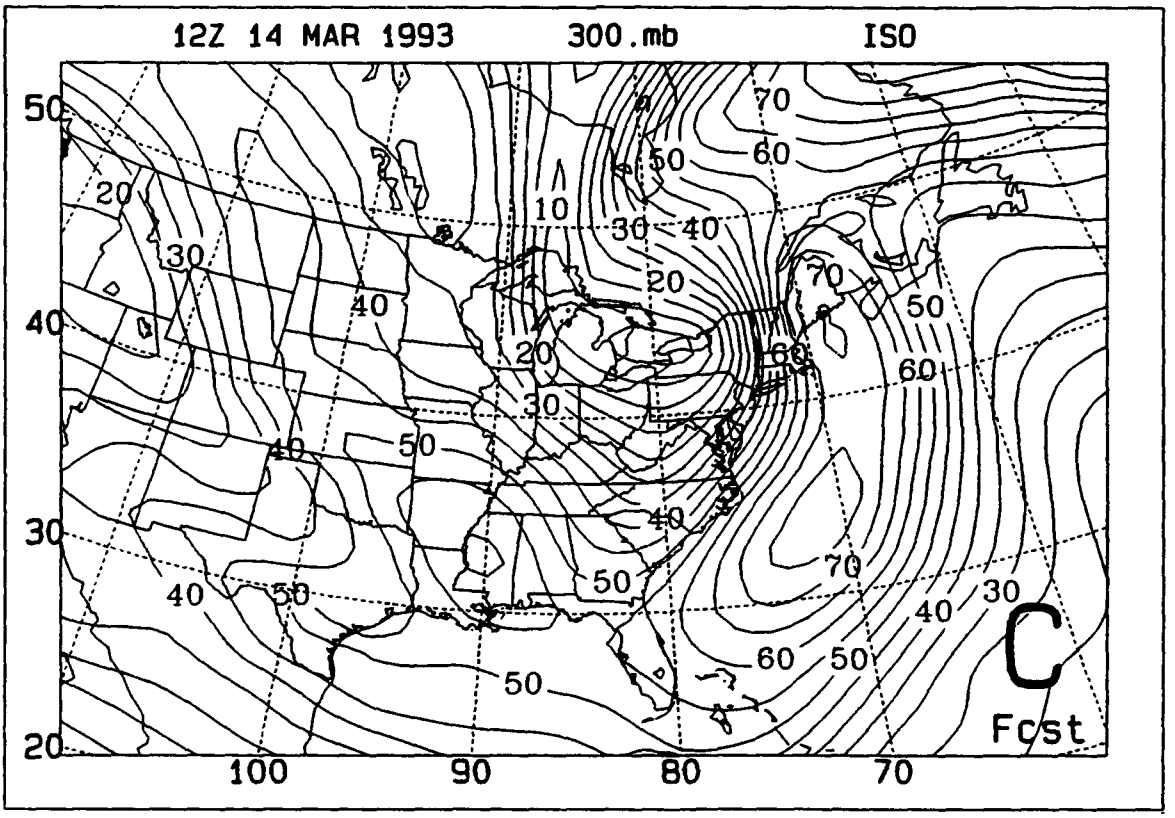
12Z 14 MAR 1993
300.mb
ISO
70
50
60
20
10
30
40
30
40
20
70
50
20
60
60
30
40
50
40
50
40
70
50
40
30
60
50
C
Fcst
50
40
30
20
100
90
80
70

AREA-AVERAGED IKE

DAY/ TIME	FORECAST			AVN ANALYSIS			NMC
(UTC)	WA	LA	p_s	WA	LA	p_s	p_s
13 / 0000	30.76	1.59	1001	32.47	1.82	1001	989
13 / 1200	35.92	2.42	992	39.78	3.05	982	973
14 / 0000	42.07	3.39	969	46.33	3.87	968	960
14 / 1200	45.15	4.29	960	44.53	4.04	967	966

Table 1. Area-averaged, Vertically Integrated Kinetic Energy. WA - whole atmosphere (950 - 100 mb), units - 10^5 J m^{-2} ; LA -- lower atmosphere (950 - 700 mb), units - 10^5 J m^{-2} ; p_s - cyclone sea-level pressure, units -mb

AREA-AVERAGED IGK

DAY/ TIME	FORECAST			AVN ANALYSIS			NMC
(UTC)	WA	LA	p_s	WA	LA	p_s	p_s
13 / 0000	11.29	2.93	1001	19.96	3.95	1001	989
13 / 1200	18.39	5.57	992	28.30	8.07	982	973
14 / 0000	30.73	9.81	969	34.35	11.47	968	960
14 / 1200	22.06	10.83	960	19.24	8.80	967	966

Table 2. Area-averaged, Vertically Integrated Generation of Kinetic Energy. WA - whole atmosphere (950 - 100 mb), units - W m^{-2} ; LA -- lower atmosphere (950 - 700 mb), units - W m^{-2} ; p_s - cyclone sea-level pressure, units -mb

LIST OF REFERENCES

Carlson, T.N., 1991: *Mid-Latitude Weather Systems*, HarperCollins Academic, 507 pp.

DeAngelis, R.M.,1993: Was it the Storm of the Century? Spring 1993. *Mariner's Weather Log*, **37**, 38-45.

Derber, J.C., D.F. Parrish, and S.J. Lord, 1991: The new Global Operational Analysis System at the National Meteorological Center. *Wea. Forecasting*, **6**, 538-547.

Haltiner, G.J., and F.L. Martin, 1957: *Dynamic and Physical Meteorology*, McGraw Hill, 470 pp.

Kanamitsu, M., 1989: Description of the NMC Global Data Assimilation and Forecast System. *Wea. Forecasting*, **4**, 335-342.

Kanamitsu, M., J.C. Alpert, K.A. Campana, P.M. Caplan, D.G. Deaven, M. Irdell, B.

Katz,H..-L. Pan, J. Sela, and G.H. White, 1991: Recent changes implemented into the Global Forecast System at NMC. *Wea. Forecasting*, **6**, 425-435.

Kung, E.C., 1966: Kinetic energy generation and dissipation in the large scale atmospheric circulation. *Mon. Wea. Rev.*, **94**, 67-84.

Kuo, H.L., 1965: On the formation and intensification of tropical cyclones through latent heat release by cumulus convection. *J. Atmos. Sci.*, **22**, 40-63.

Kuo, H.L., 1974: Further studies of the parameterization of the influence of cumulus convection on large-scale flow. *J. Atmos. Sci.*, **31**, 1232-1240.

Nuss, W.A., and D.W. Titley, 1994: Use of multiquadric interpolation for meteorological objective analysis. *Mon. Wea. Rev.*, submitted.

Nuss, W.A., S. Drake, P.A. Hirschberg, R. Pauley, T. Holt and Collaborators, 1993: VISUAL manual. Naval Postgraduate School, Meteorology Department.

Phillips, N.A., 1957: A coordinate system having some special advantage for numerical forecasting. *J. Meteor.*, **14**, 184-185.

Riehl, H., and Collaborators, 1952: *Forecasting in Middle Latitudes. Meteor.*, **1**, No. 5, 80 pp.

Sanders, F., 1986: Explosive cyclogenesis over the west central North Atlantic Ocean. *Mon. Wea. Rev.*, **114**, 1781-1794.

Sanders, F., 1987: Skill of NMC operational models in prediction of explosive cyclogenesis. *Wea. and Forecasting*, **2**, 322-336.

Sanders, F., and Auciello, E.P., 1989: Skill in prediction of explosive cyclogenesis over the Western North Atlantic Ocean, 1987/88: A forecast checklist and NMC dynamical models. *Wea. and Forecasting*, **4**, 157-172.

Sanders, F., and J.R. Gyakum, 1980: Synoptic-dynamic climatology of the "bomb". *Mon. Wea. Rev.*, **108**, 1589-1606.

Smith, P.J., 1980: The energetics of extratropical cyclones. Rev. Geophys. Space Phys.,**18**, 378-386.

Smith, P.J., and P.M. Dare, 1986: The kinetic and available potential energy budget of a winter extratropical cyclone system. *Tellus*, **38A**, 49-59.

Uccellini, L.W., 1990: Processes contributing to the rapid development of extratropical cyclones. *Extratropical Cyclones: The Erik Palmen Memorial Volume,* C. Newton and E.O. Holopainen, Eds., Amer. Meteor. Soc., 81-105.

Uccellini, L.W., and P.J. Kocin, 1987: The interaction of jet streak circulations during heavy snow events along the east coast of the United States. *Wea. Forecasting*, **2**, 289-308.

Willis, C.L., 1993: The blizzard of '93: anatomy of a monster winter storm. *Naval Oceanography Command News,* 1-4.

Wash, C.H., R.A. Hale, P.H. Dobos, and E.J. Wright, 1992: Study of explosive and nonexplosive cyclogenesis during FGGE . *Mon. Wea. Rev.*, **120**, 40-51.

INITIAL DISTRIBUTION LIST

		No. Copies
1.	Defense Technical Information Center Cameron Station Alexandria VA 22304-6145	2
2.	Library, Code 052 Naval Postgraduate School Monterey CA 93943-5002	2
3.	Oceanography Department Code OC/CO Naval Postgraduate School 833 Dyer Rd Rm 331 Monterey CA 93943-5122	1
4.	Meteorology Department Code MR/HY Naval Postgraduate School 589 Dyer Rd Rm 252 Monterey CA 93943-5114	1
5.	Dr. Patricia M. Pauley Code MR/PA Department of Meteorology Naval Postgraduate School 589 Dyer Rd RM 252 Monterey CA 93943-5114	2
6.	Dr. Paul A. Hirschberg Code MR/HS Department of Meteorology Naval Postgraduate School 589 Dyer Rd RM 233 Monterey CA 93943-5114	1
7.	LT Anton J. Kraft, USN 1637 Waterway Circle Chesapeake VA 23320	1

8. Commander
Naval Oceanography Command
Stennis Space Center
MS 39529-5000

9. Commanding Officer 1
Naval Oceanographic Office
Stennis Space Center
MS 39529-5001

10. Commanding Officer 1
Fleet Numerical Oceanography Center
7 Grace Hopper Ave Stop 4
Monterey CA 93943-0001-0120

11. Commanding Officer 1
Naval Oceanographic and Atmospheric
Research Laboratory
Stennis Space Center
MS 39529-5004

12. Superintendent 1
Naval Research Laboratory
7 Grace Hopper Way Stop 2
Monterey CA 93943-5502